2009

# Flood Attenuation Studies

Michael Bruen
*University College Dublin*, michael.bruen@ucd.ie

John O'Sullivan
*University College Dublin*, jj.osullivan@ucd.ie

Sangaralingam Ahilan
*University College Dublin*

Zeinab Bedri
*Technological University Dublin*, zeinab.bedri@tudublin.ie

**OPW Flood Studies Update Project**

**Work-Package 3.3**

**REPORT**

***for***

# FLOODPLAIN ATTENUATION STUDIES

***September 2010***


**Centre for Water Resources Research,**
**School of Engineering, Architecture and Environmental Design,**
**College of Engineering Mathematical and Physical Sciences,**
**University College Dublin**

**Postal Address:**

University College Dublin
Newstead
Belfield
Dublin 4

Phone: (01) 7163213 (Dr. John O'Sullivan)
Phone: (01) 7163212 (Prof. Michael Bruen)
Fax: (01) 7167399

E-mail: jj.osullivan@ucd.ie
m.bruen@ucd.ie

# Abstract

This report presents the findings of a study that investigates floodplain attenuation effects in Irish catchments. The work, undertaken by the Centre for Water Resources Research in UCD Civil Engineering, comprised Work-package 3.3 of the Flood Studies Update Programme (FSU).

Flood flows in river channels in Ireland are commonly influenced by the effects of floodplain storage. This influence tends to be greater than that experienced in UK catchments and may, in part, explain why many growth curves in Ireland are mildly graded. This has significance for statistical methods of flood estimation recommended in the Flood Studies Report (FSR) for Ireland. Methods include single site flood frequency analysis and regional flood frequency analysis, or the Index Flood Method. The Index Flood Method is generally carried out in two stages, the first involving an estimate of the index flood and the second using a regional growth curve to extract a multiplier for this index flood to estimate floods of required return period. The index flood recommended in the FSR is the mean annual flood, $\overline{Q}$, but in the Flood Estimation Handbook (FEH) which superseded the FSR for UK catchments and in the FSU that will supersede the FSR for Irish catchments, the median annual flood will be the index flood. For ungauged catchments, the index flood is determined from equations developed from a multivariate regression model and related to catchment descriptors that have a statistically important influence on rainfall runoff. However, these equations do not include a parameter that accounts for floodplain effects. For gauged catchments the index flood is obtained from the annual maximum series, should a record of good quality hydrometric data be available at the site in question.

Failure to include floodplain attenuation effects in either single site or regional flood frequency analysis will potentially result in errors in estimated peak flows. Floodplain attenuation effects are inherently included in single site or regional flood frequency estimation procedures that use Annual Maximum series, resulting in calculated flows that are potentially underestimated. This presents a problem when these flows are used as inputs in river models where the flows are further attenuated. Therefore, the ability to properly account for floodplain effects in the hydrological analysis of catchments is essential to unravel this 'double accounting' of floodplain attenuation, particularly in the context of the growing desire to combine hydrological and hydraulic models in a manner that provides a detailed and spatially coherent representation of flood risk. Furthermore, in the context of using groups of similar catchments or 'pooling groups' to determine growth factors that can be applied to index floods for estimating peak flows of required probabilities (return periods), data from floodplain-affected (FPA) areas has the capacity to contaminate growth curve estimates at non FPA sites.

WP 3.3 of the Flood Studies Update developed simple indices that allows floodplain effects to be either 'switched on' or switched off' depending on the application. The approach adopted involved generating flood hydrographs of specified return periods and routing these hydrographs through a generalised river reach using a flood routing model capable of simulating a variety of channel geometries and roughnesses, thus providing a downstream flow record. The index developed from this approach was validated with prototype data in the case study of the River Suir, Co. Tipperary, Ireland. Results, however were unsatisfactory with peak flow attenuations being grossly underestimated. Moderate improvements were obtained by including a scaling factor which was specific to the River Suir catchment between New Bridge and Caher Park but further work is required to a scaling factor that could reasonably predict floodplain attenuations for catchments throughout Ireland. Results from the equation for predicting the relative delay in flood wave propagation, while better, were still variable.

## Acknowledgements

The Centre for Water Resources Research in the School of Architecture, Landscape and Civil Engineering in UCD wishes to acknowledge the financial support made available by the OPW for undertaking this research.

The support and assistance of the OPW in making available data required to undertake the study is also acknowledged.

## Table of Contents

## List of Figures

## List of Tables

# 1 Introduction

Flood flows in river channels in Ireland are commonly influenced by the effects of floodplain storage. This influence tends to be greater than that experienced in UK catchments and may, in part, explain why many growth curves in Ireland are mildly graded.

Floodplain flows are significantly more complex than single channel flows and are heavily influenced by 3-dimensional interactions between the main channel and floodplain zones of the channel. The main objective of this research is to increase understanding of the influence that floodplain storage has on flood flows and how this can be effectively accounted for in flood risk estimation.

## 1.1 Background and Objective

River flows contained within channel banks are naturally attenuated. Assuming no lateral inflows or tributary influences, such attenuation is reflected in the difference in peak discharge between the upstream inflow and downstream outflow. For flows that inundate floodplains, the magnitude of this difference is influenced by the geometrical and resistance characteristics of the overbank zone but, in some situations, can be more pronounced (Figure 1-1). The main reasons for this as reported by Archer (1989) and Thomas and Nesbit (2007) amongst others, are the increase in the storage of water in the floodplain zone (influenced by both the geometrical characteristics of the floodplain and also by the hydraulic resistance of the wetted perimeter in this zone).

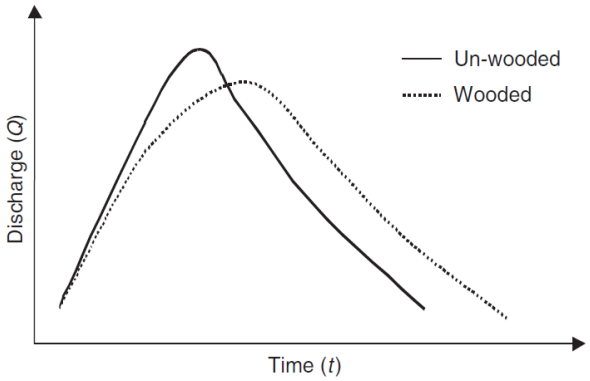


**Figure 1-1 Comparison between wooded and un-wooded floodplain in delaying and attenuating flood peak (Thomas and Nisbet, 2007)**

The increase in hydraulic resistance from the turbulent momentum exchange between the main channel and floodplain along the vertical interface between these zones will also be of influence. These impacts are likely to be more pronounced in the lower floodplain depth range where storage rather than conveyance is the dominant influence. However, in situations where the floodplain also contributes significantly to the overall compound channel conveyance, the flood peak will tend to be transferred downstream with less attenuation. Consequently and depending on the flow magnitude or return period, natural channels can be subject to a combination of these storage and attenuation effects. The net result in a given situation is complex and depends on the geometry and resistance of the river and its floodplain on the flows, and also on the width of the flood hydrograph.

The growing desire to combine hydrological and hydraulic models in a manner that provides a detailed and spatially coherent representation of flood risk requires that floodplain attenuation effects are properly accounted for in the hydrological analysis of a catchment. However, combining flood estimation methodologies with hydraulic models can be problematic. One potential difficulty is that of double-accounting for the attenuating effect of floodplain storage. This occurs when floodplain attenuation effects are represented both in the flood frequency estimation of the flow and also in hydraulic modelling.

This work-package aims to develop a simple index to represent floodplain effects on both flood frequency and magnitude. In so doing, the work-package will provide the FSU user with a method for estimating the flood frequency curve both as it is (i.e. with floodplain effects) and with the floodplain element removed. The capacity to isolate and exclude floodplain effects will allow flood estimates to be determined for situations where the floodplain effect is being allowed for elsewhere in the analysis.

Furthermore, in the context of using groups of similar catchments or 'pooling groups' to determine growth factors that can be applied to index floods for estimating peak flows of required probabilities (return periods), data from floodplain-affected (FPA) areas has the capacity to contaminate growth curve estimates at non FPA sites. The index of floodplain attenuation that is developed in this work-package will allow attenuation effects to be excluded from FPA sites in the statistical analysis to determine growth factors.

The work described in this report represents Work-Package 3.3 of the Flood Studies Update (FSU) programme. This update, initiated by the OPW in conjunction with a Management Committee comprising interested state, semi-state and other relevant organisations, is focused on providing improved methods of rainfall and flood estimation that will supersede the Flood Studies Report (NERC, 1975). In doing so, additional years of hydrometric data collected since 1969 will be utilised, as will advances in computer and digital technologies.

## 1.2 Scope of the FSU Programme

The work for the Flood Studies Update Programme comprises Research and Development in six Work-Groups. These work groups are summarised in Table 1-1.

**Table 1-1 Work Groups in Flood Studies Update programme**

| Work Group (WG) | Description |
|---|---|
| WG1 | Meteorological analysis (data preparation and frequency analysis) |
| WG2 | Hydrological analysis (statistical analysis of floods) |
| WG3 | Flood hydrograph analysis |
| WG4 | Urban catchment flood analysis |
| WG5 | Development of information systems |
| WG6 | Publication of Flood Studies Update products |

Work Groups are further divided into a number of related and complementary Work Packages. The Centre for Water Resources Research (CWRR) in UCD Civil Engineering was appointed to undertake Work-Package 3.3 in Work-Group 3 that deals with Floodplain Attenuation Studies.

## 1.3 Methodology of Project

The proposed methodology in addressing the full complexities of floodplain flows and how they relate to the overall objectives of the work-package involved:

(a) Setting up verifiable 1-D, 2D and 3-D computer models of the channels that were tested at the UK Flood Channel Facility (FCF). The 1-D model used was HEC-RAS and the 2-D and 3-D models were TELEMAC codes.
(b) Validating these models using physical data measured from the FCF;
(c) Analysing the simulated results to choose one of these models to further investigate floodplain effects in out of bank flows;
(d) Developing a generalised model of a river reach using the chosen software to run simulations for a wide range of flows, geometries and hydraulic roughness;
(e) Using the results of these simulations to identify the statistically important parameters in the capacity of floodplains to attenuate flood peaks and to develop a simple index to represent this floodplain attenuation;
(f) Using a case study to assess this index against observed data taken from a prototype scale river catchment;
(g) Producing a final report with the research conclusions and recommendations for further work.

The work throughout was supported by an extensive literature review that established the international state of knowledge and practice in the area.

The work as outlined above was undertaken by the project team in a number of well defined phases. The relationship between the various phases of the work-package is shown in Figure 1-2.

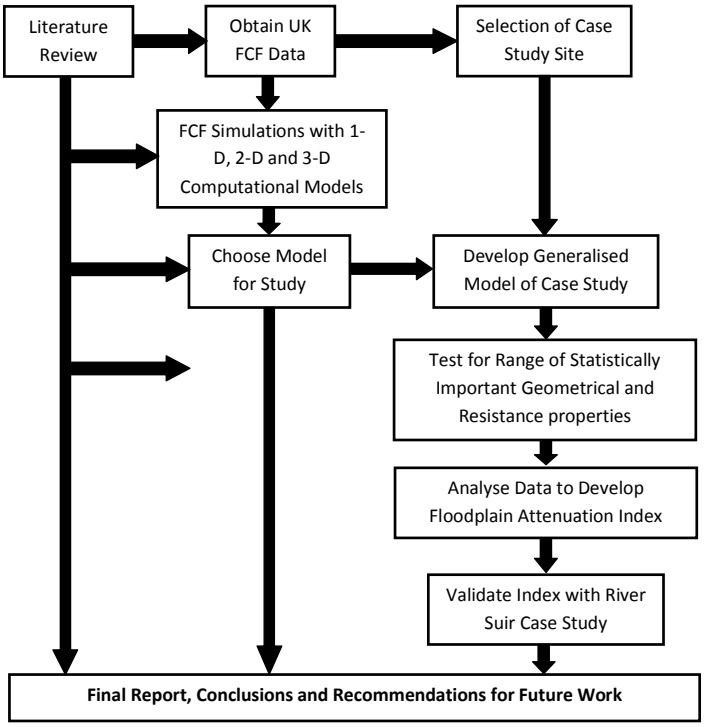


**Figure 1-2 Relationships between phases in Work-Package 3.3**

## 1.4 Outline of Report

This report is divided into six main chapters that reflect the work elements in Figure 1-2. Chapter 2 presents a literature review of aspects pertaining to the study. The review will commence with an outline of the statistical methods of flood estimation currently applied in Ireland and will continue with findings, supported by international literature, of how floodplain properties influence attenuation and in turn how this influences flood frequency. An objective of the study is to develop a simple floodplain attenuation index that may help in eliminating the 'double-accounting' of floodplain effects that can occur when a peak flow that is calculated from a flood-frequency estimation procedure is an input in a hydraulic model.

The approach that is adopted in this project involves generating flood hydrographs of specified return periods and routing these hydrographs through a generalised river reach using a flood routing model capable of simulating a variety of channel geometries and roughnesses, thus providing a downstream flow record. As this relies heavily on hydraulic modelling, Chapter 3 will include review of 1-Dimensional, 2-Dimensional and 3-Dimensional hydraulic models in their application to river channel and floodplains.

The project includes an assessment of 1-D, 2-D and 3-D hydraulic models as they are applied to data sets for straight and meandering compound channels from the large-scale UK Flood Channel Facility. The concept of this facility is presented in Chapter 4 and the performance of 1-D, 2-D and 3-D models in simulating the results from this facility are also presented.

Based on the findings of Chapter 4, a specific hydraulic modelling code is chosen to address the issue of developing the floodplain attenuation index. Chapter 5 details the development of a generalised model of a river reach within which geometrical and roughness properties can be easily changed, and through which hydrographs of specified return period are routed to provide a downstream flow record. The index that is developed in Chapter 5 is tested at prototype scale in Chapter 6 by application to a case study in which observed upstream and downstream flow records are available.

The report finishes with the overall conclusions (Chapter 7) and makes recommendations for further Research and Development.

# 2 Literature Review

## 2.1 Introduction

The ability to estimate the magnitude of design flows for specified return periods is essential for risk assessment of infrastructure projects such as roads and bridges, housing and industrial developments as well as the design of water related structures such as dams, spillways, floodwalls and levees. Current methods for this that are used in Ireland are outlined in the Flood Studies Report (NERC, 1975). The standard statistical methods for single site and regional flood frequency analysis do not have the capacity to allow for the hydraulic and hydrological effects of floodplain within the catchments and this is generally accepted as being problematic in flood frequency estimation procedures. Main channel and floodplain geometries in addition to channel resistances can have huge influence on the capacity of a floodplain to attenuate a flood peak and retard its speed of propagation down a channel. This can result in very different flood frequency distributions between sites in a catchment separated by extensive floodplain areas.

This review is structured to present detail of the current approaches to flood estimation that are used in Ireland and relating these to a body of work on floodplain effects in both a hydraulic and hydrological context.

## 2.2 Statistical Methods of Flood Estimation

In Ireland, the commonly used statistical methods for estimating design floods are based on the Flood Studies Report (FSR). This involves either:

(1) analysing the available flood record at a site or
(2) in the case of ungauged catchments, using equations based on physical characteristics that reflect the catchment response to rainfall (catchment characteristics).

## 2.3 Single Site Flood Frequency Analysis

Estimates of flow magnitude of extreme events for a specified return period, T, is relatively straightforward, if the length of record available is greater than T. However, in the majority of single site flood frequency analysis, the length of available flow records is such that the annual maximum series extracted from these flow records comprises fewer values than the required flood return period that needs

to be estimated for design or risk assessment purposes. In such circumstances, the practise is for observed flood frequency curves to be extrapolated to obtain magnitudes of higher return period flows. This technique involves fitting a probability distribution to a series of flow observations and allows the probabilities of the future occurrence of flood events to be estimated.

Three types of statistical models are recommended to establish the relationship between flood magnitude and return period, T, at a particular site. These are:

(a) Annual maximum (AM) series model;
(b) Peaks over a threshold (POT) series model;
(c) Time series model.

The basic assumptions of these models are that the flood peaks are mutually independent of each other and are identically distributed. The presence of dependence in the series of events invalidates the application of all these procedures, but a small amount of serial dependence in the events has little impact on the quality of quantile estimates. If serial dependency is significant in data series then some form of time series analysis is recommended.

The methods followed for formulating the models in (a) and (b) above are quite different and are outlined in more detail in the following sections:

### 2.3.1 Annual Maximum Series Model

An AM model uses a cumulative distribution function (cdf) to model the flood magnitudes, whereas POT models use two probabilistic models: (a) one for the probability of occurrence of peaks above a threshold, and (b) the cdf for modelling the flood exceedences.

Of these three statistical approaches, the AM model is the most widely used by hydrologists worldwide. An AM model replaces the hydrograph for each year by its largest flood and the series thus formed is called the AM series.

The choice of distribution for an AM series is not always unique. The L-moment ratio diagram (variation of L-Skewness with L-Kurtosis) can be used as a diagnostic tool to advise on which distribution is most suitable. By plotting the L-Skewness and L-Kurtosis of Irish catchments and comparing with 2-parameter and 3-parameter distributions on the L-Moment ratio diagram, the choice of distribution appropriate for the AM series can be identified.

The Flood Studies Report (NERC, 1975) recommended a Generalised Extreme Value distribution (GEV) for UK and Irish catchments. However, the Flood Estimation Handbook (Institute of Hydrology, 1999) recommended a Generalised Logistic (GLO) distribution for UK catchments. A finding from Work-package 2.2 of the FSU indicates that the AM series for Irish catchments tend to follow either the Extreme Value type 1 (EV1) distribution as recommended in the FSR or alternatively, a Generalised Logistic (GLO) distribution of the type in the FEH. Work-package 2.2 also revealed that other two parameter distributions such as the Logistic (LO2)

distribution or Lognormal Type 2 (LN2) distribution do not fit data from Irish catchments particularly well.

The GEV distribution may be expressed in the form:

$$Q_T = u + \alpha\left(\frac{1 - e^{-kyT}}{k}\right) \qquad \textbf{Eqn. 2.1}$$

where $Q_T$ is the magnitude of a flood discharge; for a specified return period, u, $\alpha$ and k are the parameters of this distribution and $y_T$ is the dimensionless EV1 reduced variate given by:

$$y_T = -\mathrm{Ln}[-\mathrm{Ln}[1 - 1/T]] \qquad \textbf{Eqn 2.2}$$

where T is the specified flood return period.

Eqn. 1.1 reduces to the following as the shape parameter k approaches zero:

$$Q_T = u + \alpha y_T \qquad \textbf{Eqn. 2.3}$$

Also, the variance of quantile estimation is:

$$\mathrm{Var}(Q_T) = \frac{\pi^2\alpha^2}{6N}\left[1 + 1.14K_T + 1.10K_T{}^2\right] \qquad \textbf{Eqn. 2.4}$$

where N is the AM series record length and $K_T$ is calculated from:

$$K_T = -\frac{\sqrt{6}}{\pi}(0.5772 - y_T) \qquad \textbf{Eqn. 2.5}$$

In the fitting of a distribution to an AM data set, the parameters u, $\alpha$ and k are estimated from the data. For the EV1 distribution (as recommended in the FSR for Ireland), a location parameter u and a scale parameter $\alpha$ are used to define the position and shape of the distribution. The value of k determines which of the three extreme value distributions encompassed by the GEV is appropriate. For $k = 0$, the Gumbel or EV1 distribution is fitted; when $k < 0$, the Frechet or EV2 distribution is specified; and with $k > 0$, the EV3 distribution is arrived at. The relationship between these distributions is shown in Figure 2-1.

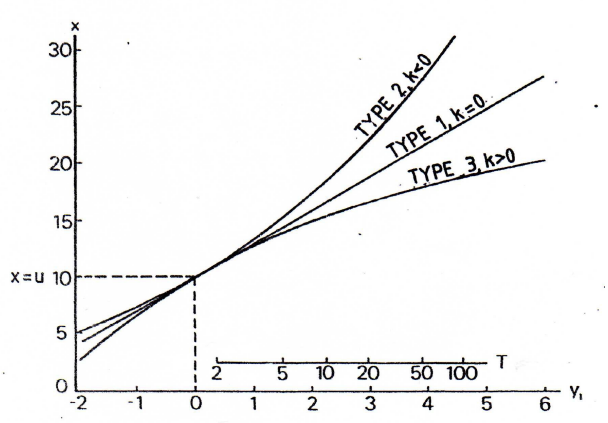


**Figure 2-1 Extreme value distributions (NERC, 1975)**

Commonly used methods for estimating $\alpha$ and u for Irish catchments are the Method of Moments, the Maximum Likelihood Method and the Method of L-Moments.

The Method of Moments involves calculating both the mean annual flood, $\overline{Q}$ and the standard deviation, $\sigma$, for the annual maximum series and relating it to $\alpha$ and u using:

$$\alpha = 0.7797\sigma \qquad \textbf{Eqn. 2.6}$$

and

$$u = \overline{Q} - 0.5772\alpha \qquad \textbf{Eqn. 2.7}$$

The Maximum Likelihood Method estimates values for $\alpha$ and u which maximise the probability of the observed discharge occurring and were the method of L-Moments to be used for fitting a distribution to the AM series, $\alpha$ and u would be calculated as from:

$$\alpha = \frac{2M_{110} - M_{100}}{Ln2} \qquad \textbf{Eqn. 2.8}$$

$$u = M_{100} - 0.5772\alpha \qquad \textbf{Eqn. 2.9}$$

where $M_{100}$ and $M_{110}$ are Probability Weighted Moments where $M_{100} = \sum_{i=1}^{n} Q_i / N$ and $M_{110} = \sum_{i=1}^{n} \left((i-1)/(N-1)\right) Q_i$ where $Q_i$ are annual maximum flow values arranged in ascending order and N is the number of years in the flow record.

An issue with AM data series is that they might tend to dominated by floods of low return period with higher return period events being less well represented. A reason for this is the inclusion in the series of only the highest flow recorded in a hydrometric year with the result that other significant flood events are omitted. For this reason,

there exists a risk that application of the AM model to a flow record would result in an underestimate of calculated flood quantiles, particularly for high return periods. This underestimation is likely to be compounded in situations where the gauging station from which the data is extracted is located downstream of active floodplains. It is therefore important to study the effect of floodplain storage on the shape of the flood frequency curve downstream of floodplains.

### 2.3.2 Peaks over Threshold Series Model

The issue of excluding significant events from analysis is overcome by using a Peaks Over Threshold (POT) Model. POT methods replace the continuous hydrograph of flows by a series of randomly spaced spikes on the time axis. The spikes themselves are of random size.

The POT series consists of all well defined peaks above a specified magnitude called the threshold flow value or the truncation level. These give rise to two random variables, namely the number of flood peaks per unit time and their magnitudes. The flood magnitudes are considered to be a random sample of a single population. Thus an appropriate continuous distributional form can represent the flood magnitudes. To formulate a relationship between $Q_T$ and T, a joint probability distribution is considered for the two random variables.

A POT analysis requires that flood peaks be modelled in both time and magnitude domains. The Poisson distribution or negative binomial distribution can be used to describe the peaks arrival rate and an exponential or Generalised Pareto Distribution (GPD) can be used to model peak magnitudes.

POT models neglect the general bunching of floods (often related to seasonal factors) that are typical in many temperate climates and although this does not matter in some applications, it casts doubt on the validity of POT rules used to determine that flood events are serially independent. However, it is still common for an exponential distribution with a Poisson arrival rate to be used to model the POT series. If the number of events per annum is regarded as a Poisson variate then both the moments and maximum likelihood estimates of $\lambda$ are given by the mean:

$$\lambda = \frac{M}{N} \qquad \textbf{Eqn. 2.10}$$

where M is the number of independent peaks for the specified flow threshold in a record of length, N years. However, it should be noted that this is the estimate of $\lambda$ that would be used even if the form of the distribution were unspecified. Hence the Poisson assumption does not play a major role here.

The magnitudes of the flows that exceed the threshold, $q_1, q_2 \ldots q_M$ are treated as a random sample from the exponential distribution with the threshold value, $q_o$ being known and $\beta$ unknown. The maximum likelihood and moment estimates of $\beta$ coincide and are:

$$\beta = \bar{q} - q_o \qquad \textbf{Eqn. 2.11}$$

where

$$\bar{q} = \sum_{i=1}^{M} \frac{q_i}{M} \qquad \textbf{Eqn. 2.12}$$

The T year flood is then written:

$$Q(T) = q_o + \beta Ln\lambda + \beta LnT = q_o + \beta Ln(\lambda T) \qquad \textbf{Eqn. 2.13}$$

and the variance of quantile estimation is:

$$VarQ_T = \frac{\beta^2}{M}\left[1 + (LnT + Ln\lambda)^2\right] \qquad \textbf{Eqn. 2.14}$$

In the POT model the exponential assumption plays a major role in quantile and sampling variance estimation.

Ahilan (2007) carried out a detailed study on Irish and UK POT data. The suitability of the exponential assumption against the GPD was investigated through two statistical tests by Van Montfort and Witter (1984) for 19 gauging stations in 15 Irish catchments. By investigating the suitability of the exponential distribution for Irish POT data, Ahilan observed that the first test, based on a probability plot accepted the exponential distribution in almost all cases while the second test, based on a Maximum Likelihood estimator of GPD parameters rejected the exponential assumption against GPD distribution in almost all cases. However, because the second test is more powerful than the first, it was concluded that Irish peaks over threshold data are more likely to follow the Generalise Pareto distribution than the exponential distribution.

Furthermore, it was observed that the Poisson distribution describes the POT data arrival rate for UK catchments reasonably well but fails to describe this arrival rate for POT data from Irish catchments.

These findings indicated that POT data from Irish and UK catchments behave differently in this respect. This may be due to differences in catchment size, variations in catchment characteristics and variations in rainfall patterns. Moreover the method of data extraction could also be a cause for these differences but efforts had been made to keep the two extraction methods the same.

In addition, Ahilan (2007) noted that negative binomial distributions describe POT data from UK and Irish catchments reasonably well. However determination of the parameters of the distribution, quantile values and sampling variances estimated using the negative binomial assumption are algebraically more complicated than those obtained using the Poisson assumption. At the same time it was noticed that quantile and sampling variance estimates based on negative binomial assumptions are nearly identical to those based on the Poisson assumption. As such, it is unnecessary to choose the negative binomial model even when the Poisson hypothesis is rejected by

the statistical tests. This is in agreement with the findings of Kirby (1969), Cunnane (1979) and Onoz and Bayazit (2001).

## 2.4 Regional Flood Frequency Analysis

The FSR recommends the use of regional flood frequency analysis for estimating design flows of specified return period at locations within river catchments. The analysis generally involves calculating the Index Flood and is often referred to as the Index Flood Method. The method has two main applications:

(1) providing a method for obtaining flood estimates in ungauged catchments;

and

(2) providing more reliable estimates of flood estimates at gauged sites for higher return periods where the flow record is of insufficient length and/ or is of poor quality.

The index flood adopted in the FSR was the mean annual flood ($\overline{Q}$). Based on the assumption of an EV1 distribution (as recommended for Irish catchments) the mean annual flood has a return period of 2.33 years. In the FEH the median annual flood having a return period of 2 years is used as the index flood.

### 2.4.1 Index Flood for Ungauged Catchments

For ungauged catchments, the index flood is linked to a set of catchment descriptors through application of a multivariate regression model. For the FSR, the selection of these catchment parameters was primarily based on their likely influence on rainfall runoff, their mutual independence and their ease of measurement from maps prepared for the FSR. These parameters account for rainfall, catchment area, stream frequency, channel slope, rainfall excess, soil type and the percentage catchment area that is urbanised or draining through lakes or reservoirs. Equations for calculating $\overline{Q}$ in terms of these parameters are provided in the FSR and include:

$$\overline{Q} = 0.677\text{AREA}^{0.77} \qquad \textbf{Eqn. 2.15}$$

$$\overline{Q} = 0.24\times10^{6}\,\text{AREA}^{0.84}\,\text{SAAR}^{2.09} \qquad \textbf{Eqn. 2.16}$$

$$\overline{Q} = 0.0236\text{AREA}^{1.19}\,\text{S1085}^{0.84} \qquad \textbf{Eqn. 2.17}$$

$$\overline{Q} = c\times\text{AREA}^{0.94}\,\text{STMFRQ}^{0.27}\,\text{S1085}^{0.16}\,\text{SOIL}^{1.23}\,\text{RSMD}^{1.03}\,(1+\text{LAKE})^{-0.85} \qquad \textbf{Eqn. 2.18}$$

where AREA ($km^2$) is the catchment area of the river to the outlet point being considered, S1085 (m/km) is the average slope of the river between 10% and 85% of its length from the outlet, SAAR (mm) is the annual average rainfall on the catchment, RSMD (mm) is the 1 day rainfall index, SOIL is the soil index, STMFRQ

(no. of stream junctions/AREA) is the stream frequency and LAKE represents the fraction of the catchment area draining through significant lakes or reservoirs. In Eqn. 2.18 the constant c relates to the location of the catchment. The FSR recommends that a value for this constant of 0.0172 be used for Irish catchments.

In the case of ungauged catchments in the FEH, the index flood ($QMED_{rural}$) is determined from catchment descriptors using:

$$QMED_{rural} = 1.172 AREA^{AE} \left(\frac{SAAR}{1000}\right)^{1.560} FARL^{2.642} \left(\frac{SPRHOST}{100}\right)^{1.211} 0.098^{REHOST} \qquad \textbf{Eqn. 2.19}$$

where AREA and SAAR are as defined above and FARL is a flood attenuation factor for reservoirs and lakes and SPRHOST is the standard percentage runoff determined from hydrology of soils type (HOST) data. AE is an area exponent given by:

$$AE = 1 - 0.015 \ln\left(\frac{AREA}{0.5}\right) \qquad \textbf{Eqn. 2.20}$$

and REHOST is a residual soils term given by:

$$REHOST = BFIHOST + 1.30\left(\frac{SPRHOST}{100}\right) - 0.987 \qquad \textbf{Eqn. 2.21}$$

where BFIHOST is a baseflow index derived from HOST data.

Eqn. 2.19 is based on data sets from 728 UK catchments with areas in excess of $0.5km^2$ and urban fractions not exceeding 0.025 Its use for catchments outside of these ranges is not recommended. In addition to availing of the additional years of hydrometric data since the FSR, methods of flood estimation in the FEH also reflected the advances in computer and digital technologies in this time. Consequently, the FEH approaches use spatial or area based quantities which can be readily determined from the digital mapping databases available in the UK rather than parameters such as stream length and slope for which unique values cannot be determined.

The Flood Studies Update (FSU) which will supersede the FSR for the analysis of Irish catchments has also adopted the QMED as the index flood and this is related to a set of catchment descriptors, some of which are specific to Ireland. This equation is:

$$QMED_{rural} = 2.557\times10^{-5} AREA^{0.878} BFI^{-0.878} SAAR^{1.254} FARL^{2.339} DRAIND^{0.438} S1085^{0.128} (1+ARTDRAIN)^{0.047} \qquad \textbf{Eqn. 2.22}$$

where parameters are as described above and where BFI is the baseflow index, DRAIND ($km^{-1}$) is a simple index that relates the length of the upstream hydrological network (km) to the area of the gauged catchment ($km^2$) and ARTDRAIN is an index of the arterial drainage extent defined as the percentage area of benefiting lands with respect to the total catchment area.

### 2.4.2 Index Flood for Gauged Catchments

The recommended alternative to calculating the index flood from the catchment characteristic equations outlined, is that $\overline{Q}$ be obtained from the annual maximum series, should a long record of good quality hydrometric data be available at the site in question.

## 2.5 Index Flood Method

As its main assumption, the Index Flood Method considers that the statistical distribution of floods within a homogeneous region is similar except for a scale parameter or index that reflects specific local features. Hence, the quantity $X_T = Q_T/Q_I$ where $Q_I$ and $Q_T$ are the index flood and flood corresponding to specified return period respectively, has the same value at all locations within the region. Values of $X_T$ are obtained by a form of regional averaging over all gauging stations in the homogeneous region and the $X_T$ with T or $X_T$ with $y_T$ relationship is referred to as a growth curve where T is the return period and $y_T$ is the variate corresponding to this return period. Using the regional growth curve, and noting that for the FSR, the index flood is $\overline{Q}$, $Q_T$ is obtained from:

$$Q_T = \overline{Q} \times X_T \qquad \textbf{Eqn. 2.23}$$

Consequently, the calculated value of the peak flow is generally carried out in two stages, the first of these is estimating a value of the mean annual flood, $\overline{Q}$, and the second is using a regional growth curve to extract a multiplier of $\overline{Q}$ to estimate floods of required return period.

### 2.5.1 $\overline{Q}$ and Regional Flood Frequency Analysis

A limitation with the FSR catchment-descriptor model for determining the index flood for unguaged catchments is that it does not include a specific term for floodplain attenuation effects. The relationship between the return periods of a bankfull river flow and the mean annual flood is of particular importance in this regard. Should the bankfull return period be less than 2 years, then for ungauged catchments, the exclusion of any index or factor to account for floodplain attenuation in the regression equations (Eqn 2.15 to Eqn 2.18) could contribute to an overestimation of the index flood. For gauged catchments, floodplain effects are inherently included in index flood estimates ($\overline{Q}$) from AM series but these are unlikely to compromise the value of the index flood.

Dissatisfaction with the omission of parameters to account for floodplain attenuation effects in FSR catchment-descriptor models has existed since the issue was raised at the first conference on the Flood Studies Report (ICE, 1975) where Dt. T.M. Prus-Chacinski commented on his surprise *at the omission of another important factor, the width of the flood valley, which affects the valley storage. …..the size of a river and*

*its valley is the integral of all climatic and geophysical factors.* It is recognised that if floodplain effects are to be included in flood estimation procedures, a means of either indexing the effect or treating it separately needs to be derived. In each case, simple effective means of identifying the floodplain effects need to be developed. In order to investigate the floodplain effects in flood risk assessment studies, much effort has been focussed into detailed hydrological modelling for specific sites where particular flood defence schemes need to be implemented. But in general, complicated floodplain models are not suitable to model floodplain effects in natural rivers (McCartney and Naden, 1995). In addition to that, any data used to identify and index the floodplain effect should be easily obtainable from data sources such as digital terrain models (DTMs).

As mentioned, failure to include floodplain attenuation effects in either single site or regional flood frequency analysis using a short AM record will result in an attenuated peak flow. This can present a problem when these peak flows are used as inputs in hydraulic models, in which simulations will further attenuate the peak flow. Therefore, the ability to properly account for floodplain effects in the hydrological analysis of catchments is essential, particularly in the context of the growing desire to combine hydrological and hydraulic models in a manner that provides a detailed and spatially coherent representation of flood risk. Furthermore, in the context of using groups of similar catchments or 'pooling groups' to determine growth factors that can be applied to index floods for estimating peak flows of required probabilities (return periods), data from floodplain-affected (FPA) areas has the capacity to contaminate growth curve estimates at non FPA sites. The focus of WP 3.3 of the Flood Studies Update is to develop a simple index that would allow floodplain effects to be either 'switched on' or switched off' depending on the application. The approach that is being adopted in this study is similar to that of Mason (1992) and involves generating flood hydrographs of specified return periods and routing these hydrographs through a generalised reach of the River Suir (Co. Tipperary, Ireland), using a flood routing model capable of simulating a variety of channel geometries and roughnesses, thus providing a downstream flow record.

Floodplain attenuation effects are only relevant in catchment hydrology when the bankfull level of a river has been exceeded. While it is recognised that this characteristic discharge and its frequency of recurrence is significant for both geomorphological and hydrological reasons (Lambert and Walling, 1987; Archer, 1989), the threshold in terms of level and flow magnitude is ambiguous. At the cross-section scale, local characteristics of erosion, sediment deposition, bank stability and vegetation interact to produce a non-obvious transition between the main-channel banks and the floodplain. This complexity of the main-channel morphology explains some of the variance in accepted definitions of both the bankfull condition and floodplains.

Speight (1965) amongst others, defines the bankfull condition as being the height of the lower limit of perennial vegetation, usually trees. Nunnally (1967) describes bankfull as the elevation of the upper limit of sand-sized particles in the sediments comprising the channel boundary. Other representations are related to the geometry of the channel. Harvey (1969) and Pickup and Warner (1976) refer to bankfull as the elevation at which the width to depth ratio of the cross section is a minimum and Williams (1978) considers that bankfull is the stage corresponding to a change in the

relation of the cross-sectional area to the channel top width. However, a simpler representation of the bankfull condition given by Nixon (1959a, 1959b) and Woodyer (1968) amongst others equates the level to that of the valley flat. This level differentiates between the main channel and floodplain but the valley flat has no universally accepted definition. In most of the scientific literature the floodplain was defined as that part of the valley floor covered by water during floods (e.g. Longwell *et al*, 1948). Other representations identify floodplains in terms of those areas where waterborne sediments have deposited (Thornbury, 1969; Shelton, 1966). Floodplains have been further defined as being either active or inactive based on the relative frequency that the bankfull level is exceeded. An inactive floodplain, known also as a terrace, is inundated so rarely that it is not influenced by river alluvial processes (Neill, 1964).

As previously noted, the bankfull flow return period (on the POT scale) is important in accurate regional flood frequency analysis. However, assessment of the bankfull flow and its associated hydrological characteristics is complex and is influenced by a number of factors. The difficulties in accurately and consistently describing the condition are a problem and significantly different recurrence periods have been obtained in studies depending on the bankfull definition used (Williams, 1978; Navratil *et al*, 2006). Early flood frequency studies relating to bankfull channel capacity generally indicated that return periods for this flow were generally accepted to be between 1 and 2 years. Other representations such as that by Dury (1961) for the White and Wabash Rivers in the US indicated that bankfull flows could be represented as a constant fraction of the mean annual flood. The concept of a single return period for bankfull flows has also been proposed (e.g. Roberts, 1989). However, as demonstrated by Hey and Davies (1975) in work on the River Severn and Tweed catchments in the UK, the assumption of a single return period for bankfull flow represents an oversimplification of the hydrological and hydraulic processes. This was supported by Williams (1978) who also questioned the concept of unique or closely grouped recurrence intervals for these flows.

Considerable work has been undertaken to establish the factors that influence the recurrence intervals of bankfull flows. In a study of gravel bed rivers in Belgium, Petit and Pauquet (1997) indicated that bankfull return periods were dependent on catchment size. In the case of small pebble bed rivers with impermeable substrata, the return period for bankfull flows was of the order of 0.5 years. However, this increased to 1.5 years for larger rivers of similar bed composition. Location within a catchment was also shown to be important. Richards (1982) showed that bankfull recurrence intervals at upstream locations were significantly lower than 1.5 years but these increased with downstream distance. This reduced frequency of bankfull discharge at downstream locations is perhaps understandable given that the flood duration of a given frequency also increases with downstream distance (Dury, 1961). This results from the increased attenuation of peak discharges in downstream river reaches where the channel gradient is lower than in upstream reaches (Petts and Foster, 1985). Castro and Jackson (2001) linked bankfull discharge recurrence intervals to regional factors (climate and physiography) in the Pacific Northwest of the US. Factors investigated included precipitation, temperature and catchment vegetation and depending on catchment location within the region, recurrence intervals varied from 1.0 to 3.1 years with an average of 1.4 years. This average value supports the assumption that the bankfull flow recurrence interval for the area is 1.5

years and suggests that regionalisation schemes have some potential for refining bankfull recurrence intervals in specified areas. Geological characteristics underlying the catchment are also significant in determining the characteristics of the flow regime. In a study of streams in Southern England, recurrence intervals for bankfull flow of 1.8 years were observed but this figure increased to values as high as 7 for catchments with an underlying chalk bedrock (Harvey, 1969). Catchments of these types are on opposite ends of the permeability spectrum but intermediate values are observed for catchments with mixed geologies. By extension, the results also suggest that the bankfull flow return period is influenced by the responsiveness of the catchment (whether catchment is sluggish or flashy) which is dependent on its geology.

Variations to the natural responses of catchments from human interventions must also be considered when considering bankfull recurrence periods. Urbanisation, cited as a major influential modification to catchment hydrology in developed areas (UNESCO, 1979), is of particular importance. Urbanisation results in an increase in impervious area within a catchment, increasing the proportion of rainfall that forms direct runoff and decreases the proportion that is available to evapotranspiration, groundwater recharge and base flow. Hollis (1975) reported that urbanisation has a greater influence on floods with short as opposed to longer return periods and that the relationship between increased peak flow in urban areas and recurrence interval falls particularly steeply for floods with recurrence intervals of between one and two years. Similar trends were observed in other studies from catchments in the US (Martens, 1968; James, 1965).

### 2.5.2 $X_T$ and Regional Flood Frequency Analysis

In addition to the mean annual flood, $\overline{Q}$, application of Eqn. 1.21 also requires a value of $X_T$. This is determined from growth curves that are specific to quasi-homogeneous regions. However, different approaches to identifying homogeneous regions have evolved. In the FSR, Ireland is treated as a single region and the curve of least gradient in Figure 2-2 is recommended.

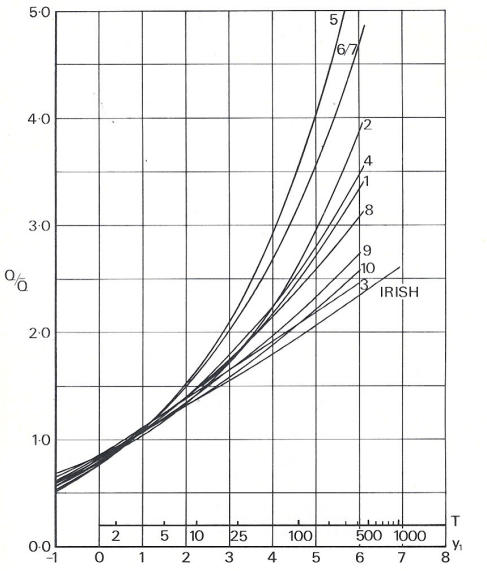


**Figure 2-2 Regional growth curve for Irish catchments from the FSR**

The mild grade of the Irish Growth Curve is generally attributed to attenuation effects that influence flows in Irish rivers. This influence tends to be greater than that experienced in UK catchments. Many reasons exist for this and these include the prevalence of bog areas, loughs and impeded drainage. However, floodplain attenuation is also likely to be important, an effect that is promoted by the mild gradients in the topography of many Irish catchments.

Using the growth curve for Ireland in Figure 2-2 represents a somewhat basic approach to regional flood frequency analysis where $X_T$ is obtained from averaging over all gauging stations in Ireland. This averaging fails to account for the very different hydrological conditions that prevail in the different regions across the country.

As an alternative, growth curves for specific regions can be developed to refine the analysis. The approach in the FSR is based on homogeneous regions that are defined on a geographical basis (usually nearby or adjacent sites). This was changed in the Flood Estimation Handbook where homogeneous regions were classified in terms of catchment similarity. Regardless of the grouping method, flood frequency analysis assumes that all sites within a given region are samples from the same distribution. Consequently, all data may be combined to yield an estimate of a regional dimensionless flood frequency relationship ($Q_T/\overline{Q}$).

A specific flood frequency distribution is valid only at a specified site. In general, distributions for multiple sites within a geographically homogeneous area can be assumed to have the same distribution and are pooled on this basis. However, the physical processes and hydraulic characteristics of floodplain flows can significantly influence flood frequency distributions (Haider, 1992; Wolff and Burges, 1994). Consequently, for catchments with active floodplains, assuming the same flood frequency distribution is likely to be erroneous. While this is indeed the case, in situations where growth curves are based on pooled data in defined geographical

regions, it is inconvenient and impractical to separate sites influenced by floodplain storage from those that are not. This can potentially result in contaminated flood frequency relationships determined for these pooled sites.

In an attempt to overcome problems with shifts in flood frequency distributions, alternative approaches to classify river basins into homogeneous groups have been developed. Such methods identified by Acreman and Sinclair (1986) suggest cluster analysis or interactive search techniques to optimise the grouping efficiency to account for both channel and floodplain effects. As an example Acreman and Sinclair used the NORMIX multivariate clustering algorithm to identify five distinct hydrologically homogeneous regions from 168 river basins in Scotland. The classification was independent of discharge data and based only on the physical characteristics of the basin, thereby avoiding the problem of regionalisation based on the highly variable, individual site estimates of flood frequency. Benn (1984), used various algorithms including that recommended in the FSR to cluster Northumbrian catchments in the UK such that a more physically based method of grouping catchments for regionalisation purposes could be developed. It was observed that catchments in which overbank storage was significant tend to be clustered together, and that their observed growth factors were generally smaller than those predicted by the FSR algorithm. In particular, the regionalised growth curve fitted to this cluster of catchments was of type EV3, and hence exhibited a finite upper bound to the flood frequency curve. Benn also noted that a further sub-group of the Northumbrian catchments, containing those having deep channels and only limited over bank storage, exhibited steeper growth curves than were predicted by the FSR algorithm.

In another study to classify basins into distinct, homogeneous groups for regional flood frequency analysis, Wiltshire (1986) used an iterative search technique through the basin characteristics database, which optimises statistics that describe the efficiency of grouping. The scheme was applied to catchments in the British Isles and yielded five groups formed on the basis of basin area, average rainfall and urban fraction. Among these five groups, four of them are homogeneous with respect to the coefficient of variance of the annual maximum flood series. Two problems exist however with this classification. The first of these is that the annual maximum of each site is referred only by the coefficient of variation of the respective annual flow records; and other valuable information relating to flood frequency such as Skewness and Kurtosis are not accommodated in the classification. The second problem is that the resulting solution in terms of basin grouping may not be unique as different basin characteristics may also produce statistically significant results. This problem however, is likely to be less serious as both physical reasoning and the behaviour of geographic regions can supplement the analysis of the test statistics.

At the point where bankfull levels are exceeded and floodplains become active for either conveyance and/ or storage, it is the physical characteristics of these overbank zones that are significant. These characteristics in terms of resistance and geometry have the capacity to both attenuate the flood peak and reduce the speed of flood wave propagation down the channel. The mechanisms of floodplain hydraulics and the manner these are contributed to by the channel and floodplain properties is therefore important in investigating flood frequency distributions and warrants mention in this review.

## 2.6 Floodplain Flows

### 2.6.1 Introduction

Channels that include floodplains in their flow cross-section are commonly referred to as compound or two-stage channels and are characterised by significantly more complex flow processes than in simple prismatic channels. A momentum exchange known as the 'kinematic effect', that takes the form of a bank of large vortices with vertical axes at the main channel edge (see Figure 2-3) has the capacity to reduce the mean velocity in a compound channel by as much as 30% and can result in discharge predictions that are overestimated by values in excess of 10% (Sellin, 1964; Zheleznyakov, 1965). These observations of reduced discharge capacity have been supported in field studies (e.g. the work by Myers and Lyness, 1989 and Martin and Myers, 1991 on the River Main, Northern Ireland).

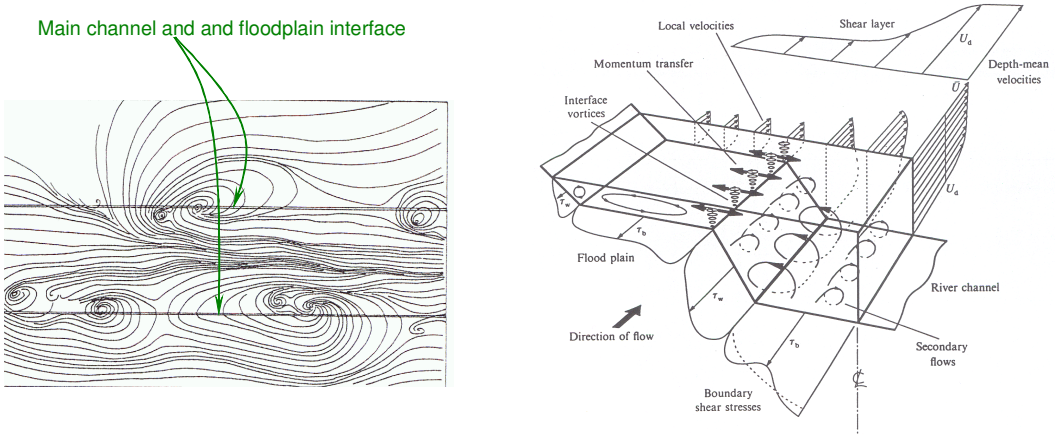


**Figure 2-3 Momentum exchanges in compound channels (Sellin, 1964; Shiono and Knight, 1991)**

According to Myers (1987), the momentum exchange is driven by the velocity gradient between the main channel and floodplain sections, the exchange being from the main channel to the floodplain for low depths but changing from the floodplain to the main channel when the highest velocities are recorded in this zone. In addition, the strength of the transfer decreases with increasing relative channel width, depth and roughness and is also influenced by the effects of channel and floodplain slope on the velocity distribution across the section (Prinos and Townsend, 1983; Holden and James, 1989; Murota *et al*, 1990).

In addition to the energy lost across the main channel and floodplain interface, the momentum exchanges also facilitate the development of secondary currents, the structure of which, according to Tominaga *et al* (1989), is mainly composed of the floodplain vortex and main channel vortex which are separated by an inclined upflow from the junction edge. This momentum exchange accelerates the floodplain flow and decelerates the main channel flow.

Natural river channels are generally comprised of meandering reaches interspersed with lengths of straight channel. In the lower extents of river basins where the

gradient is shallow, sinuous or meandering reaches characterise the planform. This is significant because it is in these shallower reaches that floodplains become active and attenuation effects impact on the flow. As reported by Mockmore (1944) and Shukry (1949), single stage channels with meanders or sinuous planforms have more complex flow patterns than straight channels and are characterised by an additional resistance to flow induced by a spiral motion in bends, the strength of which is defined as the ratio of the kinetic energy of lateral currents to the kinetic energy of the total flow.

The complexity continues to increase when the flow exceeds the bankfull level and inundates the floodplain. Research findings report reductions in discharge capacity for compound channel flows with sinuous main channel in straight floodways (Lipscomb, 1956; Leopold *et al,* 1960, James and Brown,1977; Lyness *et al* 1999). Decreased discharge, when it occurs is, according to Chang (1984) associated with the additional sources of flow resistance that occur in river bends. Chang identified these as energy lost to internal fluid friction from transverse circulation, boundary resistance associated with transverse shear and also from eddy losses resulting from flow separation in sharp bends and from sudden jumps occurring at high Froude numbers. From small scale laboratory tests, Toebes and Sooky (1967) concluded that energy losses in meandering channels were up to 2.5 times greater than those for a uniform channel of identical width, hydraulic radius and discharge and were dependent on the overbank flow depth, the mean main channel and floodplain velocities and the longitudinal channel slope. Similar influences were identified by Willetts and Hardwick (1993). These energy losses can be attributed to the full complexity of the flow field in meandering compound channels. Important mechanisms of these flows have been highlighted. Kiely (1989, 1990), Stein and Rouve (1988) and Lyness *et al* (1999) amongst others have documented the plunging of flow from floodplains into and across the inner channel and its subsequent ejection back onto the floodplain. According to Kiely, flow across the inner channel is accompanied by a depth increase on entry and a depth decrease on its exit back onto the floodplain and this expansion and contraction of the flow area induces significant energy losses. Stein and Rouve concluded that the '*welling out of*' the main channel retards the discharge on the floodplain. It was also reported by these authors that secondary currents in the main channel during overbank flow were observed to rotate in the opposite direction to those seen during inbank flow. Smith (1978) also highlighted the effect of the interaction between the main channel and floodplain flows and these flow mechanisms were further described as consisting principally of a large secondary current cell at bends and water plunging from the floodplain into the main channel near the centreline of the floodplain system (Willetts *et al*, 1990; Willetts and Hardwick, 1993, Sellin, *et al*, 1993; Ervine *et al*, 1994). These mechanisms are shown in schematic in Figure 2-4

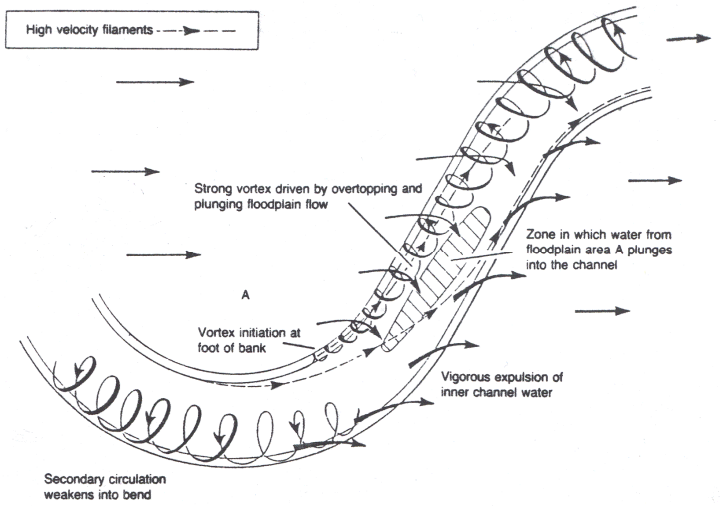


**Figure 2-4 Principal flow mechanisms in meandering compound channels (Willetts and Hardwick, 1993)**

James and Brown (1977) also observed that the overbank velocity profiles in compound meandering sections were quite distorted across the channel, a finding supported by Kiely (1989, 1990) who concluded that velocities in the main channel of a meander are as much as 50% lower than those of a similar straight channel section for the same depth.

Additional complexities and energy losses can be observed in compound channels with both sinuous main channels and floodplains. Flows in these channels tend to be characterised by additional flow separation at floodplain bends and secondary circulations in the main channel that are opposite in direction to those that occur in straight floodplain channels. These losses and the overall resistance of the channel diminish in situations where the transverse floodplain slope normal to the axis of the channel is reduced (Wieping Liu and James, 1997).

### 2.6.2 Influence of Floodplains on Flood Peak Attenuation

The above discussion highlights the full range of complexities for compound channel flows in natural river channels. Approaches in the FSR indicate that parameters for catchment area, stream frequency, rainfall and soil types can be easily applied in statistical approaches to flood estimation where the mean annual flood is estimated and related to a regional growth curve to extend to higher return periods. However, no term for floodplain attenuation effects are included in the FSR catchment-descriptor models.

Floodplains have an important role to play in flood alleviation and in sustainable flood management (ICE, 2001) and are known to decrease the speed of flood wave propagation down a channel, enhancing flood storage and reducing the magnitude of downstream flood peaks and these are important in flood wave routing. The characteristics of the floodplain have a significant role to play in this regard.

An important parameter in flood routing is the flood wave speed, c, in a river reach.

Henderson (1966) showed that at a given cross section, flood wave speed can be related to the gradient of the stage discharge curve by:

$$c = \frac{1}{B}\frac{dQ}{dy} \qquad \textbf{Eqn. 2.24}$$

where B is the channel width, Q is the discharge and y is the flow depth. Eqn. 2.24 indicates that during a flood, c will vary as Q, dQ/dh and B change with time. In addition, the variation of storage with discharge in a river reach can be expressed as a power-law relationship of the form:

$$S = kQ^m \qquad \textbf{Eqn. 2.25}$$

By noting that discharge-depth relationships (within certain discharge ranges) can be approximated by power functions ($Q = a_2 y^{b_2}$) and that channel top width to depth relationships can also be approximated by power functions in channels of regular cross-section ($B = a_3 y^{b_3}$), the flood wave speed from Wong and Laurenson (1983) in Eqn. 2.24 can be expressed as:

$$c = aQ^b \qquad \textbf{Eqn. 2.26}$$

For a simple rectangular channel the wave speed can be given by (Knight and Shiono, 1996):

$$c = \left[\frac{5}{3} - \frac{4y}{3(B+2y)}\right] \qquad \textbf{Eqn. 2.27}$$

For very wide channels where depth relative to channel width is insignificant, the wave speed from Eqn. 2.27 is c = 5/3 *x* velocity.

Natural channels are significantly more complex than simple channels, a complexity that increases with floodplain inundation, and do not follow the relationship expressed in Eqn. 2.26. Typical wave speed discharge relationships in channels with floodplains follow the form shown in Figure 2-5.

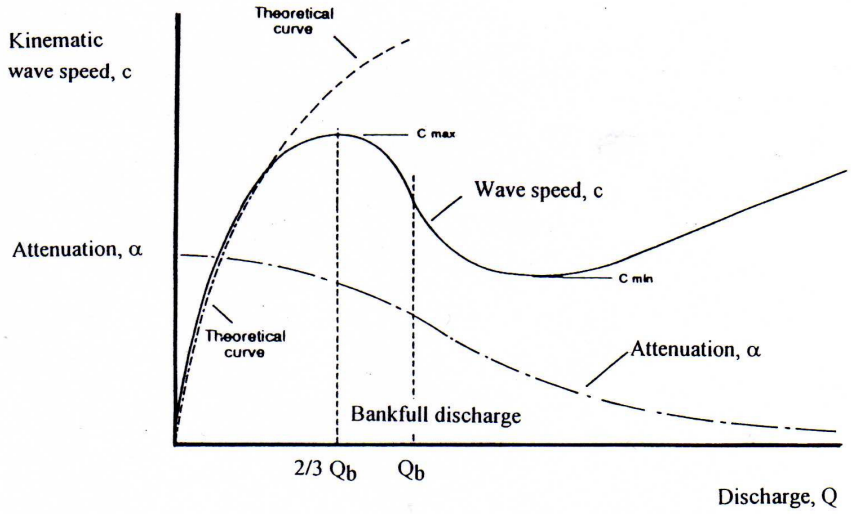


**Figure 2-5 Typical kinematic wave speed-discharge and attenuation-discharge curves (Knight and Shiono, 1996)**

Figure 2-5 indicates that these relationships are characterised by a number of distinct sections that reflect the changing conditions as flows exceed the bankfull level and inundate the overbank zone. Flood wave speed is shown typically to reach a maximum value at approximately 2/3 of the bankfull flow discharge ($Q_b$) after which it decreases to a minimum value at a shallow floodplain depth where the momentum exchanges between the main channel and floodplains are likely to be at their strongest (see Section 2.6.1). As is also reflected in Figure 2-5, a point is reached as the discharge increases where the overall channel acts as a single unit beyond which the wave speed increases. However, this single channel behaviour relates to large flows and as reported by Gillespie *et al*, (2003) for river reaches in urbanising areas of the Little Sugar Creek River, North Carolina, US, these could have return periods in excess of 25 years. Gillespie *et al* also observed a reversal in the lag time-discharge relationship at approximately the bankfull discharge of $80m^3/s$ in these rivers. For discharges up to the bankfull flow, the lag time generally decreases with increasing discharge. However when the flow exceeds the bankfull threshold, lag time increases with discharge.

The trends in Figure 2-5 are supported by results from field investigations. Price (1973) presented a wave speed ~ discharge relationship for UK rivers that was similar to that in Figure 2-5 and noted that the relationship could be expressed by two power functions, one each for the main channel and the overbank flow, joined by an elongated S-shaped transition curve. However, some inconsistencies with Figure 2-5 were observed in both the lower and upper discharge ranges. In an empirical study of flood hydrographs for six Australian river reaches, Wong and Laurenson (1983) showed that initially flood wave speed increased rapidly with discharge, then reduced markedly before returning to a much reduced speed as discharge continued to increase. The findings were in agreement with Price (1973) in that speed ~ discharge relationships could be expressed by two power law relationships with exponents between 0 and 1 that are joined by a relatively large transition curve. This transition commences at about half the bankfull discharge and extends beyond where the bankfull flow is exceeded.

However, in a study of velocity ~ discharge relationships, flood wave travel times and storage analyses on the Murrumbidgee River in Australia, Bates and Pilgrim (1982) questioned the ability of a power-law relationship to fully describe the catchment response over a wide range of discharge values and noted that significant variation in the exponent *m* in Eqn. 2.25 for changing flow. These findings were consistent with work by Laurenson (1962) who showed that the storage ~ discharge relationship from the Murrumbidgee River and from the Darling River, also in Australia, were not always consistent with Eqn. 2.25.

The characteristics of floodplain roughness play a major role in the manner and extent of flood wave attenuation in a natural channel. By analysing results from a 1-D (HEC-RAS) and 2-D (River2D) models of the River Parrett in Somerset, UK, Thomas and Nisbet (2007) predicted that the increased resistance associated with trees and woody debris on the floodplain for a 100-year flood reduced floodplain water velocity and increased water level and backwater effects. The effect of this was that the flood wave peak travel time increased by 110 minutes for the woodland roughened floodplain compared to a grassland equivalent and that flood storage increased by 56% in the same comparison. The height of the floodplain roughness with respect to floodplain depth is important in its ability to impact on the flood wave and considerable work has been done to better understand the hydraulic resistance for vegetation with different properties (e.g., Nepf, 1999; Kouwen and Fathi-Moghadam, 2000; Stephan and Gutknecht, 2002).

Ghavasieh *et al* (2006) used 1-D (Mage5 developed by French Research Institute, Cemagref) and 2-D (RUBAR20) hydraulic models to investigate the effects of discrete strips of roughened floodplain (extending from the main channel for the full floodplain width) on flood-wave propagation for a variety of channel configurations and flood hydrographs. In terms of relative attenuation and the delay in flood peak, Ghavasieh *et al* concluded that the effects on flood wave propagation are approximately proportional to the length of the roughened strips. Ghavasieh *et al* analysed results in terms of a relative indicator expressed as:

$$dVol_r(t)\% = \frac{Vol_w(t) - Vol(t)}{Vol_{tot}} \qquad \textbf{Eqn. 2.28}$$

where $dVol_r(t)\%$ is the percentage of extra water volume in the river reach resulting from the roughness strips on the floodplain, $Vol_w(t)$ and $Vol(t)$ are the volumes of water stored in the channel at time t with and without the floodplain roughness strips respectively and $Vol_{tot}$ is the total volume of the input hydrograph.

Results indicate that relative indicator values determined from Eqn. 2.28 remain almost constant with return period in the absence of any geometrical discontinuities in the floodplain for different flood levels. For a given hydrograph, the attenuation of the flood peak decreases rapidly as the downstream distance from the roughened zone increases. The peak delay values do not decrease with distance. Ghavasieh *et al* also note that while the 1-D model appears to overestimate the effects of the roughened strips, this approach is adequate for modelling symmetrical channel configurations.

Woltermade and Potter (1994) undertook watershed modelling of fluvial

geomorphological influences on flood peak attenuation using the MIKE 11 rainfall-runoff and hydrodynamic models calibrated for the Grant River watershed, Southwestern Wisconsin, US. The results indicated that floodplain attenuation effects were insignificant for small floods where floodplains were not substantially inundated and for large floods where many of the roughness elements were overtopped. However for moderate floods with recurrence intervals of between 5 and 50 years and with relatively high peak to volume ratios, attenuation effects can be significant and are influenced by channel-floodplain morphology, valley width, stream slope, and hydraulic resistance.

### 2.6.3 Influence of Floodplains on Flood Frequency

Previous studies have been undertaken that have investigated the effects of the physical processes of floodplain inundation on floodplain attenuation and the influence of this attenuation on flood frequency distributions. Furthermore, these processes that influence flood wave propagation in a river reach may change with rising depth and additional attenuation may also result from floodplain roughness and depressions in floodplain topography.

Haider (1992), using a non-linear Muskingum-Cunge flood routing model demonstrated that floodplain inundation can significantly alter the characteristics of flood waves and impact on the distribution of flood peaks. According to Wolff and Burges (1994), the degree to which the downstream flood frequency distribution is altered is influenced by physical and geometrical properties of the floodplain such as main channel and floodplain roughness, floodplain width, longitudinal slope, width/ depth ratio. However, Wolff and Burges, while concluding that there could be a change in the form of the distribution of flood peak flows as hydrographs move downstream were unable to generalise as to the form of this distribution.

Other studies have been more successful in detailing the shift in flood frequency distribution brought about by the attenuating effects of floodplains. Mason *et al* (1988) using a mathematical flood routing model systematically investigated the impact of floodplain storage on the shape of flood frequency curves for a range of different overbank geometries. By routing simulated flood hydrographs through idealised river reaches, Mason *et al* demonstrated that there is an increased tendency for the flood frequency curve to approach an EV3 distribution at sites downstream of floodplains as the volume of storage available on the floodplain increases. Similar shifts from EV2 distributions towards EV3 distributions were noted by Archer (1989) in an empirical study of sites separated by floodplains of the River Tees in Darlington, UK. Archer's study also supported the previously made assertion that the degree of flood attenuation is highly variable and is dependent on the floodplain geometry but by observing that the attenuation for a given peak inflow is greater for sharply peaked, low volume floods, concluded that the volume of the inflow is also significant.

The Mason *et al* (1988) study was based on a number of regular and uniform floodplain configurations. Natural floodplains on the other hand are irregular in shape and not directly relatable to the parameters of the idealised floodplains in these studies. Issues of this type had been previously identified by Lewin and Hughes (1980) where the effects of the significantly more complex spatial and temporal

variations of natural floodplain flows were identified. The complexity of floodplain flows in natural channels was included in a semi-empirical investigation into the influence of floodplain storage on flood flow in the River Severn (McCartney and Naden, 1995). The study investigated how the shape of the observed flood hydrograph is changed by the presence of floodplain storage and how this change influences the shape of the flood frequency curve. McCartney and Naden concluded that the transfer of flow from the main channel to the floodplain coincides with the presence of a discontinuity, referred to as a 'shoulder' on the rising limb of hydrograph. Furthermore, the availability of natural floodplain storage was shown to significantly reduce the magnitude of major floods which has a major impact on flood frequency.

# 3 Hydraulic Modelling of Rivers and Floodplains

## 3.1 Introduction

River Engineers are increasingly using computational fluid dynamics methods to improve understanding of the interactions between channel morphology, discharge, flow structure and sediment transport. If such models can provide an adequate representation of key processes, they have the potential to increase significantly our understanding of river channel dynamics.

Numerical models may increase the spatial density of information beyond what is possible through field measurement. Process investigation in the field is largely based upon point measurement of velocity or sediment transport processes. A large number of sample sites may be required to obtain sufficient representation of spatio-temporal process characteristics, and this takes time, over which the processes themselves may change.

Once confidence in model predictions has been established, the model may be used to simulate processes generated by different combinations of boundary conditions, and so address questions that have previously been restricted by the time and resources required for field or laboratory study (Lane *et al*, 1999).

## 3.2 One-Dimensional Models

The traditional one-dimensional approach to the analysis of floodplain hydraulics has been to subdivide the channel into a number of discrete sub-areas and then calculate the discharges in these sub-areas using flow resistance laws e.g. Manning's equation or the Darcy-Weisbach law. The individual discharges are then summed to give the total discharge in the whole channel.

Knight *et al* (1989) reported some difficulties when applying this approach to the River Severn, UK. Using measured friction slope and overbank velocity data, they calculated the conveyance in three sub-areas and their corresponding roughness values. The variation of Manning's *n* with depth for the whole channel was shown to decrease sharply just above bankfull level due to abrupt changes in the hydraulic radius. On the other hand, the sub-area values for the main channel had to be increased in order to obtain the correct sub-area conveyance capacity. The sub-area values for the floodplain had to be correspondingly reduced, to levels well below their

actual values (Knight and Shiono, 1996). This resulted in difficulties in obtaining the correct stage-discharge relationship for that particular site.

A second one-dimensional approach is based on the "coherence" concept developed by Ackers (1992, 1993). Where the differences in velocity and depth between the various sub-areas are large, then significant interaction between the sub-areas would be expected to occur. "Coherence" is defined as the ratio of the basic conveyance calculated by treating the channel as a single unit, with perimeter weighting of the friction factor, to that calculated by summing the basic conveyances of the separate zones. The closer to unity the coherence approaches, the more appropriate it is to treat the channel as a single unit, using the overall geometry. Where the coherence is much less than unity then discharge adjustment factors are required in order to correct the individual discharges in any sub-area (Knight and Shiono, 1996). The method is established as one of the one-dimensional (1-D) approaches, which gives best results for overbank flow (Karamisheva *et al*, 2006). Other one-dimensional approaches are based on quantifying the apparent shear stresses or forces on the sub-area division lines which are experimentally determined.

The literature comprises a wide range of applications of one-dimensional models to floodplains. Commonly used models include Mike 11 (Danish Hydraulic Institute), ISIS (Hydraulics Research Wallingford, UK) or HEC-RAS (US Army Corps of Engineers). Other models are individually developed based on the above discussed approaches.

Helmiö (2005) developed a one-dimensional unsteady flow model to predict average velocities, flow resistances, and the components of discharge in the main channel and the floodplains of a 28-km reach of the Rhine River. The one-dimensional unsteady flow model solved St. Venant equations using Nuding's method for computing flow resistance parameters for the main channel and the floodplains. Nuding's method is a calculation procedure for steady flow, in which, for a known water level, the friction factors and the components of discharge in the main channel and each floodplain are computed separately, based on e.g. the shape and vegetation of the channel. The boundary between the main channel and the floodplain or the vegetated zone is treated as an imaginary wall, for which a separate Darcy-Weisbach friction factor was estimated (Helmiö, 2005). The computed discharges and water levels for the studied reach of the River Rhine correlated well with the measured data. It was also found that a significant component of discharge was transported by the floodplains in some cross-sections during high flows.

Proust et al (2006) tested three one-dimensional models on a compound channel with abrupt floodplain contraction in order to determine whether one-dimensional (1D) models developed for straight and slightly converging channels, are valid for these geometries. The three models were compared to measurements from a physical model. Severe mass and momentum transfers from the floodplain towards the main channel were observed. The models used were: (i) the classical divided channel method (DCM) which is the reference case since it ignores both turbulent and mass transfers between subsections, (ii) exchange discharge method (EDM) developed by Bousmar and Zech (1999) which is based on a theoretical modelling of the interfacial momentum transfer and was tested for flows in slightly skewed compound channels and for a compound channel with narrowing floodplains, and (iii) the Debord formula

(Nicollet and Uan, 1979). This is an empirical method that was developed on the basis of large experimental data sets in a 60m long by 3m wide, straight compound-channel flume. Each 1D model incorporates a specific approach for the modelling of the momentum exchange at the interface boundary between the main channel and the floodplain. The increase of the lateral mass transfer generates moderate errors on the water level values but significant errors on the discharge distribution. Erroneous results arise because of incorrect estimations of both momentum exchange due to lateral mass transfers and boundary conditions which are imposed by the tested 1D models.

Karamisheva *et al* (2006) developed a number of algorithms based on one-dimensional stage-discharge models for compound channels. The Divided Resistance Approach used the Divided Channel Method (DCM) to predict flow depth corresponding to a given discharge for overbank flows in straight and meandering channels. The study also proposed a simple algorithm for stage–discharge prediction based on the lumped resistance approach. The developed algorithms were tested against experimental data of overbank flows with straight and meandering planforms from both the UK Flood Channel Facility and from a smaller scale compound channel in the University of Ulster. Despite incorporating grain resistance, the bed form resistance and the roughness characteristics of the floodplain, the divided resistance approach gave unsatisfactory prediction of the flow depth for compound channels with rough floodplains. The application of the lumped resistance approach to various flume and field data showed good agreement between the measured and predicted flow depths.

## 3.3 Two-Dimensional Models

A logical development of the one-dimensional approaches would be to divide the channel cross-section into not only many more sub-areas, but also to include in those sub-areas, the processes (e.g. lateral shear and secondary flows) that are not represented in simple bulk flow equations e.g. Darcy-Weisbach and Manning's equations. In two-dimensional models, depth-averaged parameters of velocity, lateral shear and secondary flows are used to represent the vertical distribution of these parameters at any one sub-area or element. Therefore, two-dimensional models provide a more accurate representation of the flow processes in compound channels.

A wide range of these models are used in floodplain applications: finite element models e.g. TELEMAC-2D and RMA-2 and finite difference software e.g. DIVAST and MIKE12.

The finite element model TELEMAC-2D has been applied in several studies to verify the flow patterns of a number of physical models of compound channels. The model has been used to simulate the flow patterns of the straight and meandering channel configurations of the physical models at the Flood Channel Facility, HR Wallingford, UK. Wilson *et al* (2002) investigated the effect of varying the turbulence model in TELEMAC-2D on the resulting stage-discharge relationships. The study showed that at higher water depths all turbulence models predict depth-averaged velocities for both channel configurations with greater accuracy than at lower water depths. Rameshwaran *et al* (2008) compared results derived from a physical model

representing the River Blackwater, UK, to a numerical simulation using TELEMAC-2D. The roughness height $k_s$ values were calibrated to achieve steady state flow as in the experiments. The simulated depth-averaged velocities were in good agreement with the physical model velocities and were much better than the bed shear stress prediction.

Bates *et al* (1996) studied the impact of varying the mesh resolution in TELEMAC-2D in two river channel/floodplain flow cases, namely the River Culm in Devon and River Stour in Dorset, both in the UK. The results showed that there may be an optimum resolution for particular application purposes beyond which little improvement in predictive ability is obtained for this class and scale of model application. Although the increase in spatial resolution appears to improve the quality of the results, an optimum resolution for a particular scale needs to be identified.

The current project has as its main objective the indexing of floodplain effects on a flood wave through simple empirical relationships. While the performance of multi-dimensional models in reproducing floodplain flow data, mainly from the UKFCF, has been undertaken, results from the dynamic modelling of flood waves is less common. However, Hervouet (2000) used TELEMAC-2D to study the propagation of the flood-wave down the Reyran River that resulted from the failure of the Malpasset dam in France in 1959. Topographic data was used to generate the mesh of 26000 elements and 13541 points with mesh size ranging from 5m to 300m. The model was calibrated by adjusting the channel bed friction and dispersion coefficients. By comparing the outputs of this model and a 1-D model to results obtained from a physical model, it was shown that the TELEMAC model had the capacity to simulate transit times of the flood wave reasonably accurately.

Simm *et al* (1997) applied the finite element model RMA2, to the floodplain of the lower reaches of the River Culm in southeast Devon, UK. Patterns of radiocaesium ($^{137}$Cs) accumulation by overbank accretion during flood water inundation were used to assess the potential of using such models for explaining sedimentation rates and patterns. A strong correlation was found between values of the $^{137}$Cs inventory and surface concentration and the predicted flood water patterns derived using the RMA-2 model.

## 3.4 Three-Dimensional Models

Recent research has witnessed a move away from two-dimensional to fully three-dimensional models. Lane *et al* (1995) showed that two-dimensional models were able to provide reasonable estimates of the depth-averaged velocity field. However, there remained considerable uncertainty over the extent to which the model was representing adequately the effects of three-dimensional processes upon the two-dimensional velocity field, and even then, whether or not a two-dimensional velocity field was sufficient for adequate process representation. It was argued that improved process representation was required through the use of three-dimensional models in combination with higher-quality datasets for assessment of model predictions (Lane *et al*, 1999).

Three-dimensional models provide a solution of the Reynolds-averaged Navier-Stokes set of equations but each model incorporates slightly different assumptions and formulations and offers different options for the numerical solution of the equations (Naden *et al*, 2006).

There are a number of three-dimensional computational fluid dynamics codes which are currently in use for river engineering purposes. Naden *et al*, (2006) carried out an inter-comparison of four of the available codes (PHOENICS, FLUENT, SSIIM, and TELEMAC-3D) using data of a two-stage meandering channel at the UK Flood Channel Facility. The application of each code was carried out independently and this led to a series of different valid models in terms of the mesh used and assumptions made. Standardised methods were used to compare each model with the available data. Results demonstrated that the models produce similar results overall, although there were some differences in the predicted flow field and greater differences in turbulent kinetic energy and bed shear stress.

Rameshwaran *et al* (2008) compared results derived from a physical model representing the River Blackwater, UK, to a numerical simulation using the finite volume model PHOENICS which solves the three-dimensional Reynolds-averaged continuity and Navier-Stokes equations for turbulent steady-state flow. The model was calibrated by varying the roughness height $k_s$ values until a match to the steady state flow as in the experiments was achieved. Results showed that the bed shear stress distributions were predicted reasonably well by the 3D model. The floodplain flow entering the main channel and the flow expelled from the main channel onto the floodplain were clearly observed in the cross-over region. The 3D model predicted these flow patterns very well.

Morvan *et al* (2002) used the three-dimensional code CFX (developed by the U.K. Atomic Energy Authority) to simulate experimental data from the physical model of a meandering channel at the UK Flood Channel Facility. The model solved the complete incompressible Reynolds-averaged Navier-Stokes equations using a finite volume approach on a non-staggered grid. Turbulent shearing was included by a linear $k$-$\varepsilon$ model. $k$-$\varepsilon$ turbulence models are based on the use of two parameters, namely the turbulent kinetic energy $k$ $(= 0.5\left(u'^2 + v'^2 + w'^2\right)$ where $u', v'$ and $w'$ are fluctuating components of velocity in the x, y and z directions respectively) and the rate of dissipation of $k$ due to viscous damping, which is denoted by $\varepsilon$. Sensitivity tests of mesh design, discretisation scheme, and roughness height were carried out together with the turbulence characteristics of the flow. The results of the sensitivity tests suggest that in meandering channels with overbank flow, a proper discretisation for the application is more important than the use of a complex turbulence model. It was suggested that turbulence transport was of little importance in determining the velocity field in such a configuration.

Corti and Pennati (2000) used TELEMAC-3D to simulate the hydrodynamics of a delta of the River Po, Italy. The delta is characterised by an intricate pattern with several branches in addition to strong variations in bottom topography and some sharp bends. In situations of low discharge the combined action of the river flow and of the tide can also give rise to changes of direction of the flow at some channel mouths. The hydrodynamic model was calibrated by varying the bottom friction and model results were compared to water level variations, discharge and salinity intrusion

measurements at gauged locations. The model showed a good general agreement with the measurements and reproduced the dynamics of the delta, including the salt-wedge intrusion.

Wilson *et al* (2006) used the three-dimensional finite-volume code SSIIM (developed by Olsen of the Norwegian University of Science and Technology (Olsen, 2007)) to model a willow vegetated river/floodplain system. SSIIM solves the Reynold's averaged Navier–Stokes equations for each cell, and uses the standard $k$-$\varepsilon$ model for turbulence closure. The additional hydraulic resistance of the willow stands was modelled separately to the bed resistance using a drag force term that was introduced into the Navier–Stokes equations. Flood events of varying magnitude and stages of plant development were simulated. The willow stands were modelled in bending as well as in their undisturbed vertical state. Modelling the willow stands as vertical or in bending was found to have a major impact on the computed velocity profiles.

# 4 Assessment of Hydraulic Models for Simulation of River Channels with Floodplains

## 4.1 Introduction

The use of hydraulic modelling codes in developing solutions to engineering problems is commonplace. In particular and of direct interest to this study, is the growing desire to combine flood estimation methods with river models in a way that reflects the structure of the catchments to provide a detailed and spatially coherent representation of flood risk. As reported in Chapter 3, many models exist for such applications and research has been undertaken to assess the performance for different 1D, 2D and 3D river modelling codes (e.g. Naden *et al*, 2006). In many cases, these assessments are based on the ability of these models to reproduce hydraulic parameters of the fixed boundary channels that were investigated as part of the UK Flood Channel Facility (FCF) experimental programme into compound channel flows.

The existing body of work in the assessment of river modelling codes was further supported by a component of the current study that involved an assessment of the 1D HEC-RAS, the 2D TELEMAC and the 3D TELEMAC models to reproduce the bulk hydraulic parameters and detailed flow fields of the Phase C, FCF mobile bed test series for compound channels with straight and meandering planforms. While considerable work was undertaken in simulating a range of flows in the Phase C series, consistency in the trends of the outputs for the full range of discharges in the series was observed. Consequently, the presentation in this chapter is limited to tests undertaken with flows of $0.6m^3/s$ in channels with both smooth and roughened floodplains. The assessment of the modelling approaches is based on an optimised calibration of simulated data to observed data and investigating the validity of calibration parameters to those calculated from measurement. The Manning's resistance coefficient is important in this regard.

This chapter of the report includes details of the FCF and of the modelling codes used in the assessment. Results of the assessment are then presented.

## 4.2 UK Flood Channel Facility

The Flood Channel Facility (FCF), as it later became known, was constructed in 1985-86 through funding from the Engineering and Physical Science Research Council (EPSRC) with the overall purpose of developing design methodologies for compound channels and rivers for use by statutory agencies and others responsible for flood protection and alleviation. The facility consisted of a large shallow tank, *56m* in

length by *10m* in width, within which compound channels of fixed slope were built (Figure 4-1).

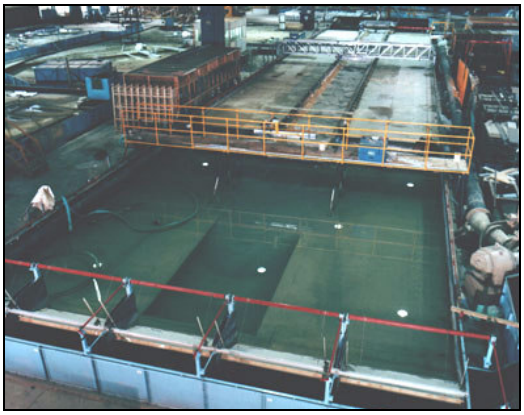

**Figure 4-1 Aerial view of FCF (Phase C straight compound channel test in progress)**

The *10m* flume width allowed a variety of channels of different planform geometry, cross-sectional shape and boundary type to be constructed. The large-scale nature of the facility assisted in overcoming discrepancies that would typically arise when modelling open channel flows in laboratory flumes that are typically *10-15m* long and generally not more than *2m* wide. The FCF facilitated the modelling of prototype rivers by making it possible to reproduce three-dimensional flows with significant momentum transfer between the main channel and floodplain flows and thus, allowed a more complete investigation of the complex interaction between these zones to be undertaken. In addition, its scale, coupled with its maximum discharge capacity of $1.08m^3/s$, facilitated the modelling of flows with complete floodplain width and sufficient floodplain depth to allow fully developed turbulent flow to be reached (Knight and Sellin, 1987).

Since its inception, the research programme of the FCF was planned to increase progressively the complexity of the configurations of compound channel geometries studied. Phases A and B were concerned with fixed bed studies of straight and meandering geometries respectively. Mobile boundaries were introduced to the experimental program in Phase C tests. Details of test series completed with the geometrical properties investigated are summarised in Figure 4-2 and Table 4-1.

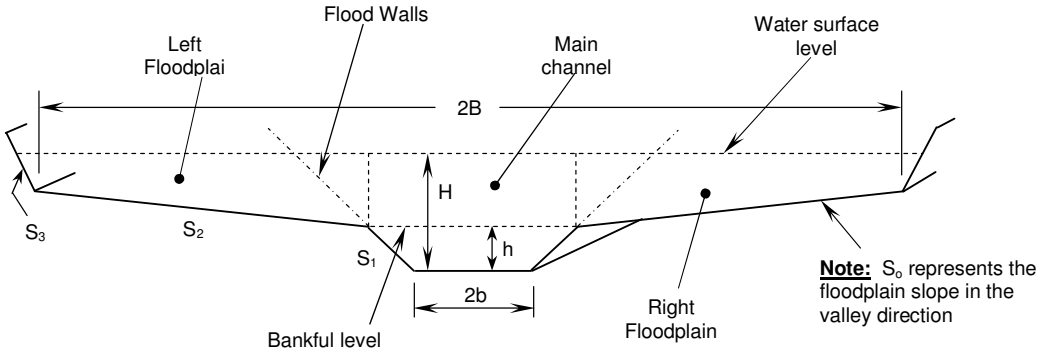


**Figure 4-2 Compound channel test series and geometrical properties tested in the FCF Programme**

**Table 4-1 Geometrical and roughness parameters of Phase A, B and C FCF channels**

| Experiments | Phase A | | | Phase B | Phase C | | | |
|---|---|---|---|---|---|---|---|---|
| | | | | | Straight | | Meandering | |
| Notation | Series 1 | Series 2 | Series 7 | | O/B smooth | O/B rough | O/B smooth | O/B rough |
| 2b | 1.5m | 1.5m | 1.5m | 0.9m | 1.6m | 1.6m | 1.2m | 1.2m |
| 2B | 10m | 6.3m | 6.3m | 10m | 8m | 8m | 8m | 8m |
| B/b | 6.67 | 4.2 | 4.2 | 11.1 | 5 | 5 | 6.67 | 6.67 |
| h | 0.15m | 0.15m | 0.15m | 0.15m | 0.2m | 0.2m | 0.2m | 0.2m |
| $S_1$ | 1:1 | 1:1 | 1:1 | 1:1 | 1:1 | 1:1 | 1:1 | 1:1 |
| $S_2$ | 0 | 0 | 0 | 0 | 0 | 0 | 0 | 0 |
| $S_3$ | Vertical | 1:1 | 1:1 | Vertical | 1:1 | 1:1 | 1:1 | 1:1 |
| $S_o$ | $1.027\times10^{-3}$ | $1.027\times10^{-3}$ | $1.027\times10^{-3}$ | $0.996\times10^{-3}$ | $1.834\times10^{-3}$ | $1.834\times10^{-3}$ | $1.8593\times10^{-3}$ | $1.8593\times10^{-3}$ |
| Sinuosity | 1 | 1 | 1 | 1.374 | 1 | 1 | 1.34 | 1.34 |
| Main Channel boundary | Smooth concrete | Smooth concrete | Smooth concrete | Smooth concrete | Sand | Sand | Sand | Sand |
| Floodplain boundary | Smooth concrete | Smooth concrete | Rod roughness | Smooth concrete | Smooth concrete | Rod roughness | Smooth concrete | Rod roughness |

The water circuit of the flume was a closed loop in which clear water was re-circulated. The flow entered the upstream channel end after passing over a knife-edged weir and through a stilling tank, and exited at the other end over a line of five parallel, variable overshot weir plates, or tailgates, used to control flume conditions. The use of flume tailgates for flow-modelling purposes are also used to simulate channels of infinite length. The knife edged weir at the upstream flume end ensured that an even supply of water entered the stilling pool. Water was supplied by one, or a combination of six varying capacity pumps, which drew water from a common sump at the downstream end of the facility. A valve on each pump controlled actual capacity. The discharge from each pump was determined by an orifice plate meter fitted in the pump delivery line.

For mobile bed experiments of the type analysed in this study, transported bed-load was collected at the downstream lip of the main channel in a sediment catcher, from where a slurry pump returned the water sand mixture to the upstream end of the main channel. Prior to joining the flow, the mixture travelled down an oscillating arm onto a wire mesh

screen that separated the sand and water. The sand was subsequently returned to the main flow and the water diverted to the sump. This separation process is shown in Figure 4-3.

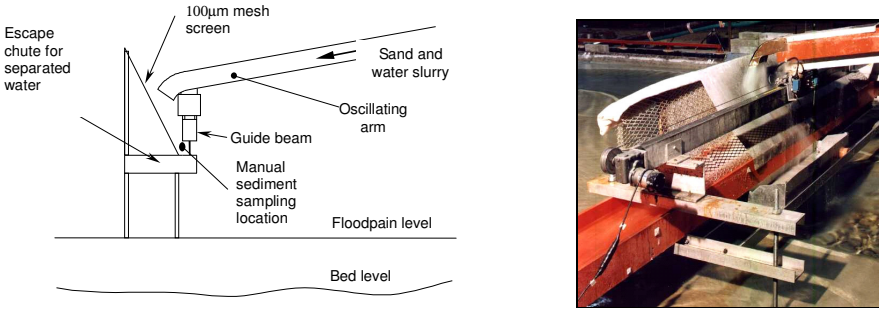


**Figure 4-3 Schematic of sediment and water separation**

For roughened floodplain tests, a single configuration of vertical rods, *25mm* in diameter, arranged in a regular rhomboidal pattern were held in place by frames that remained above the water level for all flow depths. This resulted in a roughness density of *12 rods/m*$^2$ that were surface penetrating for all flow depths as shown in Figure 4-4.

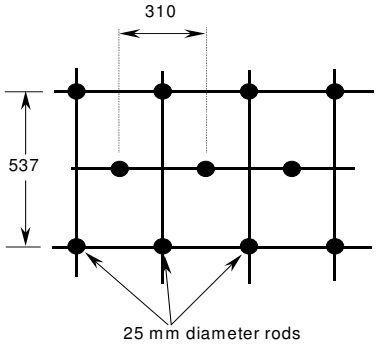


**Figure 4-4 Arrangement of roughness elements at the FCF (dimensions in *mm*)**

Water surface elevations were measured by digital pointer gauges mounted above stilling wells for the case of straight channels and mounted on an instrument carriage in the case of the meandering channel. Point velocity values in the main channel and floodplain were measured using either a miniature propeller meter or a Nortek ultrasonic velocimeter also mounted on the instrument carriage that facilitated measurement at all locations within the channel.

Data from the straight and meandering channels tested in Phase C of the FCF Programme were analysed in this study. The slot geometry of the straight channel incorporated a trapezoidal cross-section with 45$^o$ sloping sidewalls and a top width of *2m*. This differed from the *1.6m* top width of the meandering channel. The geometrical properties of the straight and meandering channels are shown in Figure 4-5.

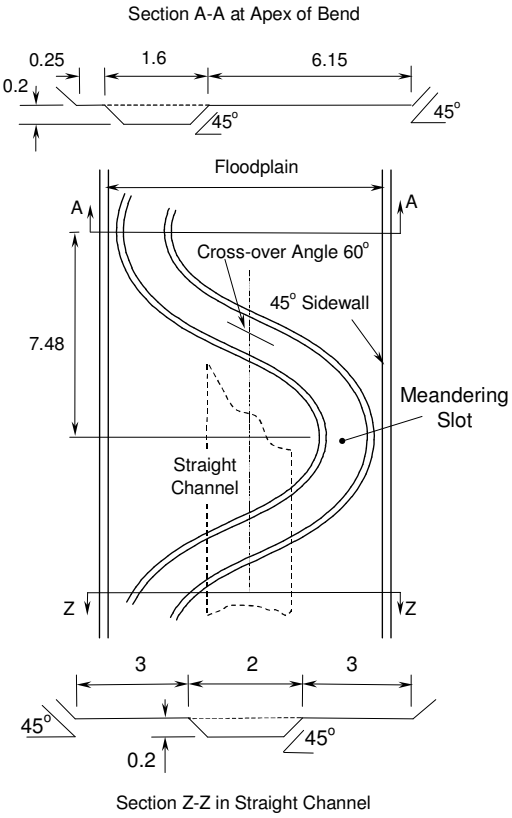


**Figure 4-5 Phase C, straight and meandering channel geometries**

The planform of the FCF meandering channel consisted of two sine-generated curves defined by the expression:

$$\theta = \theta_0 \cos\left(2\pi \frac{\ell}{L_m}\right) \qquad \textbf{Eqn. 4.1}$$

Where $\theta_0$ is the cross-over angle (angle between the main channel centre-line and the longitudinal centre-lines of the respective channels at their points of intersection), $\theta$ is the angle to the main axis at any point on the sine-wave, $L_m$ is the path length of a full meander and $\ell$ is the path length to any point on the meander. This consecutive series of uniform meanders, although different from conditions found in nature improved the reliability of results.

This expression is generally accepted to represent the planform of a regular ideal river and closely approximates the shape of real river meanders (Yalin, 1992). Transition entry and exit sections of a random curvature were required on all the constructed channels for the main channel flow to enter and exit along the flume centre-line.

An additional relationship formulated by Hey (1976) and based on the geometry of a number of natural rivers further defined the channel. This expression relates the path length of a full meander, $L_m$, to the top-width of the channel, $B$, as follows:

$$L_m = 4\pi B \qquad \textbf{Eqn. 4.2}$$

The main channel of the FCF was designed to have a $60^o$ degree cross-over angle. This resulted in a channel sinuosity of *1.34*. Sinuosity is defined as the ratio of the curved meander channel length to the straight floodplain or valley length. A sinuosity of *1.34* correlates closely with both the sinuosity range of *1.3* to *1.5* found in natural river channels formed in non-cohesive sands and gravels. Natural channels formed in cohesive sediments tend normally towards a sinuosity in the range *1.80-2.40* (Sellin, Ervine and Willetts, 1993).

A flat sand bed, *0.2m* below the bankfull level was in place along the entire length of the straight and meandering channels prior to the commencement of each experiment. The bed material in all straight and meandering channels investigated in the course of this research was closely graded, uniform sand with a $d_{50}$ value of *0.835mm*. As for the meandering channel, tests for the straight channel were carried out with a floodplain width of *8m* by installing temporary longitudinal walls on the floodplain. These walls had a vertical slope of $45^o$ giving the upper channel a trapezoidal cross-section. The floodplain of the channels had no cross-fall normal to the axis of the flume and post construction surveys showed the valley slope of straight and meandering channels to be $1.834x10^{-3}$ and $1.8593x10^{-3}$ respectively.

The measuring reach of the FCF meandering channel comprised 1 ¼ wavelengths and extended from cross-over section G to apex section Q as shown in Figure 4-6. The positive *x* and *y*-directions are also indicated in Figure 4-6. The measuring reach of the FCF straight channel extended from *24m* to *40m* measured from the upstream extent of the channel.

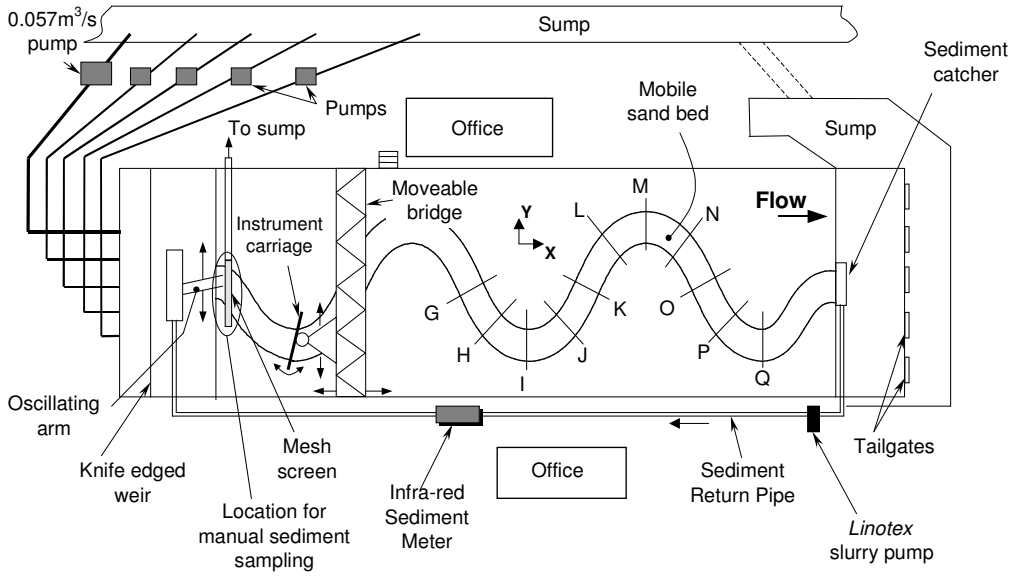


**Figure 4-6 Layout of FCF meandering channel**

All experiments were conducted under uniform flow conditions where the slope of the water surface was established to be equal to that of the longitudinal floodplain slope.

## 4.3 Hydraulic Models

Differences exist in the manner in which the hydraulic models that were used in this study execute simulations. The performance of the models investigated in this study was assessed by their ability to reproduce observed data from various tests undertaken at the FCF. This data was measured in straight and meandering planform tests with smooth and roughened floodplains. A range of discharges resulting in different overbank flow depths were included in the test matrix. These are summarised in Table 4-2 for the straight channel tests and Table 4-3 for the meandering channel tests. Tests are denoted by both alphabetical and numerical identifiers. The first letter in each test identifier, either S or M defines either a straight or meandering planform. The second letter, either S or R denotes either smooth or roughened floodplains. Each number (for e.g. *600*) represents the flow magnitude in litres/ sec. The term $S_w$ in Tables Table 4-2 and Table 4-3 is the observed average water surface slope in the floodplain.

**Table 4-2 Details of FCF Phase C straight channel tests**

| Test | Main Channel (mc) boundary | Floodplain (fp) boundary | Observed Flow ($m^3/s$) | | Observed $S_w$ (×1000) | Depth H (m) | Manning's n | |
|---|---|---|---|---|---|---|---|---|
| | | | Total Flow ($Q_{Tot.}$) | Main channel ($Q_{mc}$) | | | mc | fp |
| SS250 | Sand | Smooth concrete | 0.2476 | 0.1968 | 1.48742 | 0.2249 | 0.030 | 0.010 |
| SS350 | Sand | Smooth concrete | 0.3498 | 0.2145 | 1.88995 | 0.239 | 0.032 | 0.011 |
| SS450 | Sand | Smooth concrete | 0.4495 | 0.2303 | 1.77866 | 0.2569 | 0.031 | 0.012 |
| SS700 | Sand | Smooth concrete | 0.6970 | 0.2594 | 1.84946 | 0.2784 | 0.028 | 0.013 |
| SR250 | Sand | Rod roughness | 0.2500 | 0.2016 | 1.76931 | 0.2581 | 0.029 | 0.013 |
| SR350 | Sand | Rod roughness | 0.3475 | 0.2367 | 1.84666 | 0.2814 | 0.030 | 0.023 |
| SR450 | Sand | Rod roughness | 0.4483 | 0.2932 | 1.84332 | 0.3202 | 0.028 | 0.029 |
| SR600 | Sand | Rod roughness | 0.5984 | 0.3514 | ---- | | 0.029 | 0.034 |

**Table 4-3 Details of FCF Phase C meandering channel tests**

| Test | Slot boundary | Floodplain (fp) boundary | Observed Flow ($m^3/s$) | | Observed $S_w$ (×1000) | Depth H (m) | Manning's n | |
|---|---|---|---|---|---|---|---|---|
| | | | Total Flow ($Q_{Tot.}$) | Slot ($Q_{slot}$) | | | Slot | fp |
| MS250 | Sand | Smooth concrete | 0.2390 | 0.1118 | 0.00186 | 0.243 | 0.0230 | 0.0134 |
| MS350 | Sand | Smooth concrete | 0.3420 | 0.1389 | 0.00186 | 0.259 | 0.0196 | 0.0144 |
| MS600 | Sand | Smooth concrete | 0.5890 | 0.2010 | 0.00186 | 0.292 | 0.0165 | 0.0154 |
| MR250 | Sand | Rod roughness | 0.2440 | 0.1281 | 0.00186 | 0.265 | 0.0283 | 0.0272 |
| MR350 | Sand | Rod roughness | 0.3390 | 0.1461 | 0.00186 | 0.3 | 0.0278 | 0.0334 |
| MR600 | Sand | Rod roughness | 0.5790 | 0.2228 | 0.00186 | 0.378 | 0.0221 | 0.0459 |

While extensive work was undertaken in modelling significant components of the Phase C FCF data sets, the presentation in this chapter is limited to tests undertaken with target flows of $0.7m^3/s$ in the straight, smooth floodplain channel and $0.6m^3/s$ in

the straight, roughened floodplain channel and in the smooth and roughened floodplain meandering channel tests.

### 4.3.1 HEC-RAS

The 1-D river modelling software that was used in this study was HEC-RAS, (Hydraulic Engineering Center River Analysis System), a 1-dimensional link and node river model that computes the steady flow profiles for specified upstream flow rates and downstream water levels. The model was, and continues to be, developed by the US Army Corps of Engineers and is widely accepted by hydraulic modellers and civil engineers throughout the world. In 1995 the US Department of Defence gave permission for the HEC-RAS model to be made available without cost to the wider scientific community. The model can be executed in both steady state and dynamic mode and has found favour for a range of applications that include floodway encroachment and management, bridge and culvert analysis and levee and channel modification studies. As reported by Tate *et al* (2002), the more recent releases of HEC-RAS include large amounts of US geographical data and are used in conjunction with Geographical Information Systems (GIS).

The full theoretical basis of the model is provided in literature that accompanies the software (e.g. USACE, 2008) and only a very brief outline will be provided here.

The model essentially consists of three 1D components that facilitate:

1. Steady flow water surface profile computations;
2. Unsteady flow simulations;
3. Moveable boundary sediment transport computations.

The model assesses flow in one direction only but it accounts for 2-D parameters in the form of river channel width, depth, floodplain width, depth and length.

#### *4.3.1.1 Model Assumptions*

The HEC-RAS sub-routines that are used in the modelling computations were developed based on the following assumptions:

- Constant velocity and horizontal water surface across a channel section;
- All flows are gradually varied with hydrostatic pressure prevailing;
- Channel boundaries are fixed;
- Water is of uniform density;
- Resistance to flow can be described by empirical formulas such as Chezy or Manning's equations.

#### *4.3.1.2 Numerical Scheme*

For steady flow analysis in HEC-RAS, the one dimensional energy equation and the continuity equation are used to compute water surface profiles. The continuity

equation is:

$$Q = VA \qquad \textbf{Eqn. 4.3}$$

where Q is the discharge in the reach, V is the average velocity and A is the cross-sectional flow area. Energy losses are primarily attributed to friction and contractions and expansions of the flow in the reach under investigation. The energy equation in its general form can be expressed as:

$$y_1 + \frac{\alpha_1 V_1^2}{2g} + z_1 = y_2 + \frac{\alpha_2 V_2^2}{2g} + z_2 + h_e \qquad \textbf{Eqn. 4.4}$$

where $y$ is the flow depth, $V$ is the velocity, $z$ is the elevation of the main channel invert, $\alpha$ is the energy coefficient, $h_e$ is the energy head loss and subscripts *1* and *2* represent consecutive cross-sections *1* and *2* respectively.

For rapidly varied flow situations such as hydraulic jumps and flows over weirs and through bridges and sluice gates, in addition to cases where river confluences are being analysed, computed water surface profiles are obtained from the momentum equation based on external parameters of the flow. For steady flow, the momentum equation can be expressed as:

$$\frac{\partial(\alpha Q^2)}{\partial A} + gA\left(\frac{\partial y}{\partial x} - S_0 + S_f\right) = 0 \qquad \textbf{Eqn. 4.5}$$

where $x$ is the distance along the channel, $S_o$ is the channel bed slope and $S_f$ is the friction slope.

When using HEC-RAS in unsteady or dynamic mode, computations are based on the solution of the full 1D St. Venant Equations using an implicit, finite difference method. The St. Venant Equation of continuity is:

$$\frac{\partial Q}{\partial x} + \frac{\partial A}{\partial t} = 0 \qquad \textbf{Eqn. 4.6}$$

and the St. Venant Equation of motion can be expressed as:

$$\frac{\partial Q}{\partial t} + \frac{\partial(\alpha Q^2/A)}{\partial x} + gA\left(\frac{\partial h}{\partial x} - S_0 + S_f\right) = 0 \qquad \textbf{Eqn. 4.7}$$

where parameters are as described above.

#### *4.3.1.3 Model Inputs*

The HEC-RAS model for steady state simulations requires a peak flow and for unsteady applications requires either a flow or a stage hydrograph. In addition, the following inputs are required:

- River cross sections;
- Longitudinal distances between cross sections;
- Energy loss coefficients for both friction and the contraction and expansion of the flow.

#### *4.3.1.4 Boundary Conditions*

Boundary conditions in the HEC-RAS modelling process are necessary to establish the starting water surface at the upstream and downstream ends of the river system. For super-critical sub-critical flows, boundary conditions are necessary only at the upstream and downstream ends of the system respectively and for mixed flow regimes, boundary conditions would be required at all ends of the system. Furthermore, different boundary conditions are required for executing the flow in either steady or unsteady modes.

A number of steady flow boundary conditions are used in the HEC-RAS modelling process. These include options to execute the model using known water surface elevations, critical flow depths, normal depths represented by friction slopes or rating relationships.

For unsteady or dynamic flow simulations, boundary conditions are established at open ends of the river system. Upstream boundary conditions include any or a combination of flow hydrographs and stage hydrographs and at the downstream end of the system, similar boundary conditions can be used. Alternatively HEC-RAS can be executed using rating relationships or normal depth values at the downstream system end.

The HEC-RAS modelling of the FCF channel that was undertaken in this part of the study was executed in steady state mode with model inputs that included known discharge values. Known downstream water levels comprised the model boundary conditions. The model was calibrated by adjusting main channel and floodplain roughness values such that the correlation of the simulated water surface with the observed profile was optimised.

### 4.3.2 TELEMAC-2D

The TELEMAC project was launched in 1987 with the objective of constructing a complete system of hydro-simulation and data processing for open channel flow. The project included a number of European hydraulics research groups worked closely together in the development of the TELEMAC simulation programs. The main groups were: Électricité de France (EDF), France; Hannover University, Germany; Delft Hydraulics, Netherlands; and Ente Nazionale per l'Energia Electtrica, Italy. The responsibility of improving and maintaining the programme lies with EDF.

The TELEMAC modelling system comprises a number of simulation programmes (TELEMAC-2D and TELEMAC-3D (hydrodynamics); ESTEL-2D and ESTEL-3D (groundwater); ARTEMIS, TOMAWAC and COWADIS (wave simulation), etc.)

It calculates water depth and depth-averaged velocity component values at each node of an unstructured mesh. TELEMAC-2D has the capacity to account for the following phenomena (EDF, 2002):

- Propagation of long waves, including non-linear effects;
- Friction of the bed;
- The effects of the Coriolis force;
- The effects of meteorological phenomena such as atmospheric pressure and wind;
- Turbulence;
- Supercritical and subcritical flows; and
- Particle tracking and computation of Lagrangian drifts.

#### *4.3.2.1 Model Assumptions*

The shallow water equations are obtained from the basic equations of Navier-Stokes by making the following assumptions (EDF, 2000):

- The fluid is Newtonian, i.e. the relationship between the stress and the rate of strain is linear.
- The fluid is incompressible and homogeneous in the vertical direction. Horizontal density variations are considered through the hypothesis of Boussinesq, in which the fluid density $\rho(x, y)$ is approximated by a gradient term. Under this assumption:

  $\rho - \rho_o / \rho_o << 1.0$ , $\rho_o$ being the reference density.

- The long wave approximation assumes the pressure distribution is hydrostatic. This implies that the gauge pressure $p(x, y, z)$ at any point is caused only by the water column above that point and;

  $\frac{1}{\rho}\frac{dp}{dz} - g = 0$ where $p(x, y, z) = -\rho g z + constant$.

  Atmospheric pressure at the free surface $Z$ implies that the gauge pressure is zero and therefore $p(x, y, z) = -\rho g(Z - z)$.

- The three-dimensional set of equations is depth-averaged, resulting in two dimensional horizontal flow equations. Channel bed roughness is included as a boundary condition at the bed of the channel and surface shear stress under wind effect is accounted for in the free-surface boundary condition.

- A Reynolds decomposition and stochastic averaging (equivalent to time averaging over a short time step under the principle of ergodicity) is applied in order to model turbulence. Reynolds shear stresses resulting from this process are modelled as proposed by Boussinesq using a turbulent viscosity.

#### *4.3.2.2 Numerical Scheme*

The TELEMAC-2D code solves the depth-averaged free-surface flow described by the St. Venant equations (Barré de Saint-Venant, 1871). These are outlined in the model literature (EDF, 2001) and will only be presented in brief in this report.

The continuity equation on which the model is based is:

$$\frac{\partial h}{\partial t} + \overrightarrow{V_x}.\overrightarrow{\text{grad}}(h) + h.\text{div}(\overrightarrow{V_x}) = q \qquad \textbf{Eqn. 4.8}$$

and the momentum equations in the *x* and *y* directions can be expressed as:

$$\frac{\partial V_x}{\partial t} + \overrightarrow{V_x}.\overrightarrow{\text{grad}}(V_x) + g\frac{\partial h}{\partial x} - \text{div}(\upsilon.\overrightarrow{\text{grad}}(V_x)) = S_x - g\frac{\partial Z}{\partial x} \qquad \textbf{Eqn. 4.9}$$

$$\frac{\partial V_y}{\partial t} + \overrightarrow{V_x}.\overrightarrow{\text{grad}}(V_y) + g\frac{\partial h}{\partial y} - \text{div}(\upsilon.\overrightarrow{\text{grad}}(V_y)) = S_y - g\frac{\partial Z}{\partial y} \qquad \textbf{Eqn. 4.10}$$

where $h$ is the flow depth, $V$ is the velocity, $q$ represents the flow source or sink terms, $g$ is the gravitational acceleration, $\upsilon$ is the momentum viscosity, $S$ is the source or sink terms in the momentum equation, $Z$ is the free surface elevation, $t$ is the time and $x$ and $y$ represent the horizontal space coordinates.

Friction Representation

TELEMAC-2D offers five options for the inclusion of bottom friction. These are: Haaland's formula, Chezy's formula, Strickler's formula, Manning's formula and Nikuradse's formula. It also offers the possibility of applying a uniform bottom friction or a variable friction coefficient. When variable friction is applied, the function governing the variable friction coefficient must be programmed in a special subroutine named STRCHE.

In TELEMAC-2D, friction of the bottom is incorporated in the Momentum equations via the source terms $S_x$ and $S_y$ and it is expressed in terms of the reciprocal of the steepest slope at a point cos(α) and the elevation of the bottom, $z_f$:

$$S_x = -\frac{1}{\cos(\alpha)}.\frac{g}{h}.\text{coeff}.V_x\sqrt{V_x^{\,2} + V_y^{\,2}} \qquad \textbf{Eqn. 4.11}$$

$$S_y = -\frac{1}{\cos(\alpha)}.\frac{g}{h}.\text{coeff}.V_y\sqrt{V_x^{\,2} + V_y^{\,2}} \qquad \textbf{Eqn. 4.12}$$

where

$$\frac{1}{\cos(\alpha)} = \sqrt{1 + \left(\frac{\partial z_f}{\partial x}\right)^2 + \left(\frac{\partial z_f}{\partial y}\right)^2} \qquad \textbf{Eqn. 4.13}$$

The value of *coeff* in Eqn. 4.11 and Eqn 4.12 depends on the friction law chosen and these are shown in Table 4-4.

**Table 4-4 Value of *coeff* depending on friction laws**

| Friction Law | The value of coeff |
|---|---|
| Chezy | $\frac{1}{C^2}$, where *C* is Chezy coefficient |
| Manning | $\frac{n^2}{h^{1/3}}$, where *n* is Manning's coefficient |
| Strickler | $\frac{1}{h^{1/3}K^2}$, where *K* is Strickler coefficient |
| Nikuradse | $\frac{1}{C^2}$, where *C* is the Chezy coefficient obtained from $C = 7.83\log\left(\frac{12h}{k_s}\right)$ where $k_s$ is the grain size at the bottom |

Turbulence Modelling

Four options of turbulence modelling are presented in TELEMAC-2D (Version 5.5). These are: constant viscosity, Elder model (Hervouet, 2007), the *k-ε* model, and the Smagorinski model.

In the case of a constant viscosity, the coefficient used represents the molecular viscosity, turbulent viscosity and dispersion (EDF, 2001).

The Elder model for the Saint-Venant equations takes into account the role of dispersion and recommends two different coefficients, one, $K_l$ , along the flow (longitudinal diffusion) and the other, $K_t$, transverse to the flow (transversal diffusion) (Hervouet, 2007).

The *k-ε* model is based on the calculation of the physical quantities representing turbulence in the flow. *k* and *ε* represent turbulent kinetic energy and its dissipation respectively. In terms of velocity fluctuations these are:

$$k = \frac{1}{2}\overline{V_x' V_y'} \qquad \textbf{Eqn. 4.14}$$

$$\varepsilon = \upsilon\overline{\frac{\partial V_x'}{\partial y}\frac{\partial V_x'}{\partial y}} \qquad \textbf{Eqn. 4.15}$$

where $V_x'$ and $V_y'$ are the fluctuations about the mean of the horizontal velocities and $\upsilon$ is the fluid kinematic viscosity in $m^2/s$.

The Smagorinski model is based on the mixing length model and has a meaning only in numerical modelling. It is generally used for maritime domains with large-scale eddy phenomena. The model belongs to the category of sub-grid turbulence models. The principle is that turbulence is the solution of the Navier-Stokes equations. It would naturally appear in the numerical solutions if the size of the finite elements

allowed the reproduction of all mechanisms including the viscous dissipation of very small vortices. Only in the formulation of smaller vortices, where turbulence is inhibited by the mesh, does modelling take place in a numerical simulation. Smagorinski's idea is to add to the molecular viscosity a turbulent viscosity deduced from a mixing length model. This mixing length corresponds to the size of the vortices smaller than that of the mesh size (Hervouet, 2007).

Space Discretisation (Mesh)

The finite element method divides the problem domain into a finite number of elements (small domains) connected at nodes at which the solution is sought. The finite element mesh generation is carried out using a pre-processor software MATISSE which belongs to the TELEMAC suite of programmes. MATISSE uses as an input bathymetric data of the domain to create flexible unstructured triangular meshes that can be adjusted (refined or coarsened) locally where necessary, making the program computationally cost-effective. MATISSE is also capable of performing the interpolation of bathymetry over the computational domain and offers several options in order to improve the mesh, such as the elimination of backward dependencies, the elimination of nodes closer than a given distance to others, the cutting of over-stressed triangles, and a facility for splitting some or all the elements (Abott, 1997).

Time Discretisation

The TELEMAC model applies a finite element discretisation in order to solve the shallow water equations for the main flow variables: water depth ($y$), and the horizontal velocities ($V_x$ and $V_y$) in the $x$- and $y$- directions respectively. TELEMAC-2D offers a variety of advection schemes for the continuity and momentum equations e.g. the Method of Characteristics, the Streamline Upwind Petrov-Galerkin (SUPG) scheme and the Conservative Scheme (Hervouet, 2007). All TELEMAC-2D schemes except the method of characteristics perform the advection stage in one step (EDF, 2001). The method of characteristics employs a fractional step method. At the first fractional step, only the advection terms corresponding to transport of the hydrodynamic variables are solved. At the second stage, the propagation, diffusion, and source terms are solved (Rameshwaran and Shiono, 2003; EDF, 2001).

In the TELEMAC-2D modelling of the FCF data undertaken in this study, the Method of Characteristics which is unconditionally stable was used for the advection of velocities ($V_x$ and $V_y$), while the Conservative Scheme was used for the advection of water depth ($h$). The "Conservative Scheme" was selected for the computation of water depths because it ensures that water depths are reasonably propagated. The scheme is conservative without sub-iterations at the cost of stability. An SUPG option (EDF, 2001) was applied to the advection schemes in which the approximating functions are modified in the direction of the streamline for the discretisation of transport terms. The SUPG option ensures a better approximation and better numerical stability in the solution scheme. Thus the SUPG option was applied to both advection of velocities and water depth in the current study.

The final set of discretised equations was first preconditioned using the diagonal preconditioning option. TELEMAC-2D solved the system of equations at each time step using the Conjugate Gradient Method along with an Element by Element (EBE) matrix storage (Hervouet, 2003; 2004).

Initial Conditions

Initial conditions describe the state of the model at the start of the simulation. These can be flows or water elevations. The initial conditions may be of a fixed value (zero elevation, constant elevation, zero water depth, or constant water depth). If an initial condition does not correspond to any of the fixed value cases, it must be programmed in an ad hoc user-subroutine.

In the current study, the computation commences from quiescent initial conditions. The initial water elevation in the model domain is that of the downstream outlet. The accuracy (tolerance) between two timesteps was set to 0.0001 at all nodes for all variables ($V_x$, $V_y$, and $h$). The computation continued until a steady state was reached throughout the model domain.

Boundary Conditions

After the finite element mesh is formed by MATISSE, a boundary conditions file is formed. This is a text file in which each line is devoted to a point/node along the model boundary. Each node is assigned a string of integers representing the type of boundary conditions to be imposed. There are two types of boundaries in the computational domain, namely walls (solid boundaries) and open (liquid) boundaries.

The types of boundary conditions used in the current modelling study were:

(i) *Imposed flowrate at the upstream boundary*: At the inlet of the channel, a flow value is prescribed. To accelerate the achievement of quasi-steady state conditions, a gradual (stepwise) increment of discharge ($Q$) with time was introduced according to the following relation:

$$Q = \frac{t}{3600} Q_{ref} \quad \text{for } 0 < t \leq 3600 \qquad \textbf{Eqn. 4.16}$$

$$Q = Q_{ref} \qquad \text{for } t > 3600 \qquad \textbf{Eqn. 4.17}$$

where $t$ is the time in seconds and $Q_{ref}$ is the desired flow value at the upstream boundary.

(ii) *Water elevation at the downstream boundary*: In order to achieve and maintain the steady state condition in the channel, the water elevation at the downstream end (outlet) of the channel was fixed throughout the model computation.

(iii) *Sides of the channel (solid-slip boundary)*: This is where the water level intersects the bathymetry. No flow is allowed across this type of boundary and friction governs the relation between velocity and its gradient along the boundary wall and hence the name solid-slip. The friction relations are:

$$\frac{\partial V_x}{\partial n} = aV_x \text{ and } \frac{\partial V_y}{\partial n} = aV_y \qquad \textbf{Eqn. 4.18}$$

where $V_x$ and $V_y$ are the horizontal velocity components, $n$ is the axis normal to the boundary, and $a$ is a friction coefficient which takes the value of the assigned friction

coefficient (except when a *k-ε* model is used in which case the coefficient is computed by TELEMAC-2D).

### 4.3.3 TELEMAC-3D

TELEMAC-3D solves the full set of three-dimensional hydrostatic form Navier Stokes equations taking into account density variations in the water body.

The model studies the environmental processes in free-surface transient flow and can be applied to weirs, streams, rivers, lakes, estuaries, seas and coastal waters. The model is widely used in the study of hydrodynamics, sedimentology, water quality and free surface evolution due to short waves.

TELEMAC-3D is used in the current study to investigate the characteristics of flow in a floodplain and to investigate the complex 3-dimensional processes including flow attenuation and momentum exchange at the interface between the main channel and the floodplain.

#### *4.3.3.1 Model Assumptions*

The main assumptions of TELEMAC-3D are (EDF, 1997a,b):

- The fluid is Newtonian and incompressible.
- Hydrostatic pressure is assumed; therefore flow with high vertical accelerations cannot be modelled by TELEMAC-3D.
- In accordance to Boussinesq's approximation, the variation in density in relation to a reference density is assumed to be small.
- The computational domain can take any horizontal form, but all obstructions to the free surface flow become an integral part to the bathymetry. Thus, a submerged body cannot be represented.

#### *4.3.3.2 Numerical Scheme*

The TELEMAC-3D model solves the hydrostatic form of the Navier Stokes equations taking into account density variations in the water body. The continuity equation on which the model is based is:

$$\frac{\partial V_x}{\partial x} + \frac{\partial V_y}{\partial y} + \frac{\partial V_z}{\partial z} = 0 \qquad \textbf{Eqn. 4.19}$$

where $V$ is the velocity and $x$, $y$ and $z$ represent the Cartesian axes. The momentum equations in the $x$ and $y$ directions are:

$$\frac{\partial V_x}{\partial t} + V_x \frac{\partial V_x}{\partial x} + V_y \frac{\partial V_x}{\partial y} + V_z \frac{\partial V_x}{\partial z} = -\frac{1}{\rho_o}\frac{\partial p}{\partial x} + \frac{\partial}{\partial x}\left[\upsilon_H \frac{\partial V_x}{\partial x}\right] + \frac{\partial}{\partial y}\left[\upsilon_H \frac{\partial V_x}{\partial y}\right] + \frac{\partial}{\partial z}\left[\upsilon_z \frac{\partial V_x}{\partial z}\right] + S_x$$

**Eqn. 4.20**

$$\frac{\partial V_y}{\partial t} + V_x \frac{\partial V_y}{\partial x} + V_y \frac{\partial V_y}{\partial y} + V_z \frac{\partial V_y}{\partial z} = -\frac{1}{\rho_o}\frac{\partial p}{\partial y} + \frac{\partial}{\partial x}\left[\upsilon_H \frac{\partial V_y}{\partial x}\right] + \frac{\partial}{\partial y}\left[\upsilon_H \frac{\partial V_y}{\partial y}\right] + \frac{\partial}{\partial z}\left[\upsilon_z \frac{\partial V_y}{\partial z}\right] + S_y$$

**Eqn. 4.21**

where $p$ is the pressure, $\rho_o$ is the reference density, $\upsilon_H$ and $\upsilon_Z$ are velocity diffusion coefficients and $S$ represents source terms (wind, Coriolis Force etc.). The momentum direction in the $z$ direction for an assumed hydrostatic pressure distribution reduces to:

$$p = p_{atm} + \rho_o g(Z - z) + \rho_o g \int_z^Z \frac{\Delta\rho}{\rho_o} . \partial z \qquad \textbf{Eqn. 4.22}$$

where $p_{atm}$ is the atmospheric pressure, $\Delta\rho$ is the variation in density, $Z$ is the free surface elevation and $g$ is the gravitational acceleration.

In order to calculate the free surface elevation, the pressure continuity terms are integrated over the vertical. This cannot be solved by the three-dimensional equations listed above. Therefore, the depth-averaged hydrodynamic model TELEMAC-2D is incorporated within TELEMAC-3D to compute the free-surface elevation. Therefore, the continuity and momentum equations of TELEMAC-2D are solved again within the TELEMAC-3D model.

Presentation of Bottom Friction

Since bottom friction is a two-dimensional attribute, it is treated in the same way as that of the TELEMAC-2D model. The same options of friction law (Table 4-4) of TELEMAC-2D are available in the 3D model and the assigned value of friction coefficient in TELEMAC-3D is thus incorporated in the source terms of the momentum equations of TELEMAC-2D (which is called into TELEMAC-3D to compute the free-surface elevation).

Turbulence Modelling

In TELEMAC-3D a distinction is made between horizontal ($x$-$y$ space) and vertical turbulence for which a number of options of turbulence modelling are available (EDF, 1997a,b).

For the TELEMAC-3D model in the current study, a constant viscosity was selected to represent the horizontal turbulence modelling. The viscosity coefficient represents: the molecular viscosity, turbulent viscosity and dispersion. The velocity diffusivity/ viscosity may have a significant effect both on the shapes and sizes of recirculation zones. There are also a number of options for vertical turbulence in TELEMAC-3D. These include: constant viscosity, mixing length models, and $k$-$\varepsilon$ model. The Prandtl mixing length model was selected for the turbulence modelling of the vertical in the current study.

Space Discretisation of TELEMAC-3D (Mesh)

TELEMAC-3D offers two forms of sigma transformation, namely classical and generalised. The standard or "classical sigma" subdivides the vertical into a number of layers of equal depth (that is into equi-distant layers). As an extension of standard sigma-coordinate transformation, the "generalized transformation" applies a nonlinear

stretching to the vertical coordinate that depends on local water depth (Song and Haidvogel, 1994). This option can be used to generate a more uniform vertical resolution near the surface and consequently a better representation of the mixed layer and thermocline (Ocean-Modelling, 2002).

In order to discretise the three-dimensional domain into prisms, a two-dimensional mesh is initially constructed in the same way as that of a TELEMAC-2D mesh. Following this, the mesh is repeated over the vertical thereby producing a number of curved surfaces or "planes" with sigma coordinates. The vertical links between the nodes of the mesh and the repeated mesh form prisms. The number of horizontal planes i.e. the vertical resolution of the model is defined by the user. Each plane *I*p is defined by a single vertical coordinate *z(I*p*)* which determines the fraction of the water depth below that plane. This vertical coordinate *z(I*p*)* may be discretised using either classical or generalised sigma transformation (EDF, 1997b) as shown in Figure 4-7.

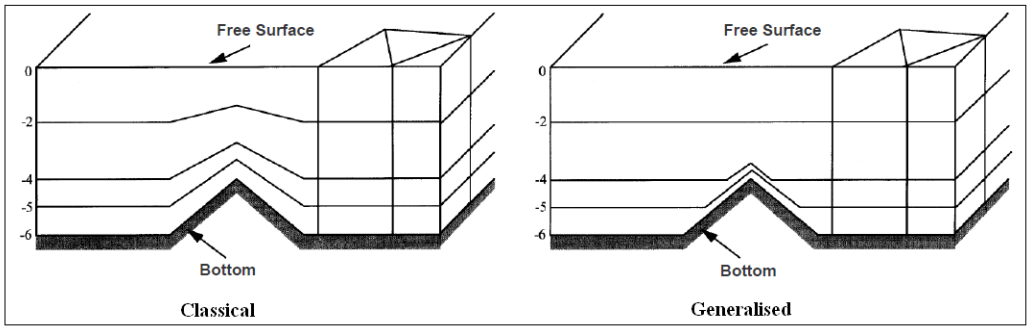


**Figure 4-7 Vertical Discretisation in TELEMAC-3D: Sigma Transformation (EDF, 1997b)**

Time Discretisation

The TELEMAC model applies a finite element discretisation in order to solve the Navier-Stokes equations for the main flow variables: the horizontal velocities ($V_x$ and $V_y$), the vertical velocity ($V_z$) and the pressure ($p$). The depth averaged model TELEMAC-2D is incorporated within TELEMAC-3D and internally called (at each timestep) to compute the water depth ($h$), and the depth-averaged horizontal velocities ($\overline{V_x}$ and $\overline{V_y}$) in the $x$- and $y$- directions respectively.

Due to the fact that the depth-averaged model is incorporated within TELEMAC-3D, the timestep requirement of TELEMAC-3D is smaller than that for a similar runs carried out in TELEMAC-2D. However, in order to avoid excessively reducing the timestep, a "3D/2D timestep ratio" is applied. Thus the two-dimensional computation within TELEMAC-3D is carried out four times within the 3D timestep and thus sub-timesteps for the 2D computations are created while running the three-dimensional model at a reasonable timestep. The 3D/2D timestep ratio results in a substantial reduction in computation time.

TELEMAC-3D offers a variety of advection schemes for the continuity and momentum equations e.g. the Method of Characteristics, the Streamline Upwind

Petrov-Galerkin (SUPG), the Multi-dimensional Upwind Residual Distribution (MURD) scheme and the Conservative Scheme (Hervouet, 2007).

To facilitate the comparison with the TELEMAC-2D model in the current study, the advection of velocities in the momentum equation was computed by the Method of Characteristics, a method which is unconditionally stable (EDF, 1997b). The "Conservative Scheme" was selected for the computation of water depths because it ensures that water depths are reasonably propagated. The scheme is conservative without sub-iterations at the cost of stability. The conservative scheme is the same as in TELEMAC-2D with the exception that the SUPG decentring is disabled in TELEMAC-3D (EDF, 1997b).

The final set of discretised equations was first preconditioned using the diagonal preconditioning option. TELEMAC-3D solved the system of equations at each time step using the Generalised Minimum Residual method (GMRES) for velocities and propagation. The Element by Element (EBE) matrix storage was used (Hervouet, 2003; 2004).

Initial Conditions

The computation commences from quiescent initial conditions i.e. the computation starts from rest. The initial conditions of the straight channel model were different than those of the meandering channel simulations. In the TELEMAC-3D model of the FCF straight channel, the initial water elevation in the model domain was the average of the upstream and downstream water elevations (Figure 4-8). The accuracy (tolerance) between any two timesteps was set to 0.0001 at all nodes for all variables ($V_x$ *(m/s)*, $V_y$*(m/s)*, $V_z$*(m/s)*, and *h(m)*). The computation continued until a steady state was reached.

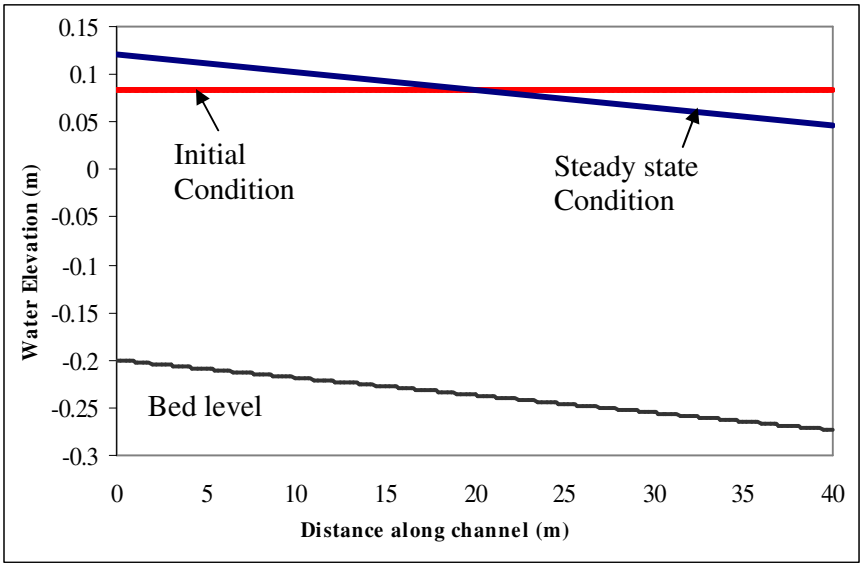


**Figure 4-8 Initial conditions of the TELEMAC-3D model of the FCF Straight channel**

In the TELEMAC-3D models of the meandering channel configuration, the initial water elevation in the model domain is that of the downstream outlet.

Boundary Conditions
The types of boundary conditions available in TELEMAC-3D are similar to those of the TELEMAC-2D model. The types of boundary conditions used in the current modelling study are different for the straight and meandering channel configurations:

*Straight Channel Model:*
*(i) Imposed water elevation at the upstream and downstream boundaries:* The water elevation at both the upstream (inlet) and downstream (outlet) of the channel were fixed throughout the duration of the model run.

*(ii) Sides of the channel (solid-slip boundary):* This is where the water level intersects the bathymetry. No flow is allowed across this type of boundary and friction governs the relation between velocity and its gradient along the boundary wall and hence the name solid-slip.

*Meandering Channel Model:*
*(i) Imposed water elevation at downstream boundary:* The water elevation at downstream end of the channel (outlet) was fixed throughout the duration of the model run.
*(ii) Solid-slip boundary conditions at the sides of the channel.*
*(iii) Imposed flowrate at the upstream boundary:* At the inlet of the channel, a flow value is prescribed. A step-wise increment in the flow value was applied in order to accelerate the achievement of quasi-steady state conditions in the channel.

## 4.4 Model Development

### 4.4.1 HEC-RAS

The HEC-RAS models of the straight and meandering channel in this study were developed by incorporating channel cross-sections of known elevation at defined longitudinal intervals into the model geometry. The HEC-RAS schematics for the straight channel are shown in Figure 4-9 and that for the meandering channel is in Figure 4-10.

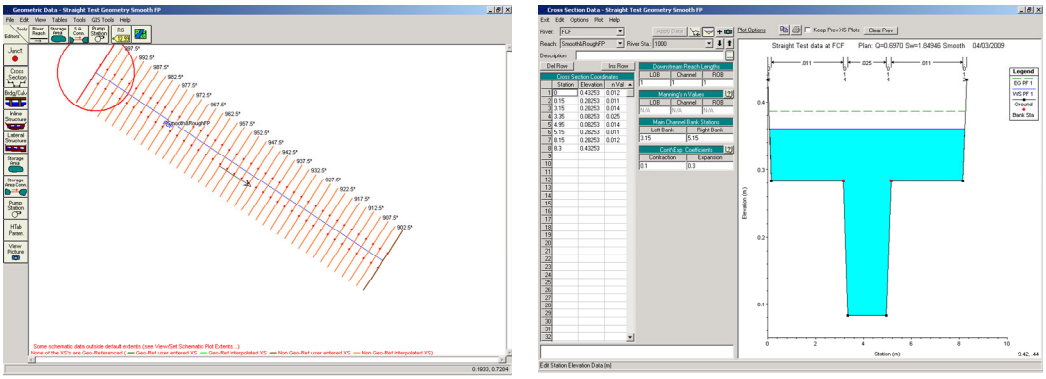

**Figure 4-9 HEC-RAS river reach of FCF Phase C straight compound channel**

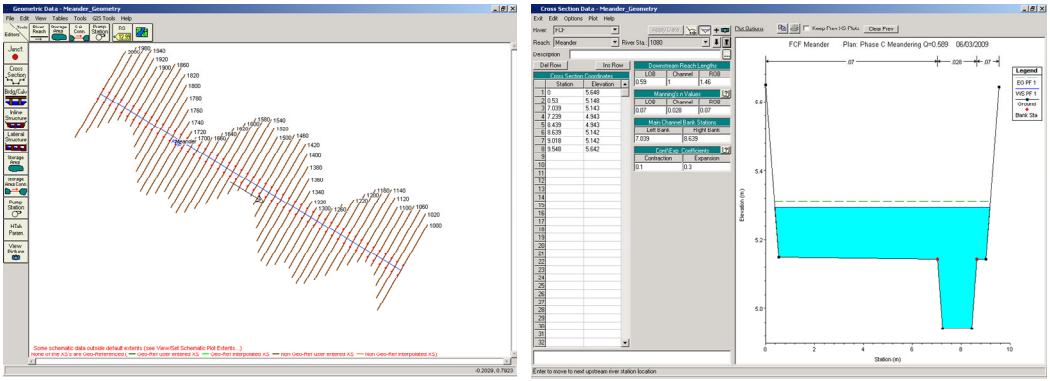

**Figure 4-10 HEC-RAS river reach of FCF Phase C meandering compound channel**

### 4.4.2 TELEMAC-2D

The finite element meshes for the TELEMAC-2D bathymetries for the straight and meandering channels were constructed using the mesh generator software MATISSE. These discretised the geometries that consisted of trapezoidal sections in both the main channel (slot) and overbank zones of the channel The straight channel mesh consisted of *5327* nodes and *10240* triangular elements (Figure 4-11) and that for the meandering channel (Figure 4-12) consisted of *2719* nodes and *5202* elements. The floodplain mesh was coarse ranging from *0.2m* to *0.54m* for the straight and meandering channels. However a finer mesh with elements that ranged from *0.1* to *0.2m* was utilised in the main channel.

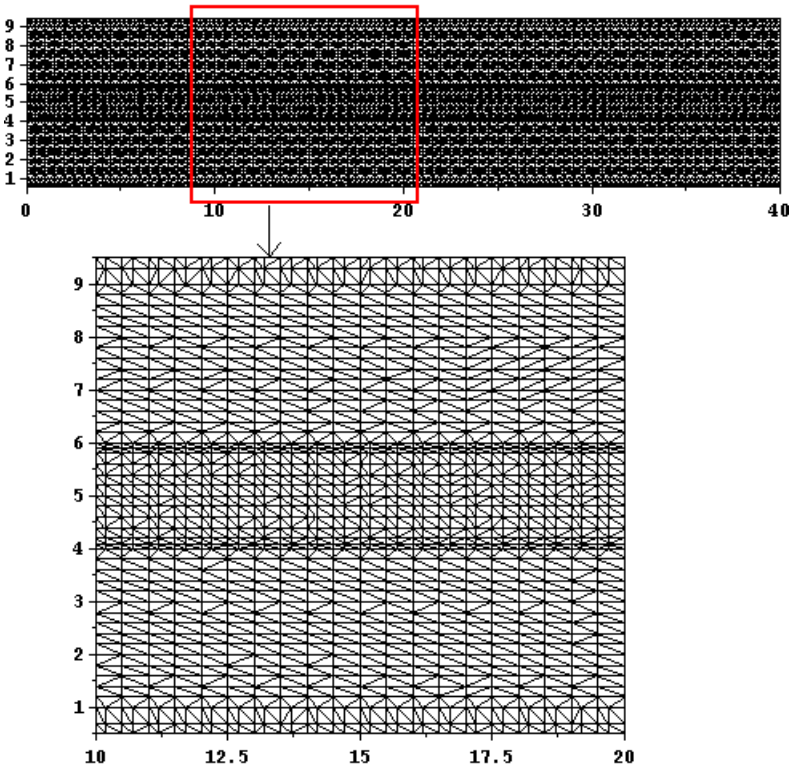


**Figure 4-11 Finite element mesh of FCF straight compound channel generated in TELEMAC**

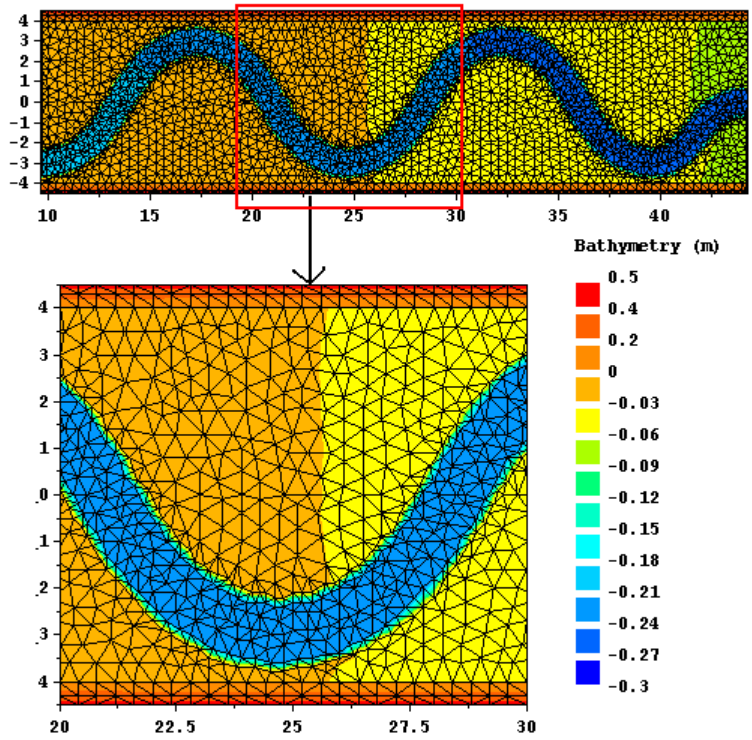


**Figure 4-12 Finite element Mesh of the meandering channel**

### 4.4.3 TELEMAC-3D

TELEMAC-3D meshes were constructed by applying the sigma transformation with eight vertical planes to the 2D meshes used in the TELEMAC-2D models. The eight planes were located at: the bottom, *0.2y, 0.4y, 0.5y, 0.65y, 0.8y and 0.9y* (where *y* is the water depth) and at the water surface. This user-defined positioning of planes was programmed in a special TELEMAC-3D subroutine. These 3D meshes are shown in Figure 4-13 for the straight channel and Figure 4-14 for the meandering channel.

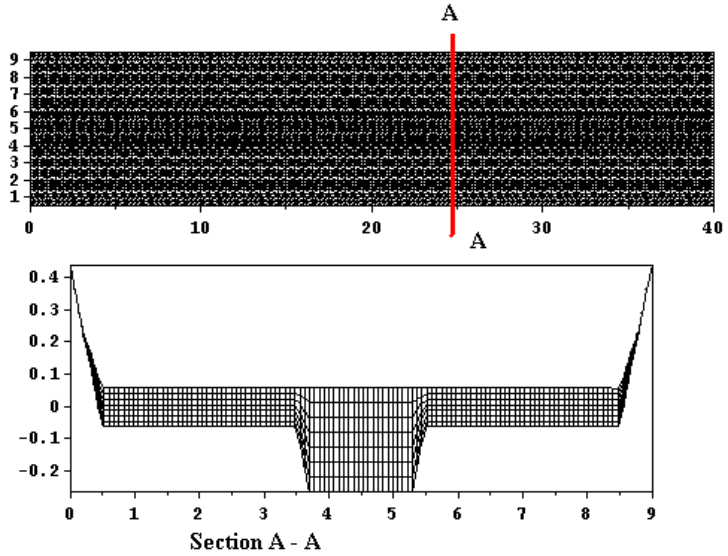


**Figure 4-13 Finite element 3D mesh of the straight FCF channel**

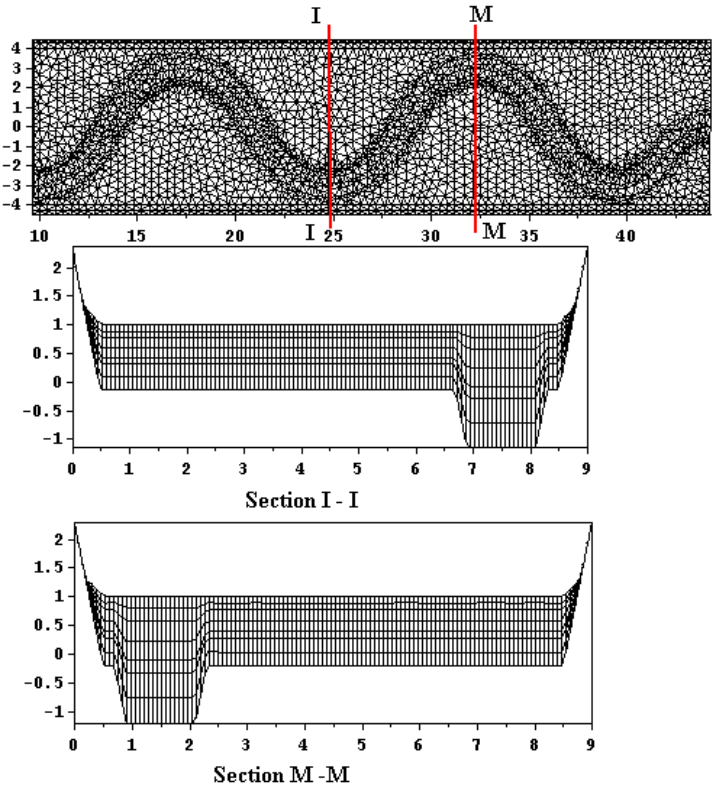


**Figure 4-14 Finite element 3D mesh of the meandering FCF channel**

## 4.5 Model Calibration

### 4.5.1 HEC-RAS

As may be expected, calibration of the 1D HEC-RAS model was considerably more straight-forward than that required for the TELEMAC-2D and 3D models. The model was executed for calibration simulations in steady state model using known values of both upstream flow and downstream water level. Calibration for a straight channel test involved setting the resistance in the main channel to a Manning's *n* of 0.03 and adjusting the floodplain roughness coefficients so that the water surface profile correlated as closely as possible with that measured at the FCF. This main channel *n* value was calculated from measured data and was considered to be an accurate representation of main channel resistance. An optimised calibration was not solely based on matching the simulated and measured water surface profiles but rather, represented the best compromise between matching the profiles, average velocity values and flow proportions to those determined from measurement. Water surface profiles for calibration of the 0.6m$^3$/s straight channel test with roughened floodplains are shown in Figure 4-15. The channel bed is also shown in Figure 4-15 and it should be noted that data relates to a datum that was arbitrarily chosen for modelling purposes. Profiles of this type were typical and a similar set of profiles were observed for calibration of the smooth floodplain test.

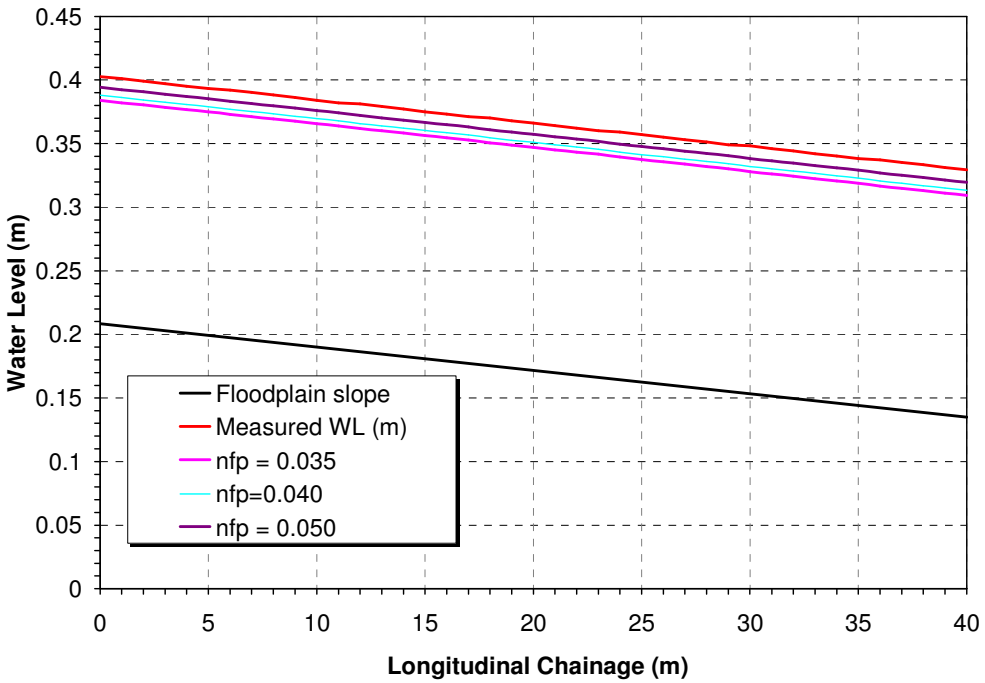


**Figure 4-15 Calibrated water surface profiles for the roughened floodplain 0.6m$^3$/s straight channel test**

Meandering channel calibration was somewhat more involved. Two-stage flows in meandering channels are significantly more complex than those in straight channels and are characterised by 'plunging' flows from the floodplain to the main channel across the meander belt overbank zone. These structures result in considerable energy losses that will not be reflected in a 1-Dimensional model such as HEC-RAS. As a consequence, the approach to model calibration adopted for the straight channel tests, where only floodplain resistance was adjusted, could not be adopted. Calibration therefore was based on iterative adjustments of both main channel and floodplain resistance until good correlations between observed and simulated water surface profiles were obtained. Calibration water surface profiles for the 0.6m$^3$/s meandering channel test with roughened floodplains are shown in Figure 4-16.

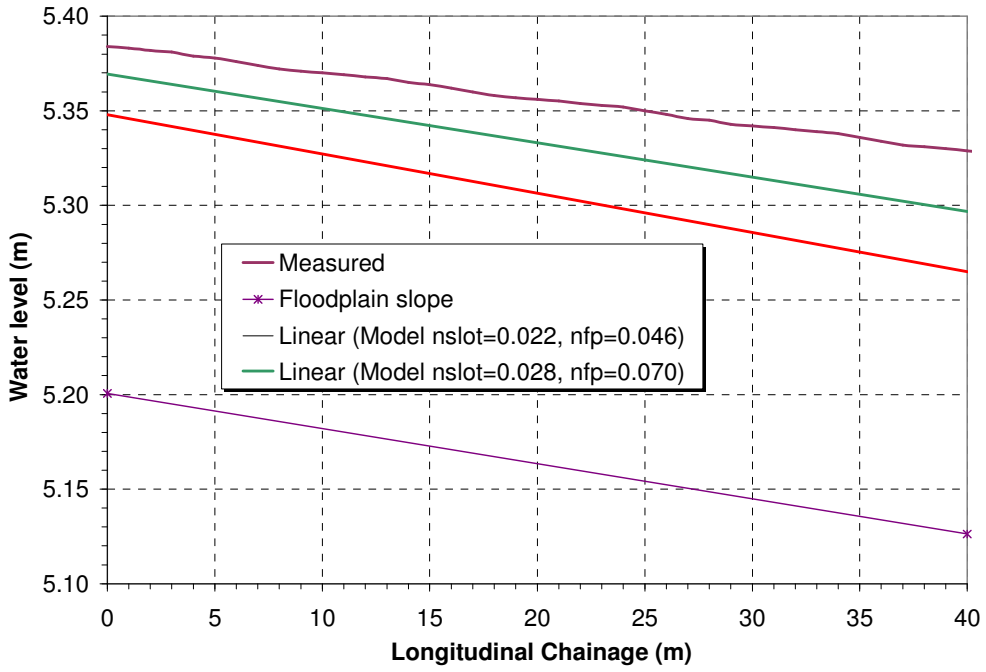


**Figure 4-16 Calibrated water surface profiles for the roughened floodplain 0.6m$^3$/s meandering channel test**

### 4.5.2 TELEMAC-2D

Model calibration is the process of varying physical and/or empirical parameters until a good agreement is reached between observed data and model predictions. Parameters that were important in this regard were the selected timestep, the turbulence scheme, the diffusion coefficient and the friction law.

Timestep

Simulations were initially set to times up to *5.5* hours (*19800*s). In the initial period, up to a maximum of *2* hours, the flow was gradually increased until it reached the magnitude of the flows recorded in the FCF tests. The remaining time, up to *3.5* hours, ensured that steady state conditions were established in the model. The choice of a suitable timestep depends on the number of iterations required at each timestep for values of the variables to converge (solver accuracy/tolerance = *0.0001*). A timestep of *2* seconds was initially applied. This was reduced to *1* second due to the high number of iterations required. Finally a timestep of *0.5s* was considered optimum in terms of the number of iterations required for each timestep and the computation time required to finish the simulation. Approximately *25* minutes were required to complete a model simulation of up to *5.5* hours. On average, four iterations were necessary at a time step of *0.5s* to achieve an accuracy of *0.0001* in the estimation of velocities and water depth.

Turbulence Scheme

For the straight and meandering channels investigated in this study, a constant viscosity was selected to represent the turbulence modelling. Constant viscosity is

sufficient when flow is governed by the pressure gradient and by advection (Hervouet, 2007).

Friction Law
The friction coefficient for the FCF channels was estimated using Manning's friction law. In order to facilitate the comparison with estimated/measured values of friction coefficient, Manning's friction law was used in the calibration of the TELEMAC-2D model of the straight and meandering compound channel.

Diffusion Coefficient
The diffusion coefficient represents the molecular viscosity, the turbulent viscosity and dispersion characteristics of the flow. The velocity diffusivity/viscosity may have a significant effect both on the shapes and sizes of recirculation zones.

#### *4.5.2.1 Straight Channel Calibration*

Preliminary calibration involved undertaking a number of simulations to identify the sensitive parameters and functions in the model. From this, the dispersion coefficient (velocity diffusivity) and the bottom friction were found to be the significant influences on water surface profiles, flow velocities and the flow proportions that were conveyed in the main channel and on the floodplain. These parameters required calibration to optimised values of average water surface slope and main channel and floodplain flow proportions. The calibration approach involved a two-step procedure. In the first step, a range of values for the diffusion coefficient were tested and the diffusion coefficient that yielded the best combined results (velocity profile and values of flow and water surface slope) was chosen. Following this and after endorsing an appropriate value for diffusion coefficient from the first calibration step, a number of runs are performed to calibrate the friction coefficients in the main channel and floodplain.

Diffusion Coefficient
The model's sensitivity to the magnitude of the diffusion coefficient was explored by running the TELEMAC-2D straight model for a range of diffusivity values ranging from *.001*$m^2/s$ to *.025*$m^2/s$. The Manning's resistance coefficients were kept constant and had values of *0.013* and *0.028* in the main channel and floodplain respectively.

The impact of these variations in diffusion coefficients on water surface slopes and on the main channel ($Q_{mc}$) and floodplain ($Q_{fp}$) flow distributions are shown in Table 4-5.

**Table 4-5 Influence of diffusion coefficient on surface slope and flow distribution**

| Run | Diff. Coeff. ($m^2/s$) | Observed Variables | | | Simulated Variables | | | Percentage Error | | |
|---|---|---|---|---|---|---|---|---|---|---|
| | | $Q_{mc}$ ($m^3/s$) | $Q_{Tot.}$ ($m^3/s$) | $S_w$ (x1000) | $Q_{mc}$ ($m^3/s$) | $Q_{Tot.}$ ($m^3/s$) | $S_w$ (x1000) | $Q_{mc}$ % | $Q_{Tot.}$ % | $S_w$ % |
| SS700-2D_1 | 0.025 | 0.358 | 0.697 | 1.8495 | 0.382 | 0.6996 | 0.00231 | 6.7 | 0.24 | 24.87 |
| SS700-2D_2 | 0.01 | 0.358 | 0.697 | 1.8495 | 0.372 | 0.6992 | 0.00221 | 3.9 | 0.32 | 19.26 |
| SS700-2D_3 | 0.005 | 0.358 | 0.697 | 1.8495 | 0.368 | 0.6999 | 0.00216 | 2.7 | 0.43 | 16.83 |
| SS700-2D_4 | 0.001 | 0.358 | 0.697 | 1.8495 | 0.364 | 0.7009 | 0.00211 | 1.6 | 0.55 | 14.32 |

The average water surface slopes for the varying dispersion coefficients in Table 4-5 are shown graphically in Figure 4-17.

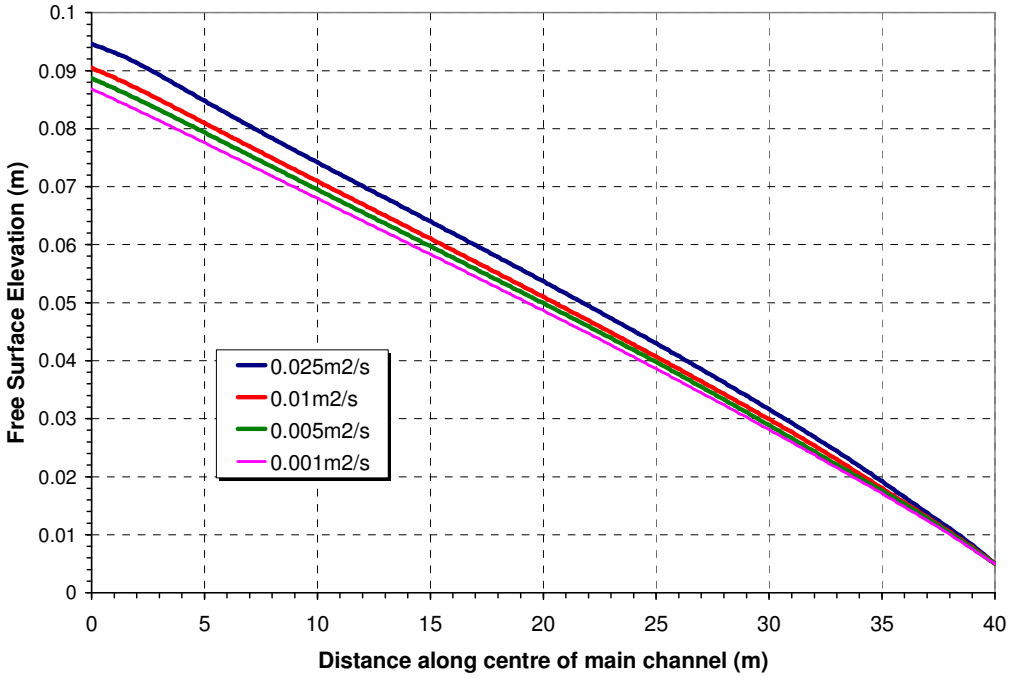


**Figure 4-17 Influence of varying diffusion coefficient on water surface slope**

Table 4-5 and Figure 4-17 show that average water surface slope values decrease with decreasing diffusion coefficient. Furthermore, decreasing the diffusion coefficient also results in a reduction in the main channel flow proportion and an increasing proportion of the total flow being conveyed on the floodplain.

Velocity data only in the longitudinal main channel flow direction were recorded in the FCF straight channel tests. These were recorded at a number of cross-sections in the measuring reach that were located between the chainages of *34m* and *36m*. Main channel and floodplain velocity data was recorded at *0.4y* (where *y* is the water depth) in accordance with an assumed logarithmic velocity profile in the vertical water column. These values facilitated a reasonable comparison with the depth average velocity values produced by TELEMAC-2D. Simulated transverse velocity profiles for the range of diffusion coefficients that were investigated are compared against observed values in Figure 4-18.

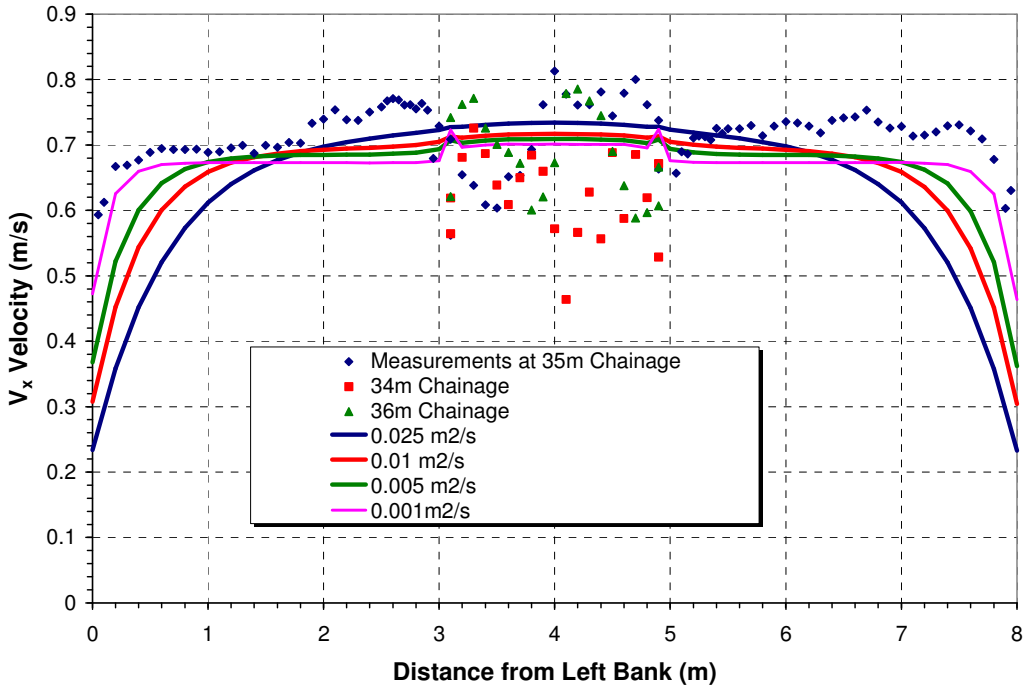


**Figure 4-18 Influence of diffusion coefficient on velocity profile across floodplain**

The significant scatter in the observed main channel point velocities (from approximately *0.5m/s* to *0.8m/s*) in Figure 4-18 result from significant bedforms (primarily dunes) that characterised the channel bed in these mobile bed tests. Values increased in the vicinity of the main channel and floodplain interface, before returning to a reasonably constant value across the floodplain. Significant decreases in velocity were observed towards the floodplain edges reflecting the frictional characteristics of the boundary.

Figure 4-18 indicates that the value of the diffusion coefficient impacts significantly on both the magnitude, but more particularly, the shape of simulated velocity profiles. The highest simulated velocity profile in the main channel corresponds to the highest diffusion coefficient of $0.025m^2/s$. However, this profile was characterised by low velocities across the floodplains. The lowest diffusion coefficient ($0.001m^2/s$) on the other hand, resulted in the best estimate of the discharge in the main channel $Q_{mc}$, being only *1.6%* higher than the measured flow. This coefficient also produced the best estimate of the water surface slope in the main channel.

It is observed from Figure 4-18 that the shape of the velocity profile is also dependent on the diffusion coefficient. The profile corresponding to a value of $0.001m^2/s$ is characterised by a profile that has a constant $V_x$ magnitude across the main channel, increasing suddenly at the interface with the floodplain and reducing in the floodplain. Comparison of all the profiles in Figure 4-18 suggests that s suitable compromise in terms of the velocity magnitudes and profile shape is achieved with a diffusion coefficient of $0.005m^2/s$. The flow proportion in the main channel ($Q_{mc}$) is further improved by calibrating the bottom roughness.

Channel Friction

The second part of the calibration process requires that this diffusion coefficient is kept constant while an iterative procedure of adjusting main channel and floodplain roughness coefficients is undertaken until the match between observed and simulated water surface and velocity profiles is optimised.

Compound channels are characterised by hydraulic roughness values that can vary considerably along the length of the wetted perimeter. The FCF tests that were investigated in this study were no exception – tests were undertaken with smooth and roughened floodplains. Because of the variations in resistance, it was necessary to program a TELEMAC-2D subroutine called STRCHE that facilitated assigning different roughness coefficients to difference sub-sections of the flow cross-section. Summarised results of the optimised friction parameters for calibration are shown in Table 4-6.

**Table 4-6 Effect of varying the friction coefficient on the resulting surface slope and flow**

| Run | Manning's n | | Observed Variables | | | Simulated Variables | | | Percentage Error | | |
|---|---|---|---|---|---|---|---|---|---|---|---|
| | | | $Q_{mc}$ | $Q_{Tot.}$ | $S_w$ | $Q_{mc}$ | $Q_{Tot.}$ | $S_w$ | $Q_{mc}$ | $Q_{Tot.}$ | $S_w$ |
| | mc | fp | ($m^3/s$) | ($m^3/s$) | (x1000) | ($m^3/s$) | ($m^3/s$) | (x1000) | % | % | % |
| SS700-2D_3 | 0.028 | 0.013 | 0.358 | 0.697 | 1.8495 | 0.368 | 0.699 | 0.00216 | 2.7 | 0.427 | 16.8 |
| SS700-2D_5 | 0.025 | 0.013 | 0.358 | 0.697 | 1.8495 | 0.385 | 0.700 | 0.00207 | 7.6 | 0.424 | 12.1 |
| SS700-2D_6 | 0.020 | 0.010 | 0.358 | 0.697 | 1.8495 | 0.406 | 0.700 | 0.00168 | 13.5 | 0.419 | -9.4 |
| SS700-2D_7 | 0.023 | 0.011 | 0.358 | 0.697 | 1.8495 | 0.390 | 0.700 | 0.00185 | 8.8 | 0.412 | 0.3 |

Calibration of the main channel and floodplain roughness values in Table 4-6 commenced with an initial assumption that the main channel Manning's *n* was *0.028* and that on the floodplain was *0.013*. These correspond to the measured values determined from the geometrical and flow properties of the test. Table 4-6 indicates that average surface slope values decrease with reducing resistance coefficients. A comparison of runs *SS700-2D_3*, *SS700-2D_5,* and *SS700-2D_6* also reflect the increases in main channel flow proportion that results from a decrease in main channel roughness. These higher main channel flow proportions are reflected in the simulated transverse velocity profiles shown in Figure 4-19 for the combinations of resistance coefficients in Table 4-6.

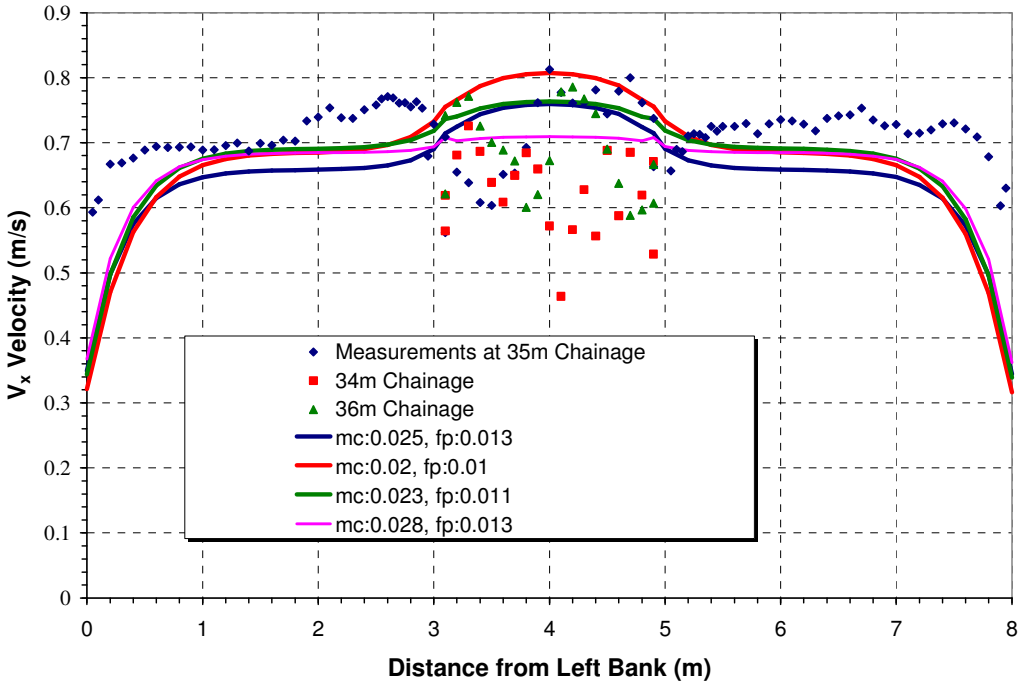


**Figure 4-19 Influence of resistance coefficients on velocity profiles across floodplain (diffusion coefficient: *0.005m²/s*)**

The calibration involved optimising physical and empirical parameters required in the model such that acceptable agreement is reached between observed data and model predictions. The analysis indicates that in the case of the straight channel investigated, optimum results are obtained for a diffusion coefficient of *0.005m²/s* and friction coefficients of *0.023* and *0.011* for the main channel and the floodplains respectively. Resistance coefficients of this magnitude are consistent with values for sand bed channels and screeded concrete.

### *4.5.2.2 Meandering Channel Calibration*

The straight channel calibration data presented in Section 4.5.2.1 related to the *0.6m³/s* smooth floodplain test. For the full comparison of the 1D, 2D and 3D models that were tested, calibration of tests with all floodplain configurations was undertaken. The meandering channel calibrations that are being presented are for the roughened floodplain *0.6m³/s* test.

Diffusion Coefficient

A similar approach to that carried out for the straight channel was undertaken for calibrating the physical and empirical parameters in the FCF meandering channel TELEMAC-2D model. The influence of diffusion coefficients that vary in value from *0.1m²/s* to *0.001m²/s* was assessed against measured water surface slopes and slot (below bankfull) and overbank flow distributions for constant Manning's resistance values of *0.022* in the slot and *0.046* in the floodplain. These values correspond to those obtained at the UK FCF for the meandering channel with rough floodplains and a target flow of *0.6m³/s*. Data for this calibration is shown in Table 4-7.

**Table 4-7 Influence of diffusion coefficient on surface slope and flow distribution**

| Run | Diff. Coeff. ($m^2/s$) | Observed Variables | | | Simulated Variables | | | Percentage Error | | |
|---|---|---|---|---|---|---|---|---|---|---|
| | | $Q_{slot}$ ($m^3/s$) | $Q_{Tot.}$ ($m^3/s$) | $S_w$ (x1000) | $Q_{slot}$ ($m^3/s$) | $Q_{Tot.}$ ($m^3/s$) | $S_w$ (x1000) | $Q_{slot}$ % | $Q_{Tot.}$ % | $S_w$ % |
| MR600-2D_1 | 0.0001 | 0.223 | 0.579 | 1.8593 | 0.1965 | 0.5923 | 0.00218 | -11.8 | 1.60 | 17.0 |
| MR600-2D_2 | 0.001 | 0.223 | 0.579 | 1.8593 | 0.1961 | 0.5874 | 0.00215 | -12.0 | 1.54 | 15.7 |
| MR600-2D_3 | 0.01 | 0.223 | 0.579 | 1.8593 | 0.1948 | 0.5883 | 0.00200 | -12.6 | 1.53 | 7.8 |
| MR600-2D_4 | 0.1 | 0.223 | 0.579 | 1.8593 | 0.1879 | 0.5886 | 0.00146 | -15.7 | 1.66 | -21.4 |

Diffusion coefficients in the TELEMAC model are a measure of the speed at which a pulse of water passes an element. Increasing this coefficient therefore results in a greater mass of water flowing into the domain per time step. With regard to Table 4-7, increases in the diffusion coefficient are shown not to have a significant influence on the total flow because this is controlled by an applied boundary condition. However, the increases are reflected in the slot flow proportions which are reduced in order to increase the floodplain flow which is the dominant flow conveyer in the channel. Table 4-7 also indicates that the average surface slope decreases with the increase in the diffusion coefficient.

In order to investigate the complex main channel and floodplain interaction in the FCF meandering channel, data collection was more detailed than that for the straight channel tests and included the measurement of velocity components in the longitudinal ($V_x$) and transverse ($V_y$) channel directions (see Figure 4-6 of FCF layout for sign convention). Calibration again involved assessing the models capability to reproduce in shape, the measured transverse velocity profiles in two directions. These are shown for an apex section in Figure 4-20 for the longitudinal direction and Figure 4-21 for the transverse direction.

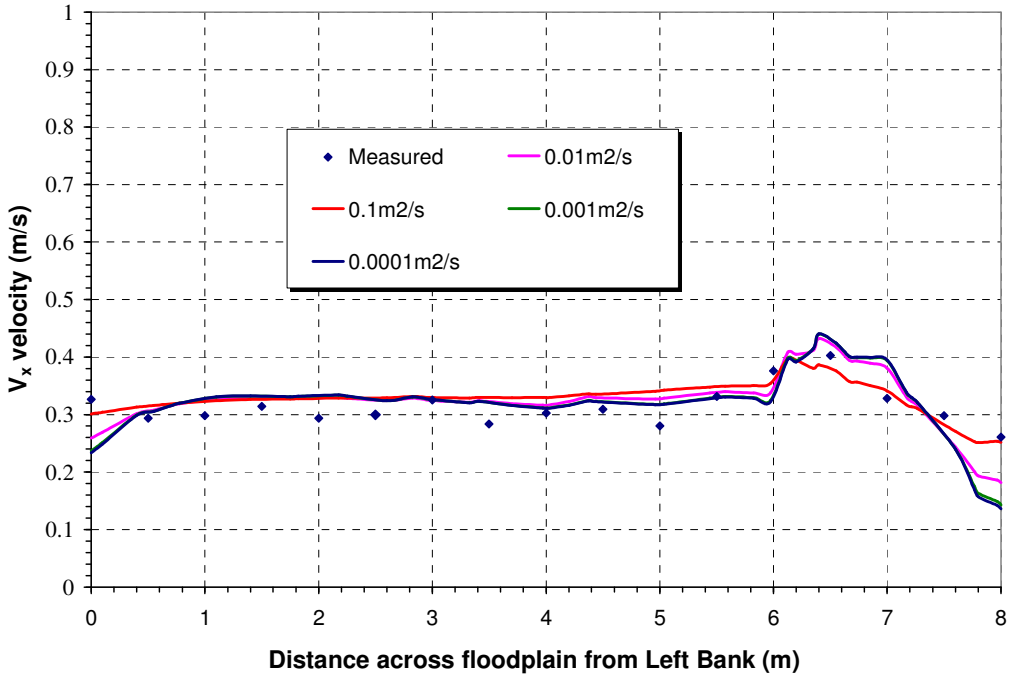


**Figure 4-20 Influence of diffusion coefficient on velocity profile in *x*-direction at Apex *I***

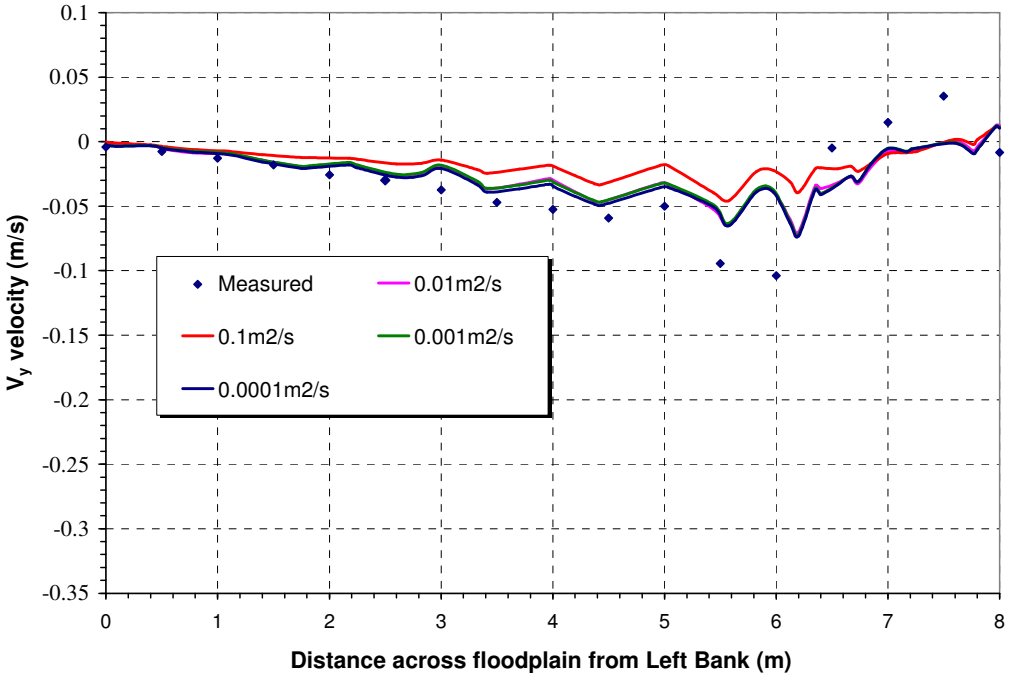


**Figure 4-21 Influence of diffusion coefficient on velocity profile in *y*-direction at Apex *I***

Table 4-7 with Figure 4-20 and Figure 4-21 suggest that an optimum diffusion coefficient of $0.01m^2/s$ produces a reasonable compromise between simulating the observed water surface slope, transverse velocity profiles in the longitudinal and transverse channel directions and distributing the slot and floodplain flow in proportion to measured values. This value formed the basis of the second stage of the calibration that involved varying the slot and overbank resistance coefficients and the turbulence scheme such that further optimisation was achieved.

Channel Friction and Turbulence Scheme

Summarised results of varying the slot and floodplain resistance in the meandering channel 2D model are summarised in Table 4-8

**Table 4-8 Effect of varying the slot and main channel friction coefficient and the model turbulence scheme on the resulting surface slope and flow (*CV* is constant viscosity and k-ε is k-epsilon model)**

| Run | Manning's n | | Turbulence | Observed Variables | | | Simulated Variables | | | Percentage Error | | |
|---|---|---|---|---|---|---|---|---|---|---|---|---|
| | slot | fp | | $Q_{slot}$ ($m^3/s$) | $Q_{Tot.}$ ($m^3/s$) | $S_w$ (x1000) | $Q_{slot}$ ($m^3/s$) | $Q_{Tot.}$ ($m^3/s$) | $S_w$ (x1000) | $Q_{slot}$ % | $Q_{Tot.}$ % | $S_w$ % |
| MR600-2D_5 | 0.0150 | 0.0459 | CV | 0.223 | 0.579 | 1.8593 | 0.1981 | 0.5825 | 0.00184 | -11.10 | 0.60 | -0.90 |
| MR600-2D_3 | 0.0221 | 0.0459 | CV | 0.223 | 0.579 | 1.8593 | 0.1948 | 0.5883 | 0.00200 | -12.60 | 1.33 | 7.80 |
| MR600-2D_6 | 0.0221 | 0.0479 | CV | 0.223 | 0.579 | 1.8593 | 0.1962 | 0.5875 | 0.00203 | -12.00 | 1.47 | 9.00 |
| MR600-2D_7 | 0.0180 | 0.0459 | CV | 0.223 | 0.579 | 1.8593 | 0.1955 | 0.5879 | 0.00194 | -12.30 | 1.54 | 4.50 |
| MR600-2D_8 | 0.0250 | 0.0459 | CV | 0.223 | 0.579 | 1.8593 | 0.1941 | 0.5879 | 0.00204 | -12.90 | 1.53 | 9.70 |
| MR600-2D_9 | 0.0221 | 0.0479 | k-ε | 0.223 | 0.579 | 1.8593 | 0.1977 | 0.5867 | 0.00216 | -11.30 | 1.33 | 16.40 |
| MR600-2D_10 | 0.0221 | 0.0459 | k-ε | 0.223 | 0.579 | 1.8593 | 0.1964 | 0.5876 | 0.00212 | -11.90 | 1.49 | 14.10 |

The impact of changing the main channel and floodplain resistance coefficients shown in Table 4-8 confirms trends that would be expected. Decreases in the slot roughness contribute to a higher simulated flow in this sub-section with a compensating reduction in the flow proportion being conveyed in the floodplain. Furthermore, these decreases are also shown to reduce the average gradient of the water surface slope through the reach. Table 4-8 also indicates that changing the turbulence scheme from a constant viscosity model to a *k-ε* model (model runs *MR600-2D_9* and *MR600-2D_10*) has only a minor influence on the simulated results.

Refining the friction coefficients in the second part of the calibration process ensured that in addition to the profile shape being well simulated, the magnitude of velocity values was also similar to observed values. The longitudinal and transverse velocity profiles are shown for Apex *M* in Figure 4-22 and Figure 4-23 for the combinations of slot and floodplain resistance values in Table 4-8.

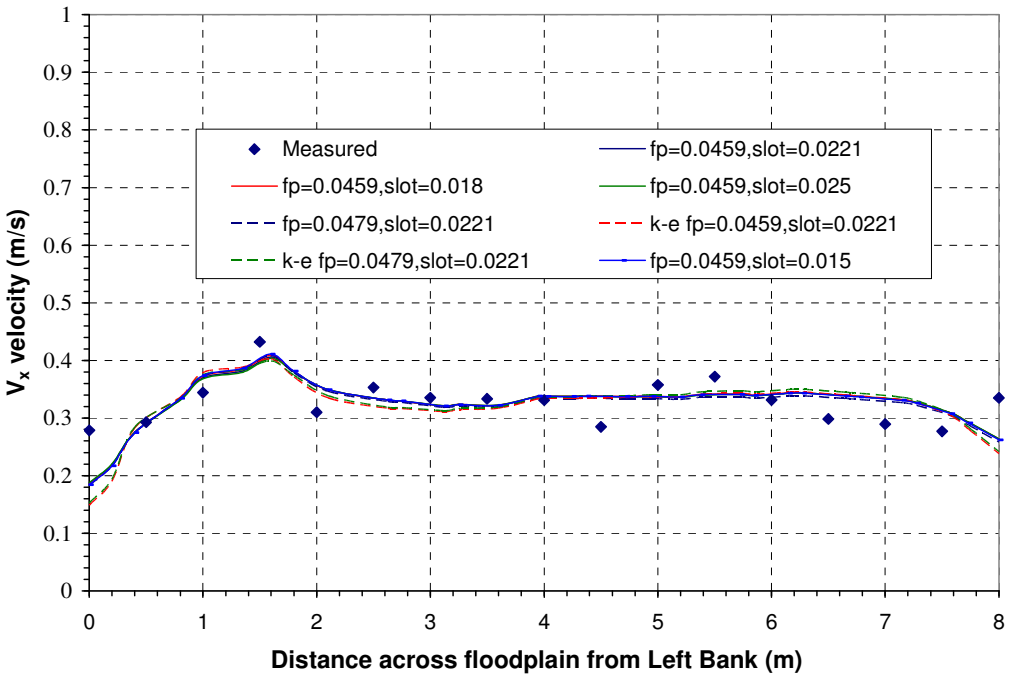


**Figure 4-22 Influence of resistance coefficients and turbulence scheme on velocity profiles in *x*-direction at Apex *M* (diffusion coefficient: *0.01m²/s*)**

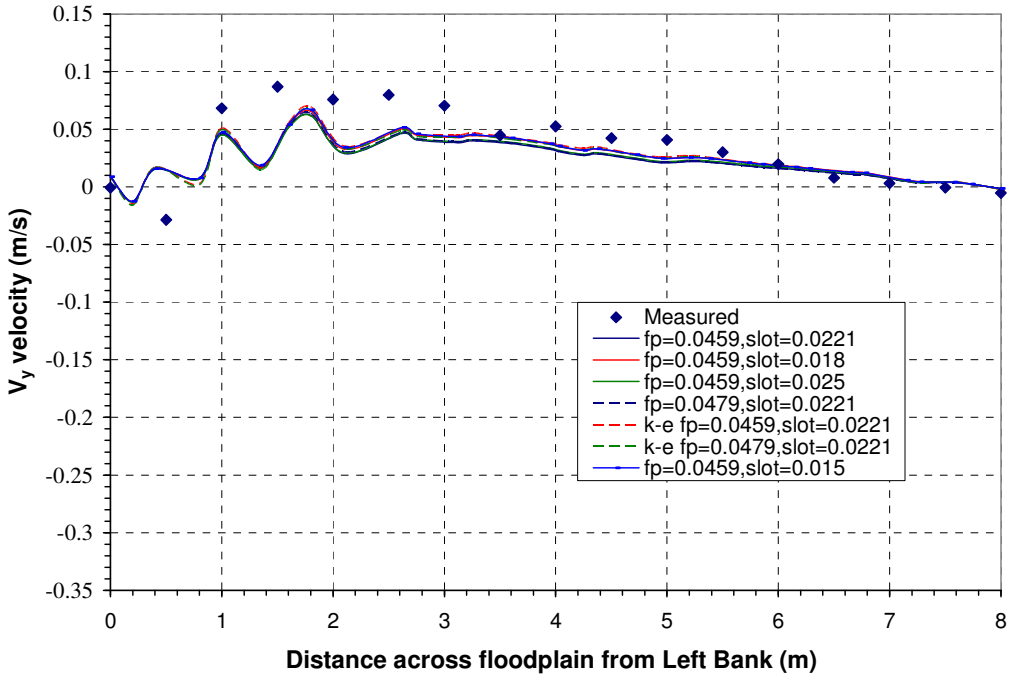


**Figure 4-23 Influence of resistance coefficients and turbulence scheme on velocity profiles in *y*-direction at Apex *M* (diffusion coefficient: *0.01m²/s*)**

Measured $V_x$ velocities at Apex *M* show a similar trend to those at Apex *I*. The $V_x$ velocities fluctuate around a value of approximately 0.*3m/s* until the flow approaches the inner channel (Figure 4-22). At this points both $V_x$ and $V_y$ velocities increase sharply across the slot. These sudden velocity changes highlight the plunging nature of the flow in the proximity of a meander bend as water from both left and right floodplains flows towards the inner channel.

Apex sections of meandering channels are characterised by conditions where the main channel and floodplain interaction is at a minimum. At other cross-sections, particularly cross-overs, the interaction is significantly more vigorous and is characterised by the 'plunging' of floodplain flow into the main channel and the 'welling out' of the main channel flow back onto the floodplain. As discussed in Section 2.6 these exchanges contribute significantly to energy losses in meandering compound channels and it is necessary that the model be calibrated for such cross-sections. Velocity profiles at Crossover *O* in the longitudinal transverse channel directions are shown in Figure 4-24 and Figure 4-25.

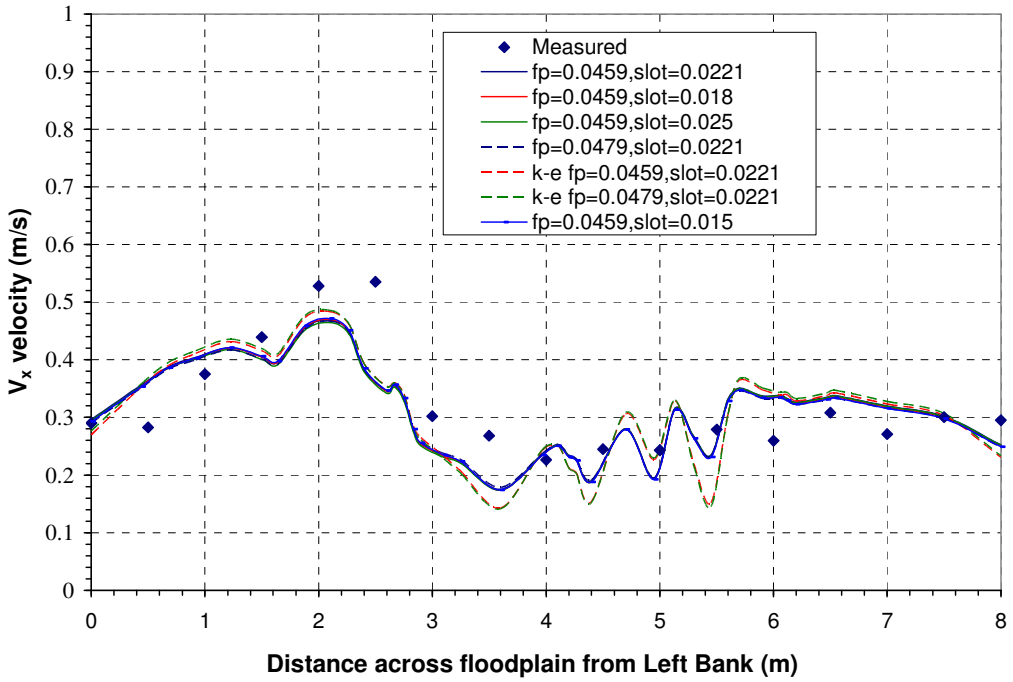


**Figure 4-24 Influence of resistance coefficients and turbulence scheme on velocity profiles in *x*-direction at Cross-over *O* (diffusion coefficient: *0.01m²/s*)**

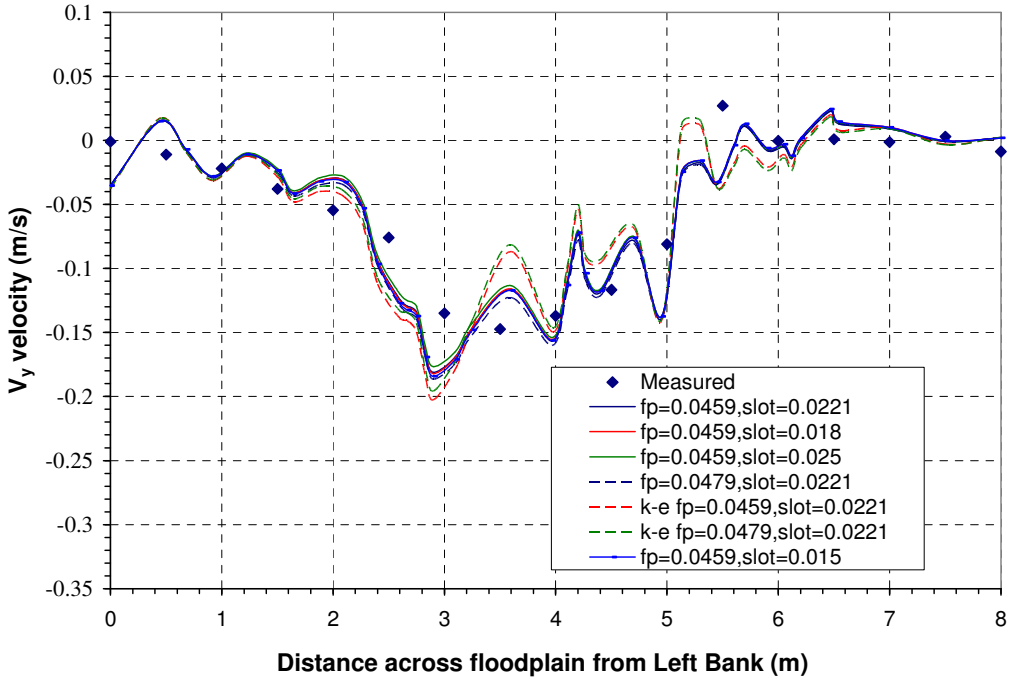


**Figure 4-25 Influence of resistance coefficients and turbulence scheme on velocity profiles in *y*-direction at Cross-over *O* (diffusion coefficient: *0.01m²/s*)**

Depth averaged overbank velocity components at Cross-over *O* differ from those observed at Apex *I* and *M* and are affected more definitively by the presence of the inner channel. Velocities in the valley direction for the roughened floodplain test case increase steadily across the left floodplain until they are in the vicinity of the inner channel, at which point they increase sharply. This sudden increase in $V_x$ is mirrored by a similar sized decrease in the transverse velocity component in the valley direction and in this case is representative of the plunging of water from the left floodplain to the inner channel. A minimum overbank transverse velocity ( $V_y$) at this section of *-0.15m/s* compared with a value of approximately *-0.10m/s* at Apex *I*, suggests, as would be expected, that this plunging flow is more pronounced at cross-over sections. Overbank velocity values in the longitudinal direction decrease across the slot and those in the transverse direction increase in the same region after which they tend to more constant values on the right side floodplain. This variation in overbank velocities above the slot reflects the influence of the shearing effect created at the interface of the inbank and overbank zones from the slot flow which is predominantly in the inner channel direction and the overbank flow which approaches along the valley direction.

The calibration for the TELEMAC-2D meandering channel indicates that variations in the assigned main channel and floodplain resistance coefficients and the model turbulence scheme have only a minor impact on the simulated $V_x$ and $V_y$ velocity components at all cross-sections. Consequently, the model was assumed calibrated for a diffusion coefficient of $0.01m^2/s$ and for slot and floodplain Manning's resistance coefficients in Run *MR600-2D_5* of *0.015* and *0.0459* in the main channel and floodplain respectively. The high floodplain resistance indicates that floodplains for this calibration were roughened with the elements described in Section 4.2. Little difference between simulated parameters was observed for the constant viscosity and $k$-$\varepsilon$ turbulence schemes and because of the additional considerable time required using the $k$-$\varepsilon$ model, the constant viscosity model was used to represent turbulence.

### 4.5.3 TELEMAC-3D

As with the TELEMAC-2D calibration, parameters that were likely to be important in establishing good agreement between model predictions and observed data were the selected timestep, the turbulence scheme, the diffusion coefficient and the friction law.

Timestep

As previously reported, the TELEMAC-3D model was constructed by a sigma transformation of the TELEMAC-2D depth averaged model. As a consequence, the timestep requirement of TELEMAC-3D is smaller than that for a similar run carried out in TELEMAC-2D (*0.5* seconds in TELEMAC-2D and *0.25* seconds in TELEMAC-3D). However, to avoid excessively reducing the timestep the '3D/2D timestep ratio' was applied. This ratio was set to *4*. On average four iterations were necessary at each time step (*0.25* seconds) to achieve an accuracy of *0.0001* in the estimation of velocities. This contrasted with the single iteration that was on average required by the solver to achieve an acceptable accuracy in predicted water surface elevations.

Turbulence Scheme
For the TELEMAC-3D models of the straight and meandering FCF compound channels investigated, a constant viscosity was selected to represent the horizontal turbulence modelling while the Prandtl mixing length was chosen for the modelling of vertical turbulence.

Bottom Friction
To enable a comparison with both measurements from the FCF and with results of the TELEMAC-2D simulations, the same Manning's resistance law as that used in TELEMAC-2D represented the bottom friction of the channel.

Diffusion Coefficient
As previously stated, the diffusion coefficient value of represents the molecular viscosity, the turbulent viscosity and dispersion characteristics of the flow and can have a significant influence on both on the shapes and sizes of recirculation zones produced in model simulations.

As with TELEMAC-2D, initial calibration involved a number of initial runs to investigate the sensitivity of the physical and empirical parameters and functions in the 3D model. From these, the dispersion coefficient (velocity diffusivity) and the bottom friction of the channel were found to be the significant influences on water surface profiles, flow velocities and the flow proportions that were conveyed in the main channel and on the floodplain of the compound section. These parameters required further calibration to optimise values for both the straight and meandering channels.

It should be noted at this time that unlike the output/result file of TELEMAC-2D which is readily readable by the analysis and graphical display programme RUBENS, TELEMAC-3D results file require some processing. A post-processor programme POSTEL3D is run on the TELEMAC-3D result files to produce both horizontal and vertical cross-sections along and/or across any axis of the model domain. These sections can then be read by RUBENS. The locations and dimensions of the cross-sections are determined by the model user. As such, horizontal and vertical cross-sections that facilitated comparison with measured FCF data sets required careful selection.

#### *4.5.3.1 Straight Channel Calibration*

Diffusion Coefficient
The model's sensitivity to the magnitude of the diffusion coefficient was explored by running the model on the straight channel with smooth floodplains using four values for the diffusion coefficient. Initially, a diffusion coefficient of *0.005* was applied and this was increased to values of *0.05*, *0.075* and *0.1*$m^2/s$. Friction coefficients in the floodplain and the main channel were maintained at constant values of *0.013* and *0.028* respectively.

The effect on the simulated water surface slopes and main channel and floodplain flow distributions for these increasing diffusion coefficients is shown in Table 4-9. Variations in the simulated water surface profiles are shown in Figure 4-26.

**Table 4-9 Influence of diffusion coefficient on surface slope and flow distribution**

| Run | Diff. Coeff. ($m^2/s$) | Observed Variables | | | Simulated Variables | | | Percentage Error | | |
|---|---|---|---|---|---|---|---|---|---|---|
| | | $Q_{mc}$ ($m^3/s$) | $Q_{Tot.}$ ($m^3/s$) | $S_w$ (x1000) | $Q_{mc}$ ($m^3/s$) | $Q_{Tot.}$ ($m^3/s$) | $S_w$ (x1000) | $Q_{mc}$ % | $Q_{Tot.}$ % | $S_w$ % |
| SS700-3D_1 | 0.05 | 0.358 | 0.697 | 1.849 | 0.348 | 0.672 | 0.00185 | -2.80 | -3.60 | 0.07 |
| SS700-3D_2 | 0.075 | 0.358 | 0.697 | 1.849 | 0.345 | 0.667 | 0.00185 | -3.60 | -4.30 | 0.20 |
| SS700-3D_3 | 0.1 | 0.358 | 0.697 | 1.849 | 0.343 | 0.665 | 0.00185 | -4.20 | -4.60 | 0.23 |

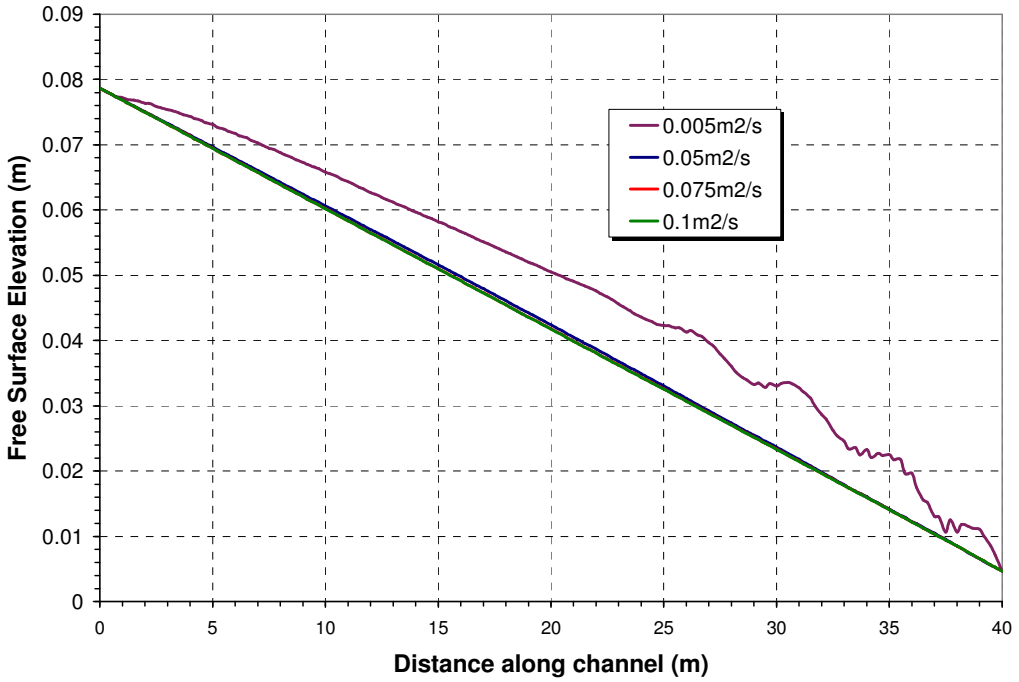


**Figure 4-26 Influence of varying diffusion coefficient on water surface slope**

Table 4-9 and Figure 4-26 indicate that with the exception of the diffusion coefficient of *0.005$m^2/s$* which produced a water surface profile that was unstable at the downstream channel end, little difference exists between the simulated and observed water surface slopes. This similarity results from the prescribed elevation boundary conditions at the upstream and downstream extents of the channel. The fixed nature of these boundary conditions in the model is compensated for by allowing a free or unfixed flow into the model domain. Consequently, the ability of the model to simulate the observed main channel and floodplain flow proportions is a superior indicator of a suitable diffusion coefficient. On this basis, and as shown in Table 4-5, increases in diffusion coefficient result in reduced flows into the system as a whole and also in the main channel and floodplain zones.

Figure 4-27 shows both the observed and simulated main channel and floodplain transverse velocity profiles through the measuring reach (chainage from *34m - 36m*) of the straight channel for the diffusion coefficients in Table 4-9. Simulated point velocities in the main channel and floodplains are depth averaged values and those observed were recorded at 60% of the main channel and floodplain flow depth

measured from the water surface. The considerable scatter in the observed point velocities in the main channel reflects the influence of migrating bedforms that were associated with the FCF Phase C mobile bed experiments. This data therefore represents, in general terms, velocity magnitudes rather than representative variations in velocity across the main channel.

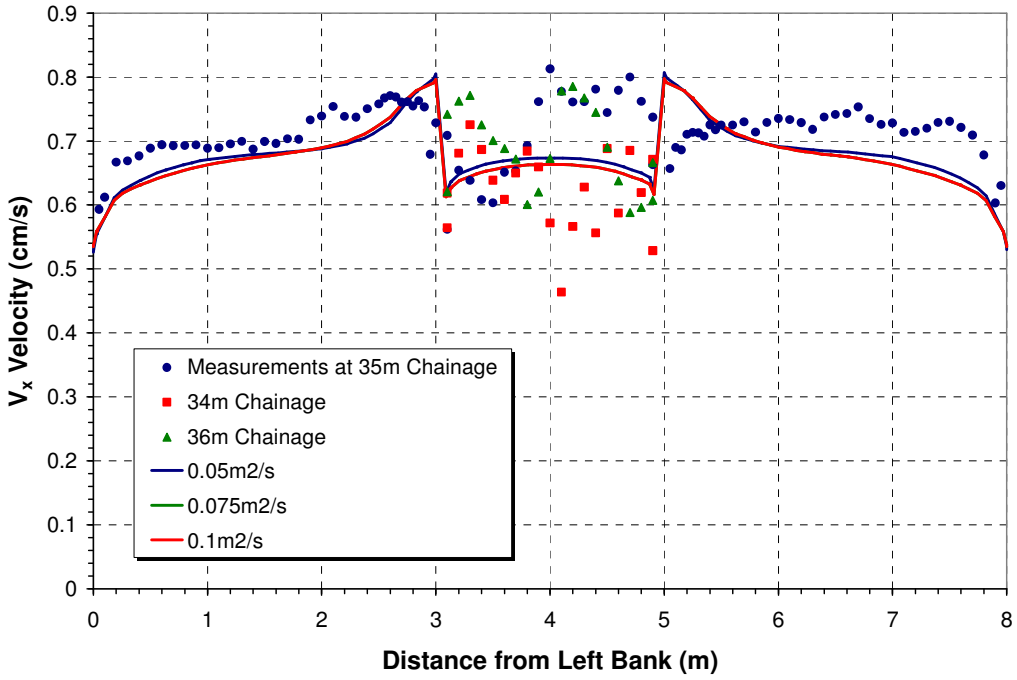


**Figure 4-27 Influence of diffusion coefficient on main channel and floodplain velocity profiles in x-direction**

Figure 4-27 indicates that the velocity profiles in both magnitude and shape are similar for the range of diffusion coefficients investigated. Simulated main channel velocities are highest in the channel centre and decrease as the main channel and floodplain interface approaches. At this point, velocities increase sharply, beyond which values decrease to a more constant value before further decreasing as the floodplain boundary approaches. Figure 4-27 indicates that although reasonably consistent in shape, simulated floodplain profiles show slight underestimates from those measured. Simulations were undertaken with flat or 'screeded' channel beds and although the simulated main channel values do not reflect the scatter of the observed measurements, their magnitudes are considered to be a reasonable estimate of an average of the point velocity measurements.

The TELEMAC-3D model facilitates the variation of velocity with channel depth to be investigated. Simulated vertical velocity profiles in the main channel centre for the range of diffusion coefficients in Table 4-9 are shown with observed values in Figure 4-28.

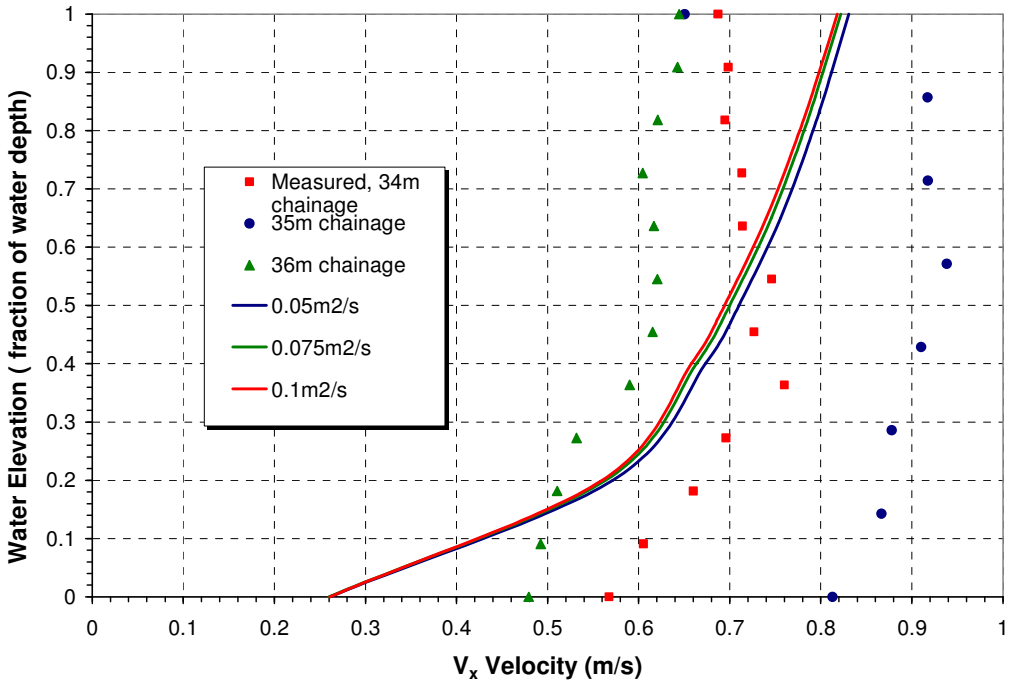


**Figure 4-28 Influence of diffusion coefficient on vertical velocity profiles**

Figure 4-28 shows that simulated vertical velocity profiles while not being significantly influence by varying diffusion coefficient are reasonably consistent with observed values. When comparing this data however, it must be noted that simulated values are determined for flat or 'screeded' channel beds and measured values are influence by the downstream migration of bedforms in the main channel. Consequently a direct comparison of simulated and observed data must be treated with an element of caution.

In summary, variations in diffusion coefficient have little influence on simulated water surface profiles and transverse and vertical velocity profiles. However, as shown in Table 4-9, the simulated flow proportions for model run *SS700-3D_1* correspond most closely with those determined from measured velocity data. The diffusion coefficient for this simulation was *0.05m$^2$/s* and this was adopted for the friction calibration runs.

Channel Friction

In order to facilitate a comparison of friction coefficients from both the measured FCF data and the TELEMAC-2D simulations, the Manning's friction law was again used in the calibration of the TELEMAC-3D model. Due to the variability of friction coefficient in space, there was a need for programming the subroutine STRCHE. The subroutine is the same as that used in the TELEMAC-2D model but the set of variables used and the added program lines for the 3D model were different. In STRCHE, the main channel (*mc*) was assigned a value of Manning's *n* while a separate value for the friction coefficient was assigned for the floodplains (*fp*). The combinations of main channel and floodplain coefficients and the corresponding average water surface slopes and flow distributions are summarised in Table 4-10.

The simulated data in Table 4-10 is determined for a constant diffusion coefficient of $0.05m^2/s$ determined from the initial stage of the calibration process.

**Table 4-10 Effect of varying the main channel and floodplain friction coefficient on the resulting surface slope and flow distribution**

| Run | Manning's n | | Observed Variables | | | Simulated Variables | | | Percentage Error | | |
|---|---|---|---|---|---|---|---|---|---|---|---|
| | mc | fp | $Q_{mc}$ ($m^3/s$) | $Q_{Tot.}$ ($m^3/s$) | $S_w$ (x1000) | $Q_{mc}$ ($m^3/s$) | $Q_{Tot.}$ ($m^3/s$) | $S_w$ (x1000) | $Q_{mc}$ % | $Q_{Tot.}$ % | $S_w$ % |
| SS700-3D_1 | 0.028 | 0.013 | 0.358 | 0.697 | 1.849 | 0.3481 | 0.67 | 0.00185 | -2.77 | -3.56 | 0.07 |
| SS700-3D_4 | 0.025 | 0.013 | 0.358 | 0.697 | 1.849 | 0.3793 | 0.70 | 0.00185 | 5.95 | 0.69 | 0.25 |
| SS700-3D_5 | 0.025 | 0.010 | 0.358 | 0.697 | 1.849 | 0.3789 | 0.79 | 0.00186 | 5.84 | 13.46 | 0.73 |

Table 4-10 indicates that as expected, decreases in the hydraulic resistance of the channel sub-sections results in increases in the flow proportion being conveyed in these sub-sections. Although its main channel flow proportion was underestimated by approximately *6%*, the total flow in model run *SS700-3D_4* correlated most closely with that measured. This main channel and floodplain resistance coefficients for this simulation were *0.025* and *0.013* respectively.

Transverse velocity profiles corresponding to *0.4y* (where *y* is the flow depth) for longitudinal channel chainages of *34m*, *35m* and *36m* are compared to simulated profiles in Figure 4-29 for the combinations of main channel and floodplain resistance coefficients in Table 4-10.

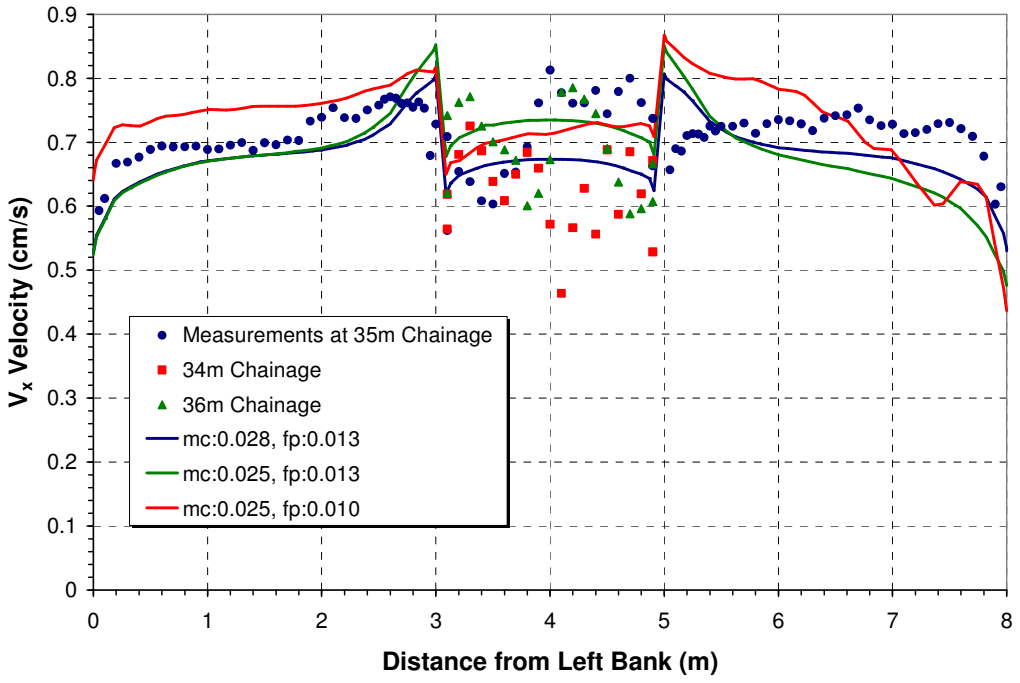


**Figure 4-29 Influence of resistance coefficients on main channel and floodplain velocity profiles (diffusion coefficient: $0.05m^2/s$)**

The asymmetrical profile for model run *SS700-3D_5* in Figure 4-29 indicates that instability of the water mass in the model domain exists for this simulation. This may result from the constraint on the upstream and downstream water levels in addition to an excessive reduction in the friction coefficients. It is noted that the reduction in the main channel friction coefficient between model runs *SS700-3D_1* and *SS700-3D_4* has resulted in an increase in the $V_x$ velocity in the main channel by approximately *0.06m/s* but had little effect if any on the floodplain velocity. However, *SS700-3D_1* shows a superior fit to the measured velocity in the main channel.

Simulated vertical velocity profiles in the water column in the centre of the main channel for the combinations of main channel and floodplain resistance in Table 4-10 are compared to measured profiles in Figure 4-30.

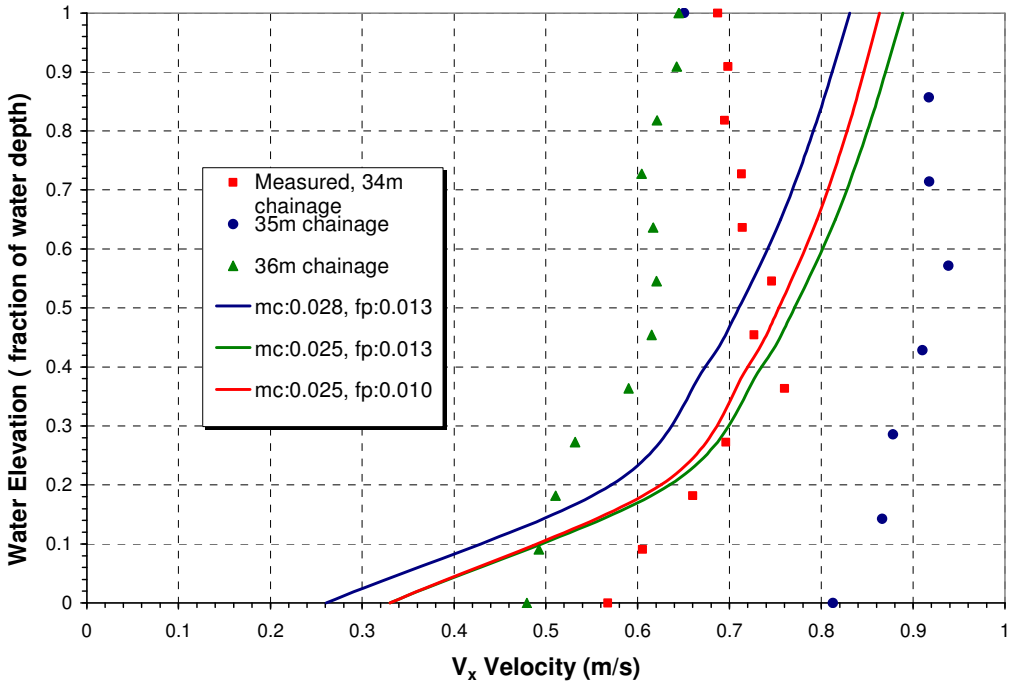


**Figure 4-30 Influence of main channel and floodplain resistance coefficients on vertical velocity profiles**

Figure 4-30 indicates that the highest simulated velocities by approximately *0.05m/s* are produced in model run *SS700-3D_4* for main channel and floodplain resistance coefficients of *0.025* and *0.013* respectively. Based on an analysis of the simulated slope and velocity data it is considered that model run *SS700-3D_1* with a diffusion coefficient of $0.05m^2/s$ and with main channel and floodplain resistance coefficients of *0.028* and *0.013* is considered to optimise the calibration for the $0.697m^3/s$ straight channel test.

### *4.5.3.2 Meandering Channel*

As with the 2D TELEMAC model of the meandering channel, the 3D calibration presented is that for the roughened floodplain $0.6m^3/s$ test.

Diffusion Coefficient and Channel Friction

The sensitivity of the meandering channel model to the variation of diffusion coefficient and friction factor was explored by running the model for a number of diffusion coefficients. The first of these was *0.001m²/s*. A diffusion coefficient of this magnitude required a comparatively small time-step of 0.005s for the model to remain stable. This imposed a significant computational burden on the calibration process and as a result, calibration of the diffusion coefficient was limited to two values of *0.01m²/s* and *0.1m²/s*. These values were compared in combination with a range of slot and floodplain resistance coefficients as summarised in Table 4-11.

**Table 4-11 Calibration data for TELEMAC-3D meandering channel (rough floodplains)**

| Run | Diff. Coeff. ($m^2/s$) | Manning's n | | Observed Variables | | | Simulated Variables | | | Percentage Error | | |
|---|---|---|---|---|---|---|---|---|---|---|---|---|
| | | slot | fp | $Q_{slot}$ ($m^3/s$) | $Q_{Tot.}$ ($m^3/s$) | $S_w$ (x1000) | $Q_{slot}$ ($m^3/s$) | $Q_{Tot.}$ ($m^3/s$) | $S_w$ (x1000) | $Q_{slot}$ % | $Q_{Tot.}$ % | $S_w$ % |
| MR600-3D_1 | 0.01 | 0.0221 | 0.0459 | 0.223 | 0.579 | 1.8593 | 0.18847 | 0.5857 | 0.00220 | -15.42 | 1.16 | 18.50 |
| MR600-3D_2 | 0.01 | 0.0221 | 0.0479 | 0.223 | 0.579 | 1.8593 | 0.18855 | 0.5866 | 0.00225 | -15.39 | 1.32 | 20.90 |
| MR600-3D_3 | 0.01 | 0.0150 | 0.0459 | 0.223 | 0.579 | 1.8593 | 0.19305 | 0.5860 | 0.00218 | -13.37 | 1.21 | 17.30 |
| MR600-3D_4 | 0.1 | 0.0221 | 0.0459 | 0.223 | 0.579 | 1.8593 | 0.18252 | 0.5879 | 0.00244 | -18.10 | 1.55 | 31.30 |
| MR600-3D_5 | 0.1 | 0.015 | 0.0459 | 0.223 | 0.579 | 1.8593 | 0.18666 | 0.5880 | 0.00242 | -16.24 | 1.56 | 30.30 |

Table 4-11 shows the effect of varying the diffusion and friction coefficients on the average water surface slope in the channel and the computed flow composition in the slot *($Q_{slot}$)* and the total flow *($Q_{Tot.}$)*. The surface slope was computed from the water surface elevation (which is an output of TELEMAC-3D). The model also produces as an output the scalar flowrate which was integrated to obtain the flowrate in the main channel and floodplains.

It is observed by comparing model runs *MR600-3D_1* and *MR600-3D_3* to *MR600-3D_4* and *MR600-3D_5* that increases in diffusion coefficient increase the water surface slope. The reason for this is that a more rapid passage of flow through the elements which define the model mesh associated with increasing diffusion coefficients results in a greater mass of water flowing into the domain per time step. This increase has not reflected on the total flow (as it is controlled by the imposition of a boundary condition) but has resulted in a reduction in slot flow in order to increase the floodplain flow (which happens to be the dominant flow conveyer in the channel). In other words, the increase in floodplain flow was on the expense of slot flow.

When comparing model runs *MR600-3D_1* to *MR600-3D_3* and Runs *MR600-3D_4* to *MR600-3D_5* in which the friction coefficient was varied, it was observed that decreasing the roughness in the slot would result in a higher value for flow in the slot ($Q_{slot}$) and a lower water surface slope. This is because reducing the friction would increase the velocity and hence the flow in the slot. On the other hand, increasing the roughness on the floodplain resulted in a slight increase in flow in the slot and also an increase in the surface slope (model runs *MR600-3D_1* and *MR600-3D_2*).

The responses to changes in diffusion and friction coefficients are similar to those obtained in the TELEMAC-2D simulations of the meandering channel in Table 4-7 and Table 4-8. The optimum results were obtained in model run *MR600-3D_3* (Table 4-11) as it resulted in the best slope and flow in the slot.

Measurements of depth averaged overbank velocity components in the longitudinal and transverse channel directions are shown for Apex *M* in Figure 4-31 and Figure 4-32.

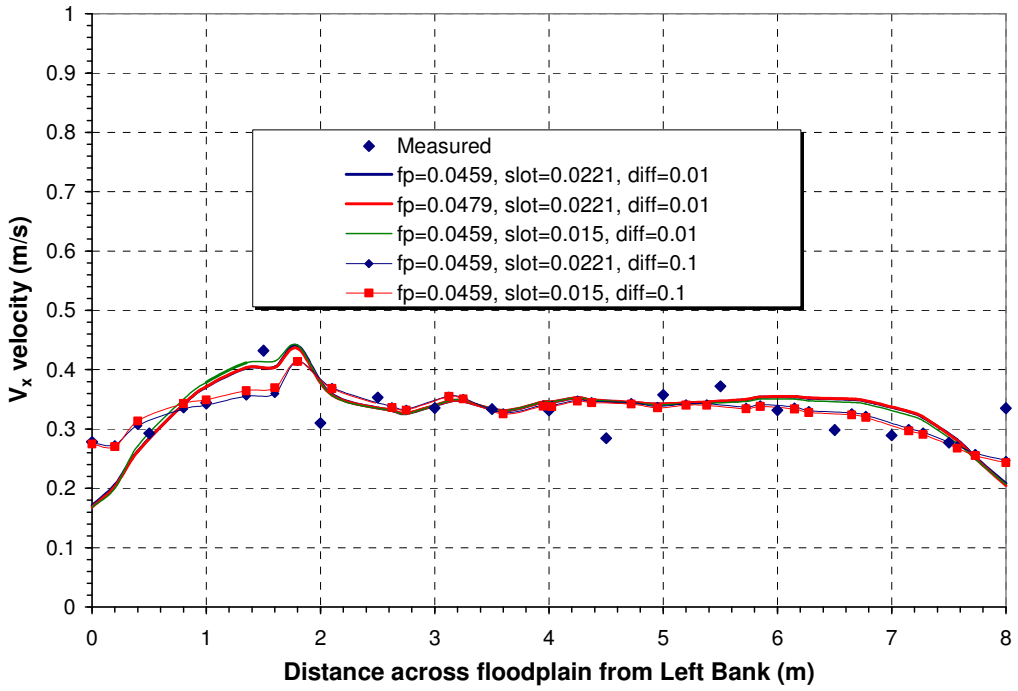


**Figure 4-31 Influence of diffusion and resistance coefficients on velocity profiles in x-direction at Apex *M***

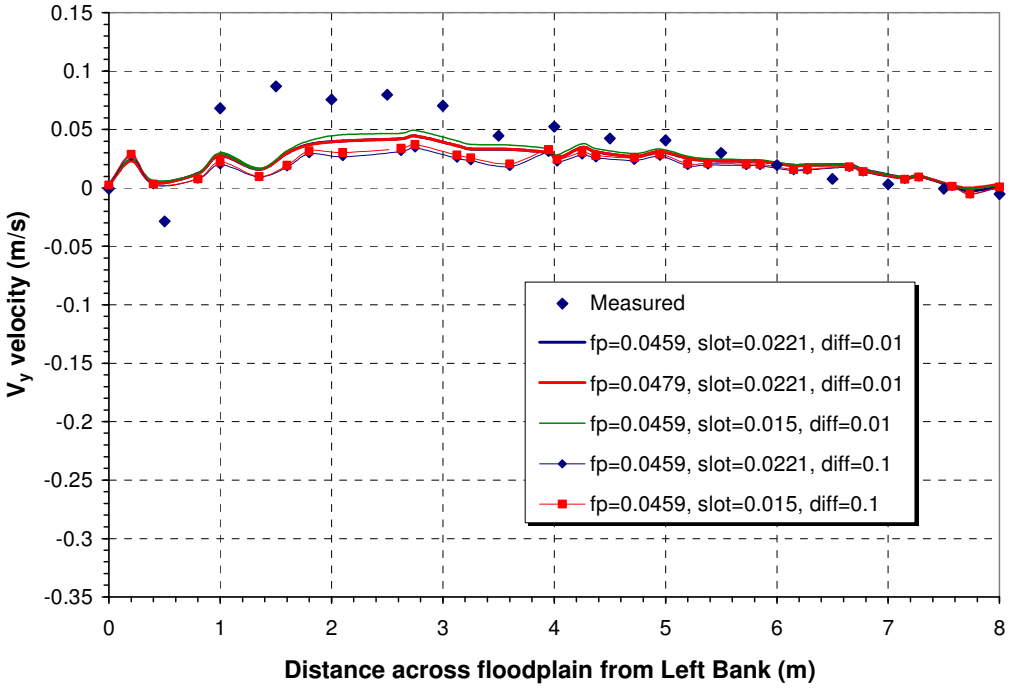


**Figure 4-32 Influence of diffusion and resistance coefficients on velocity profile in y-direction at Apex *M***

The TELEMAC-3D velocities are depth averaged for comparison with measured values recorded at *60%* of the main channel and floodplain depths (measured from water surface). In the legend the runs are labelled according to the assigned value of Manning's *n* of the floodplain (*fp*) and the slot and the corresponding diffusion coefficient.

TELEMAC-3D has satisfactorily simulated the $V_x$ velocities at section *M* but has underestimated the $V_y$ in the vicinity of the slot (Figure 4-32). In Figure 4-31 it is observed that model runs *MR600-3D_4* and *MR600-3D_5* corresponding to a diffusion coefficient of $0.1m^2/s$, have resulted in lower velocities than in other results, the influence being most pronounced in the slot area. This is also evident in Figure 4-32. It can also be observed that for a diffusion coefficient of *0.1* or $0.01m^2/s$, varying the friction coefficient (Manning's *n*) has no effect on the simulated $V_x$ velocities but has slightly changed the $V_y$ velocities.

Good calibration should ensure a good correlation between measured and simulated results at all cross-sections in the channel. Longitudinal and transverse velocity profiles at Cross-over *O* are shown in Figure 4-33 and Figure 4-34.

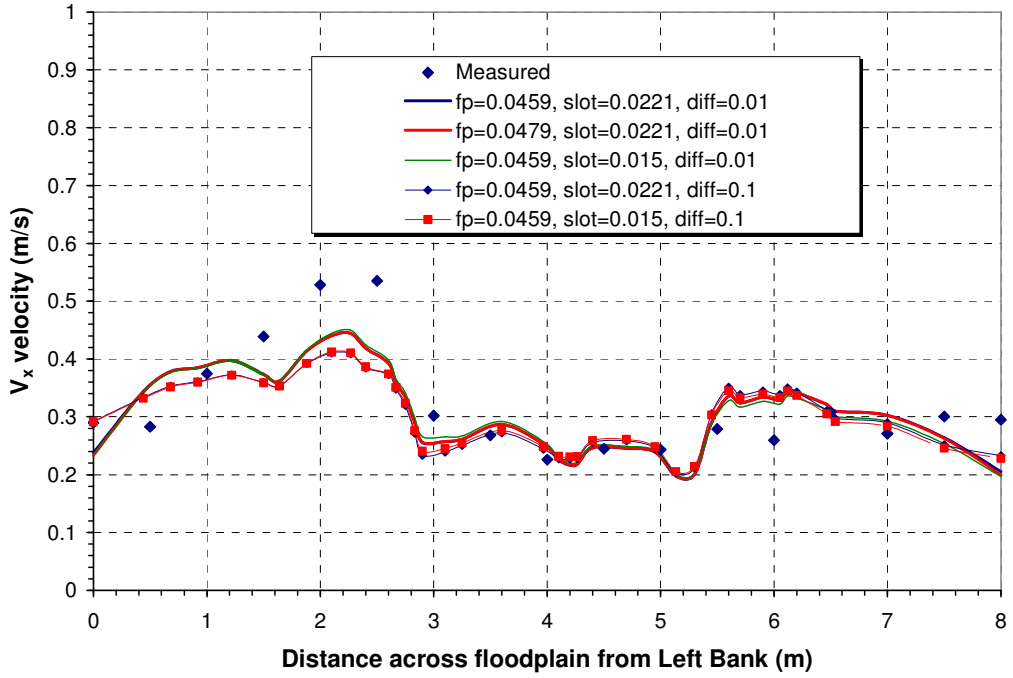


**Figure 4-33 Influence of diffusion and resistance coefficients on velocity profiles in x-direction at Cross-over *O***

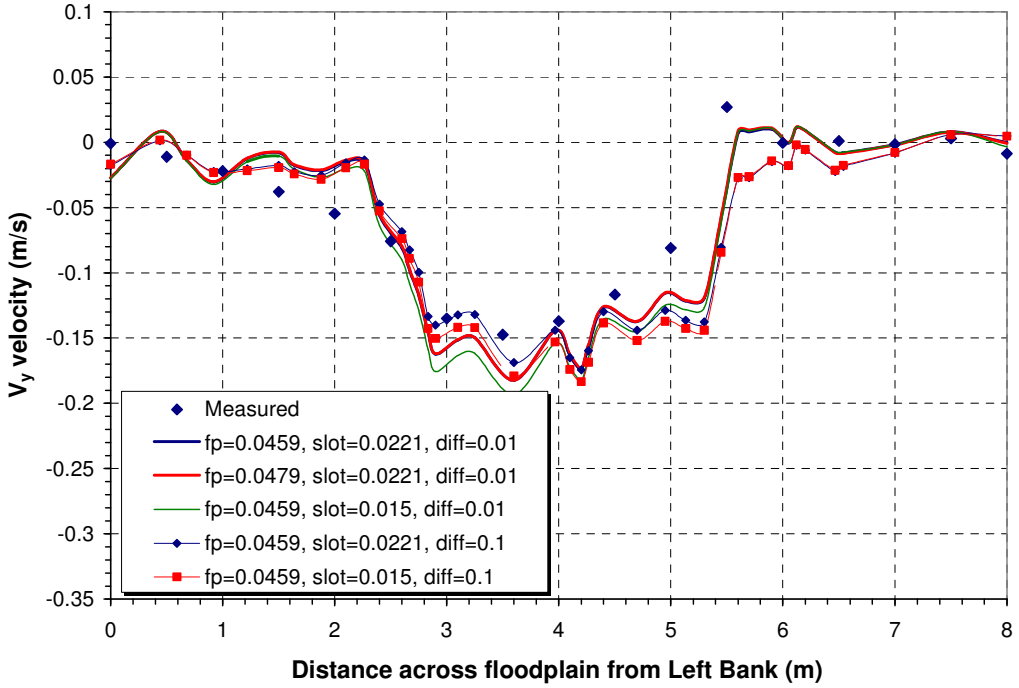


**Figure 4-34 Influence of diffusion and resistance coefficients on velocity profiles in y-direction at Cross-over *O***

Profiles in Figure 4-33 and Figure 4-34 again corresponding to *40%* of the main channel and floodplain depths TELEMAC-3D are a better fit to those presented at the apex section in Figure 4-31 and Figure 4-32 indicating better model performance at cross-over sections of the meandering channel that was tested. Again model runs *MR600-3D_4* and *MR600-3D_5* with diffusion coefficients of $0.1m^2/s$ have resulted in lower velocities than other results. It is also observed that as with apex sections, variations of friction coefficients for diffusion coefficients of *0.1* or $0.01m^2/s$, have little effect on the simulated $V_x$ velocities but do slightly influence the $V_y$ velocities.

## 4.6 Comparison of Models

The above sections detailed the principles of the HEC-RAS and TELEMAC models and the approaches to model calibration adopted in each of the cases. As previously explained, the assessment of the modelling approaches was based on each of the models ability to reproduce the measured results from the Phase *C* mobile bed experimental programme undertaken at the Flood Channel Facility. For the purposes of this report the straight channel calibration process was presented for the $0.7m^3/s$ smooth floodplain test and that for the meandering channel was presented for the $0.6m^3/s$ roughened floodplain test. For full comparison of the models tested, the data set is extended to include data for the $0.6m^3/s$ rough and $0.7m^3/s$ smooth floodplain tests in the FCF straight and meandering channels.

### 4.6.1 Straight Channel

#### *4.6.1.1 Smooth Floodplain Test*

The initial comparison was based on the ability of each of the three models to reproduce the observed water surfaces for the test discharge of $0.7m^3/s$. These are shown in Figure 4-35. Figure 4-35 indicates that measured water surface profiles include fluctuations with time that reflect the migration of bedforms along the channel. Sediment movement was considered to be in a state of dynamic equilibrium during tests.

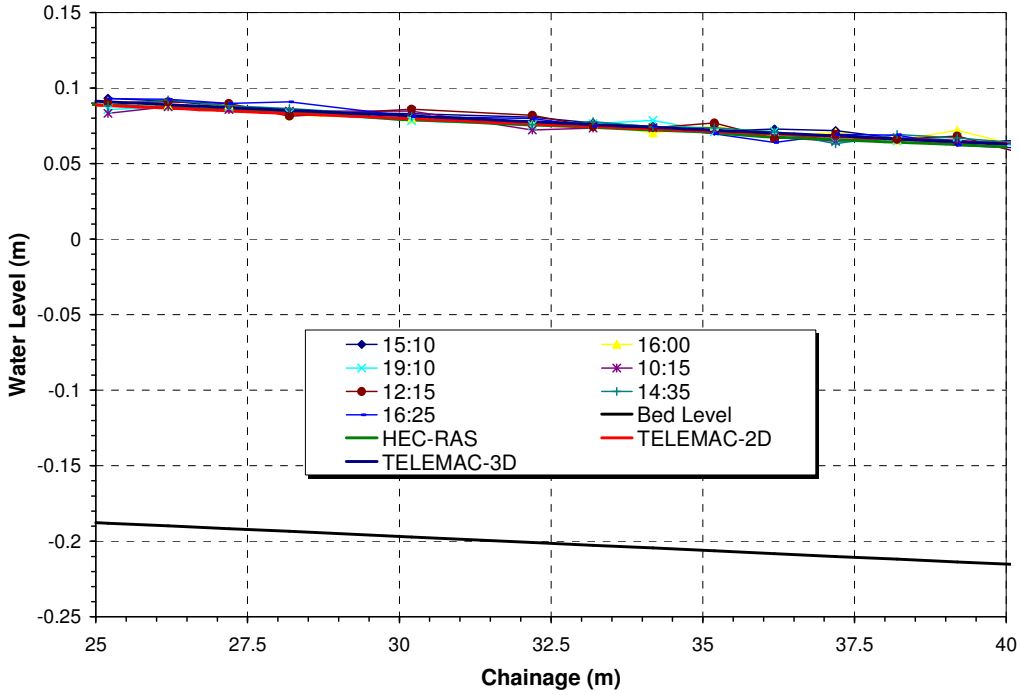


**Figure 4-35 Measured and simulated water surface profiles – *0.7m³/s* straight channel with smooth floodplains**

The data in Figure 4-35 was obtained from the calibrated main channel and floodplain resistance coefficients summarised for the three models in Table 4-12. The error in the computed average water surface slopes in addition to the simulated flow distribution in the channel sub-sections compared to values determined from the integration of velocity measurements is also shown.

**Table 4-12 Comparison of HEC-RAS, TELEMAC-2D and 3D models – *0.7m³/s* straight channel with smooth floodplains**

| Model | Manning's n | | Simulated Variables | | | Percentage Error | | |
|---|---|---|---|---|---|---|---|---|
| | mc | fp | $Q_{mc}$ ($m^3/s$) | $Q_{Tot.}$ ($m^3/s$) | $S_w$ (x1000) | $Q_{mc}$ % | $Q_{Tot.}$ % | $S_w$ % |
| Observed | 0.028 | 0.013 | 0.358 | 0.697 | 0.001850 | --- | --- | ----- |
| HEC-RAS | 0.030 | 0.011 | 0.372 | 0.698 | 0.001868 | 3.90 | 0.14 | 0.97 |
| TELEMAC-2D | 0.023 | 0.011 | 0.390 | 0.700 | 0.001854 | 8.80 | 0.41 | 0.26 |
| TELEMAC-3D | 0.028 | 0.013 | 0.348 | 0.672 | 0.0018541 | -2.80 | -3.56 | 0.07 |

Figure 4-35 indicates that all three models produced a surface slope that is comparable to the measured slope and Table 4-12 shows that the average slope determined from the simulated data in each of the three models is within *1%* of the measured value.

The one-dimensional HEC-RAS model produced this data for calibrated friction coefficients that compared most closely with those determined from measurement with slight underestimation in main channel Manning's n and a slight overestimation in floodplain values. TELEMAC-2D resulted in a slightly lower friction coefficient

in the floodplain but has significantly underestimated Manning's $n$ in the main channel. The discrepancy in the estimation of friction coefficient could be attributed to the difference in the bathymetry between the experiments and the modelled scenarios. The measured/estimated friction coefficients at the UK FCF are those of experiments carried out on a mobile sand bed channel while the simulations were done assuming a flat or 'screeded' bed. Bedforms in the channel might be expected to increase the turbulence and with this, the velocities in the main channel. The effect of underestimation of Manning's $n$ in the main channel has directly reflected on the computed TELEMAC-2D flow distribution. Main channel flows were overestimated by approximately *9%* and this does not compare favourably with HEC-RAS where the error in simulated channel flow was approximately *4%*.

Table 4-12 also indicates that the TELEMAC-3D model has the ability to simulate measured water surfaces for the calibrated resistance coefficients that are similar to those determined from measured data.

Further comparison between TELEMAC-2D and 3D was undertaken to assess the model's ability to measured velocity fields over the compound channel section. HEC-RAS, being a 1D model was not included in this comparison. Measured and simulated transverse velocity profiles in the longitudinal ($V_x$) direction are shown in Figure 4-36. Data corresponds to that determined for *40%* of the main channel and floodplain depth.

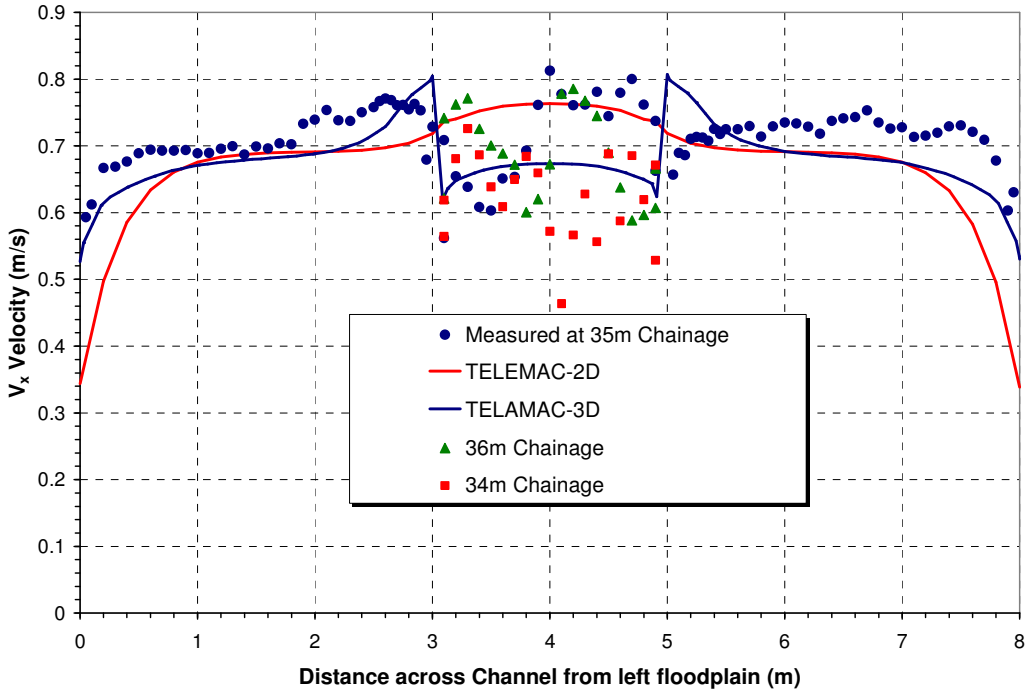


**Figure 4-36 Measured and simulated main channel and floodplain velocity profiles in x-direction (*0.7m³/s* straight channel with smooth floodplains)**

Figure 4-36 indicates that TELEMAC-2D and 3D, while similar in magnitude, have produced profiles that vary in shape. The $V_x$ profile of the TELEMAC-2D model peaks at the mid-point of the main channel and decreases gradually towards the

floodplain. The velocity is fairly constant in the floodplain and then rapidly decreases as the floodplain approaches the tank walls. The 2D model showed a decrease in velocity at the main channel/floodplain interface as a response to the difference in roughness between the main channel and the floodplain. Simulated main channel velocities produced from the 2D model would appear to be higher than those measured. This data contrasts with the 3D profile which shows a marked increase in velocity at the main channel and floodplain interface followed by a reasonably rapid decrease away from the main channel before more constant values are produced. The main channel velocity profile from the 3D model represents a better average of the measured values than from the 2D data set. The high 2D values are associated with the high main channel flow proportion already mentioned.

The trends of the 2D and 3D velocity profiles in Figure 4-36 are also represented in the depth-averaged vector plots in Figure 4-37

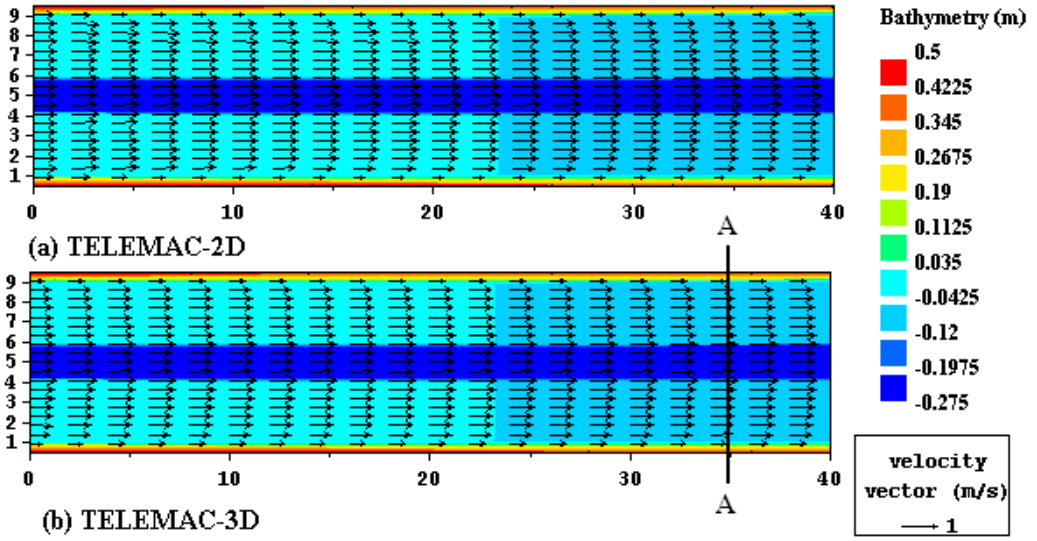


**Figure 4-37 Velocity vector fields produced in the TELEMAC-2D and 3D models (*0.7m³/s* straight channel with smooth floodplains)**

Figure 4-37 shows that the predominant velocity component for both TELEMAC models is in the longitudinal ($V_x$) channel direction. The 2D vector plot again indicated that the velocities are highest in the centre of the main channel, reasonably constant across the floodplains before further decreasing towards the edge of the floodplain. The highest velocity components for the 3D model, as also shown in Figure 4-36, are at the main channel and floodplain interface. These high velocity values at the main channel interface can also be observed in data produced from Section A-A shown in Figure 4-38.

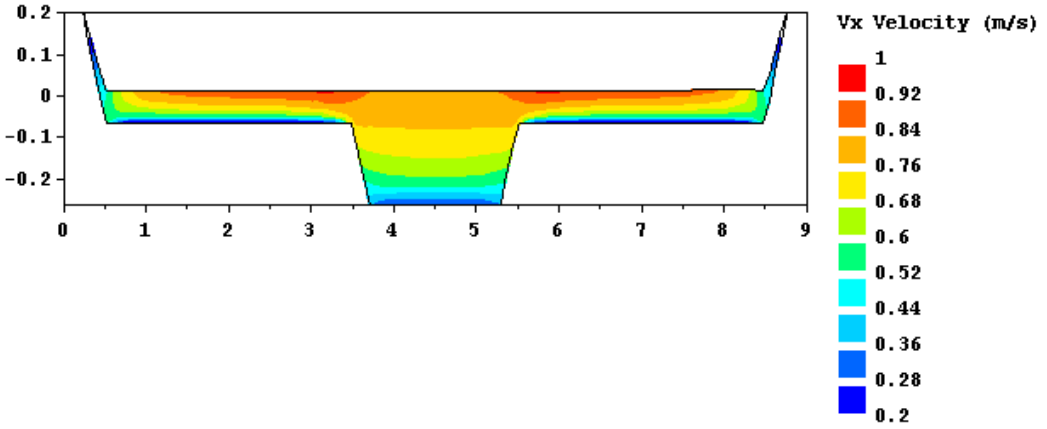


**Figure 4-38 Variation of velocity in x-direction across Section A-A (*0.7m³/s* straight channel with smooth floodplains)**

### *4.6.1.2 Rough Floodplain Test*

Simulated water surface profiles for the *0.6m³/s* straight channel test with roughened floodplains are shown in Figure 4-39 for the HEC-RAS, TELEMAC-2D and 3D models. The calibrated resistance coefficients with computed errors in average water surface slopes and flow proportions are summarised in Table 4-13.

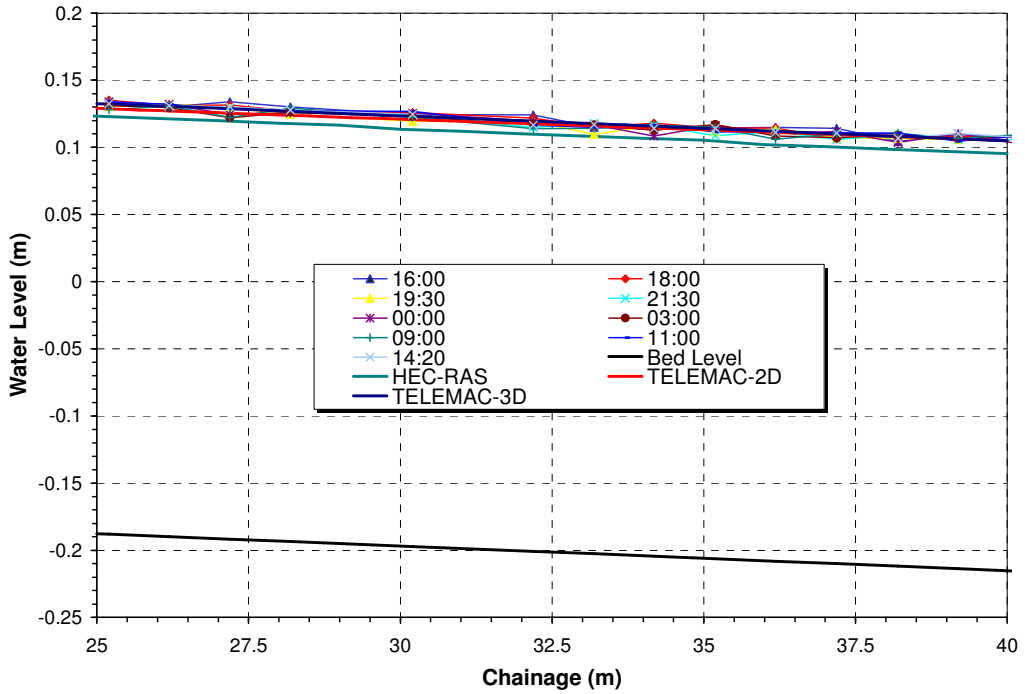


**Figure 4-39 Measured and simulated water surface profiles – *0.6m³/s* straight channel with rough floodplains**

**Table 4-13 Comparison of HEC-RAS, TELEMAC-2D and 3D models – *0.6m³/s* straight channel with rough floodplains**

| Model | Manning's n | | Simulated Variables | | | Percentage Error | | |
|---|---|---|---|---|---|---|---|---|
| | mc | fp | $Q_{mc}$ ($m^3/s$) | $Q_{Tot.}$ ($m^3/s$) | $S_w$ (x1000) | $Q_{mc}$ % | $Q_{Tot.}$ % | $S_w$ % |
| Observed | 0.029 | 0.034 | 0.351 | 0.599 | 0.001843 | ---- | ---- | ---- |
| HEC-RAS | 0.030 | 0.050 | 0.461 | 0.599 | 0.001870 | 31.3 | 0 | 1.5 |
| TELEMAC-2D | 0.026 | 0.030 | 0.367 | 0.602 | 0.001848 | 4.5 | 0.5 | 0.3 |
| TELEMAC-3D | 0.023 | 0.034 | 0.404 | 0.771 | 0.001830 | 14.9 | 28.7 | -0.7 |

Results indicate that as was the case for the smooth floodplain test, all models can produce reasonably accurate water surface profiles. The data in Figure 4-39 is based on the optimised resistance coefficients in Table 4-13 and indicates that calibration for the HEC-RAS model was achieved for a floodplain resistance coefficient of *0.05* compared to the value of *0.034* determined from measured FCF data. This has directly reflected on the simulated main channel flow as the high friction coefficient in the floodplain has significantly reduced the floodplain flow and increased the flow into the main channel resulting in an overestimation of approximately *30%*. Calibrating the simulated TELEMAC-2D model to measured data required resistance coefficients lower than those from the FCF and resulted in an increase in the estimated flow in the main channel. As was the case with the smooth floodplain test data in Table 4-12, calibration of the 3D model for the roughened floodplain required a resistance that was consistent with the FCF value but a main channel coefficient that was significantly underestimated. This in comparison to the 2D model has resulted in a higher proportion of flow being conveyed. The influence of channel bedforms inherent in the measured data is perhaps not being represented in the simulated data and may be contributing to some of the observed variations. The presence of bedforms increases channel turbulence and main channel velocities and this is not reflected in the flat bed condition of the tests that were analysed.

Measured and simulated transverse depth averaged velocity profiles in the longitudinal ($V_x$) direction from the TELEMAC-2D and 3D models are shown in Figure 4-40.

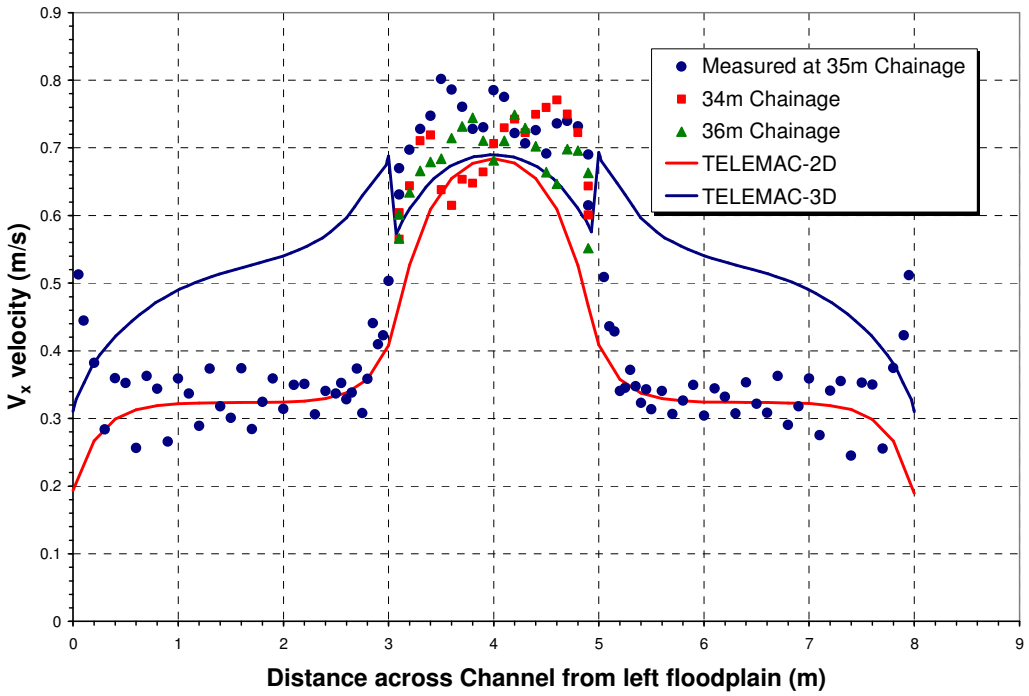


**Figure 4-40 Measured and simulated main channel and floodplain velocity profiles in x-direction (*0.6m³/s* straight channel with rough floodplains)**

Figure 4-40 indicated that again, although similar in magnitude, the two models have produced significant variations in the shape of the $V_x$ velocity profiles. This may suggest differences in the ability of the models to simulate the complexities of the main channel and floodplain interactions that characterise compound channel flows. The $V_x$ profile of the TELEMAC-2D model is at its highest at the centre of the main channel and decreases sharply towards the floodplain. The velocity is fairly constant in the floodplain and then gradually decreases as the floodplain approaches the tank walls. The 2D model satisfactorily reproduced the velocities in the floodplain but has slightly underestimated the main channel velocities by approximately *0.05m/s*. The 3D model showed a better fit to the velocities in the main channel but has failed to capture the velocities in the floodplain.

Trends consistent with the data in Figure 4-40 are shown in the TELEMAC vector plots in Figure 4-41 and the cross-sectional flow field produced by TELEMAC 3D in Figure 4-42.

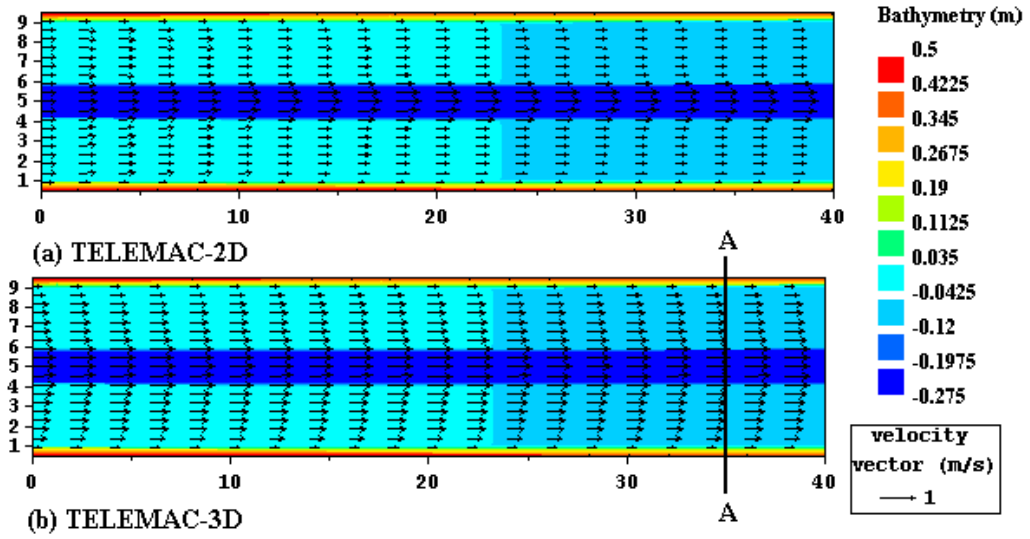


**Figure 4-41 Velocity vector fields produced in the TELEMAC-2D and 3D models (*0.6m³/s* straight channel with rough floodplains)**

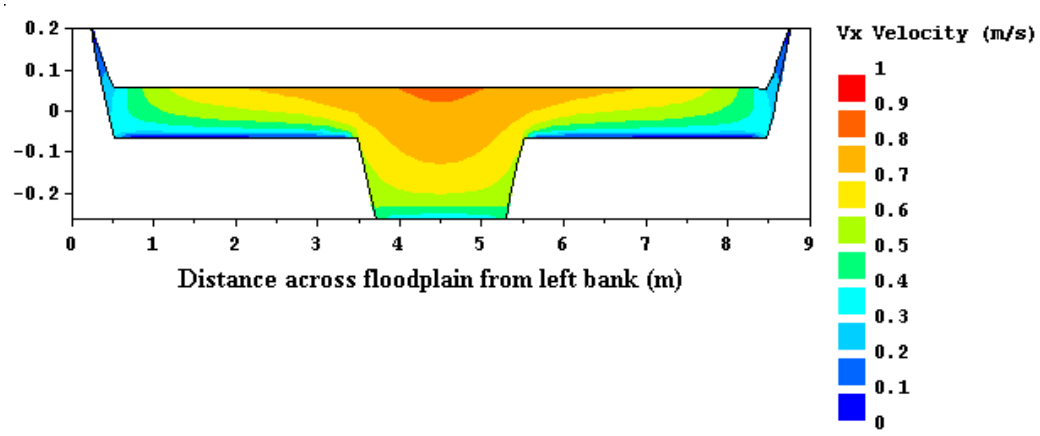


**Figure 4-42 Variation of simulated velocity in x-direction across Section A-A (*0.6m³/s* straight channel with rough floodplains)**

## 4.6.2 Meandering Channel

### *4.6.2.1 Smooth Floodplain Test*

Simulated water surface profiles are compared to observed profiles in Figure 4-43. As discussed in Section 4.2, flow conditions in the FCF were controlled by downstream tailgates. Individual experiments required testing flow conditions for a range of tailgate settings until a quasi-uniform flow was obtained. Although the recirculation system ensured that overall sediment volumes remained in equilibrium for the duration of all tests (sediment loads being added at the upstream channel end equalled that leaving at the downstream, channel end), bedforms were continuously

migrating in the channel, resulting in fluctuations in water level at given locations with time. The calibration data for which the profiles were obtained are summarised in Table 4-14. Simulated flow distributions in the channel sub-sections are also shown in Table 4-14.

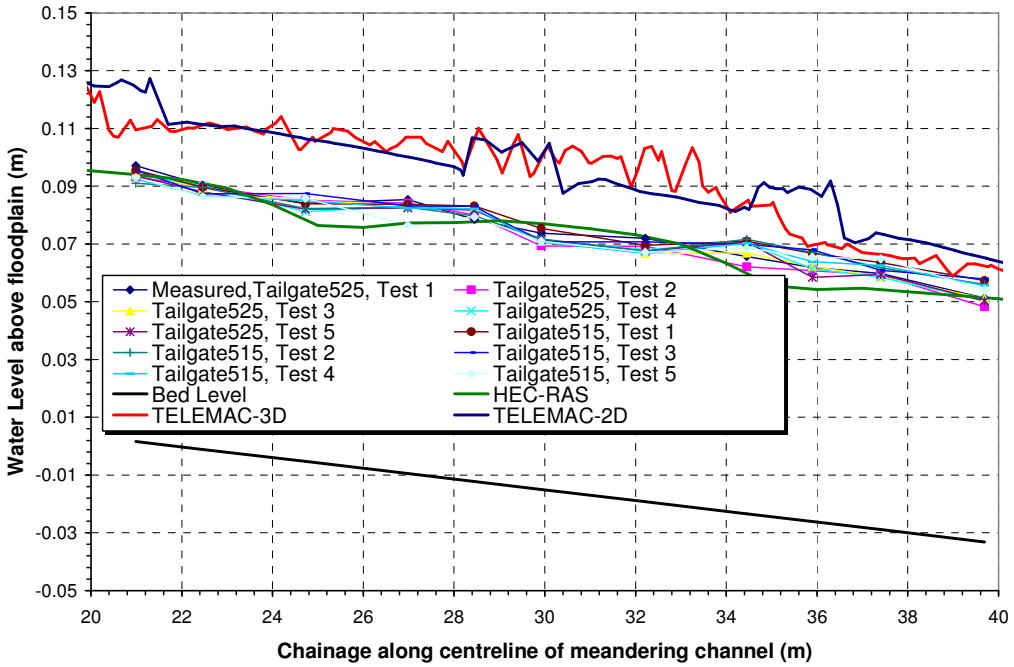


**Figure 4-43 Measured and simulated water surface profiles (*0.6m³/s* meandering channel with smooth floodplains)**

**Table 4-14 Comparison of HEC-RAS, TELEMAC-2D and 3D models (*0.6m³/s* meandering channel with smooth floodplains)**

| Model | Manning's n | | Simulated Variables | | | Percentage Error | | |
|---|---|---|---|---|---|---|---|---|
| | slot | fp | $Q_{slot}$ ($m^3/s$) | $Q_{Tot.}$ ($m^3/s$) | $S_w$ (x1000) | $Q_{slot}$ % | $Q_{Tot.}$ % | $S_w$ % |
| Observed | 0.017 | 0.015 | 0.201 | 0.589 | 0.00186 | ---- | ---- | ------ |
| HEC-RAS | 0.028 | 0.016 | 0.215 | 0.589 | 0.00167 | 7.0 | 0 | -10.0 |
| TELEMAC-2D | 0.017 | 0.025 | 0.213 | 0.598 | 0.00243 | 6.0 | 1.5 | 30.5 |
| TELEMAC-3D | 0.015 | 0.015 | 0.219 | 0.598 | 0.00294 | 9.3 | 1.5 | 58.1 |

Figure 4-43 indicated superior performance of HEC-RAS in simulating observed water surface profiles than both TELEMAC-2D and 3D which produced profiles of greater average depth than those measured. Discrepancies averaged over the profile through the measuring reach were approximately *0.04m*.

Results indicate that calibration of the HEC-RAS model required significantly higher resistance coefficients in the channel slot than those determined from measured data and reflects the inability of the 1D model to account for the complexities of main channel and floodplain interactions that are significant in meandering channels. Even with these high values, slot discharges were overestimated by *7%*. TELEMAC-2D

resistance coefficients in the floodplain were higher than those determined from measured data and contributed to the significant discrepancy in the simulated water surface profile which was *30.5%* higher than the observed profile. TELEMAC-3D simulations, although corresponding reasonably well to the FCF values, result in a water surface profile, the slope of which is significantly overestimated.

Velocity profiles produced by the TELEMAC-2D and 3D models in the longitudinal ($V_x$) and transverse ($V_y$) channel directions are shown for Apex *M* and Cross-over *O* in Figure 4-44 to Figure 4-47.

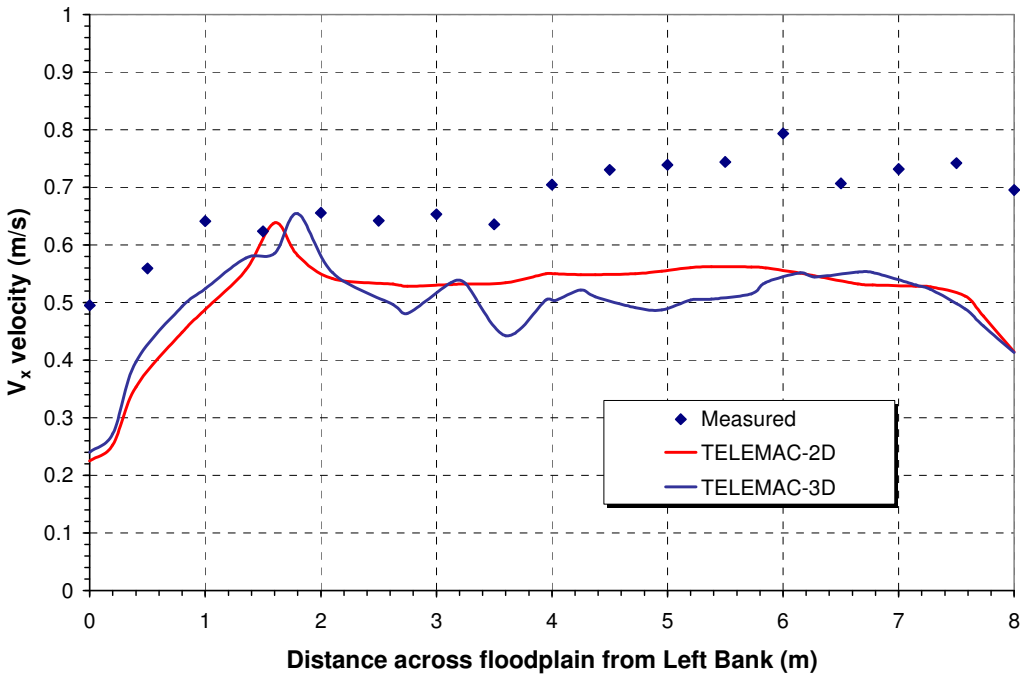


**Figure 4-44 Measured and simulated velocity profiles in x-direction at Apex *M* (*0.6m$^3$/s* meandering channel with smooth floodplains)**

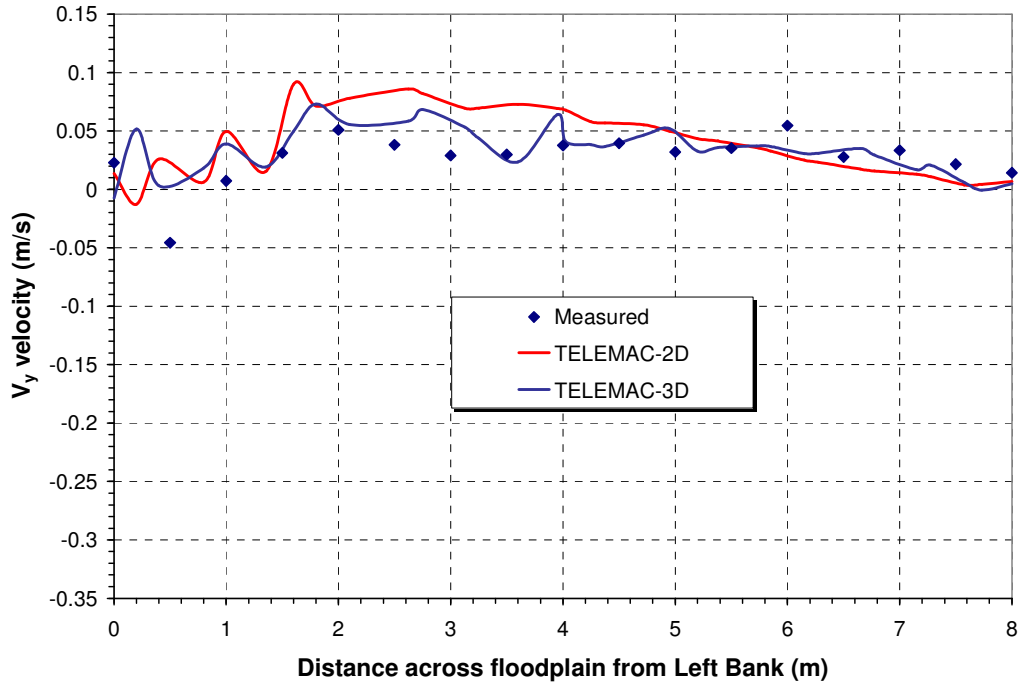


**Figure 4-45 Measured and simulated velocity profiles in y-direction at Apex *M* (*0.6m³/s* meandering channel with smooth floodplains)**

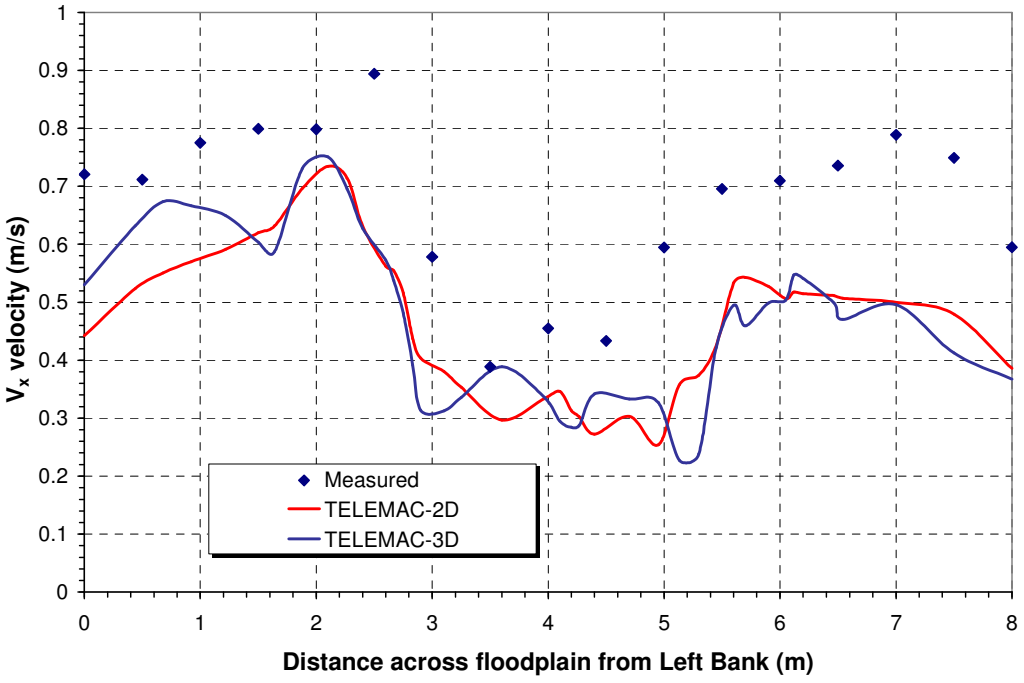


**Figure 4-46 Measured and simulated velocity profiles in x-direction at Cross-over *O* (*0.6m³/s* meandering channel with smooth floodplains)**

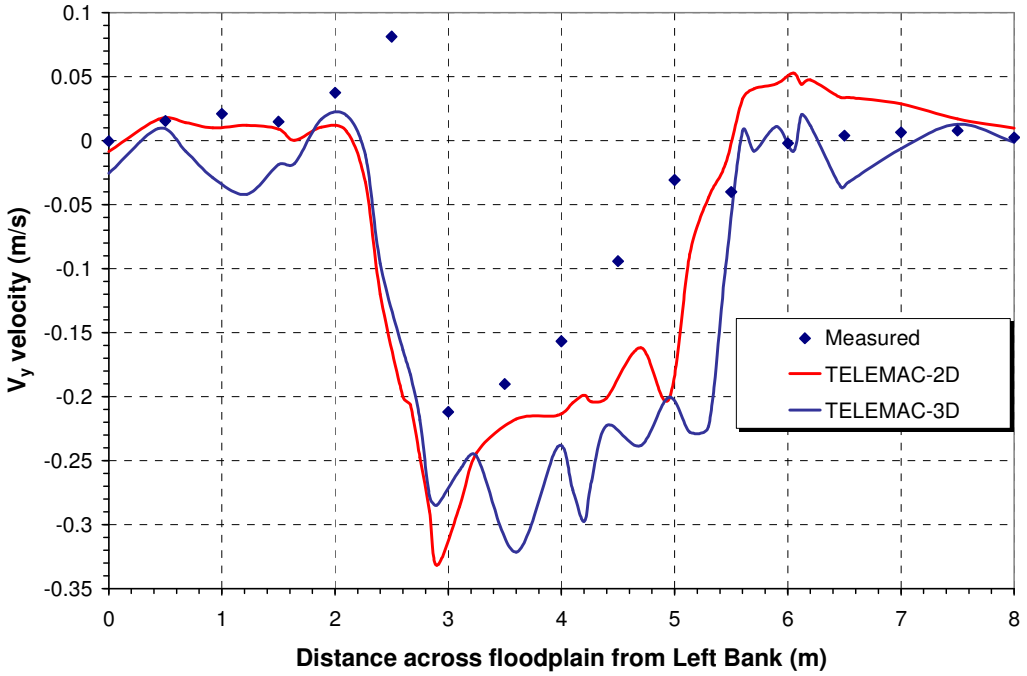


**Figure 4-47 Measured and simulated velocity profiles in y-direction at Cross-over *O* (*0.6m³/s* meandering channel with smooth floodplains)**

Figure 4-44 to Figure 4-47 indicate that both models capture the changing patterns of the $V_x$ and $V_y$ velocity components although some discrepancies do exist in velocity magnitude. However, these discrepancies may be considered to be within acceptable limits.

Velocity vector outputs from the TELEMAC-2D and 3D models and cross-sectional velocity profiles from the 3D model at Apex *I* and *M* are shown in Figure 4-48 and Figure 4-49.

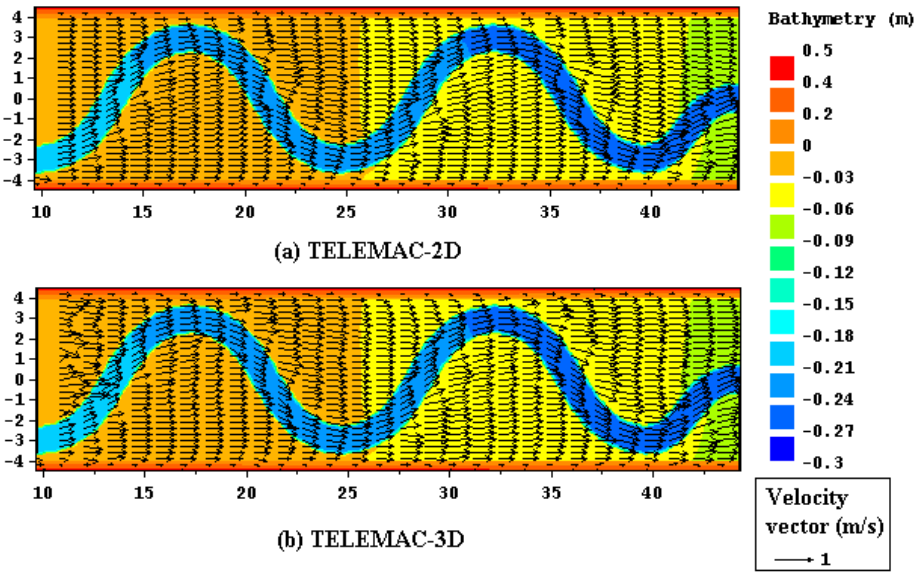


**Figure 4-48 Velocity vector fields produced in the TELEMAC-2D and 3D models (*0.6m³/s* meandering channel with smooth floodplains)**

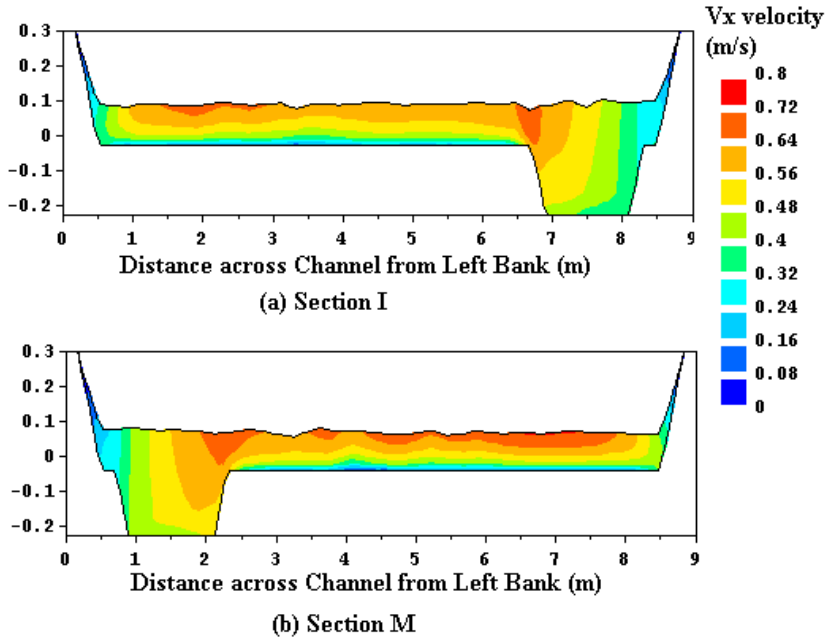


**Figure 4-49 Variation of simulated velocity in x-direction across Apex sections (*0.6m³/s* meandering channel with smooth floodplains)**

Figure 4-48 shows that a significant velocity component below bankfull is in the main channel direction and that on the overbank region is in the valley direction. The plots that the overbank and inner channel interactions result in floodplain and main channel

interactions results in deviated and reduced velocity values in the overbank flow immediately above the slot. This is due to the retarding effect of the slower moving inbank flow which primarily follows the direction of the main channel. The output from the 3D model shows inconsistencies at the upstream end of the channel and these can be attributed to instabilities in the computational model associated with initial (entry) conditions.

### *4.6.2.2 Rough Floodplain Test*

Simulated water surface profiles for the $0.6m^3/s$ meandering channel test with roughened floodplains are shown in Figure 4-50 for the models tested. The calibrated resistance coefficients with computed errors in average water surface slopes and flow proportions are summarised in Table 4-15.

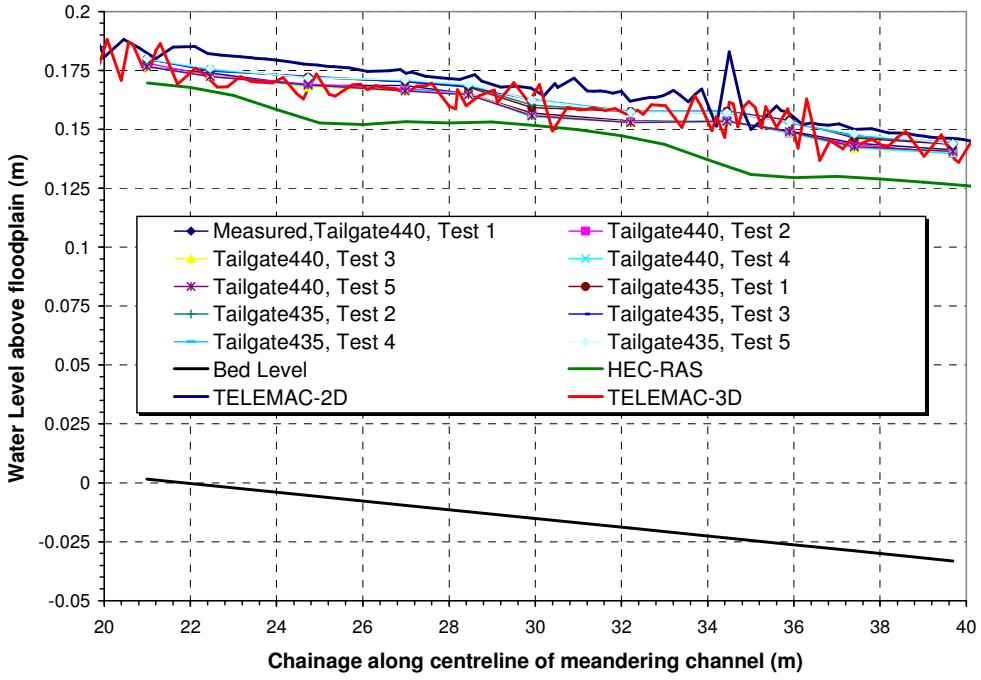


**Figure 4-50 Measured and simulated water surface profiles ($0.6m^3/s$ meandering channel with rough floodplains)**

**Table 4-15 Comparison of HEC-RAS, TELEMAC-2D and 3D models ($0.6m^3/s$ meandering channel with roughened floodplains)**

| Model | Manning's n | | Simulated Variables | | | Percentage Error | | |
|---|---|---|---|---|---|---|---|---|
| | slot | fp | $Q_{slot}$ ($m^3/s$) | $Q_{Tot.}$ ($m^3/s$) | $S_w$ (x1000) | $Q_{slot}$ % | $Q_{Tot.}$ % | $S_w$ % |
| Observed | 0.022 | 0.046 | 0.2228 | 0.5790 | 0.00186 | ---- | ---- | ------ |
| HEC-RAS | 0.028 | 0.070 | 0.3360 | 0.5790 | 0.00170 | 51.0 | 0 | -8.4 |
| TELEMAC-2D | 0.015 | 0.046 | 0.1980 | 0.5830 | 0.00184 | -11.1 | 0.6 | -0.9 |
| TELEMAC-3D | 0.015 | 0.046 | 0.1930 | 0.5860 | 0.00218 | -13.4 | 1.2 | 17.3 |

Figure 4-50 demonstrates that as with the smooth floodplain tests, TELEMAC-2D and TELEMAC-3D profiles overestimate the measured water depths. Depths were underestimated in the HEC-RAS model. The HEC-RAS model required a very high estimate for the friction coefficient in the floodplain to reproduce the FCF measured data. This has significantly reduced the overbank flow leading to an overestimation of slot flow by *51%*. Both the TELEMAC-2D and TELEMAC-3D models were calibrated with significantly underestimated friction coefficient in the channel slot. The discrepancy in the estimation of friction coefficient could perhaps be explained by the difference in the bathymetry between the experiments and the modelled scenarios. The measured/estimated friction coefficients at the UK FCF are those of experiments carried out on a mobile sand bed channel while the simulations were done assuming a flat/screeded sand bed.

Velocity profiles across the channel in the x-direction and y-direction are shown in Figure 4-51 and Figure 4-52.

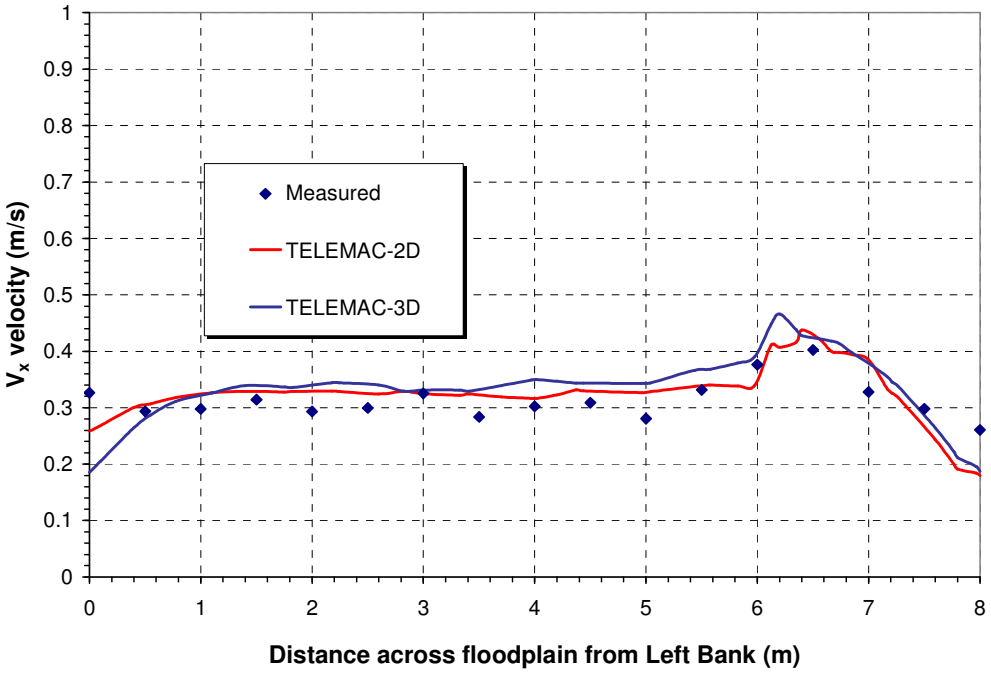


**Figure 4-51 Measured and simulated floodplain velocity profiles in x-direction at Apex *I* (*0.6m$^3$/s* meandering channel with rough floodplains)**

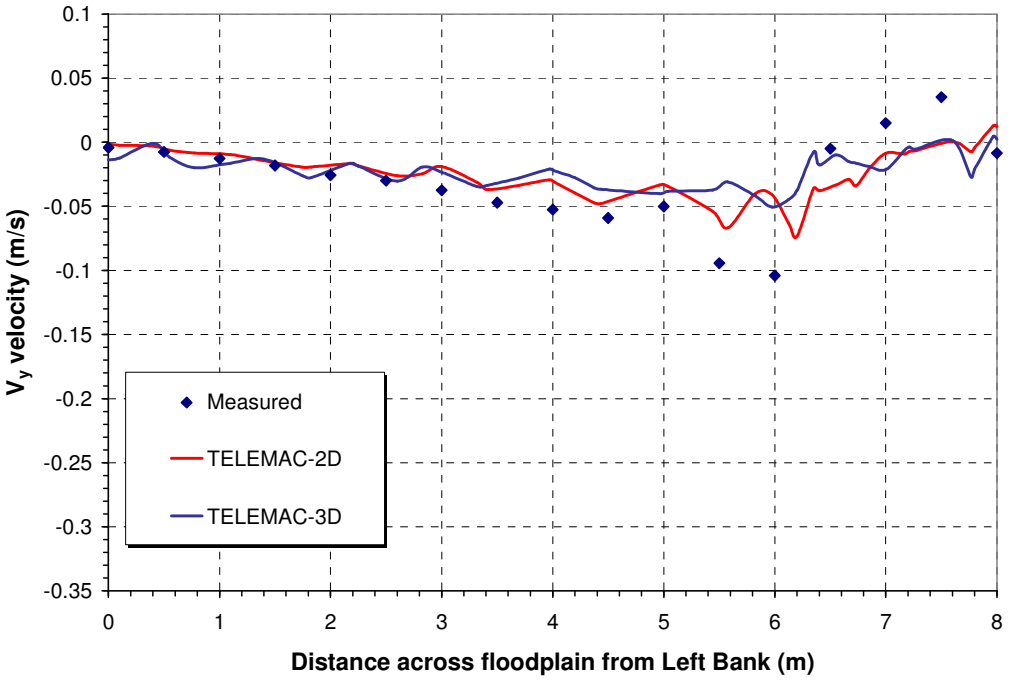


**Figure 4-52 Measured and simulated floodplain velocity profiles in y-direction at Apex *I* (*0.6m³/s* meandering channel with rough floodplains)**

Overbank velocities in the longitudinal channel direction, $V_x$, reflect the surface penetrating nature of the roughness elements and are in the same order of magnitude across the channel that fluctuates around a value of approximately *0.3m/s* until the flow approaches the inner channel. At this point the longitudinal velocities, $V_x$, increase sharply and transverse components, $V_y$, decrease and show significant negative velocities across the slot. These sudden velocity changes highlight the plunging nature of the flow in the proximity of a meander bend as water from both left and right floodplains flows towards the inner channel. This behaviour was satisfactorily simulated by both TELEMAC-2D and TELEMAC-3D which show the sharp increase in $V_x$ coupled with the decrease in $V_y$ in the vicinity of the slot.

Vector data produced for this test generated from the 2D and 3D models is shown in Figure 4-53 and cross-section velocity fields are shown in Figure 4-54 for Apex *I* and Apex *M*.

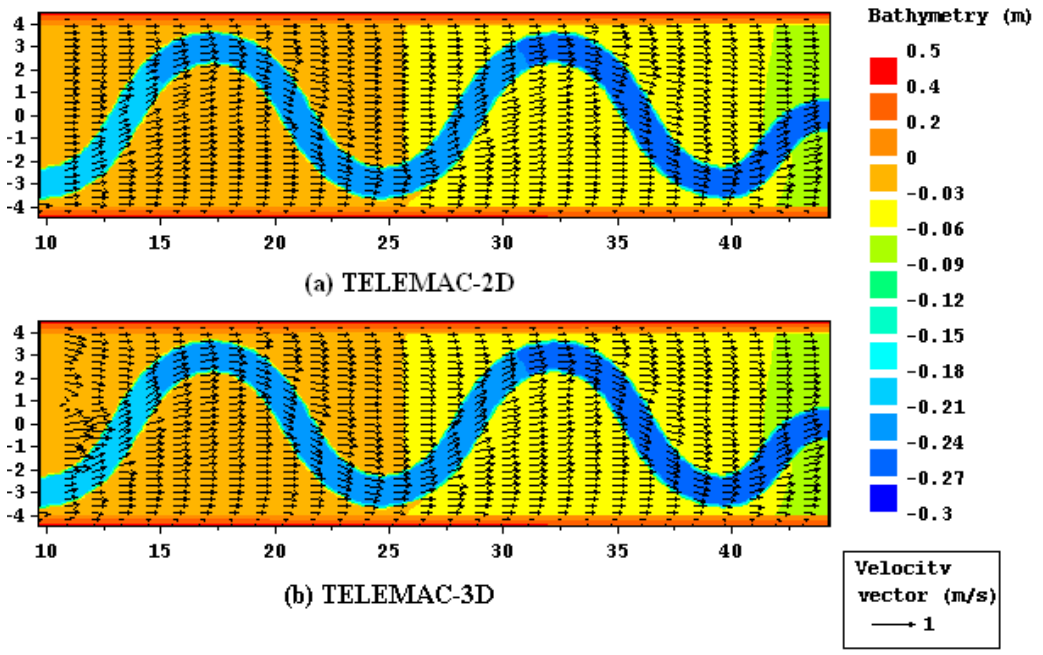


**Figure 4-53 Velocity vector fields produced in the TELEMAC-2D and 3D models (*0.6m³/s* meandering channel with rough floodplains)**

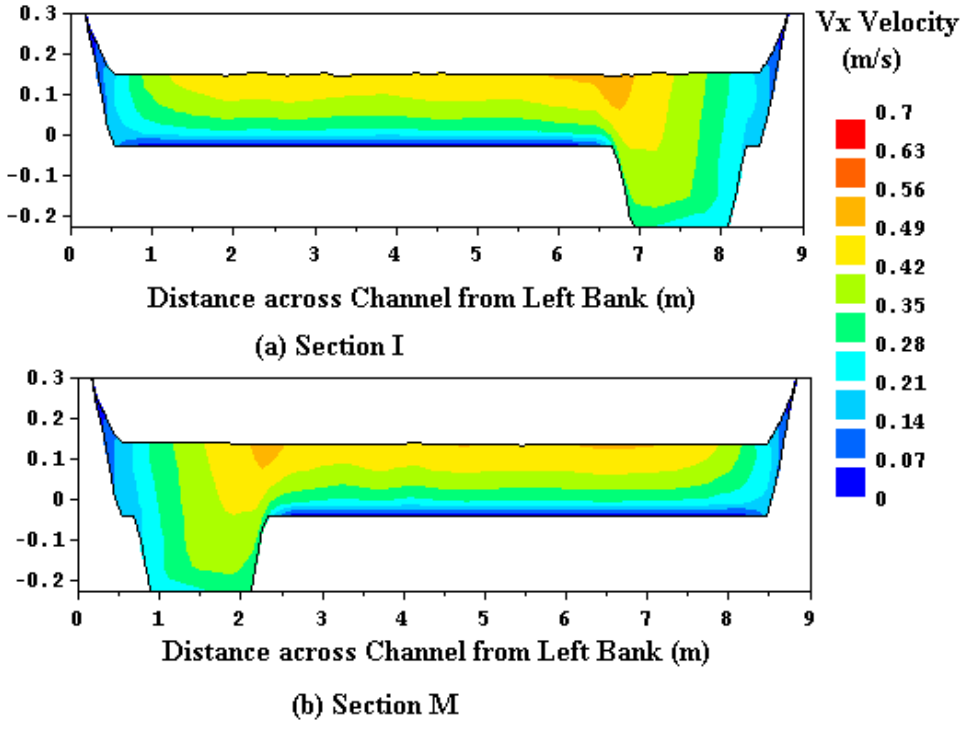


**Figure 4-54 Variation of simulated velocity in x-direction at Apex I (top) and Apex M (*0.6m³/s* meandering channel with rough floodplains)**

# 5 Indexing of Floodplain Effects

## 5.1 Introduction

Attenuation of flood peaks due to floodplain storage is common, particularly in rivers with low slopes and it is suggested that the consequent suppression of flood growth is widespread for most Irish rivers. The effect may be greater than that experienced in the UK and may, in part, explain why many growth curves in Ireland are mildly graded.

To develop a reliable future flood frequency estimation procedure, some means of either indexing the effect or treating it separately is required. The objective of this study is to index floodplain attenuation effects on flood frequency for design floods. The shape, the size, the extent, and the spread of floodplains are important in this regard and are the end-products of the dynamics of streams and river systems which have been working on the earth's crust from prehistoric times (Bhowmik, 1984).

The prediction of a design flood hydrographs at a particular site on a river may be based on the derivation of a discharge or stage hydrograph at an upstream section, together with a method to route this hydrograph through downstream sections (NERC, 1975). Floodplain attenuation effects are known to alter the timing and magnitude of large flood peaks in natural rivers when flood waves travel along a channel. A one-dimensional flood routing model (HEC-RAS) was used in this study to simulate the propagation of the flood wave downstream and to explore the influence of a range of floodplain hydraulic and geometric properties and hydrograph properties on both its peak and delay. This approach required that inflow hydrographs from a known flood frequency distribution (EV1) were derived for selected return periods. A comparison of these inflow hydrographs with those simulated through the computer modelling facilitated an assessment of various floodplain and main channel properties together with hydrograph properties on flood peak attenuation and on the delay of propagation of flood waves along a channel. A multi-variate regression model that included these parameters was developed to provide indices for peak flow attenuation and the delay in flood wave propagation.

## 5.2 Flood Routing Approach

In addition to estimating flood peaks at a single location, the engineer may require estimates of both stage and discharge along a watercourse resulting from the passage of a flood wave. Flood routing is used for this purpose and its importance is reflected in the large number of flood routing methods that have been developed since the early

1900's (NERC, 1975).

Flood-routing procedures may be classified as either hydrological or hydraulic (Choudhury *et al*., 2002). Hydrological methods use the principle of continuity and an empirical or assumed relationship between discharge and the temporary storage volumes of water during the flood period (Shaw, 1994). A typical example of a simple hydrological flood-routing technique used in natural channels is the Muskingum flood-routing method (Shaw, 1994).

Hydraulic methods of routing involve the numerical solutions of either the convective diffusion equation or the one–dimensional Saint–Venant equation of gradually varied unsteady flow in open channels (Tewolde and Smithers, 2006). The factors that should be considered in selecting a method include the floodplain characteristics, channel slope, hydrograph characteristics, the overall flow network and the flow regime (sub critical or supercritical flow). The presence of backwater effects are also important.

Furthermore, the selection of a routing model is also influenced by the required accuracy, the type and availability of data, the available computational facilities, the computational costs, the extent of flood information desired and the familiarity of the user with a given model (NERC, 1975).

The prediction of flows over a complex topography remains a challenging area in floodplain hydraulics, particularly for 1-D models where results are more susceptible to variations in topographical features within a floodplain. Furthermore, 1-D models comprising a network of channels, while suitable for many applications, do not allow for point changes in the direction of water flow at a point. Issues of this type are better dealt with in 2-D models.

In this study, the one-dimensional Saint-Venant equations of gradually varied unsteady flow are used to investigate the influence of floodplain hydraulic and geometric properties on flood peaks. The adopted methodology involves solving these equations using the HEC-RAS 1-D flood routing model. HEC-RAS is a 1-Dimensional link and node river model that has and continues to be developed by the US Army Corps of Engineers. Unsteady or dynamic conditions are analysed in the study to account for the influence of channel storage on the shape and peak of the flood hydrograph as it propagated down the channel. Such influences would not be assessed by executing the channel in steady-state mode. In addition, the issues with topographical variations in the floodplain topography and their potential impact on the results from 1-D models are minimised by assuming uniformity along and across channel floodplains. An evaluation of 1-D and 2-D models (Horritt and Bates, 2002) indicates for situations of river flood inundation, both model types are capable of predicting flood extent and travel times to similar levels of accuracy at optimum calibration. The use of a 1-D model in this case is further supported by previous research where channel routing by numerical integration of the Saint-Venant equations has been shown to be appropriate (e.g. Amein, 1968, Amein and Fang, 1970, Samuels, 1985). A further benefit of the HEC-RAS model is that it is readily available and has the required flexibility to perform flood routing for various floodplain geometric configurations.

For unsteady flow, the HEC-RAS model solves the full 1D dynamic Saint-Venant equations using an implicit, finite difference method. These equations are expressed as:

$$\frac{\partial A}{\partial t} + \frac{\partial \phi Q}{\partial x_c} + \frac{\partial (1-\phi) Q}{\partial x_f} = 0 \qquad \textbf{Eqn. 5.1}$$

$$\frac{\partial Q}{\partial t} + \frac{\partial}{\partial x_c}\left(\frac{\phi^2 Q^2}{A_c}\right) + \frac{\partial}{\partial x_f}\left(\frac{(1-\phi)^2 Q^2}{A_f}\right) + gA_c\left(\frac{\partial z}{\partial x_c} + S_c\right) + gA_f\left(\frac{\partial z}{\partial x_f} + S_c\right) = 0 \qquad \textbf{Eqn. 5.2}$$

where $\phi = \frac{K_c}{K_c + K_f}$, $K = \frac{A^{5/3}}{nP^{2/3}}$, $S_c = \frac{\phi^2 Q^2 n_c^2}{R_c^{4/3} A_c^2}$ and $S_f = \frac{(1-\phi)^2 Q^2 n_f^2}{R_f^{4/3} A_f^2}$

In these equations, $Q$ is the total flow down the reach, $A_c$ and $A_f$ are the cross sectional areas of the flow in the main channel and floodplain, $x_c$ and $x_f$ are distances along the channel and floodplain (these may differ between cross sections to allow for channel sinuosity), $P$ is the wetted perimeter, $R$ is the hydraulic radius $(A/P)$, $n$ is the Manning's roughness value and $S$ is the friction slope. The parameter $\phi$ specifies how flow is partitioned between the floodplain and main channel and as shown, is dependent on the conveyance in the main channel and floodplain, represented by $K_c$ and $K_f$ respectively. These equations are discretised using the finite difference method and solved using a four point implicit (box) method.

## 5.3 Methodology

The main objective of this study was to develop simple indices that allow floodplain influences on both the attenuation of flood peak and the delay in flood wave propagation to be properly accounted for in flood estimation methodologies. The approach adopted in this study involved a numerical solution of the one–dimensional Saint–Venant equations of gradually varied unsteady flow in open channels. Solutions to the equations were obtained for hydrographs with peaks of known return period using the HEC-RAS river modelling software by routing these hydrographs through a generalised reach of the River Suir in Co. Tipperary. Basing the model on geometrical properties of the River Suir ensured that its scale and slope were within the limits of a channel that may typically be affected by floodplain effects. Furthermore, the River Suir and its tributary network form the basis of the case study in which the index is to be validated. The generalised model facilitated a detailed investigation of floodplain effects for a broad range of dimensions and parameters.

The approach adopted in this study to examine the effects of channel and floodplain properties on downstream flood frequency distributions was assessed in the generalised model using a three step approach:

(1) Select the maximum flow for a given return period from a specified flood frequency distribution (EV1) at the upstream end of the channel reach. Hydrographs with a common base length and similar shapes are defined for each peak flood flow magnitude derived from the postulated parent distribution.

    Natural hydrographs are characterised by base lengths which increase with peak flows. The increased flood volume associated with increasing duration was included in the analysis by incorporating FSR relationships between hydrograph base length ($T_B$) and the time to peak ($T_P$).

(2) Route the selected flood hydrograph of specified return periods down a single river reach whose channel and floodplain sections are maintained constant over the length.

(3) Analyse the downstream hydrographs produced in computer simulations. These will be broader that upstream hydrographs but will have peaks that are lower than those upstream, reflecting the attenuation of the channel floodplains.

The process was repeated for various floodplain geometries and hydraulic configurations for a wide range of flood events with return periods of between 25 years and 1000 years. As reported in Section 2.5.1, bankfull return periods may typically be expected to be between 1 and 2 years and return periods greater than this would be expected to significantly exceed the bankfull flow and inundate the adjacent floodplains. However, in the case of the River Suir and on which the generalised model is based, bankfull return periods are less than 5-years and for the floodplains to be influential in flow attenuation, the analysis of higher return periods is required.

### 5.3.1 Hydrograph Development

The approach to this study required that characteristic flood hydrographs were developed for the upstream end of the reach. These were based on flow data from New Bridge gauging station (Station No. 16008) on the River Suir that is available from 1954 to 2006. Constructing the generalised model to correspond with the geometrical properties of the River Suir ensured that this data could form suitable flow inputs to this model. The AM series at this station conforms to an Extreme Value Type 1 Distribution with a mean value of 90.64$m^3$/s and a standard deviation of 11.35$m^3$/s. The coefficient of variation of 0.12 for this distribution is typical for rivers in the centre and south of Ireland.

For the purposes of simplifying the analysis, hydrographs of specified return period were defined for upstream locations (x = 0) corresponding to peak flood flows. The input hydrograph was derived from the methodology and its associated software that was developed in WP 3.1 of the FSU for gauged catchments and involved six stages as follows:

(1) The first stage of the process involved identifying the annual exceedence series for the New Bridge gauging station (16008). This series is comprised of the 54 maximum flood events from the 54 year flow record.

(2) The identified annual exceedence flood hydrographs are decoupled by simply discarding the complex segments on each side of the peak, leaving just the observed part of the main component hydrograph. In this approach, only that part of the observed complex flood hydrograph which contains the largest peak and also has substantial segments each side of the peak that are clearly not part of the immediately preceding or following floods is considered as being relevant for deriving a generalised shape of the design flood hydrograph. This decoupling is shown in Figure 5-1 for event No. 2 and No. 30 at the New Bridge gauging station (16008).

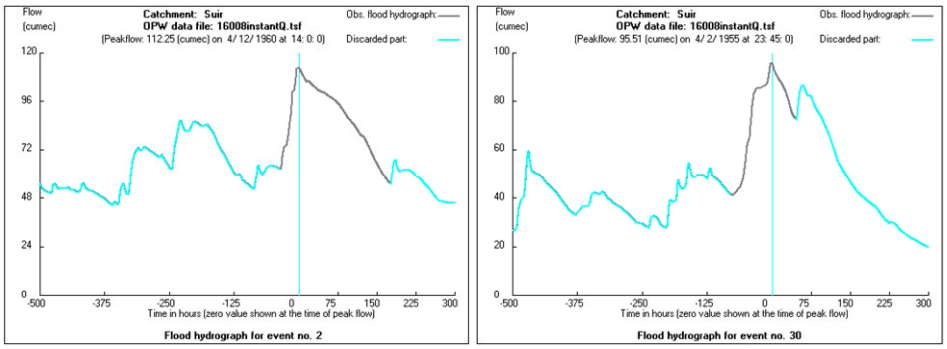


**Figure 5-1 The decoupled hydrographs for flood event 2 and 30 at the New Bridge gauging station (16008)**

(3) The decoupled or isolated flood hydrographs (Figure 5-1) is standardised to have a unit valued peak by dividing its flow ordinate by the peak flow of the flood.

(4) At each of the selected percentiles, the values of the available widths of exceedence on the rising and receding side of the hydrograph, measured in units of time from the peak of each standardised flood hydrograph, are separately extracted.

(5) A modified form of the Gamma curve having a peak value of unity defines the rising limb of the hydrograph. An exponential curve joins the gamma curve at its peak and defines the recession limb of the hydrograph. Rising limb timesteps are negative and recession limb timesteps have positive values.

(6) The derived hydrograph (Figure 5-2) is scaled up for different peaks and a base flow is added at each ordinate corresponding to a range of specified return periods (Figure 5-3).

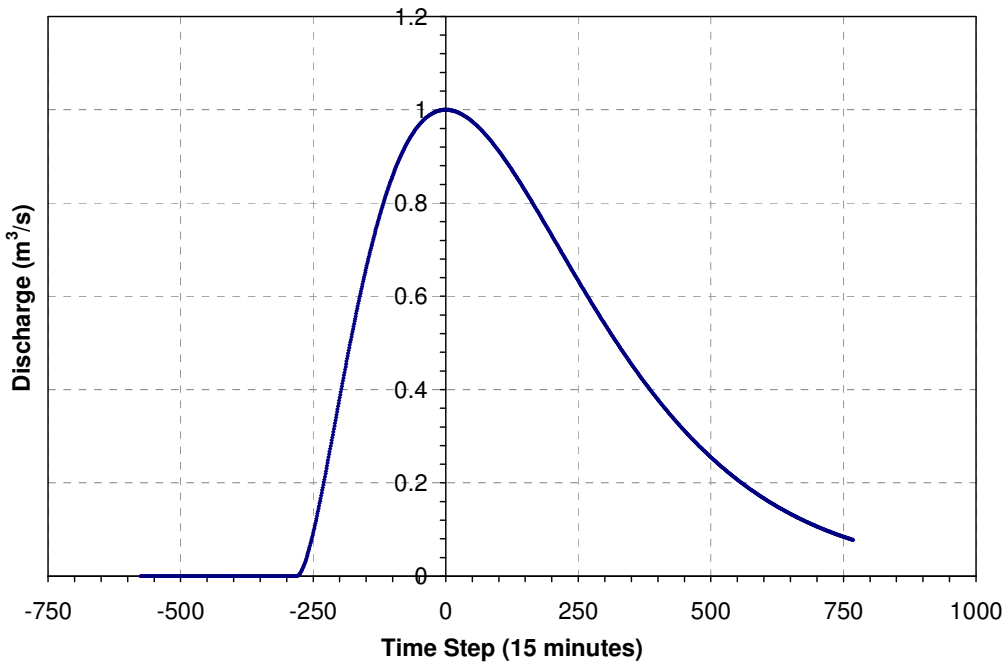


**Figure 5-2 Derived hydrograph using methodology in WP 3.1**

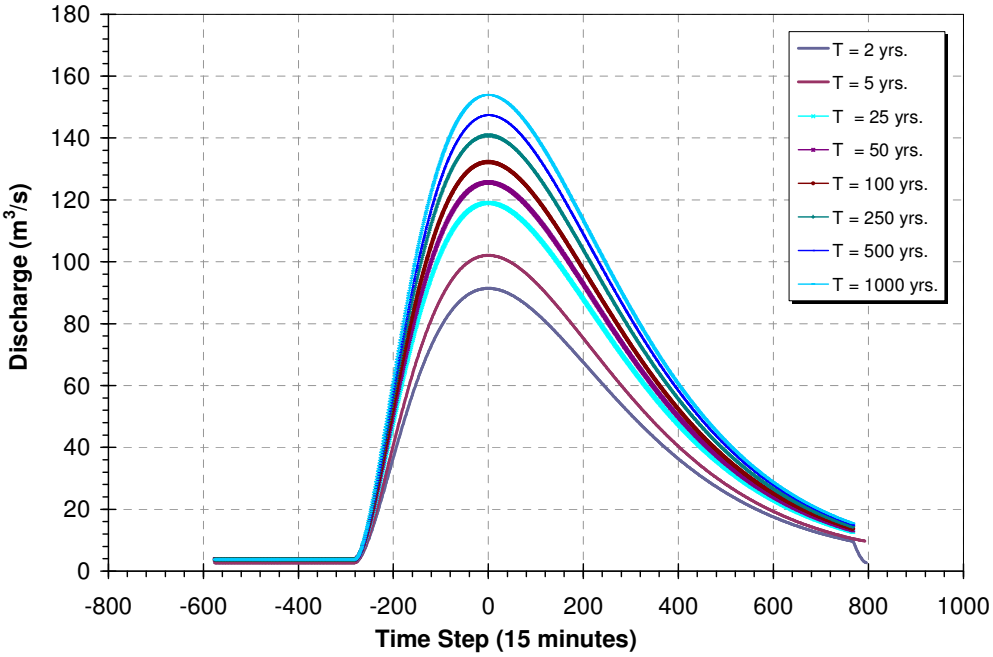


**Figure 5-3 Input hydrographs for specified return periods**

The flood quantiles estimated from the Annual Maximum flow record from the New Bridge gauging station (Station 16008) are based on an Extreme Value Type 1 distribution. These are summarised in Table 5-1.

**Table 5-1 Estimated flood quantiles at New Bridge (Stn. 16008)**

| T (Yrs) | $Q_T$ (cumec) |
|---|---|
| 2 | 91.41 |
| 5 | 102.06 |
| 10 | 110.12 |
| 25 | 119.03 |
| 50 | 125.64 |
| 100 | 132.21 |
| 250 | 140.85 |
| 500 | 147.38 |
| 1000 | 153.90 |

The hydrographs for the specified return periods in Figure 5-3 are simplified by the assumption that they have the same base length and therefore flood volume is being represented by flood peak only. The relationship between flood volume and flood peak of direct runoff is of fundamental importance in a wide variety of hydrologic analyses, especially where hydrologic data are scarce. Attempts have been made (for example Rogers, 1980, Mimikou, 1983, Singh and Aminian, 1986) to develop relationships between volume and peak of direct runoff from a large number of catchments in the United States, Australia, Italy and Greece. However, a validated relationship for Irish catchments has not existed and an attempt to develop such a relationship as part of the Flood Studies Update programme has proved inconclusive.

For the current study, flood volume is an important parameter in terms of assessing the capacity of a floodplain to attenuate a flood and therefore representing flood duration, in addition to flood peak in any index or indices is important. This was done by taking the 1000 year hydrograph in Figure 5-3, and developing a triangular hydrograph of the same volume. This volume was linked to the hydrograph characteristics by:

$$\text{Volume} = \frac{1}{2} \times T_B \times Q_P \qquad \textbf{Eqn. 5.3}$$

The duration of the 1000-year hydrograph corresponding to this volume is approximately 265 hours. The duration $T_B$ in Eqn. 5.3 is linked to the time to peak, $T_P$, by the Flood Studies Report relationship:

$$T_B = 2.52 T_P \qquad \textbf{Eqn. 5.4}$$

By further scaling the 1000-year hydrograph, this approach facilitated the development of a range of hydrographs of varying durations as shown in Figure 5-4. The actual 1000-year hydrograph from Figure 5-3 is shown in Figure 5-4 for indicative purposes.

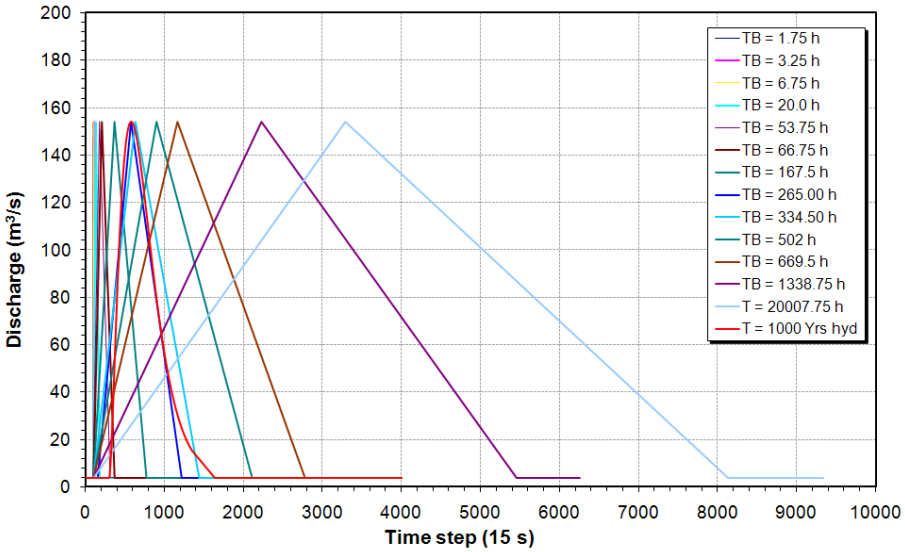


**Figure 5-4 Triangular hydrographs of different duration**

A limitation of this approach is that the influence of flood duration and flood peak on floodplain attenuation is treated independently. This is not the case in reality where increased flood peaks are generally associated with longer durations. However, in the context of the current study, the approach adopted is considered acceptable.

### 5.3.2 Floodplain Properties

Floodplains only become inundated when bankfull levels are exceeded and when this happens will behave differently depending on the level to which they are exceeded. Lower return period floods which do not substantially inundate the floodplain may remain largely unaffected, but once the floodplain is substantially inundated the flood conveyance is affected and thus the peak flood and its timing are altered. The effects are very complex. For low to mid-range floods which have shallow inundation of the floodplain, its roughness (characterised by its boundary, but including the presence of bushes, trees, ditches and walls) determines its impact on attenuation and delay of the flood peak. However, for more severe floods, where many of the roughness elements are overtopped and become submerged, the floodplain may begin to provide an enhanced flood conveyance for flows which no longer will follow the meanders of the main channel but rather, will flow directly downstream in the main valley direction. Consequently, very severe floods may be conveyed more quickly and with less attenuation, pro-rata, than less severe floods.

Section 2.6 of this report identified and discussed the channel properties and characteristics that have been shown to influence the ability of a floodplain to attenuate flow. These parameters are important in the context of this study and include (i) floodplain length; (ii) floodplain width; (iii) longitudinal floodplain slope, (iv) transverse floodplain slope (v) floodplain resistance and (vi) main channel resistance. In addition to these, the characteristics of the flood represented in terms of the (vii) flood peak and (viii) flood duration are also important. For the purpose of this study, floodplain and main channel resistance is characterised in terms of

Manning's *n* resistance coefficients. While literature highlights extensive energy losses (see Section 2.6) that result from the complexities of main channel and floodplain interactions in compound channels, the influences of these (sinuosity, width-depth ratio, channel side slope etc) will be most pronounced in the low floodplain depth range and will diminish as the depth and flow increase. In the high flood flow range, the influence of the main channel in terms of the flow that it conveys and in terms of the energy losses from the turbulent momentum exchange between it and floodplain will be much less significant.

The approach in this study involved using the hydraulic model of a generalised river reach of the River Suir to investigate a wide range of geometrical and resistance properties that would encompass the majority of river channels in Ireland. The dimensions of the reach cross-section were based on approximated averaged values between New Bridge and Caher Park as determined from detailed topographical data provided by the OPW. Analysis of this data indicated that the bankfull width of the main channel ($b_{bf}$) was 25m and, from flood polygons also made available by the OPW, the active floodplain on each side of the main channel extended for a width ($b_{fp}$) of 25m. The main channel banks were 45° to the horizontal plane and the estimated bankfull depth was 2.5m. The floodplain boundaries were also assumed to be at 45° to the horizontal resulting in a trapezoidal overbank section in the generalised model. The observed longitudinal floodplain slope between New Bridge and Caher Park ($S_{fp}$) was approximately 1.0 m/km and this slope was use in all model simulations where parameters other than slope were being investigated. The notation pertaining to the cross-sectional parameters is shown in Figure 5-5.

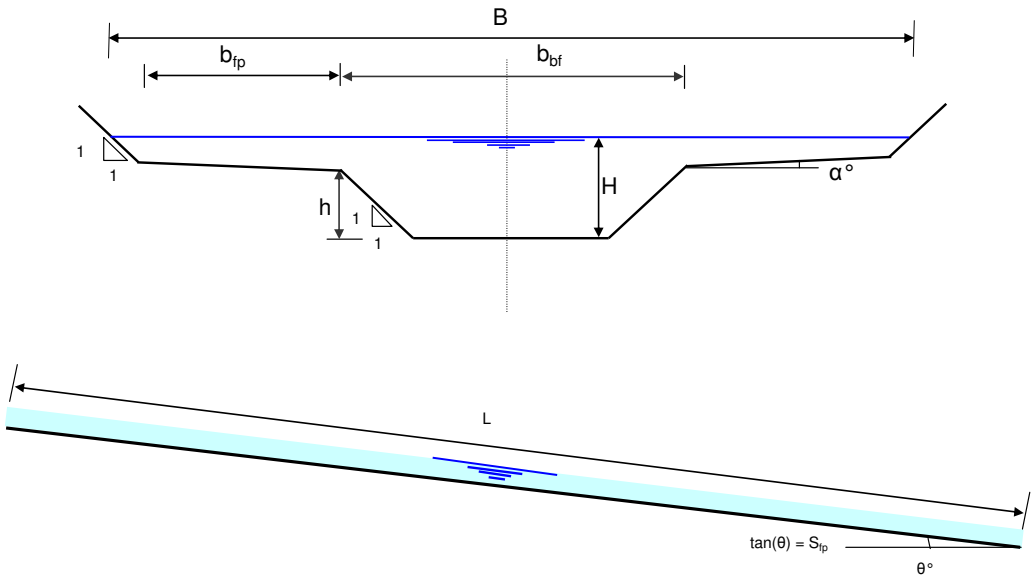


**Figure 5-5 Channel notation adopted in study**

The base Manning's resistance coefficient in the main channel and on the floodplain were taken to be 0.03 and 0.25 respectively and this allowed for irregularities, alignment, the presence of obstructions and vegetation and the meandering planform of the channel and floodplains. These values were reasonably consistent with those that can be derived from literature or by an application of the Soil Conservation

Service Method of resistance estimation. A standard channel length (L) of 50km was chosen for the generalised model where floodplain length was not being investigated and when the influence of floodplain length was being investigated, lengths of between 10km and 50km were tested.

Individual simulations were undertaken for incremental changes of each of the parameters that were tested. Eight cases, denoted by A-H, were examined and the influence on attenuation observed. Case A investigated the channel length (L), Case B the longitudinal floodplain slope ($S_{fp}$), Case C the floodplain hydraulic resistance ($n_{fp}$), Case D the floodplain width ($b_{fp}$), Case E, the transverse floodplain slope ($\alpha$), Case F, the magnitude of the flood peak ($Q_P$), Case G, the main channel hydraulic resistance ($n_{mc}$) and Case H, the flood duration ($T_B$). Details of all model parameters for these cases are summarised in Table 5-2.

**Table 5-2 Floodplain and flow magnitudes investigated in Case A to Case H simulations**

| | L (km) | $S_{fp}$ (m/km) | $n_{fp}$ ($s/m^{1/3}$) | $b_{fp}$ (m) | α (deg) | $n_{mc}$ ($s/m^{1/3}$) | $T_B$ (hrs) | $Q_P$ ($m^3/s$) |
|---|---|---|---|---|---|---|---|---|
| **A1.** | **10** | 1.00 | 0.25 | 25 | 0 | 0.03 | 335.5 | 153.90 |
| **A2.** | **20** | 1.00 | 0.25 | 25 | 0 | 0.03 | 335.5 | 153.90 |
| **A3.** | **30** | 1.00 | 0.25 | 25 | 0 | 0.03 | 335.5 | 153.90 |
| **A4.** | **40** | 1.00 | 0.25 | 25 | 0 | 0.03 | 335.5 | 153.90 |
| **A5.** | **50** | 1.00 | 0.25 | 25 | 0 | 0.03 | 335.5 | 153.90 |
| **B1.** | 50 | **0.05** | 0.25 | 25 | 0 | 0.03 | 335.5 | 153.90 |
| **B2.** | 50 | **0.10** | 0.25 | 25 | 0 | 0.03 | 335.5 | 153.90 |
| **B3.** | 50 | **0.14** | 0.25 | 25 | 0 | 0.03 | 335.5 | 153.90 |
| **B4.** | 50 | **0.28** | 0.25 | 25 | 0 | 0.03 | 335.5 | 153.90 |
| **B5.** | 50 | **0.42** | 0.25 | 25 | 0 | 0.03 | 335.5 | 153.90 |
| **B6.** | 50 | **0.75** | 0.25 | 25 | 0 | 0.03 | 335.5 | 153.90 |
| **B7.** | 50 | **1.00** | 0.25 | 25 | 0 | 0.03 | 335.5 | 153.90 |
| **B8.** | 50 | **1.40** | 0.25 | 25 | 0 | 0.03 | 335.5 | 153.90 |
| **B9.** | 50 | **2.00** | 0.25 | 25 | 0 | 0.03 | 335.5 | 153.90 |
| **B10.** | 50 | **2.25** | 0.25 | 25 | 0 | 0.03 | 335.5 | 153.90 |
| **B11.** | 50 | **2.50** | 0.25 | 25 | 0 | 0.03 | 335.5 | 153.90 |
| **B12.** | 50 | **2.80** | 0.25 | 25 | 0 | 0.03 | 335.5 | 153.90 |
| **B13.** | 50 | **3.00** | 0.25 | 25 | 0 | 0.03 | 335.5 | 153.90 |
| **C1.** | 50 | 1.00 | **0.01** | 25 | 0 | 0.03 | 335.5 | 153.90 |
| **C2.** | 50 | 1.00 | **0.05** | 25 | 0 | 0.03 | 335.5 | 153.90 |
| **C3.** | 50 | 1.00 | **0.10** | 25 | 0 | 0.03 | 335.5 | 153.90 |
| **C4.** | 50 | 1.00 | **0.25** | 25 | 0 | 0.03 | 335.5 | 153.90 |
| **C5.** | 50 | 1.00 | **0.50** | 25 | 0 | 0.03 | 335.5 | 153.90 |
| **C6.** | 50 | 1.00 | **1.00** | 25 | 0 | 0.03 | 335.5 | 153.90 |
| **C7.** | 50 | 1.00 | **2.00** | 25 | 0 | 0.03 | 335.5 | 153.90 |
| **C8.** | 50 | 1.00 | **5.00** | 25 | 0 | 0.03 | 335.5 | 153.90 |
| **D1** | 50 | 1.00 | 0.25 | **12.5** | 0 | 0.03 | 335.5 | 153.90 |
| **D2.** | 50 | 1.00 | 0.25 | **25** | 0 | 0.03 | 335.5 | 153.90 |
| **D3.** | 50 | 1.00 | 0.25 | **50** | 0 | 0.03 | 335.5 | 153.90 |
| **D4.** | 50 | 1.00 | 0.25 | **75** | 0 | 0.03 | 335.5 | 153.90 |
| **D5.** | 50 | 1.00 | 0.25 | **100** | 0 | 0.03 | 335.5 | 153.90 |
| **D6.** | 50 | 1.00 | 0.25 | **150** | 0 | 0.03 | 335.5 | 153.90 |
| **D7.** | 50 | 1.00 | 0.25 | **300** | 0 | 0.03 | 335.5 | 153.90 |
| **D8.** | 50 | 1.00 | 0.25 | **400** | 0 | 0.03 | 335.5 | 153.90 |
| **D9.** | 50 | 1.00 | 0.25 | **500** | 0 | 0.03 | 335.5 | 153.90 |
| **D10.** | 50 | 1.00 | 0.25 | **600** | 0 | 0.03 | 335.5 | 153.90 |
| **D11.** | 50 | 1.00 | 0.25 | **750** | 0 | 0.03 | 335.5 | 153.90 |
| **D12.** | 50 | 1.00 | 0.25 | **900** | 0 | 0.03 | 335.5 | 153.90 |
| **D13.** | 50 | 1.00 | 0.25 | **1000** | 0 | 0.03 | 335.5 | 153.90 |
| **D14.** | 50 | 1.00 | 0.25 | **1175** | 0 | 0.03 | 335.5 | 153.90 |
| **D15.** | 50 | 1.00 | 0.25 | **1250** | 0 | 0.03 | 335.5 | 153.90 |
| **D16.** | 50 | 1.00 | 0.25 | **1500** | 0 | 0.03 | 335.5 | 153.90 |
| **D17.** | 50 | 1.00 | 0.25 | **1700** | 0 | 0.03 | 335.5 | 153.90 |
| **D18.** | 50 | 1.00 | 0.25 | **2000** | 0 | 0.03 | 335.5 | 153.90 |

**Table 5-2 Ctd. Floodplain and flow magnitudes investigated in Case A to Case H simulations**

| | L (km) | $S_{fp}$ (m/km) | $n_{fp}$ ($s/m^{1/3}$) | $b_{fp}$ (m) | α (deg) | $n_{mc}$ ($s/m^{1/3}$) | $T_B$ (hrs) | $Q_{P1}$ ($m^3/s$) |
|---|---|---|---|---|---|---|---|---|
| **E1** | 50 | 1.00 | 0.25 | 25 | **0** | 0.03 | 335.5 | 153.90 |
| **E2.** | 50 | 1.00 | 0.25 | 25 | **2** | 0.03 | 335.5 | 153.90 |
| **E3.** | 50 | 1.00 | 0.25 | 25 | **5** | 0.03 | 335.5 | 153.90 |
| **E4.** | 50 | 1.00 | 0.25 | 25 | **10** | 0.03 | 335.5 | 153.90 |
| **E5.** | 50 | 1.00 | 0.25 | 25 | **15** | 0.03 | 335.5 | 153.90 |
| **E6.** | 50 | 1.00 | 0.25 | 25 | **30** | 0.03 | 335.5 | 153.90 |
| **F1.** | 50 | 1.00 | 0.25 | 25 | 0 | 0.03 | 335.5 | **91.41** |
| **F2.** | 50 | 1.00 | 0.25 | 25 | 0 | 0.03 | 335.5 | **102.06** |
| **F3.** | 50 | 1.00 | 0.25 | 25 | 0 | 0.03 | 335.5 | **110.12** |
| **F4.** | 50 | 1.00 | 0.25 | 25 | 0 | 0.03 | 335.5 | **119.03** |
| **F5.** | 50 | 1.00 | 0.25 | 25 | 0 | 0.03 | 335.5 | **125.64** |
| **F6.** | 50 | 1.00 | 0.25 | 25 | 0 | 0.03 | 335.5 | **132.21** |
| **F7.** | 50 | 1.00 | 0.25 | 25 | 0 | 0.03 | 335.5 | **140.85** |
| **F8.** | 50 | 1.00 | 0.25 | 25 | 0 | 0.03 | 335.5 | **147.38** |
| **F9.** | 50 | 1.00 | 0.25 | 25 | 0 | 0.03 | 335.5 | **153.90** |
| **G1.** | 50 | 1.00 | 0.25 | 25 | 0 | **0.03** | 335.5 | 153.90 |
| **G2.** | 50 | 1.00 | 0.25 | 25 | 0 | **0.06** | 335.5 | 153.90 |
| **G3.** | 50 | 1.00 | 0.25 | 25 | 0 | **0.10** | 335.5 | 153.90 |
| **G4.** | 50 | 1.00 | 0.25 | 25 | 0 | **0.15** | 335.5 | 153.90 |
| **G5.** | 50 | 1.00 | 0.25 | 25 | 0 | **0.20** | 335.5 | 153.90 |
| **G6.** | 50 | 1.00 | 0.25 | 25 | 0 | **0.30** | 335.5 | 153.90 |
| **G7.** | 50 | 1.00 | 0.25 | 25 | 0 | **0.50** | 335.5 | 153.90 |
| **G8.** | 50 | 1.00 | 0.25 | 25 | 0 | **1.00** | 335.5 | 153.90 |
| **G9.** | 50 | 1.00 | 0.25 | 25 | 0 | **2.00** | 335.5 | 153.90 |
| **G10.** | 50 | 1.00 | 0.25 | 25 | 0 | **5.00** | 335.5 | 153.90 |
| **H1.** | 50 | 1.00 | 0.25 | 25 | 0 | 0.03 | **1.75** | 153.90 |
| **H2.** | 50 | 1.00 | 0.25 | 25 | 0 | 0.03 | **3.25** | 153.90 |
| **H3.** | 50 | 1.00 | 0.25 | 25 | 0 | 0.03 | **6.75** | 153.90 |
| **H4.** | 50 | 1.00 | 0.25 | 25 | 0 | 0.03 | **20.00** | 153.90 |
| **H5.** | 50 | 1.00 | 0.25 | 25 | 0 | 0.03 | **53.75** | 153.90 |
| **H6.** | 50 | 1.00 | 0.25 | 25 | 0 | 0.03 | **66.75** | 153.90 |
| **H7.** | 50 | 1.00 | 0.25 | 25 | 0 | 0.03 | **167.50** | 153.90 |
| **H8.** | 50 | 1.00 | 0.25 | 25 | 0 | 0.03 | **265.00** | 153.90 |
| **H9.** | 50 | 1.00 | 0.25 | 25 | 0 | 0.03 | **334.50** | 153.90 |
| **H10.** | 50 | 1.00 | 0.25 | 25 | 0 | 0.03 | **502.01** | 153.90 |
| **H11.** | 50 | 1.00 | 0.25 | 25 | 0 | 0.03 | **669.50** | 153.90 |
| **H12.** | 50 | 1.00 | 0.25 | 25 | 0 | 0.03 | **1338.75** | 153.90 |
| **H13.** | 50 | 1.00 | 0.25 | 25 | 0 | 0.03 | **2007.75** | 153.90 |

The geometrical parameters of a channel determine its storage capacity and conveyance. They are, therefore, important factors in peak attenuation and hydrograph deformation. With the exception of Case A where length varied, the downstream valley length was 50 km. With the exception of Case B, the river longitudinal slope was constant with a gradient of 0.001. The hydraulic roughness of the floodplain was represented in terms of Manning's *n* and increased from 0.01 to 5 in Case C and for Case D floodplain widths from 12.5m to 1500m were investigated. These values corresponded to convenient multiples of the main channel width (0.5 for

a narrow valley to 60 for the widest valley). Simulations other than those in Case D were undertaken with a floodplain width of 25m. Case E simulations were undertaken with transverse floodplain slopes up to 30°. Other simulations were undertaken with floodplains that were laterally horizontal to facilitate a greater proportion of the total flow being retained in the floodplain. Flow magnitudes from 91.41$m^3$/s to 153.5$m^3$/s corresponding to flood return periods between 2 years and 1000 years were analysed in the Case F simulations. Main channel Manning's resistances from 0.03 to 5 were included in Case G and flood durations from 1.75 hours to approximately 2008 hours were represented in the Case H simulations.

The time interval in the model simulations was set at 15 minutes and correlated with the time intervals of the input hydrographs. Typically, model parameters were determined at longitudinal channel intervals of 400m. This distance interval coincided with longitudinal distances between cross-sections of the topographical data for the River Suir catchment provided by the OPW. However, for some simulations where computational time was excessive, this interval was lengthened and lower resolution data was extracted for analysis.

## 5.4 Results for Attenuation of Flood Peaks

The influence of each of the eight variables in Table 5-2 on flood hydrograph attenuation is assessed by comparing the flood peaks of inflow hydrographs to the outflow hydrographs generated in model simulations. This is shown in schematic in Figure 5-6.

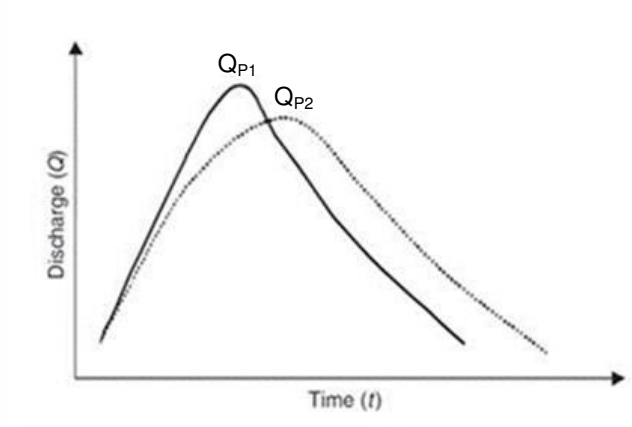


**Figure 5-6 Inflow and attenuated outflow hydrographs**

Differences in upstream inflow and downstream hydrographs are represented in terms of Relative Attenuation defined as:

$$\text{Relative Attenuation } (\%) = \frac{Q_{P1} - Q_{P2}}{Q_{P1}} \qquad \textbf{Eqn. 5.5}$$

where $Q_{P1}$ and $Q_{P2}$ are the peaks of the inflow and outflow hydrographs in Figure 5-6.

### 5.4.1 Influence of Reach Length

In Case A simulations, the effects of reach length on flood peak attenuation is examined. The magnitudes of the computed peak flow rate are extracted at every 400m interval in the 50 km reach being investigated. The variation with distance along the floodplain of the relative attenuation of the peak flow in the downstream direction based on the summarised data in Table 5-3 is shown in Figure 5-7.

**Table 5-3 Variation of $Q_{P1}$ with $Q_{P2}$ with floodplain length**

| | L (km) | $S_{fp}$ (m/km) | $n_{fp}$ ($s/m^{1/3}$) | $b_{fp}$ (m) | α (deg) | $n_{mc}$ ($s/m^{1/3}$) | $T_B$ (hrs) | $Q_{P1}$ ($m^3/s$) | $Q_{P2}$ ($m^3/s$) | Rel. Att (%) |
|---|---|---|---|---|---|---|---|---|---|---|
| **A1.** | **10** | 1.00 | 0.25 | 25 | 0 | 0.03 | 335.5 | 153.90 | 153.86 | 0.03 |
| **A2.** | **20** | 1.00 | 0.25 | 25 | 0 | 0.03 | 335.5 | 153.90 | 153.81 | 0.06 |
| **A3.** | **30** | 1.00 | 0.25 | 25 | 0 | 0.03 | 335.5 | 153.90 | 153.76 | 0.09 |
| **A4.** | **40** | 1.00 | 0.25 | 25 | 0 | 0.03 | 335.5 | 153.90 | 153.72 | 0.12 |
| **A5.** | **50** | 1.00 | 0.25 | 25 | 0 | 0.03 | 335.5 | 153.90 | 153.67 | 0.15 |

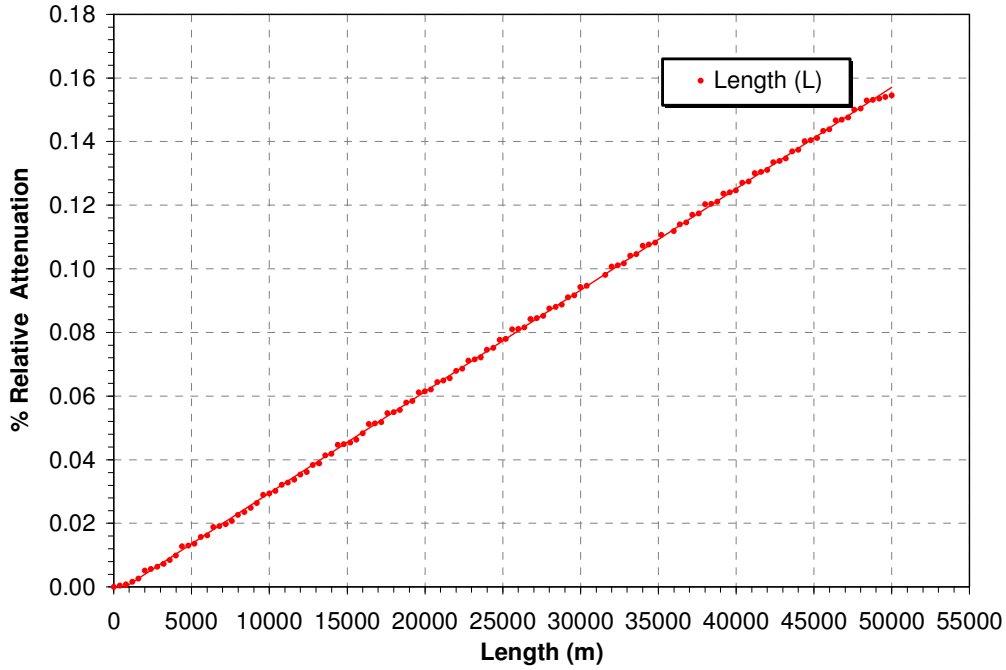


**Figure 5-7 Variation or relative attenuation with reach length (L)**

Figure 5-7 shows that relative attenuation increases linearly with increases in reach length. This finding is consistent with other research where the influence of floodplain properties on flow attenuation were investigated (e.g. Wolff and Burges 1994).

### 5.4.2 Influence of Longitudinal Floodplain Slope ($S_{fp}$)

The effects of longitudinal floodplain slope on flood peak attenuation are examined for nine different slopes, ranging from a relatively flat slope of 0.01 m/km in Case B1, to a steeper slope of 3 m/km in case B11. Two additional simulations for floodplain slopes of 0.05 m/km and 2.8 m/km were also undertaken to further define the relationship between slope and attenuation. The variation of relative attenuation with these longitudinal floodplain slopes is summarised in Table 5-4 and shown graphically in Figure 5-8.

**Table 5-4 Variation of $Q_{P1}$ with $Q_{P2}$ with floodplain slope ($S_{fp}$)**

| | L (km) | $S_{fp}$ (m/km) | $n_{fp}$ ($s/m^{1/3}$) | $b_{fp}$ (m) | α (deg) | $n_{mc}$ ($s/m^{1/3}$) | $T_B$ (hrs) | $Q_{P1}$ ($m^3/s$) | $Q_{P2}$ ($m^3/s$) | Rel. Att (%) |
|---|---|---|---|---|---|---|---|---|---|---|
| **B1.** | 50 | **0.05** | 0.25 | 25 | 0 | 0.03 | 335.5 | 153.90 | 138.17 | 10.22 |
| **B2.** | 50 | **0.10** | 0.25 | 25 | 0 | 0.03 | 335.5 | 153.90 | 146.84 | 4.59 |
| **B3.** | 50 | **0.14** | 0.25 | 25 | 0 | 0.03 | 335.5 | 153.90 | 148.57 | 3.46 |
| **B4.** | 50 | **0.28** | 0.25 | 25 | 0 | 0.03 | 335.5 | 153.90 | 151.61 | 1.49 |
| **B5.** | 50 | **0.42** | 0.25 | 25 | 0 | 0.03 | 335.5 | 153.90 | 152.84 | 0.69 |
| **B6.** | 50 | **0.75** | 0.25 | 25 | 0 | 0.03 | 335.5 | 153.90 | 153.62 | 0.18 |
| **B7.** | 50 | **1.00** | 0.25 | 25 | 0 | 0.03 | 335.5 | 153.90 | 153.71 | 0.13 |
| **B8.** | 50 | **1.40** | 0.25 | 25 | 0 | 0.03 | 335.5 | 153.90 | 153.75 | 0.10 |
| **B9.** | 50 | **2.00** | 0.25 | 25 | 0 | 0.03 | 335.5 | 153.90 | 153.80 | 0.07 |
| **B10.** | 50 | **2.25** | 0.25 | 25 | 0 | 0.03 | 335.5 | 153.90 | 153.83 | 0.05 |
| **B11.** | 50 | **2.50** | 0.25 | 25 | 0 | 0.03 | 335.5 | 153.90 | 153.87 | 0.02 |
| **B12.** | 50 | **2.80** | 0.25 | 25 | 0 | 0.03 | 335.5 | 153.90 | 153.87 | 0.02 |
| **B13.** | 50 | **3.00** | 0.25 | 25 | 0 | 0.03 | 335.5 | 153.90 | 153.87 | 0.02 |

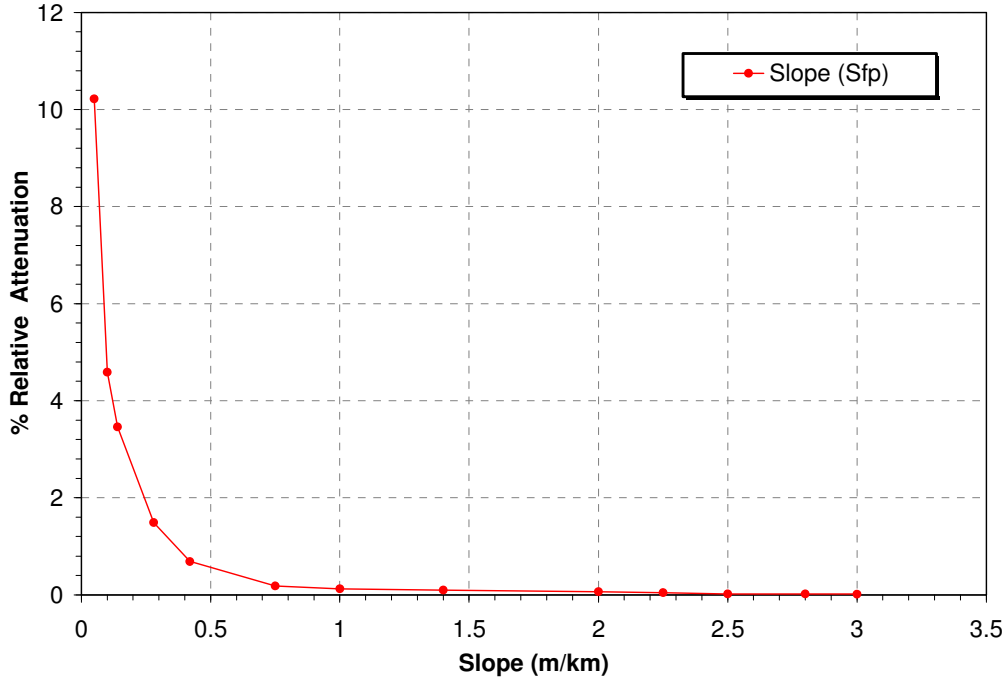


**Figure 5-8 Variation of relative attenuation with floodplain slope**

Figure 5-8 suggests that a power-law relationship defines the variation of relative attenuation with floodplain slope. The relative attenuations in Figure 5-8 cover a range of values that are consistent with channel gradients in Irish catchments. The OPW register of gauges indicate that S1085 values for Irish channels vary from approximately 0.2 m/km to 30 m/km and while very high gradients were not included in simulations, Figure 5-8 indicates that relative attenuation decreases to a limiting upper slope value of 1 m/km beyond which attenuation is negligible. The surveyed average slope of the River Suir reach between New Bridge and Caher Park) is approximately 1 m/km. Differences in the computed upstream peak flows for these slopes are significant. Figure 5-8 indicates that for the lower gradient slopes tested, significant attenuation of the flood peak occurs with respect to that for the steeper slopes. The lower attenuation of the steeper catchments reflects the higher conveyance associated with high gradient channels and the associated reduction in storage of the flood volume in the reach.

These findings are consistent with Ghavasieh *et al*. (2006) where it was shown that for a range of floodplain roughness configurations in four differing compound channel configurations, the storage of the flood volume in a reach is influenced significantly by longitudinal slope. The slope versus relative attenuation relationship in Figure 5-8 is also supported by Wolff and Burges (1994) who verified significant peak attenuation with a sharp reduction in the variability of the cumulative distribution for low gradient floodplains than for steep floodplains.

### 5.4.3 Influence of Floodplain Roughness ($n_{fp}$)

The selection of an appropriate value for the Manning's roughness coefficient ($n$) is crucial to the accuracy of the computed hydraulic parameters. The value of the Manning's resistance coefficient is highly variable and depends on several factors including surface roughness, vegetation, channel irregularities, channel alignment, scour and deposition, obstructions, size and shape of the channel, stage and discharge, seasonal changes, water temperature, and suspended material and bed load (Thomas and Nisbet, 2006).

Emergent or surface penetrating vegetation is common in natural floodplains, particularly for low floodplain depths and has a strong influence on physical and biological processes (Jarvela, 2002).

The use of conventional resistance equations, such as those of Manning and Chézy account for resistance arising from boundary shear and do not adequately represent the resistance exerted by drag through the flow depth. In situations where vegetation is surface penetrating, velocity is essentially uniform over the flow depth, rather than being depth-dependent as it is when resistance is exerted along the boundary. The consequent dependence on depth of average velocity implied by these equations should in theory require compensation through depth-dependent resistance coefficients in vegetated sections of channels and has led to the development of more fundamental approaches for estimating resistance values that account for the drag force on vegetation stems (e.g. by Petryk and Bosmajian, 1975). However, the use of these equations has not been adopted on a widespread basis and the Manning's equation where the coefficient $n$ constitutes a lumped parameter to account for all

energy loss influences and estimated largely on the basis of qualitative descriptions and "judgement" (e.g. Soil Conservation Service, 1963, Chow, 1959) is still the most popular for natural rivers. Consequently, hydraulic resistance in the generalised HEC-RAS model being used in this study is represented in terms of the Manning's resistance coefficient. This, as discussed is appropriate for relatively short roughness elements along a channel boundary such as grass but is less suitable for defining the hydraulic resistance of taller, non-submerged vegetation where drag effects are likely to be significant.

Literature indicates that extensive research has been undertaken in numerical and physical modelling studies in compound channel with varying floodplain resistance in terms of both characteristics and configuration. The majority of the effort has focussed on steady state flow regimes with considerably less literature available for dynamic flow conditions.

In the current study, eight floodplain roughness conditions represented by Manning's *n* varying from 0.01, 0.05, 0.10, 0.25, 0.50, 1.00, 2.00 and 5.00 are presented. These are summarised in Case C in Table 5-2. The effect of these floodplain roughness values on relative attenuation are summarised in Table 5-5 and shown in Figure 5-9.

**Table 5-5 Variation of $Q_{P1}$ with $Q_{P2}$ with floodplain roughness**

| | L (km) | $S_{fp}$ (m/km) | $n_{fp}$ ($s/m^{1/3}$) | $b_{fp}$ (m) | α (deg) | $n_{mc}$ ($s/m^{1/3}$) | $T_B$ (hrs) | $Q_{P1}$ ($m^3/s$) | $Q_{P2}$ ($m^3/s$) | Rel. Att (%) |
|---|---|---|---|---|---|---|---|---|---|---|
| **C1.** | 50 | 1.00 | **0.01** | 25 | 0 | 0.03 | 335.5 | 153.90 | 153.85 | 0.03 |
| **C2.** | 50 | 1.00 | **0.05** | 25 | 0 | 0.03 | 335.5 | 153.90 | 153.77 | 0.09 |
| **C3.** | 50 | 1.00 | **0.10** | 25 | 0 | 0.03 | 335.5 | 153.90 | 153.72 | 0.12 |
| **C4.** | 50 | 1.00 | **0.25** | 25 | 0 | 0.03 | 335.5 | 153.90 | 153.68 | 0.14 |
| **C5.** | 50 | 1.00 | **0.50** | 25 | 0 | 0.03 | 335.5 | 153.90 | 153.66 | 0.15 |
| **C6.** | 50 | 1.00 | **1.00** | 25 | 0 | 0.03 | 335.5 | 153.90 | 153.65 | 0.16 |
| **C7.** | 50 | 1.00 | **2.00** | 25 | 0 | 0.03 | 335.5 | 153.90 | 153.65 | 0.16 |
| **C8.** | 50 | 1.00 | **5.00** | 25 | 0 | 0.03 | 335.5 | 153.90 | 153.65 | 0.16 |

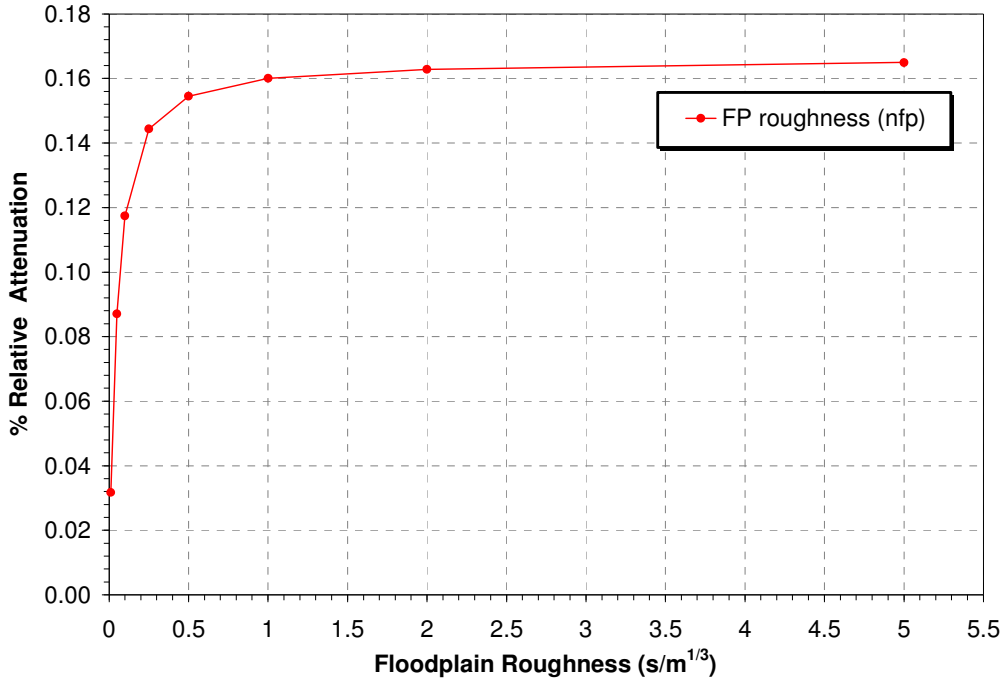


**Figure 5-9 Variation of relative attenuation with floodplain roughness**

Table 5-5 and Figure 5-9 highlight a limitation with the current analysis. Roughness in the hydraulic model is exerted along the wetted perimeter of the channel. In real rivers, floodplain roughness will have a different influence depending on the depth. For low flow depths, roughness may be expected to be emergent or surface penetrating. In this case, the resistance to the flow will primarily result from the drag influence of the elements and attenuation would be significant. As flow and water levels continue to increase, the same floodplain roughness would be expected to become submerged, resulting in an increase in floodplain conveyance and a corresponding reduction in attenuation.

The relationship in Figure 5-9 shows that relative attenuation increases with resistance before approaching a constant value as roughness continues to increase. The use of such a simple relationship to define the variation of relative attenuation with roughness in a regression model will not facilitate the inclusion of the complexities associated with the roughness influence at different flow depths.

### 5.4.4 Influence of Floodplain Width ($b_{fp}$)

Simulations for Case D assessed the effects of floodplain width on floodplain attenuation. For a given discharge, the width of the valley determines whether over-bank water will flow slowly as a thin layer spread over a wide valley or whether it will rise within the confines of a narrow valley to depths at which even overbank water is rapidly flowing. The floodplain widths investigated were set to be convenient multiples of the main channel width and ranged from a narrow valley of 12.5m to extensive floodplains with widths of 1500m. The variation of relative attenuation with floodplain width is shown in Table 5-6 and Figure 5-10.

**Table 5-6 Variation of $Q_{P1}$ with $Q_{P2}$ with floodplain width**

| | L (km) | $S_{fp}$ (m/km) | $n_{fp}$ ($s/m^{1/3}$) | $b_{fp}$ (m) | α (deg) | $n_{mc}$ ($s/m^{1/3}$) | $T_B$ (hrs) | $Q_{P1}$ ($m^3/s$) | $Q_{P2}$ ($m^3/s$) | Rel. Att (%) |
|---|---|---|---|---|---|---|---|---|---|---|
| **D1** | 50 | 1.00 | 0.25 | **12.5** | 0 | 0.03 | 335.5 | 153.90 | 153.77 | 0.08 |
| **D2.** | 50 | 1.00 | 0.25 | **25** | 0 | 0.03 | 335.5 | 153.90 | 153.66 | 0.15 |
| **D3.** | 50 | 1.00 | 0.25 | **50** | 0 | 0.03 | 335.5 | 153.90 | 153.37 | 0.35 |
| **D4.** | 50 | 1.00 | 0.25 | **75** | 0 | 0.03 | 335.5 | 153.90 | 153.01 | 0.58 |
| **D5.** | 50 | 1.00 | 0.25 | **100** | 0 | 0.03 | 335.5 | 153.90 | 152.61 | 0.84 |
| **D6.** | 50 | 1.00 | 0.25 | **150** | 0 | 0.03 | 335.5 | 153.90 | 152.46 | 0.94 |
| **D7.** | 50 | 1.00 | 0.25 | **300** | 0 | 0.03 | 335.5 | 153.90 | 150.33 | 2.32 |
| **D8.** | 50 | 1.00 | 0.25 | **400** | 0 | 0.03 | 335.5 | 153.90 | 148.35 | 3.60 |
| **D9.** | 50 | 1.00 | 0.25 | **500** | 0 | 0.03 | 335.5 | 153.90 | 147.55 | 4.12 |
| **D10.** | 50 | 1.00 | 0.25 | **600** | 0 | 0.03 | 335.5 | 153.90 | 144.09 | 6.38 |
| **D11.** | 50 | 1.00 | 0.25 | **750** | 0 | 0.03 | 335.5 | 153.90 | 138.52 | 10.00 |
| **D12.** | 50 | 1.00 | 0.25 | **900** | 0 | 0.03 | 335.5 | 153.90 | 134.63 | 12.52 |
| **D13.** | 50 | 1.00 | 0.25 | **1000** | 0 | 0.03 | 335.5 | 153.90 | 133.55 | 13.22 |
| **D14.** | 50 | 1.00 | 0.25 | **1175** | 0 | 0.03 | 335.5 | 153.90 | 129.67 | 15.74 |
| **D15.** | 50 | 1.00 | 0.25 | **1250** | 0 | 0.03 | 335.5 | 153.90 | 129.61 | 15.78 |
| **D16.** | 50 | 1.00 | 0.25 | **1500** | 0 | 0.03 | 335.5 | 153.90 | 129.58 | 15.80 |
| **D17.** | 50 | 1.00 | 0.25 | **1700** | 0 | 0.03 | 335.5 | 153.90 | 129.54 | 15.83 |
| **D18.** | 50 | 1.00 | 0.25 | **2000** | 0 | 0.03 | 335.5 | 153.90 | 129.70 | 15.73 |

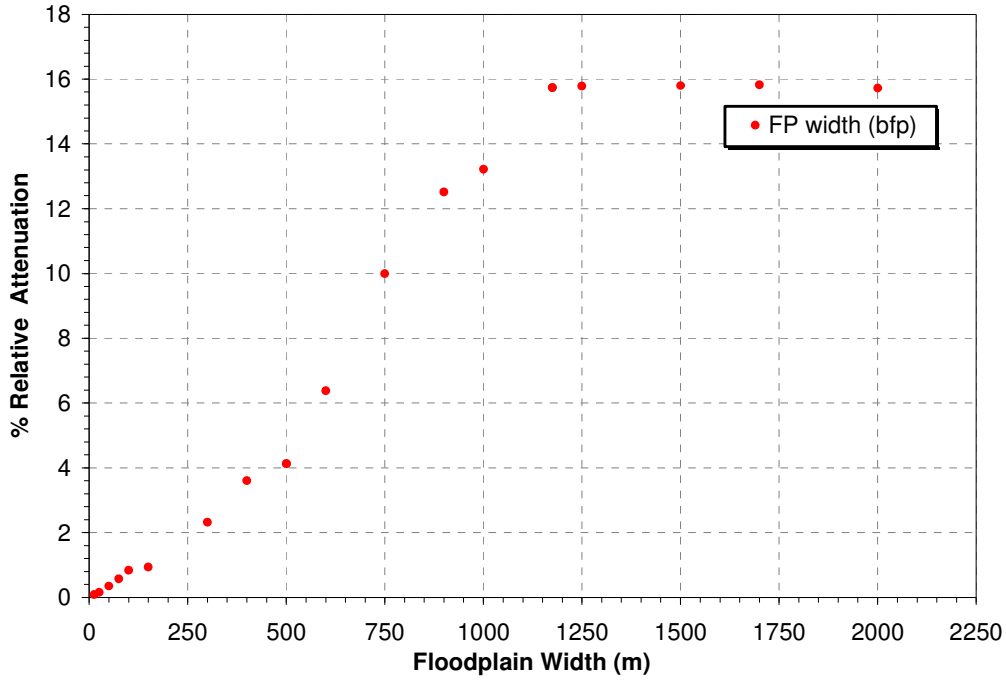


**Figure 5-10 Variation of relative attenuation with floodplain width**

Figure 5-10 indicates that floodplain width is a significant parameter in the capacity of a channel to attenuate flood peaks. Increasing the floodplain width results in an increased storage capacity in the overbank zone of the compound section and as would be expected, promotes attenuation. Figure 5-10 suggests that the relationship between relative attenuation and floodplain width is complex. As would be expected, attenuation increases with floodplain width. However, a point will be reached where

the floodplain width for a specified flow ($Q_P$ = 153.9$m^3$/s in this case) is such that floodplain depths have decreased to a limiting value below which, further increases in floodplain width will have inconsequential effects on depth and no discernible change on the relative attenuation of the flood peak is observed. This limiting value for the channel geometry and flow investigated is approximately 1000m.

### 5.4.5 Influence of Transverse Floodplain Slope (α)

Case E investigated the influence on attenuation of changes to the transverse or lateral floodplain slope. A total of five slopes increasing from the horizontal to 30° as shown in Figure 5-8 were investigated. The variation of relative attenuation with floodplain transverse slope is shown in Figure 5-11.

**Table 5-7 Variation of $Q_{P1}$ with $Q_{P2}$ with transverse floodplain slope**

| | L (km) | $S_{fp}$ (m/km) | $n_{fp}$ ($s/m^{1/3}$) | $b_{fp}$ (m) | α (deg) | $n_{mc}$ ($s/m^{1/3}$) | $T_B$ (hrs) | $Q_{P1}$ ($m^3/s$) | $Q_{P2}$ ($m^3/s$) | Rel. Att (%) |
|---|---|---|---|---|---|---|---|---|---|---|
| **E1** | 50 | 1.00 | 0.25 | 25 | **0** | 0.03 | 335.5 | 153.90 | 153.68 | 0.144 |
| **E2.** | 50 | 1.00 | 0.25 | 25 | **2** | 0.03 | 335.5 | 153.90 | 153.72 | 0.117 |
| **E3.** | 50 | 1.00 | 0.25 | 25 | **5** | 0.03 | 335.5 | 153.90 | 153.81 | 0.058 |
| **E4.** | 50 | 1.00 | 0.25 | 25 | **10** | 0.03 | 335.5 | 153.90 | 153.83 | 0.045 |
| **E5.** | 50 | 1.00 | 0.25 | 25 | **15** | 0.03 | 335.5 | 153.90 | 153.84 | 0.039 |
| **E6.** | 50 | 1.00 | 0.25 | 25 | **30** | 0.03 | 335.5 | 153.90 | 153.85 | 0.032 |

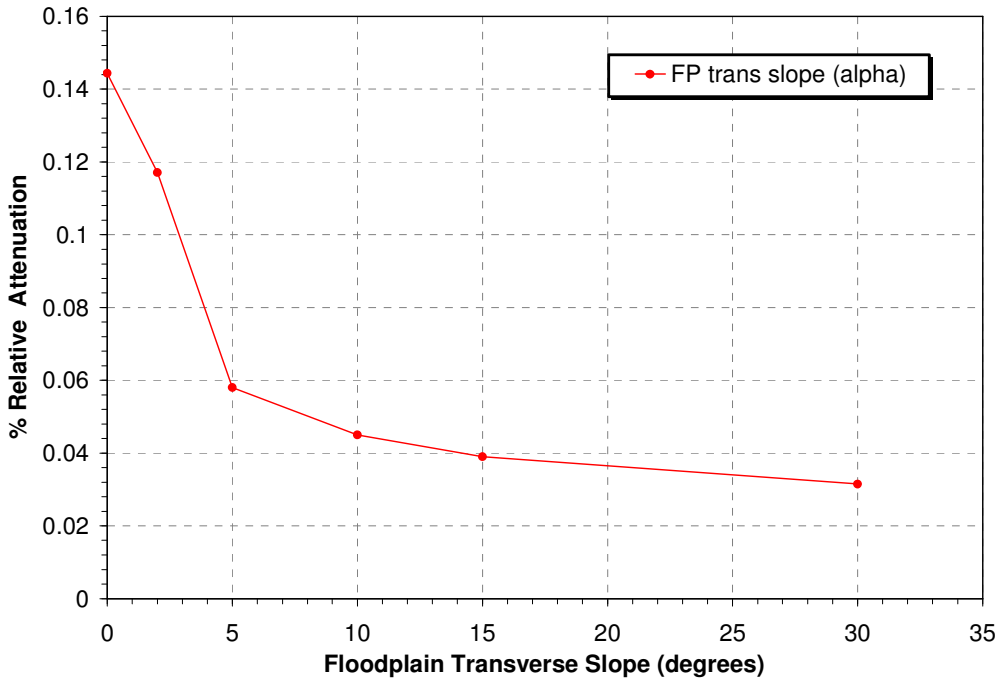


**Figure 5-11 Variation of relative attenuation with transverse floodplain slope**

The gradient towards the main channel from floodplains with steep lateral slopes results in a geometry where overbank flow is continually redirected back towards the main channel. This is reflected in Figure 5-11 where it is shown that floodplains with

increasing lateral gradients attenuate a progressively decreasing proportion of the flood peak. As a result compound channels with steep lateral slopes convey more water through the main channel than those with flatter slopes. Furthermore, floodplain resistance is typically higher than that in the main channel and the low attenuations corresponding to the steeper lateral slopes are added to as the proportion of flow being retarded by this roughness is lower than would be the case in floodplains with lower transverse gradients.

### 5.4.6 Influence of Flood Magnitude ($Q_P$)

Simulations in Case F investigated the relationship between relative attenuation and flow magnitude. Floods with return periods varying from 2 years to 1000 years as shown in Table 5-2 formed the basis of this analysis. The variation of relative attenuation for these flows is summarised in Table 5-8 and graphed in Figure 5-12.

**Table 5-8 Variation of $Q_{P1}$ with $Q_{P2}$ with flow magnitude**

| | L (km) | $S_{fp}$ (m/km) | $n_{fp}$ ($s/m^{1/3}$) | $b_{fp}$ (m) | α (deg) | $n_{mc}$ ($s/m^{1/3}$) | $T_B$ (hrs) | $Q_{P1}$ ($m^3/s$) | $Q_{P2}$ ($m^3/s$) | Rel. Att (%) |
|---|---|---|---|---|---|---|---|---|---|---|
| **F1.** | 50 | 1.00 | 0.25 | 25 | 0 | 0.03 | 335.5 | **91.41** | 91.38 | 0.036 |
| **F2.** | 50 | 1.00 | 0.25 | 25 | 0 | 0.03 | 335.5 | **102.06** | 101.95 | 0.107 |
| **F3.** | 50 | 1.00 | 0.25 | 25 | 0 | 0.03 | 335.5 | **110.12** | 109.95 | 0.150 |
| **F4.** | 50 | 1.00 | 0.25 | 25 | 0 | 0.03 | 335.5 | **119.03** | 118.85 | 0.153 |
| **F5.** | 50 | 1.00 | 0.25 | 25 | 0 | 0.03 | 335.5 | **125.64** | 125.45 | 0.157 |
| **F6.** | 50 | 1.00 | 0.25 | 25 | 0 | 0.03 | 335.5 | **132.21** | 132.02 | 0.144 |
| **F7.** | 50 | 1.00 | 0.25 | 25 | 0 | 0.03 | 335.5 | **140.85** | 140.66 | 0.136 |
| **F8.** | 50 | 1.00 | 0.25 | 25 | 0 | 0.03 | 335.5 | **147.38** | 147.17 | 0.142 |
| **F9.** | 50 | 1.00 | 0.25 | 25 | 0 | 0.03 | 335.5 | **153.90** | 153.68 | 0.144 |

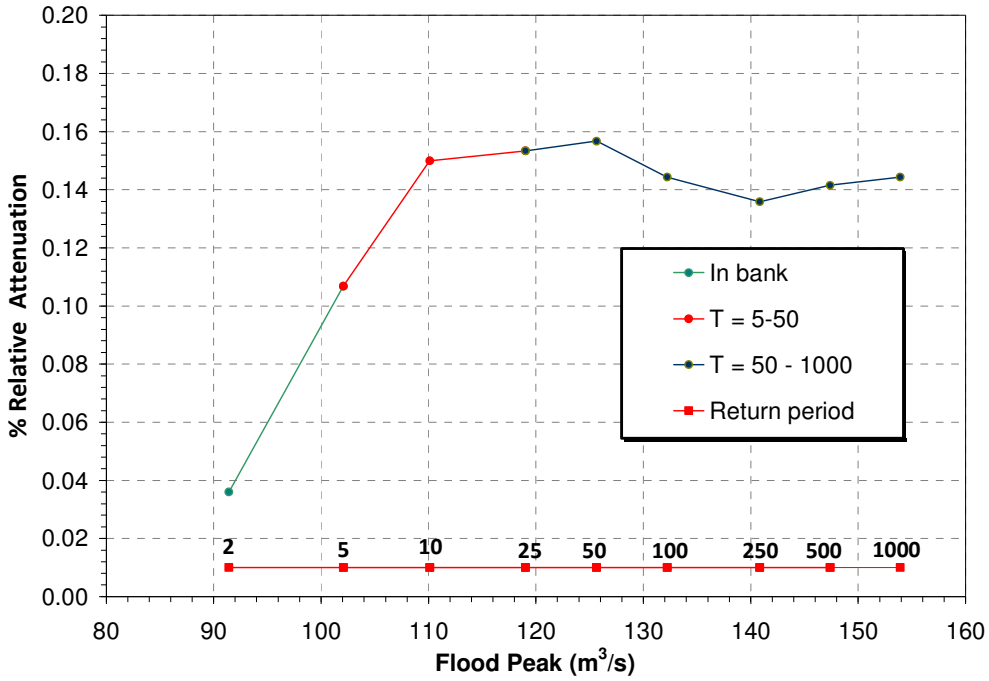


**Figure 5-12 Variation of relative attenuation with flow**

The influence of floodplains on flow attenuation is complex and is dependent on flow magnitude and floodplain depth. For return periods less than the bankfull return periods (typically between 1 and 2 years), floods will not significantly inundate the floodplain and will not be affected by the additional attenuation attributed to floodplain characteristics. Attenuation in these cases will result solely from the natural attenuation in the main channel alone and as shown in Figure 5-12 will be reasonably low. For moderate floods in the 5-year to 50-year return period range, the floodplain provides a significant area for extra storage of water and may result in decreased conveyance in the overbank channel zone. This is consistent with findings by Woltemade and Potter (1994) who observed that the attenuation of moderate volume floods, while being influenced by channel-floodplain morphology, valley width, stream slope, and hydraulic resistance, can be significant. As flows continue to increase to values for return periods greater than 50 years attenuation is shown to decrease and then approach a reasonably constant value. Floodplain resistance in the hydraulic model is defined in terms of Manning's *n* which represents a boundary resistance as opposed to drag resistance which would be significant for emergent vegetation. As flow and depth increase, this boundary resistance becomes relatively less significant in the context of the overbank flow volume being conveyed, resulting in an increase in overall velocity and a corresponding decrease in attenuation as shown.

A trend of this type is consistent with that which may be observed in natural rivers where increasing flow will for some value result in floodplain depths which are sufficient to overtop and submerge many floodplain roughness elements. When this occurs the floodplain may provide enhanced conveyance for flows that no longer follow the meanders of the main channel but rather, flow directly downstream in the

main valley direction. These more extreme floods may be conveyed more quickly and with less attenuation than less severe floods.

Experiments that were undertaken at prototype channel scale in the UK Flood Channel Facility (FCF) for smooth surface penetrating roughened floodplains assessed the functional relationship between floodplain flows and floodplain depth and indicated that the turbulent momentum exchange between the main channel and floodplain that characterises compound channel flows is most intense for relative depths (relative depth = (H-h)/H) where *H* is the total depth and *h* is the bankfull depth) in the range between 0.1 and 0.3 with typical values approximately 0.2 (Knight and Shiono, 1996). Attenuation of the flood peak from floodplain effects may also be expected to be at a maximum in this relative depth range.

A relative depth based on average water depths at cross-sections through the generalised model was extracted from flood routing of the inflow hydrographs for return periods from 2 to 100 years. These depths with corresponding relative attenuation values are shown in Table 5-9 and plotted in Figure 5-13.

**Table 5-9 Average relative depth and corresponding relative attenuation values for return periods from 2 to 1000 years**

| T (Yrs) | $Q_T$ (cumec) | Overbank Depth (H-h) (m) | Relative depth (H-h)/H | Rel. attn in $Q_P$ (% ) |
|---|---|---|---|---|
| 2 | 91.41 | In bank | 0 | 0.04 |
| 5 | 102.06 | 0.087 | 0.033 | 0.11 |
| 10 | 110.12 | 0.205 | 0.076 | 0.15 |
| 25 | 119.03 | 0.324 | 0.115 | 0.15 |
| 50 | 125.64 | 0.406 | 0.140 | 0.16 |
| 100 | 132.21 | 0.487 | 0.163 | 0.14 |
| 250 | 140.85 | 0.589 | 0.191 | 0.14 |
| 500 | 147.38 | 0.662 | 0.209 | 0.14 |
| 1000 | 153.90 | 0.734 | 0.227 | 0.14 |

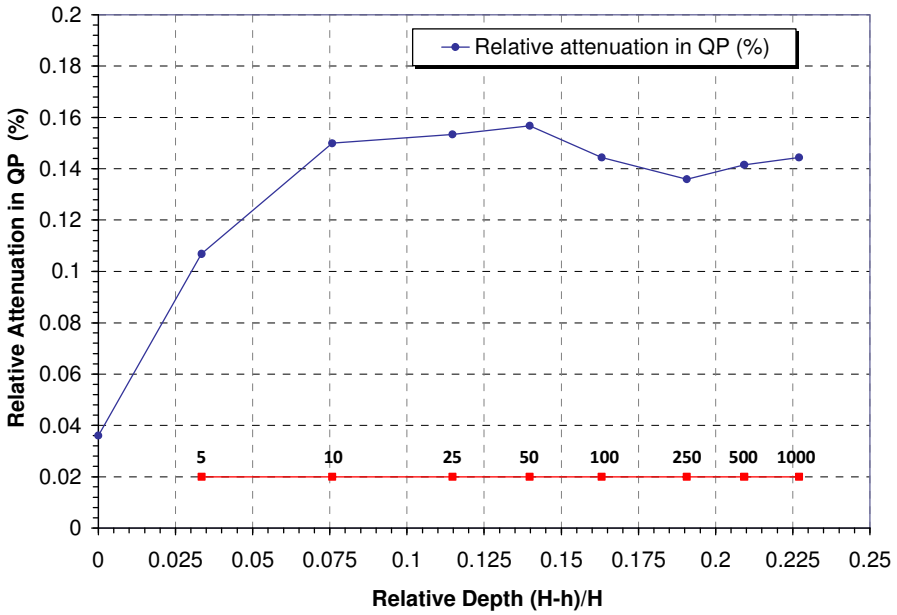


**Figure 5-13 Variation of relative attenuation with relative depth for return periods from 2 to 1000 years**

Although not related to turbulent momentum exchanges between the main channel and floodplains because of limitations with the use of a 1-Dimensional model, Figure 5-13 suggests that for the case investigated, maximum relative attenuation occurs at an average relative depth of approximately 0.14 but serves to indicate the significance of floodplain depth on attenuation effects. Other studies, albeit those that analyse main channel and floodplain interaction processes in greater detail, have recognised the relationship between floodplain flows and depth (for example Imamoto and Kuge 1974; Knight *et al.*, 1983, 1984, 1990, 1991; Tominaga and Nezu 1991; Ackers, 1992b, 1993a and 1993b as cited in Knight and Shiono (1996).

### 5.4.7 Influence of Main Channel Resistance ($n_{mc}$)

In unsteady open channel modelling, direct or explicit estimation of the main channel roughness coefficient remains a challenge in flow routing. Roughness depends on several factors including surface roughness characteristics, the presence of vegetation, channel irregularity, bed form characteristics, depth and flow magnitude.

Simulations in Case G investigated the influence of main channel Manning's roughness ($n_{mc}$) on the relative attenuation of peak flows. Ten main channel roughness values varying from 0.03 to 5.0 as shown in Table 5-2 formed the basis of this analysis and the variation of these with relative attenuation is tabulated in Table 5-10 and plotted in Figure 5-14.

**Table 5-10 Variation of $Q_{P1}$ with $Q_{P2}$ with main channel roughness ($n_{mc}$)**

| | L (km) | $S_{fp}$ (m/km) | $n_{fp}$ ($s/m^{1/3}$) | $b_{fp}$ (m) | α (deg) | $n_{mc}$ ($s/m^{1/3}$) | $T_B$ (hrs) | $Q_{P1}$ ($m^3/s$) | $Q_{P2}$ ($m^3/s$) | Rel. Att (%) |
|---|---|---|---|---|---|---|---|---|---|---|
| **G1.** | 50 | 1.00 | 0.25 | 25 | 0 | **0.03** | 335.5 | 153.90 | 153.68 | 0.143 |
| **G2.** | 50 | 1.00 | 0.25 | 25 | 0 | **0.06** | 335.5 | 153.90 | 153.50 | 0.260 |
| **G3.** | 50 | 1.00 | 0.25 | 25 | 0 | **0.10** | 335.5 | 153.90 | 153.23 | 0.435 |
| **G4.** | 50 | 1.00 | 0.25 | 25 | 0 | **0.15** | 335.5 | 153.90 | 152.64 | 0.819 |
| **G5.** | 50 | 1.00 | 0.25 | 25 | 0 | **0.20** | 335.5 | 153.90 | 152.00 | 1.235 |
| **G6.** | 50 | 1.00 | 0.25 | 25 | 0 | **0.30** | 335.5 | 153.90 | 150.83 | 1.995 |
| **G7.** | 50 | 1.00 | 0.25 | 25 | 0 | **0.50** | 335.5 | 153.90 | 149.09 | 3.125 |
| **G8.** | 50 | 1.00 | 0.25 | 25 | 0 | **1.00** | 335.5 | 153.90 | 146.89 | 4.555 |
| **G9.** | 50 | 1.00 | 0.25 | 25 | 0 | **2.00** | 335.5 | 153.90 | 145.33 | 5.569 |
| **G10.** | 50 | 1.00 | 0.25 | 25 | 0 | **5.00** | 335.5 | 153.90 | 144.18 | 6.316 |

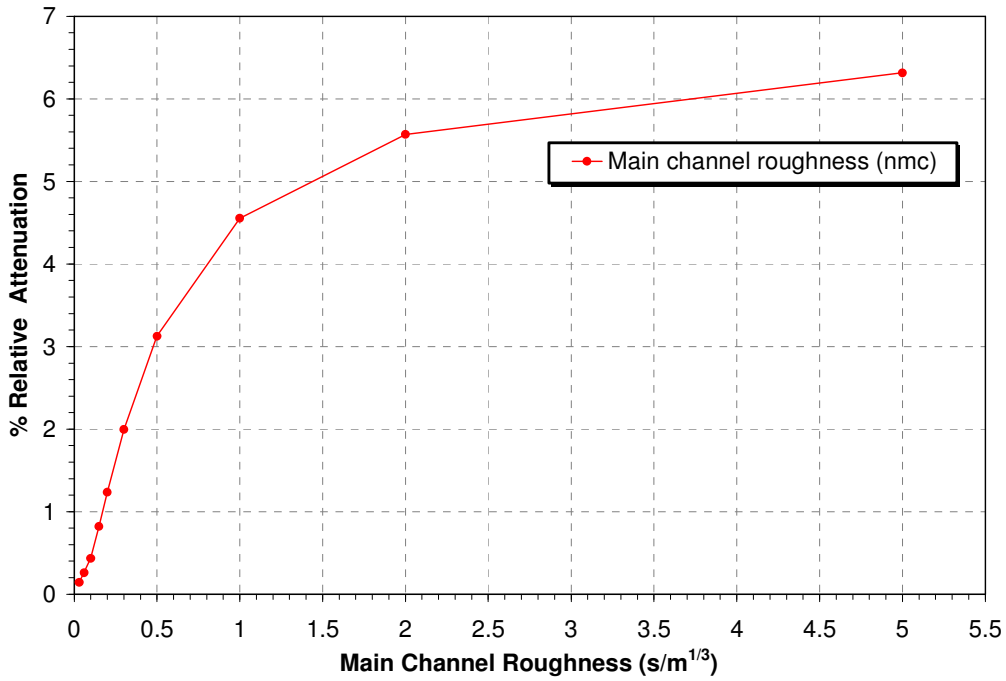


**Figure 5-14 Variation of relative attenuation with main channel roughness**

Figure 5-14 indicates that relative attenuation increases with main channel roughness and represents the lower velocities associated with greater energy dissipation in high resistance channels. As main channel resistance continues to increase, a point is reached where the flow approaches stagnation and further changes in relative attenuation in this high roughness range are small.

### 5.4.8 Influence of Flow Duration ($T_B$)

The factors that affect the shape of the hydrograph can be broadly grouped into climatic factors and physiographic factors. The climatic factors reflect the storm

characteristics, initial loss and evapo-transpiration. The physiographic factors include river basin, infiltration and channel characteristics.

Simulations in Case F assessed the flow peak ($Q_P$), an important parameter in defining hydrograph shape and Case H investigated the influence of flood duration ($T_B$) on the relative attenuation. When combined, $Q_P$ and $T_B$ define the flood volume. Flood durations varying from 1.75 hours to 2007.75 hours as shown in Figure 5-4 were assessed. The influence on relative attenuation for these durations are summarised in Table 5-11 and shown graphically in Figure 5-15.

**Table 5-11 Variation of $Q_{P1}$ with $Q_{P2}$ with flood duration**

| | L (km) | $S_{fp}$ (m/km) | $n_{fp}$ ($s/m^{1/3}$) | $b_{fp}$ (m) | α (deg) | $n_{mc}$ ($s/m^{1/3}$) | $T_B$ (hrs) | $Q_{P1}$ ($m^3/s$) | $Q_{P2}$ ($m^3/s$) | Rel. Att (%) |
|---|---|---|---|---|---|---|---|---|---|---|
| **H1.** | 50 | 1.00 | 0.25 | 25 | 0 | 0.03 | **1.75** | 153.90 | 25.62 | 83.35 |
| **H2.** | 50 | 1.00 | 0.25 | 25 | 0 | 0.03 | **3.25** | 153.90 | 47.65 | 69.04 |
| **H3.** | 50 | 1.00 | 0.25 | 25 | 0 | 0.03 | **6.75** | 153.90 | 90.24 | 41.36 |
| **H4.** | 50 | 1.00 | 0.25 | 25 | 0 | 0.03 | **20.00** | 153.90 | 124.77 | 18.93 |
| **H5.** | 50 | 1.00 | 0.25 | 25 | 0 | 0.03 | **53.75** | 153.90 | 141.09 | 8.32 |
| **H6.** | 50 | 1.00 | 0.25 | 25 | 0 | 0.03 | **66.75** | 153.90 | 143.57 | 6.71 |
| **H7.** | 50 | 1.00 | 0.25 | 25 | 0 | 0.03 | **167.50** | 153.90 | 149.79 | 2.67 |
| **H8.** | 50 | 1.00 | 0.25 | 25 | 0 | 0.03 | **265.00** | 153.90 | 151.35 | 1.66 |
| **H9.** | 50 | 1.00 | 0.25 | 25 | 0 | 0.03 | **334.50** | 153.90 | 151.83 | 1.35 |
| **H10.** | 50 | 1.00 | 0.25 | 25 | 0 | 0.03 | **502.01** | 153.90 | 152.52 | 0.90 |
| **H11.** | 50 | 1.00 | 0.25 | 25 | 0 | 0.03 | **669.50** | 153.90 | 152.86 | 0.68 |
| **H12.** | 50 | 1.00 | 0.25 | 25 | 0 | 0.03 | **1338.75** | 153.90 | 153.38 | 0.34 |
| **H13.** | 50 | 1.00 | 0.25 | 25 | 0 | 0.03 | **2007.75** | 153.90 | 153.56 | 0.22 |

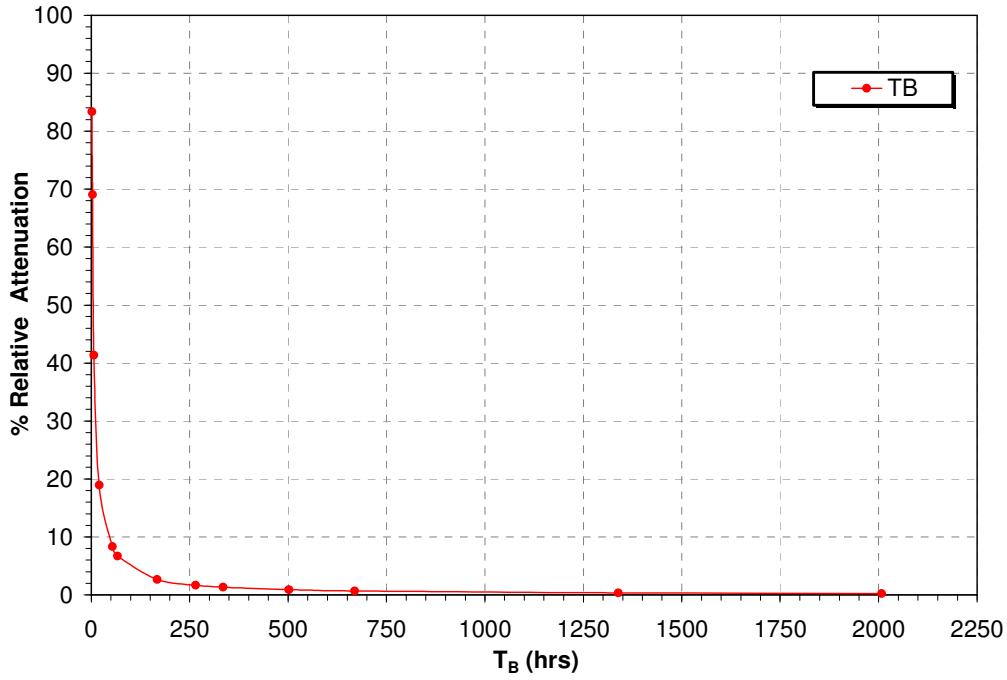


**Figure 5-15 Variation of relative attenuation with flood duration**

As expected, Figure 5-15 indicates that hydrographs with sharp peaks but low volumes (short duration) experience significantly higher attenuation than those hydrographs with higher volumes. Floods that are characterised by high volumes on the rising limb of the hydrograph will tend to occupy floodplain storage that is available and once occupied, this storage is no longer available for the remainder of the flood. The attenuation provided by the floodplain in these high volume floods is therefore less significant. In contrast, hydrographs with low rising limb volumes disperse most of the flood volume to storage resulting in relative attenuations that are high.

## 5.5 Development of Flood Peak Attenuation Index

The simple index that allows for floodplain effects was developed from a multivariate regression model related to parameters that typically influence the capacity of a floodplain to attenuate flow. For this analysis, geometrical properties of the main channel and floodplain are important and include bankfull width ($b_{bf}$), floodplain length (L), floodplain width ($b_{fp}$) and the transverse or lateral slope of the floodplain ($\alpha$). Hydraulic resistance is represented in terms of Manning's *n* and is assigned to both the main channel ($n_{mc}$) and floodplain ($n_{fp}$) zones. The flood characteristics are also influential and are represented in terms of the hydrograph properties of flood peak ($Q_P$) and duration ($T_B$). From the results presented in Section 5.4 the influence of these parameters in contributing to floodplain attenuation has been assessed in terms of relative attenuation and forms the basis of the regression model. The regression analysis was undertaken to produce a single index that reflects the influences of these parameters on the attenuation of the flood peak.

The optimised equation for the attenuation index from the regression model was based on minimising the square of the errors (least squares fit) between attenuation values determined from simulations and those determined from the equation. The floodplain width ($b_{fp}$) and the bankfull width ($b_{bf}$) were expressed as a single parameter defined by the ratio of these widths. $b_{fp}/b_{bf}$. Grouping these channel widths in this ratio is consistent with other compound channel research (example Knight and Shiono, 1996) and is convenient in representing the diffusion effects of the flow along the interface between the floodplain and main channel of the overall cross-section.

Furthermore, the analysis detailed in Sections 5.4.3, 5.4.4 and 5.4.7 included an assessment of main channel and floodplain Manning's *n* up to maximum values of 5 and of floodplain widths up to 2 km as summarised in Table 5-2. This range of values far exceeds the range that could be considered relevant to Irish catchments and for this reason the regression model was limited to main channel and floodplain Manning's n values up to 2 and floodplain widths up to 1 km. It should also be noted that the floodplain width ($b_{fp}$) is as shown in Figure 5-5 and the 1km floodplain width refers to a single floodplain only and the term $b_{fp}/b_{bf}$ in effect represents a shape parameter by which the discharge term is multiplied.

This optimised equation was found to be:

$$\% \text{ Relative Attenuation} = 14050 \frac{L \; n_{fp} \; n_{mc} \left(\frac{b_{fp}}{b_{bf}}\right)^{1.54} \left(\frac{Q_P}{B}\right)^{0.44}}{S_{fp}^{1.54} \alpha^{0.18} \left(12.97+T_B\right)^{1.96}} \qquad \textbf{Eqn. 5.6}$$

The total channel width (B) is also included in Eqn 5.6 and is defined as $2b_{fp} + b_{bf}$.

Application of Eqn. 5.6 requires that $\alpha > 0$ and therefore horizontal floodplains are represented by a near-zero value of $\alpha$. Similarly, the equation assesses floodplain effects and therefore $Q_P > Q_{bf}$ where $Q_{bf}$ is the estimated bankfull discharge in the river.

It should be noted at this point that Eqn. 5.6 is based solely on the assessed influence of the above mentioned parameters on relative attenuation using the HEC-RAS model and has therefore accepted limitations. The values of parameter exponents are based on the simulated data only and therefore, as with regression models of this type, parameters that may intuitively be considered to be important do not necessarily come to the fore in the analysis. Eqn. 5.6 represents an optimised equation for the full range of parameters investigated. However, the authors are continuing to investigate the performance of other equations developed from the regression model which include a selection of parameters (not all) that were shown to be dominant in attenuating the flood peak.

The performance of this index is shown in Figure 5-16 where the simulated relative attenuation values are plotted on linear scales against those calculated using Eqn. 5.6 for the parameters investigated.

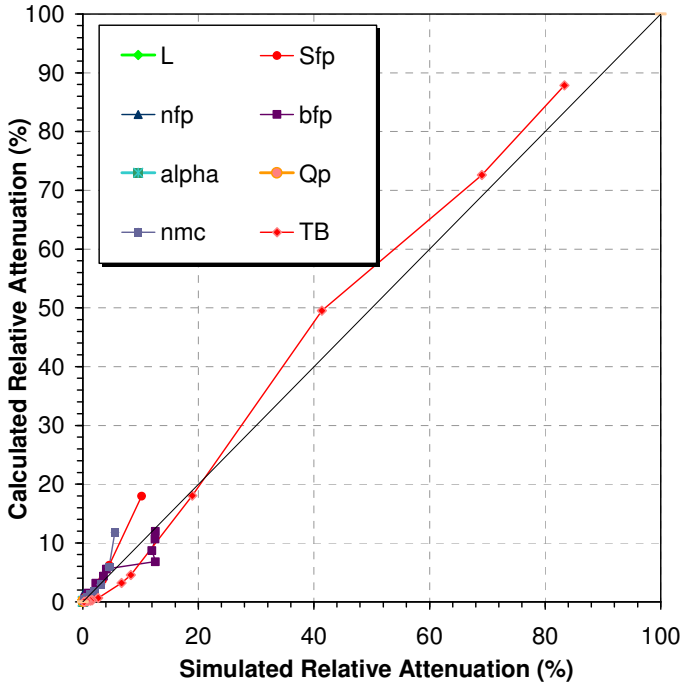


**Figure 5-16 Comparison of simulated attenuation to that calculated using index plotted on linear scales**

Figure 5-16 indicates that the generalised model resulted in relative attenuations of the peak flow that were low for many of the properties investigated and are clustered in the bottom left corner of the graph. Floodplain width ($b_{fp}$), floodplain longitudinal slope ($S_{fp}$), main channel resistance ($n_{mc}$) and flood duration ($T_B$), the latter being more dominant, were the only parameters investigated where significant attenuations were recorded.

Results in Figure 5-16 conflict with what might intuitively be expected. For example, it would be expected that significant floodplain roughness would result in reasonably large attenuations. However, a limitation of the analysis that was undertaken is that the influence of geometrical, resistance and hydrograph properties were assessed individually. Therefore, in the case of floodplain resistance, high values (up to Manning's *n* of 5) were assessed in combination with much lower main channel resistance values of 0.03 that remained constant for simulations in which floodplain roughness was being assessed. As the floodplain resistance increases, the proportion of flow being conveyed in the main channel increases and attenuation is very low. Allowing for hydraulic resistance in the generalised model through Manning's resistance represented a low value of roughness that for most conditions does not reflect the significant energy losses that would be associated with floodplain flows in most natural channels.

Furthermore, flood attenuation is sensitive to channel slope where channels with steep slopes have low attenuation properties. All simulations, with the exception of those where slope is being investigated were undertaken with an assumed slope of 0.001. This represents a reasonably steep value for slope in comparison to other Irish catchments and contributes to the cluster of low attenuation data in Figure 5-16.

Figure 5-17 shows simulated attenuations plotted against calculated attenuations on logarithmic scales. This broadens the clustered data in Figure 5-16 and facilitates more readily an evaluation of the individual parameters in Eqn. 5.6.

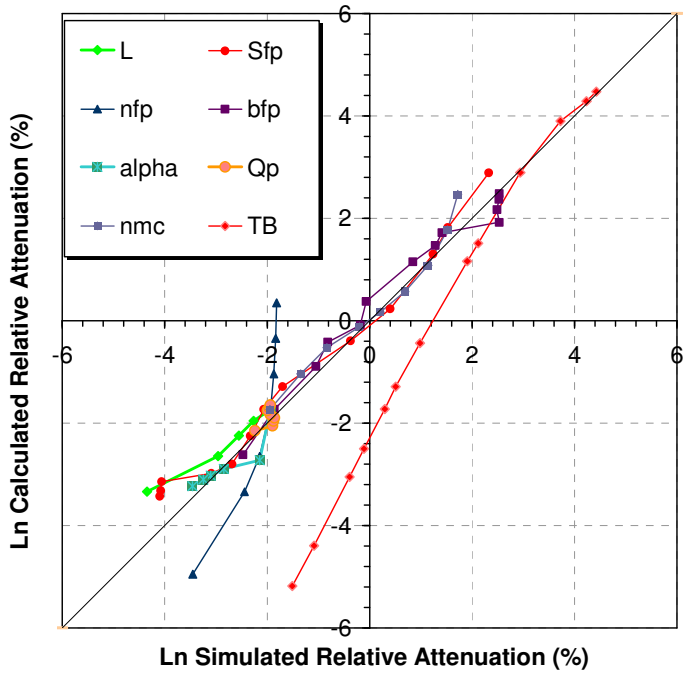


**Figure 5-17 Comparison of simulated attenuation to that calculated using index**

Figure 5-17 indicates that Eqn. 5.6 reproduces reasonably well the simulated data for most of the geometrical, resistance and hydrograph properties. The data indicates that the main sources of error in Eqn. 5.6 arise from the representation of flood duration ($T_B$) and floodplain resistance ($n_{fp}$). A reason for the poor fit of flood duration to simulated values may relate to the assumption of independence between the flood peak ($Q_P$) and the flood duration that was made when including duration as a parameter in the regression model.

Figure 5-17 also indicates that Eqn. 5.6 is more accurate at predicting high flood peak attenuations. Therefore the poor fit that is evident in the bottom left corner of Figure 5-17 is likely to be less of a concern to the flood estimator who will typically be unconcerned with low values of attenuation.

## 5.6 Results for Delay in Propagation of Flood Wave

The influence of each of the eight variables in Table 5-2 on flood hydrograph delay is assessed by comparing the time to peak of the inflow hydrograph with the time to peak of the outflow hydrograph generated in model simulations. This is shown in schematic in Figure 5-18.

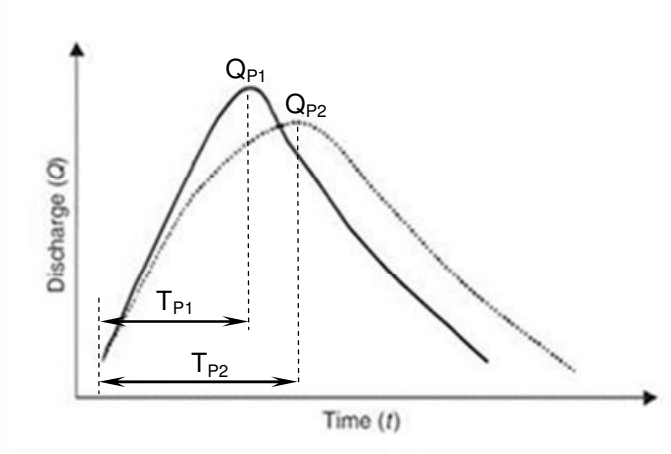


**Figure 5-18 Inflow and delayed outflow hydrographs**

Differences in upstream inflow and downstream hydrographs are represented in terms of the relative delay in flood peaks defined as:

$$\text{Relative delay in time to peak } (\%) = \frac{T_{P2} - T_{P1}}{T_{P1}} \qquad \textbf{Eqn. 5.7}$$

where $T_{P1}$ and $T_{P2}$ are the times to peak of the inflow and outflow hydrographs in Figure 5-18.

It should be noted that the shape of inflow hydrographs was kept constant throughout the study and this was defined by a start time (first point) that was arbitrarily set as 29/12/2008 at 24:00 hours. This was followed by a 'warm up' period until 2/1/09 at 02:00hours (74 hours) at the end of which the hydrograph begins to rise. The time at the peak of the inflow hydrograph ($T_{P1}$) is 04/01/2009 at 11:30 hours and represents a time to peak ($T_P$) of 69.5 hours. Hydrographs were defined in 15-minute time intervals and were defined by upwards of 4000 points.

### 5.6.1 Influence of Reach Length (L)

Simulations in Case A represent the influence of reach length on the delay of propagation of the flood wave. Reach lengths from 10km to 50 km were investigated and other parameters are as defined in Table 5-2. Results are summarised in Table 5-12 and shown graphically in Figure 5-19.

**Table 5-12 Variation of $T_{P1}$ with $T_{P2}$ with main channel length (L)**

| | L (km) | $S_{fp}$ (m/km) | $n_{fp}$ ($s/m^{1/3}$) | $b_{fp}$ (m) | α (deg) | $n_{mc}$ ($s/m^{1/3}$) | $T_B$ (hrs) | $Q_P$ ($m^3/s$) | $T_{P1}$ | $T_{P2}$ | Rel. delay (%) |
|---|---|---|---|---|---|---|---|---|---|---|---|
| A1. | 10 | 1.00 | 0.25 | 25 | 0 | 0.03 | 335.5 | 153.90 | 04/01/2009 23:30 | 05/01/2009 01:45 | 3.237 |
| A2. | 20 | 1.00 | 0.25 | 25 | 0 | 0.03 | 335.5 | 153.90 | 04/01/2009 23:30 | 05/01/2009 04:30 | 7.194 |
| A3. | 30 | 1.00 | 0.25 | 25 | 0 | 0.03 | 335.5 | 153.90 | 04/01/2009 23:30 | 05/01/2009 06:30 | 10.072 |
| A4. | 40 | 1.00 | 0.25 | 25 | 0 | 0.03 | 335.5 | 153.90 | 04/01/2009 23:30 | 05/01/2009 08:45 | 13.309 |
| A5. | 50 | 1.00 | 0.25 | 25 | 0 | 0.03 | 335.5 | 153.90 | 04/01/2009 23:30 | 05/01/2009 11:45 | 17.626 |

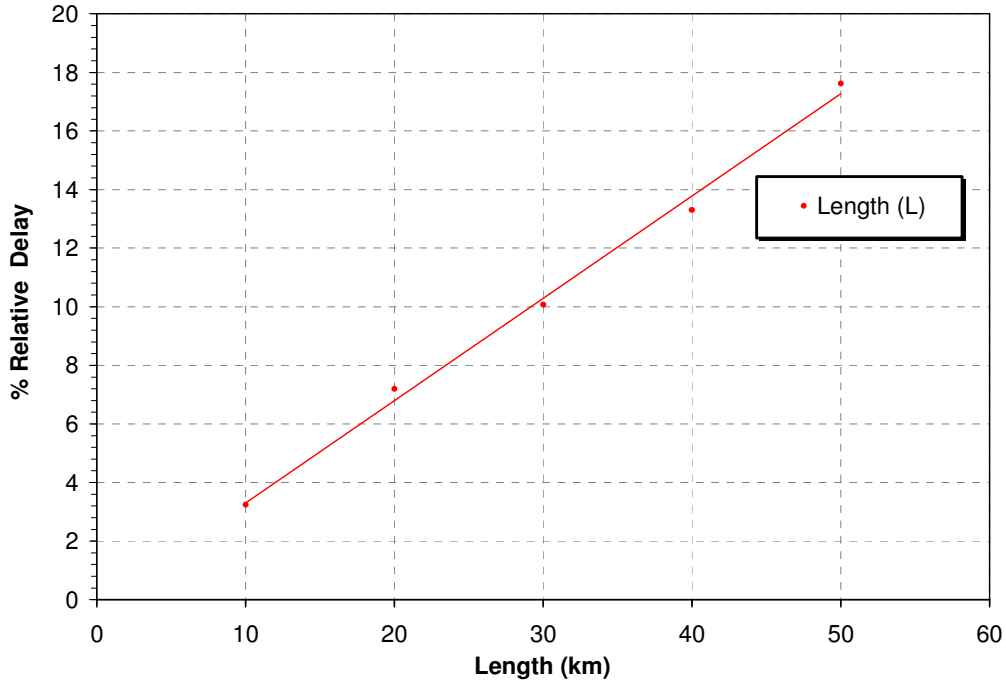


**Figure 5-19 Variation of relative delay with reach length (L)**

Figure 5-19 indicates that the relative delay in flood peak increases linearly with increasing floodplain (reach) length.

### 5.6.2 Influence of Longitudinal Floodplain Slope ($S_{fp}$)

The effects of longitudinal floodplain slope on the delay in flood peak were investigated for a range of gradients from 0.1 m/km in Case B1 to 3m/km in Case B 11. The variation of relative delay with floodplain slope is summarised in Table 5-13 and shown graphically in Figure 5-20.

**Table 5-13 Variation of $T_{P1}$ with $T_{P2}$ with floodplain slope ($S_{fp}$)**

| | L (km) | $S_{fp}$ (m/km) | $n_{fp}$ ($s/m^{1/3}$) | $b_{fp}$ (m) | α (deg) | $n_{mc}$ ($s/m^{1/3}$) | $T_B$ (hrs) | $Q_P$ ($m^3/s$) | $T_{P1}$ | $T_{P2}$ | Rel. delay (%) |
|---|---|---|---|---|---|---|---|---|---|---|---|
| **B1.** | 50 | **0.10** | 0.25 | 25 | 0 | 0.03 | 335.5 | 153.90 | 04/01/2009 23:30 | 06/01/2009 04:30 | 41.73 |
| **B2.** | 50 | **0.14** | 0.25 | 25 | 0 | 0.03 | 335.5 | 153.90 | 04/01/2009 23:30 | 06/01/2009 03:00 | 39.57 |
| **B3.** | 50 | **0.28** | 0.25 | 25 | 0 | 0.03 | 335.5 | 153.90 | 04/01/2009 23:30 | 05/01/2009 21:00 | 30.94 |
| **B4.** | 50 | **0.42** | 0.25 | 25 | 0 | 0.03 | 335.5 | 153.90 | 04/01/2009 23:30 | 05/01/2009 17:15 | 25.54 |
| **B5.** | 50 | **0.75** | 0.25 | 25 | 0 | 0.03 | 335.5 | 153.90 | 04/01/2009 23:30 | 05/01/2009 12:00 | 17.99 |
| **B6.** | 50 | **1.00** | 0.25 | 25 | 0 | 0.03 | 335.5 | 153.90 | 04/01/2009 23:30 | 05/01/2009 11:00 | 16.55 |
| **B7.** | 50 | **1.40** | 0.25 | 25 | 0 | 0.03 | 335.5 | 153.90 | 04/01/2009 23:30 | 05/01/2009 09:45 | 14.75 |
| **B8.** | 50 | **2.00** | 0.25 | 25 | 0 | 0.03 | 335.5 | 153.90 | 04/01/2009 23:30 | 05/01/2009 09:15 | 14.03 |
| **B09.** | 50 | **2.25** | 0.25 | 25 | 0 | 0.03 | 335.5 | 153.90 | 04/01/2009 23:30 | 05/01/2009 07:00 | 10.79 |
| **B10.** | 50 | **2.50** | 0.25 | 25 | 0 | 0.03 | 335.5 | 153.90 | 04/01/2009 23:30 | 05/01/2009 03:15 | 5.40 |
| **B11.** | 50 | **3.00** | 0.25 | 25 | 0 | 0.03 | 335.5 | 153.90 | 04/01/2009 23:30 | 05/01/2009 03:00 | 5.04 |

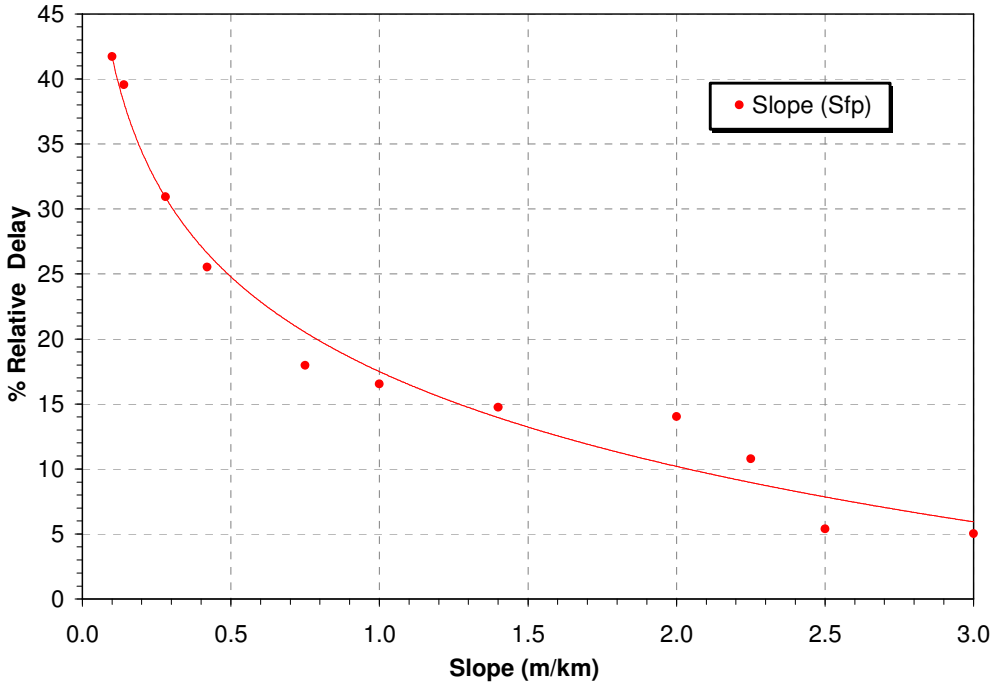


**Figure 5-20 Variation of relative delay with floodplain slope ($S_{fp}$)**

Figure 5-20 indicates that the delay in the inflow hydrograph being propagated downstream decreases as the longitudinal floodplain slope increases. Steeper catchments have the capacity to convey floodwater more quickly that lower gradient catchments, reducing the storage of the flood volume in the reach. The relationship between slope and flood peak delay in Figure 5-20 is consistent with Ghavasieh *et al.* (2006) where, for a range of floodplain resistances in different compound channel geometries, the longest delays in time to peaks were observed in low gradient channels with small bankfull discharge capacities.

### 5.6.3 Influence of Floodplain Roughness ($n_{fp}$)

As summarised in Table 5-2, floodplain resistances in terms of Manning's *n* varying from 0.01 to 5 were investigated in this study. The influence of the delay of flood wave propagation for these resistances is summarised in Table 5-14 and shown in Figure 5-21.

**Table 5-14 Variation of $T_{P1}$ with $T_{P2}$ with floodplain roughness ($n_{fp}$)**

| | L (km) | $S_{fp}$ (m/km) | $n_{fp}$ ($s/m^{1/3}$) | $b_{fp}$ (m) | α (deg) | $n_{mc}$ ($s/m^{1/3}$) | $T_B$ (hrs) | $Q_P$ ($m^3/s$) | $T_{P1}$ | $T_{P2}$ | Rel. delay (%) |
|---|---|---|---|---|---|---|---|---|---|---|---|
| **C1.** | 50 | 1.00 | **0.01** | 25 | 0 | 0.03 | 335.5 | 153.90 | 04/01/2009 23:30 | 05/01/2009 04:00 | 6.47 |
| **C2.** | 50 | 1.00 | **0.05** | 25 | 0 | 0.03 | 335.5 | 153.90 | 04/01/2009 23:30 | 05/01/2009 09:00 | 13.67 |
| **C3.** | 50 | 1.00 | **0.10** | 25 | 0 | 0.03 | 335.5 | 153.90 | 04/01/2009 23:30 | 05/01/2009 10:30 | 15.83 |
| **C4.** | 50 | 1.00 | **0.25** | 25 | 0 | 0.03 | 335.5 | 153.90 | 04/01/2009 23:30 | 05/01/2009 11:00 | 16.55 |
| **C5.** | 50 | 1.00 | **0.50** | 25 | 0 | 0.03 | 335.5 | 153.90 | 04/01/2009 23:30 | 05/01/2009 11:30 | 17.27 |
| **C6.** | 50 | 1.00 | **1.00** | 25 | 0 | 0.03 | 335.5 | 153.90 | 04/01/2009 23:30 | 05/01/2009 11:45 | 17.63 |
| **C7.** | 50 | 1.00 | **2.00** | 25 | 0 | 0.03 | 335.5 | 153.90 | 04/01/2009 23:30 | 05/01/2009 12:00 | 17.99 |
| **C8.** | 50 | 1.00 | **5.00** | 25 | 0 | 0.03 | 335.5 | 153.90 | 04/01/2009 23:30 | 05/01/2009 12:00 | 17.99 |

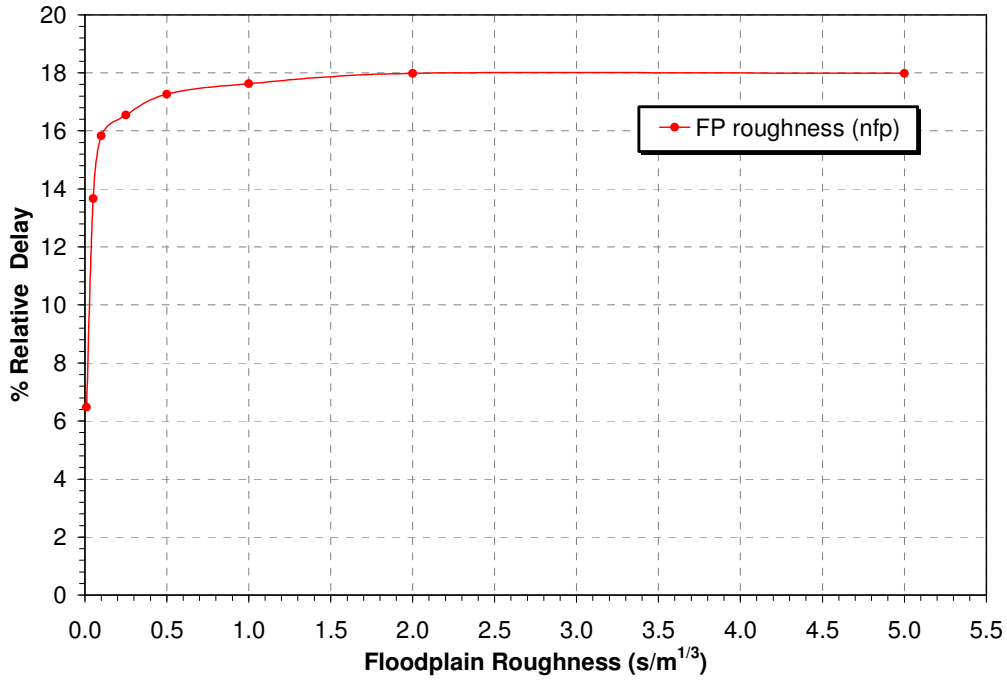


**Figure 5-21 Variation of relative delay with floodplain roughness ($n_{fp}$)**

Figure 5-21 indicates that the relative delay of the time to peak increases rapidly for Manning's resistances up to 0.1 but tends to a constant value (18% for the case shown) as roughness continues to increase. Increasing resistance causes decreases in velocity values across the channel that serve to reduce the flood wave travel time.

However, Figure 5-21 does not represent a relationship between floodplain roughness and attenuation that would be expected in natural channels. In natural channels attenuation would increase as the resistance on floodplain also increases but for high flows and depths roughness in many channels may be expected to become submerged with a resulting increase in velocity and reduction in attenuation.

### 5.6.4 Influence of Floodplain Width ($b_{fp}$)

Effects of floodplain width on the delay of the flood peak were assessed in Case D simulations. A general feature of floodplain flows is their strong dependence on the over-bank flow depth (Knight and Shiono, 1996). For wider floodplains, a given discharge may be conveyed along the channel at a low overbank depth. Low overbank depths promote significant momentum transfer between the river and the floodplain reducing the overall flow velocity and increasing the time of travel of the flood peak. Channels with narrow floodplains typically convey flood flows at higher depths and with higher velocities. In an attempt to represent these varying floodplain characteristics, floodplain widths from 12.5m to 2000m (convenient multiples of the bankfull width of 25m) were included in the analysis. The variation of the delay in the flood peak with these floodplain widths is summarised in Table 5-15 and shown graphically in Figure 5-22.

**Table 5-15 Variation of $T_{P1}$ with $T_{P2}$ with floodplain width ($b_{fp}$)**

| | L (km) | $S_{fp}$ (m/km) | $n_{fp}$ ($s/m^{1/3}$) | $b_{fp}$ (m) | α (deg) | $n_{mc}$ ($s/m^{1/3}$) | $T_B$ (hrs) | $Q_P$ ($m^3/s$) | $T_{P1}$ | $T_{P2}$ | Rel. delay (%) |
|---|---|---|---|---|---|---|---|---|---|---|---|
| **D1** | 50 | 1.00 | 0.25 | **12.5** | 0 | 0.03 | 335.5 | 153.90 | 04/01/2009 23:30 | 05/01/2009 07:45 | 11.87 |
| **D2.** | 50 | 1.00 | 0.25 | **25** | 0 | 0.03 | 335.5 | 153.90 | 04/01/2009 23:30 | 05/01/2009 11:45 | 17.63 |
| **D3.** | 50 | 1.00 | 0.25 | **50** | 0 | 0.03 | 335.5 | 153.90 | 04/01/2009 23:30 | 05/01/2009 19:00 | 28.06 |
| **D4.** | 50 | 1.00 | 0.25 | **75** | 0 | 0.03 | 335.5 | 153.90 | 04/01/2009 23:30 | 05/01/2009 23:30 | 34.53 |
| **D5.** | 50 | 1.00 | 0.25 | **100** | 0 | 0.03 | 335.5 | 153.90 | 04/01/2009 23:30 | 06/01/2009 09:15 | 48.56 |
| **D6.** | 50 | 1.00 | 0.25 | **150** | 0 | 0.03 | 335.5 | 153.90 | 04/01/2009 23:30 | 06/01/2009 15:00 | 56.83 |
| **D7.** | 50 | 1.00 | 0.25 | **300** | 0 | 0.03 | 335.5 | 153.90 | 04/01/2009 23:30 | 07/01/2009 14:15 | 90.29 |
| **D8.** | 50 | 1.00 | 0.25 | **400** | 0 | 0.03 | 335.5 | 153.90 | 04/01/2009 23:30 | 08/01/2009 06:15 | 113.31 |
| **D9.** | 50 | 1.00 | 0.25 | **500** | 0 | 0.03 | 335.5 | 153.90 | 04/01/2009 23:30 | 08/01/2009 22:00 | 135.97 |
| **D10.** | 50 | 1.00 | 0.25 | **600** | 0 | 0.03 | 335.5 | 153.90 | 04/01/2009 23:30 | 09/01/2009 01:45 | 141.37 |
| **D11.** | 50 | 1.00 | 0.25 | **750** | 0 | 0.03 | 335.5 | 153.90 | 04/01/2009 23:30 | 09/01/2009 05:45 | 147.12 |
| **D12.** | 50 | 1.00 | 0.25 | **900** | 0 | 0.03 | 335.5 | 153.90 | 04/01/2009 23:30 | 09/01/2009 08:15 | 150.72 |
| **D13.** | 50 | 1.00 | 0.25 | **1000** | 0 | 0.03 | 335.5 | 153.90 | 04/01/2009 23:30 | 09/01/2009 08:15 | 150.72 |
| **D14.** | 50 | 1.00 | 0.25 | **1175** | 0 | 0.03 | 335.5 | 153.90 | 04/01/2009 23:30 | 09/01/2009 05:30 | 146.76 |
| **D15.** | 50 | 1.00 | 0.25 | **1250** | 0 | 0.03 | 335.5 | 153.90 | 04/01/2009 23:30 | 09/01/2009 08:30 | 151.08 |
| **D16.** | 50 | 1.00 | 0.25 | **1500** | 0 | 0.03 | 335.5 | 153.90 | 04/01/2009 23:30 | 09/01/2009 10:45 | 154.32 |
| **D17.** | 50 | 1.00 | 0.25 | **1700** | 0 | 0.03 | 335.5 | 153.90 | 04/01/2009 23:30 | 09/01/2009 07:45 | 150.00 |
| **D18.** | 50 | 1.00 | 0.25 | **2000** | 0 | 0.03 | 335.5 | 153.90 | 04/01/2009 23:30 | 09/01/2009 05:45 | 147.12 |

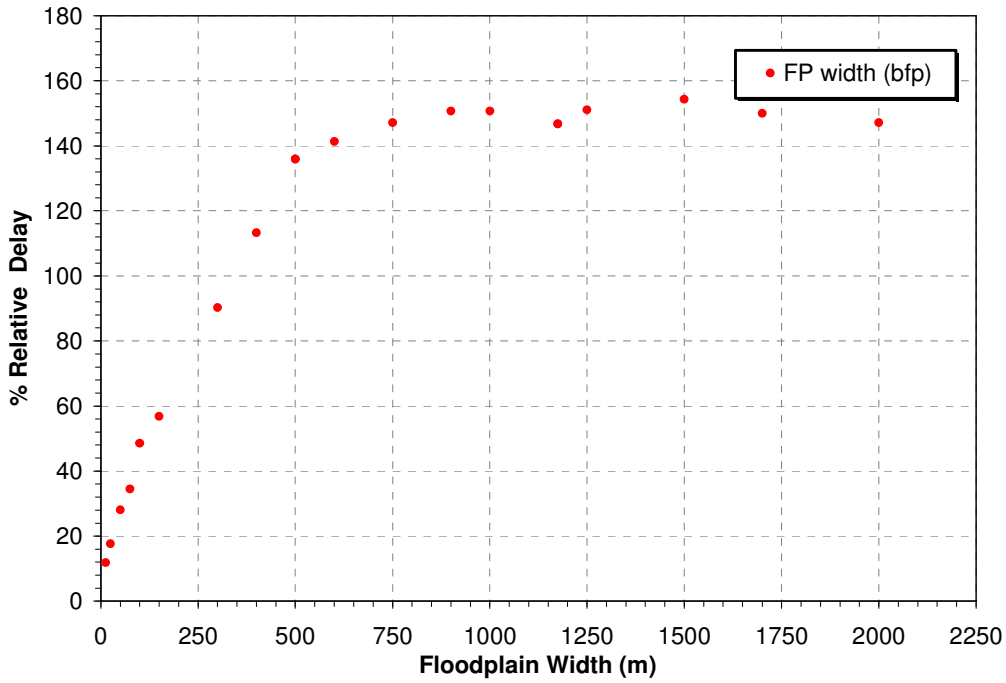


**Figure 5-22 Variation of relative delay with floodplain width ($b_{fp}$)**

Increasing the floodplain width results in an increased storage capacity in the overbank zone of the channel section and as would be expected, results in greater delay of the flood peak. Figure 5-22 suggests that for the generic model investigated in this study, the relationship between relative delay and floodplain width can be reasonably well represented by a linear relationship up to values of approximately 500m. Floodplain widths beyond this value result in relative delays that become constant. As width continues to increase, floodplain depth for a specified flow ($Q_P$ = 153.9$m^3$/s in this case) decreases and reaches a low and limiting value associated with this constant relative delay value, below which further decreases in floodplain depth have no discernible influence on the relative delay of the flood wave.

### 5.6.5 Influence of Transverse Floodplain Slope (α)

Case E simulations investigated the influence of the transverse (lateral) floodplain slope on the delay of the flood peak. This influence for transverse slopes that increase from being horizontal ($\alpha = 0^o$) to being sloped at $30^o$ are summarised in Table 5-16 and shown in Figure 5-23.

**Table 5-16 Variation of $T_{P1}$ with $T_{P2}$ with transverse floodplain slope (α)**

| | L (km) | $S_{fp}$ (m/km) | $n_{fp}$ ($s/m^{1/3}$) | $b_{fp}$ (m) | α (deg) | $n_{mc}$ ($s/m^{1/3}$) | $T_B$ (hrs) | $Q_P$ ($m^3/s$) | $T_{P1}$ | $T_{P2}$ | Rel. delay (%) |
|---|---|---|---|---|---|---|---|---|---|---|---|
| **E1.** | 50 | 1.00 | 0.25 | 25 | **0** | 0.03 | 335.5 | 153.90 | 04/01/2009 23:30 | 05/01/2009 11:00 | 16.55 |
| **E2.** | 50 | 1.00 | 0.25 | 25 | **2** | 0.03 | 335.5 | 153.90 | 04/01/2009 23:30 | 05/01/2009 10:00 | 15.11 |
| **E3.** | 50 | 1.00 | 0.25 | 25 | **5** | 0.03 | 335.5 | 153.90 | 04/01/2009 23:30 | 05/01/2009 06:15 | 9.71 |
| **E4.** | 50 | 1.00 | 0.25 | 25 | **10** | 0.03 | 335.5 | 153.90 | 04/01/2009 23:30 | 05/01/2009 05:45 | 8.99 |
| **E5.** | 50 | 1.00 | 0.25 | 25 | **15** | 0.03 | 335.5 | 153.90 | 04/01/2009 23:30 | 05/01/2009 05:00 | 7.91 |
| **E6.** | 50 | 1.00 | 0.25 | 25 | **30** | 0.03 | 335.5 | 153.90 | 04/01/2009 23:30 | 05/01/2009 04:15 | 6.83 |

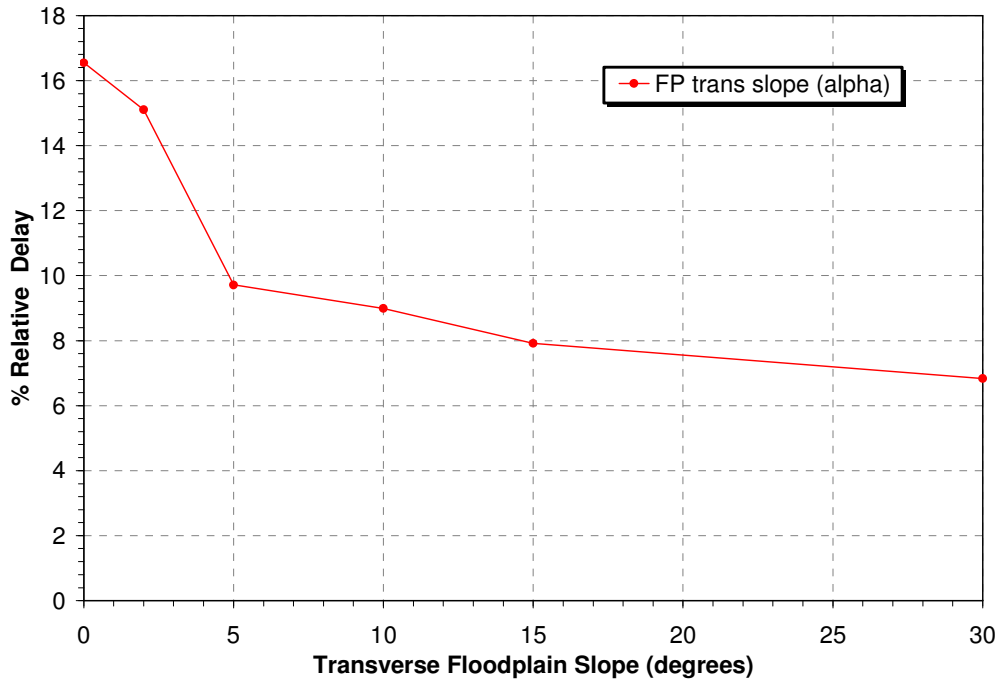


**Figure 5-23 Variation of relative delay with transverse floodplain slope (α)**

Channels with floodplains that slope steeply towards the main channel will convey a greater proportion of the total flow in the main channel than channels with flatter floodplains. Main channel resistance is typically lower than that on the floodplain and consequently, there is less floodplain attenuation in compound channels with significant lateral floodplain slopes. As a result and as indicated in Figure 5-23, channels with more steeply sloping lateral floodplains have the capacity to deliver a flood downstream than channels with lower lateral gradient floodplains.

### 5.6.6 Influence of Flow Magnitude ($Q_P$)

In Case F simulations the relationship between the delay in flood wave propagation along a channel with flood magnitude was investigated. Flow magnitudes corresponding to return periods from 2 years to 1000 years in Table 5-2 formed the basis of this analysis. The variation of relative delay of time to peak for these flows is summarised in Table 5-17 and plotted in Figure 5-24.

**Table 5-17 Variation of $T_{P1}$ with $T_{P2}$ with flow magnitude ($Q_P$)**

| | L (km) | $S_{fp}$ (m/km) | $n_{fp}$ ($s/m^{1/3}$) | $b_{fp}$ (m) | α (deg) | $n_{mc}$ ($s/m^{1/3}$) | $T_B$ (hrs) | $Q_P$ ($m^3/s$) | $T_{P1}$ | $T_{P2}$ | Rel. delay (%) |
|---|---|---|---|---|---|---|---|---|---|---|---|
| **F1.** | 50 | 1.00 | 0.25 | 25 | 0 | 0.03 | 335.5 | **91.41** | 04/01/2009 23:30 | 05/01/2009 05:45 | 8.99 |
| **F2.** | 50 | 1.00 | 0.25 | 25 | 0 | 0.03 | 335.5 | **102.06** | 04/01/2009 23:30 | 05/01/2009 09:30 | 14.39 |
| **F3.** | 50 | 1.00 | 0.25 | 25 | 0 | 0.03 | 335.5 | **110.12** | 04/01/2009 23:30 | 05/01/2009 13:00 | 19.42 |
| **F4.** | 50 | 1.00 | 0.25 | 25 | 0 | 0.03 | 335.5 | **119.03** | 04/01/2009 23:30 | 05/01/2009 13:00 | 19.42 |
| **F5.** | 50 | 1.00 | 0.25 | 25 | 0 | 0.03 | 335.5 | **125.64** | 04/01/2009 23:30 | 05/01/2009 13:00 | 19.42 |
| **F6.** | 50 | 1.00 | 0.25 | 25 | 0 | 0.03 | 335.5 | **132.21** | 04/01/2009 23:30 | 05/01/2009 11:30 | 17.27 |
| **F7.** | 50 | 1.00 | 0.25 | 25 | 0 | 0.03 | 335.5 | **140.85** | 04/01/2009 23:30 | 05/01/2009 11:00 | 16.55 |
| **F8.** | 50 | 1.00 | 0.25 | 25 | 0 | 0.03 | 335.5 | **147.38** | 04/01/2009 23:30 | 05/01/2009 11:30 | 17.27 |
| **F9.** | 50 | 1.00 | 0.25 | 25 | 0 | 0.03 | 335.5 | **153.90** | 04/01/2009 23:30 | 05/01/2009 11:45 | 17.63 |

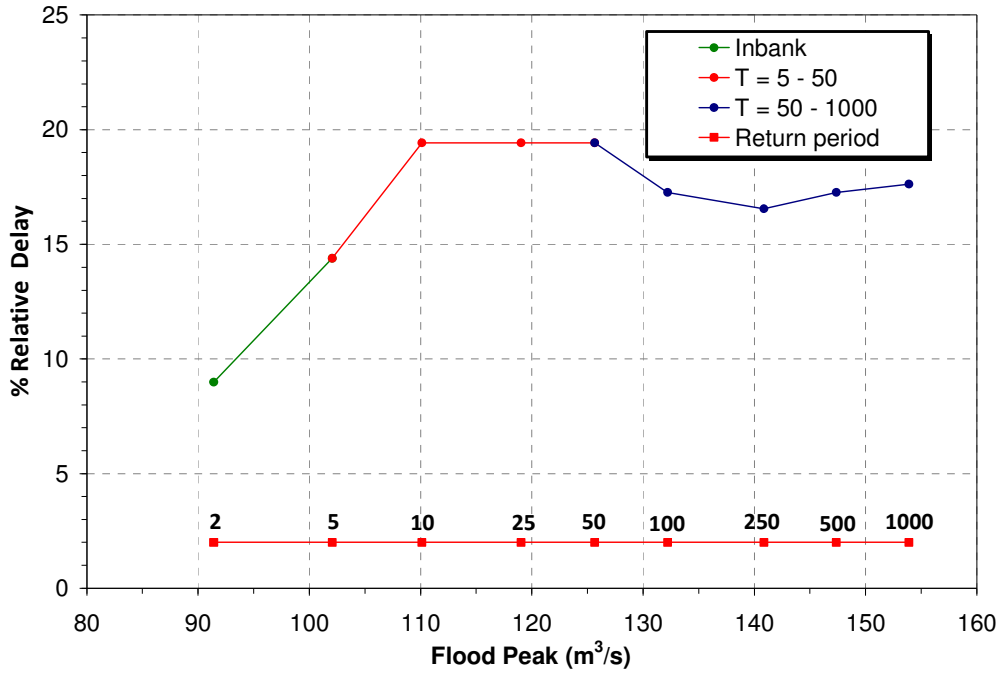


**Figure 5-24 Variation of relative delay with flow magnitude ($Q_P$)**

Figure 5-24 is consistent with Figure 5-12 and again reflects the complexities of floodplain influences on flow behaviour.

### 5.6.7 Influence of Main Channel Resistance ($n_{mc}$)

The effect of main channel hydraulic resistance on flood wave travel time was investigated in Case G simulations for Manning's roughness coefficients varying from 0.03 to 5. Results are summarised in Table 5-18 and shown in Figure 5-25.

**Table 5-18 Variation of $T_{P1}$ with $T_{P2}$ with main channel resistance ($n_{mc}$)**

| | L (km) | $S_{fp}$ (m/km) | $n_{fp}$ ($s/m^{1/3}$) | $b_{fp}$ (m) | α (deg) | $n_{mc}$ ($s/m^{1/3}$) | $T_B$ (hrs) | $Q_P$ ($m^3/s$) | $T_{P1}$ | $T_{P2}$ | Rel. delay (%) |
|---|---|---|---|---|---|---|---|---|---|---|---|
| **G1.** | 50 | 1.00 | 0.25 | 25 | 0 | **0.03** | 335.5 | 153.90 | 04/01/2009 23:30 | 05/01/2009 11:00 | 16.55 |
| **G2.** | 50 | 1.00 | 0.25 | 25 | 0 | **0.06** | 335.5 | 153.90 | 04/01/2009 23:30 | 05/01/2009 15:30 | 23.02 |
| **G3.** | 50 | 1.00 | 0.25 | 25 | 0 | **0.10** | 335.5 | 153.90 | 04/01/2009 23:30 | 05/01/2009 19:15 | 28.42 |
| **G4.** | 50 | 1.00 | 0.25 | 25 | 0 | **0.15** | 335.5 | 153.90 | 04/01/2009 23:30 | 06/01/2009 00:45 | 36.33 |
| **G5.** | 50 | 1.00 | 0.25 | 25 | 0 | **0.20** | 335.5 | 153.90 | 04/01/2009 23:30 | 06/01/2009 05:00 | 42.45 |
| **G6.** | 50 | 1.00 | 0.25 | 25 | 0 | **0.30** | 335.5 | 153.90 | 04/01/2009 23:30 | 06/01/2009 10:45 | 50.72 |
| **G7.** | 50 | 1.00 | 0.25 | 25 | 0 | **0.50** | 335.5 | 153.90 | 04/01/2009 23:30 | 06/01/2009 17:30 | 60.43 |
| **G8.** | 50 | 1.00 | 0.25 | 25 | 0 | **1.00** | 335.5 | 153.90 | 04/01/2009 23:30 | 07/01/2009 00:15 | 70.14 |
| **G9.** | 50 | 1.00 | 0.25 | 25 | 0 | **2.00** | 335.5 | 153.90 | 04/01/2009 23:30 | 07/01/2009 04:30 | 76.26 |
| **G10.** | 50 | 1.00 | 0.25 | 25 | 0 | **5.00** | 335.5 | 153.90 | 04/01/2009 23:30 | 07/01/2009 07:30 | 80.58 |

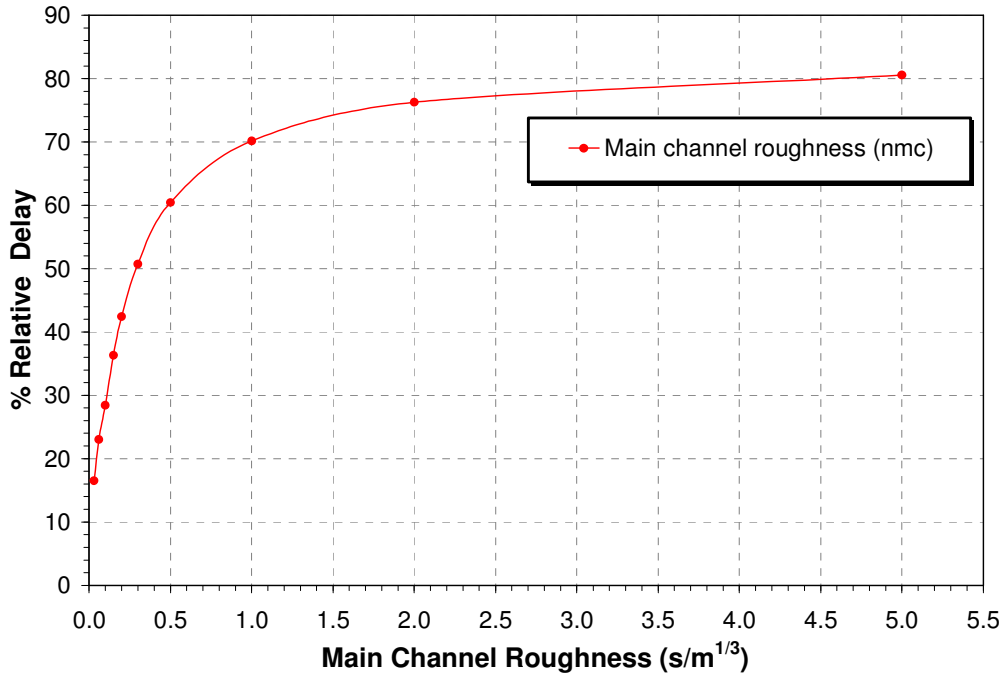


**Figure 5-25 Variation of relative delay with main channel resistance ($n_{mc}$)**

Figure 5-25 indicates that the relative delay of the time to peak increases with increasing main channel hydraulic resistance. Increasing resistance retards flow velocity and increases the travel time of the flood wave in the channel. For extreme values of resistance, a constant value of relative delay is approached where main channel velocity values are almost zero and where further increases in resistance no longer influence the flow velocity or the flood wave travel time.

### 5.6.8 Influence of Flow Duration ($T_B$)

In Case H simulations, the influence of flood duration ($T_B$) on the flood wave travel time was investigated. The basis of the relationship for determining durations for a given flood peak (100-year return period) was outlined in Section 5.3.1 and while the limitations of treating flood peak and duration independently in the context of flood volume is recognised, the approach for the purpose of this study is considered acceptable. Results of the simulations for the range of flood durations in Table 5-2 are summarised in Table 5-19 and the variation of relative delay with flood duration is shown in Figure 5-26.

**Table 5-19 Variation of $T_{P1}$ with $T_{P2}$ with flow duration ($T_B$)**

| | L (km) | $S_{fp}$ (m/km) | $n_{fp}$ ($s/m^{1/3}$) | $b_{fp}$ (m) | α (deg) | $n_{mc}$ ($s/m^{1/3}$) | $T_B$ (hrs) | $Q_P$ ($m^3/s$) | $T_{P1}$ | $T_{P2}$ | Rel. delay (%) |
|---|---|---|---|---|---|---|---|---|---|---|---|
| **H1.** | 50 | 1.00 | 0.25 | 25 | 0 | 0.03 | **1.75** | 153.90 | 31/12/2008 01:30 | 31/12/2008 10:15 | 1312.50 |
| **H2.** | 50 | 1.00 | 0.25 | 25 | 0 | 0.03 | **3.25** | 153.90 | 31/12/2008 02:00 | 31/12/2008 09:30 | 562.50 |
| **H3.** | 50 | 1.00 | 0.25 | 25 | 0 | 0.03 | **6.75** | 153.90 | 31/12/2008 03:30 | 31/12/2008 10:00 | 243.75 |
| **H4.** | 50 | 1.00 | 0.25 | 25 | 0 | 0.03 | **20.00** | 153.90 | 31/12/2008 08:45 | 31/12/2008 18:15 | 118.75 |
| **H5.** | 50 | 1.00 | 0.25 | 25 | 0 | 0.03 | **53.75** | 153.90 | 31/12/2008 21:00 | 01/01/2009 09:15 | 92.54 |
| **H6.** | 50 | 1.00 | 0.25 | 25 | 0 | 0.03 | **66.75** | 153.90 | 01/01/2009 03:15 | 01/01/2009 15:30 | 46.12 |
| **H7.** | 50 | 1.00 | 0.25 | 25 | 0 | 0.03 | **167.50** | 153.90 | 02/01/2009 19:15 | 03/01/2009 07:30 | 18.45 |
| **H8.** | 50 | 1.00 | 0.25 | 25 | 0 | 0.03 | **265.00** | 153.90 | 04/01/2009 23:30 | 05/01/2009 11:30 | 11.39 |
| **H9.** | 50 | 1.00 | 0.25 | 25 | 0 | 0.03 | **334.50** | 153.90 | 05/01/2009 13:30 | 06/01/2009 01:45 | 9.22 |
| **H10.** | 50 | 1.00 | 0.25 | 25 | 0 | 0.03 | **502.01** | 153.90 | 08/01/2009 08:00 | 08/01/2009 20:15 | 6.15 |
| **H11.** | 50 | 1.00 | 0.25 | 25 | 0 | 0.03 | **669.50** | 153.90 | 11/01/2009 02:15 | 11/01/2009 14:30 | 4.61 |
| **H12.** | 50 | 1.00 | 0.25 | 25 | 0 | 0.03 | **1338.75** | 153.90 | 22/01/2009 04:00 | 22/01/2009 16:00 | 2.26 |
| **H13.** | 50 | 1.00 | 0.25 | 25 | 0 | 0.03 | **2007.75** | 153.90 | 02/02/2009 05:30 | 02/02/2009 17:30 | 1.51 |

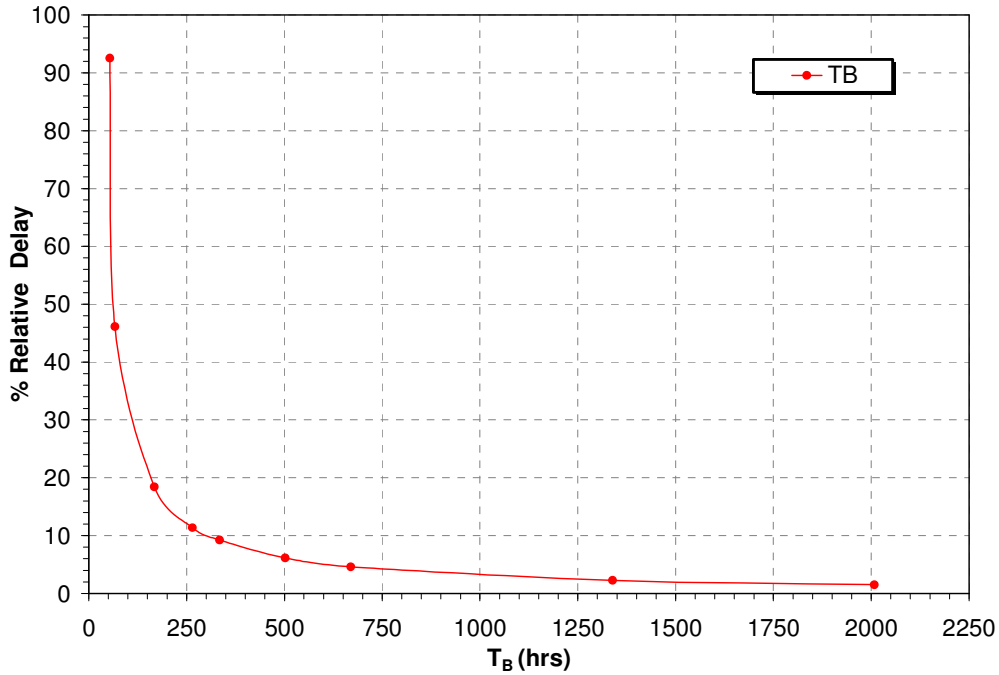


**Figure 5-26 Variation of relative delay with flow duration ($T_B$)**

Results in Table 5-19 and Figure 5-26 indicate that flood volume, as represented by flood duration ($T_B$) in the Case H simulations is important in assessing flood wave

travel times along a channel. Low volume floods with sharp peaks experience significant delays in travel times compared to high volume events that are characterised by hydrographs with rising and receding limbs that respond slowly. High volume floods have sufficient volume to fill the available storage in the reach, thereby facilitating an efficient downstream transfer of the flood wave.

### 5.6.9 Wave Speed and Discharge Relationship

An important parameter in flood routing is the speed or celerity *c* at which the flood wave travels along a river reach. The celerity of the flood wave for the hydrographs with return periods from 2 to 100 years (Figure 5-3) were determined for the 50km river reach using the peak time data in Table 5-17. These are summarised in Table 5-20 and shown varying with flood peak in Figure 5-27.

**Table 5-20 Wave celerity for return periods from 2 to 1000 years**

| Return period (Yrs) | Flow ($m^3/s$) | Wave Speed (m/s) |
|---|---|---|
| 2 | 91.41 | 2.22 |
| 5 | 102.06 | 1.39 |
| 10 | 110.12 | 1.03 |
| 25 | 119.03 | 1.03 |
| 50 | 125.64 | 1.03 |
| 100 | 132.21 | 1.16 |
| 250 | 140.85 | 1.21 |
| 500 | 147.38 | 1.16 |
| 1000 | 153.90 | 1.13 |

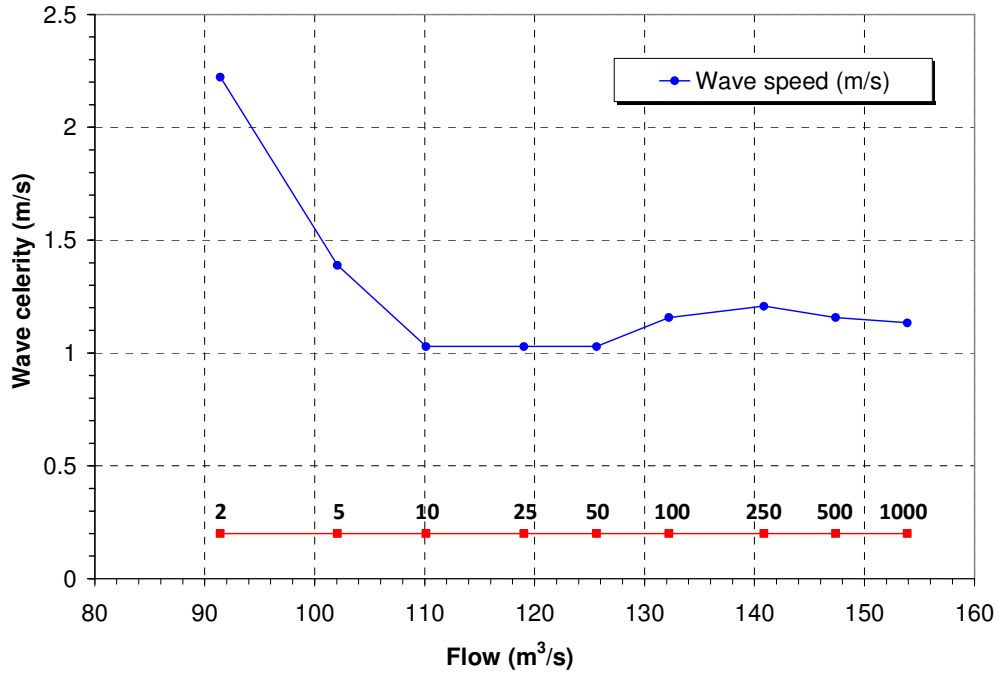


**Figure 5-27 Variation of flood wave celerity with flood peak magnitude for various return periods**

Figure 5-27 indicates that wave speed is relatively high for inbank/ bankfull flows represented by return periods up to approximately 2-years and then decreases for overbank flows up to return periods of about 50 years. Wave speed would be expected to be at a minimum for the lower floodplain depths that would be typical for this low to moderate flow range and although not represented in the simulated data in Figure 5-27, the low attenuation for shallow floodplain depths would be contributed to by the turbulent momentum exchange from the main channel to the floodplain that is most pronounced at low overbank depths. As flow and depth increase further for higher return periods, the mean velocity in the floodplain will increase further and reach a value that is equal to the main channel flow velocity. This represents a limiting value beyond which further increases in floodplain velocity promote a reversed momentum interaction where the exchange is now from the floodplain to the main channel. This is accompanied by increasing flood wave celerity that is consistent with that reported by Knight and Shiono (1996) and shown in Figure 5-28.

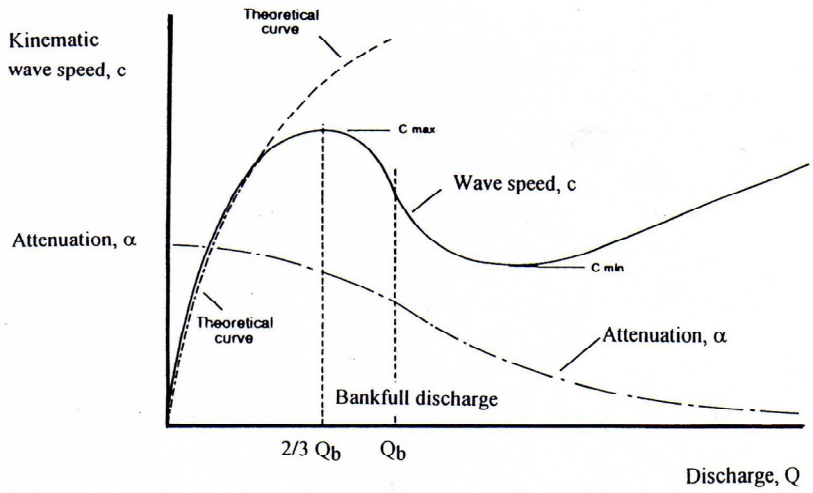


**Figure 5-28 Typical kinematic wave speed-discharge and attenuation-discharge curves (Knight and Shiono, 1996)**

The trend in Figure 5-27 is also consistent with Woltemade and Potter (1994) where the influences of fluvial geomorphology on peak flow attenuation was undertaken. As previously noted in this report, this study indicated that moderate floods (in the 5 to 50-year return period range) with relatively high peak-to-volume ratios are attenuated most. In contrast, both small and large floods are attenuated to a lower degree. For high flood volumes (recurrence intervals typically greater that 50 years), the main channel and floodplain can act as a single unit that is dominated by the floodplain component with the result that flood wave celerity can increase as flow further increases.

## 5.7 Development of Flood Wave Delay Index

The simple index that combines floodplain properties with the delay in time to peak was developed from a multivariate regression model. Important parameters that were analysed comprise geometrical and resistance properties of the channel and include length, floodplain width, longitudinal and lateral floodplain slopes and the main channel and floodplain resistances. The peak and duration of flood hydrographs of specified return period were also included. By incorporating the results in Section 5.6 into the regression model, an optimised index giving the relative delay in flood wave travel time along a channel was produced. This equation is:

$$\% \text{ Relative Delay} = 181 \frac{L\, n_{fp}^{0.17}\, n_{mc}^{0.46} \left( \frac{b_{fp}}{b_{bf}} \right)^{0.38}}{S_{fp}^{0.55}\, \alpha^{0.07}\, T_B^{0.8} \left( \frac{Q_P}{B} \right)^{0.36}} \qquad \textbf{Eqn. 5.8}$$

where $b_{bf}$ is the bankfull width (m), L is the floodplain length (km), $b_{fp}$ is the floodplain width (m), B is the total channel width (m), $S_{fp}$ is the longitudinal floodplain slope (m/km), $\alpha$ is the transverse or lateral floodplain slope (degrees), $n_{mc}$ and $n_{fp}$ are the main channel and floodplain Manning's resistances respectively, $Q_P$ is

the peak flow ($m^3/s$) and $T_B$ is the flood duration (hrs). Application of Eqn. 5.8 requires that $\alpha > 0$ and therefore horizontal floodplains are represented by a near-zero value of $\alpha$. Similarly, the equation assesses floodplain effects and therefore $Q_P > Q_{bf}$ where $Q_{bf}$ is the estimated bankfull discharge in the river.

The performance of this index is assessed on linear scales where the simulated relative delay values are compared to those calculated using Eqn. 5.8 in Figure 5-29.

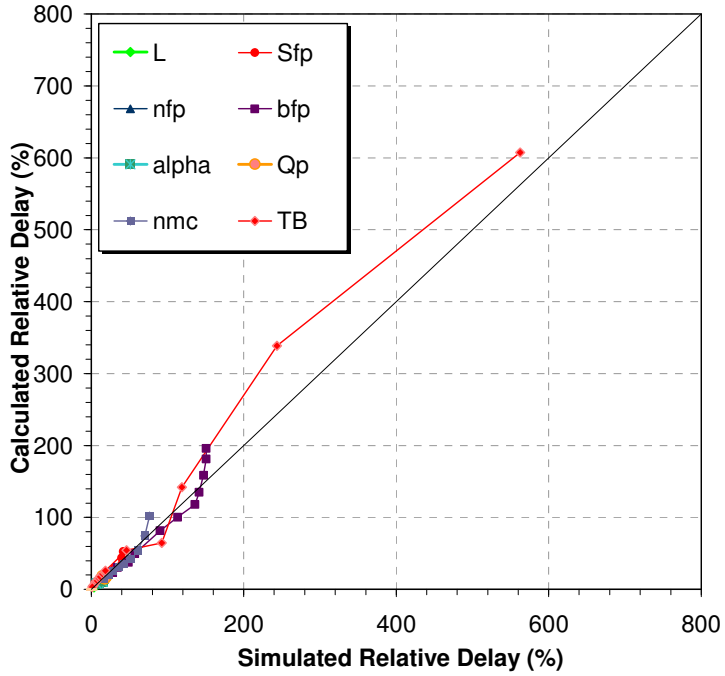


**Figure 5-29 Comparison of simulated and calculated relative delays plotted on linear scales**

As with Figure 5-16, data in Figure 5-29 is clustered in the bottom left corner of the plot and indicates that flood duration ($T_B$) is the dominant parameter that influences the delay of propagation of the flood wave in the generalised model. As before and as shown in Figure 5-30, this clustering is less pronounced when calculated and simulated relative delays are compared on logarithmic scales.

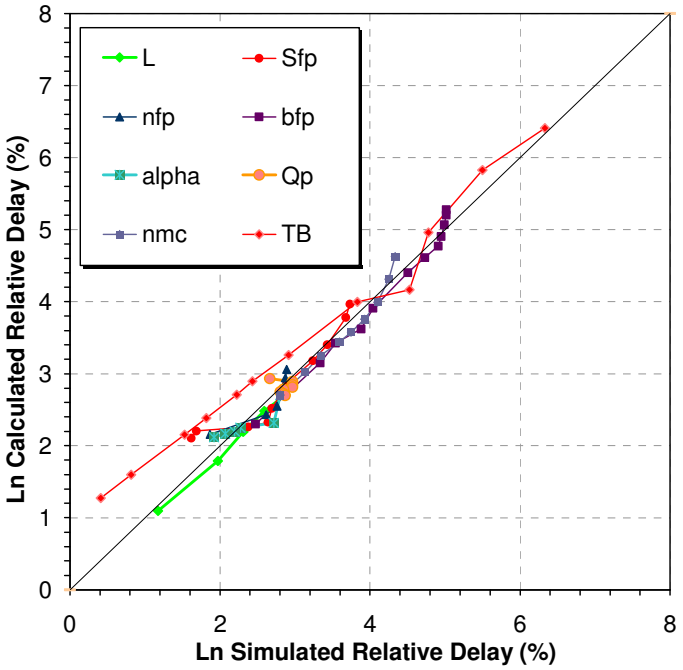


**Figure 5-30 Comparison of simulated and calculated relative delays plotted on logarithmic scales**

Figure 5-30 indicates that relative delays calculated from Eqn. 5.8 represent a good fit to the simulated data from the generalised model. As was the case for Eqn. 5.6 for peak flow attenuation, Eqn. 5.8 is again shown to predict relative delays more accurately in the high value range.

# 6 Validation of Indices by Case Study

## 6.1 Introduction

It was recognised at the outset of this project that the indices that were developed in Chapter 5 would require validation in a defined case study. Validation required the construction of a hydraulic model of a river reach which could be calibrated from relationships derived from measured data at the downstream boundary. For this reason, it was desirable that the case study would assess a recently surveyed natural river reach with active floodplains and with gauged data at its upstream and downstream extents. After careful consideration and in consultation with OPW, a reach of the River Suir in Co. Tipperary between New Bridge and Caher Park was chosen for the case study. A HEC-RAS hydraulic model of this river reach was constructed with required topographical information being made available from OPW and executed using flow records at the upstream and downstream gauging stations again made available by OPW. This chapter provides detail on the site selection process, model development and comparison of the results determined from the developed indices with measured data from the case study.

## 6.2 Site Selection

The site selection process for the case study was largely driven by the availability upstream and downstream flood hydrographs over a reasonable period in addition to extensive topographical data that defines the main channel and floodplain geometry between these upstream and downstream limits. The site selection process was assisted by OPW and after careful consideration, the reach of the River Suir between New Bridge (Station 16008) and Caher Park (Station 16009) emerged as being the most suitable for this study.

However, other sites worthy of mention were considered and for different reasons were excluded. At the outset of the project, the UCD research team had originally intended using the Camlin River downstream of Longford Town for this case study but investigation of the site indicated that the floodplain of this river provides mostly storage and contributes very little to the conveyance of flood flows, precluding an investigation of momentum transfer effects. The flows are further complicated by a major constriction at the railway bridge. It was for this reason, combined with quality issues of the hydrometric data that was available, that the project team decided to look elsewhere for suitable sites. Sites on the Rivers Suir, Suck, Slaney, Boyne, Blackwater, Brosna and Little Brosna were also considered and some investigation of each option was undertaken. However, for reasons that included the scarcity of

required high quality hydrometric and topographical data and the fact that for some river reaches floodplain inundation was very rare and when it did occur was shallow and not very extensive, these too were excluded.

## 6.3 The River Suir Case Study

### 6.3.1 The River Suir Catchment

The River Suir and its tributary network which comprises the Aherlow, Anner, Clodiagh, Multeen, Drish, Tar, Linguan, Clodaigh (Portlaw) and Pollanassa rivers, flows through areas of Counties Tipperary, Kilkenny and Waterford. The river rises in the Devil's Bit near Moneygall in County Tipperary and flows in a southerly direction past Templemore to the west, through Thurles and Cahir to the county boundary of Tipperary and Waterford near Newcastle. Along its course, the river passes through varying geological regions. Upstream of Waterford City, the meanders of the Suir criss-cross the Devonian sandstone rim. In the vicinity of Carrick-on-Suir the river follows the limestone floor of the Carrick Syncline. Upstream of Clonmel the river and its tributaries transverse Upper Palaeozoic Rocks, mainly the Lower Carboniferous Visean and Tournaisian. The Aherlow River flows through a Carboniferous limestone valley, with outcrops of Old Red Sandstone forming the Galtee Mountains to the south and the Slivenamuck range to the north. Glacial deposits of sand and gravels are common along the valley bottom.

At present, significant areas of the River Suir and tributary catchments are covered by grassland pasture and forestry (for example the main River Suir catchment covers approximately 85% pasture and 9% forestry and the River Aherlow catchment covers 70% pasture, 18% forest and 11% peat).

Spatial descriptors of the River Suir and River Aherlow catchments are tabulated in Table 6-1. The alluvial extent of the floodplain as a proportion of the total catchment area (ALLUV) is determined by reference to a national dataset of soil parent material developed by Teagasc as component dataset of the national indicative forestry strategy project. The alluvial extent represents a measure of the floodplain area that is at risk of flooding. Previously mapped information such as the FSR Soil maps, OPW maps of lands benefitting from drainage or maps of ecological typologies are also indicative in identifying areas that may ne at risk from flooding.

**Table 6-1 Spatial catchment descriptors of River Aherlow (16007) and River Suir catchments (16008 and 16009)**

| | 16007 | 16008 | 16009 | Description<br>Station code |
|---|---|---|---|---|
| Waterbody | Aherlow | Suir | Suir | Station waterbody |
| Location | Killardry | New Bridge | Caher Park | Station location |
| POLY_AREA | 273.2596 | 1090.2520 | 1582.6908 | Catchment area ($km^2$) |
| CENTE | 189160 | 209000 | 202800 | Catchment centroid easting |
| CENTN | 128650 | 158030 | 150350 | Catchment centroid northing |
| ALTBAR | 183.3 | 137.7 | 139.5 | Catchment mean elevation |
| SAAR | 1330.55 | 1029.63 | 1078.57 | SAAR rainfall (mm/year) |
| URBEXT | 0.67 | 0.67 | 0.77 | % Urban extent |
| FOREST | 17.86 | 8.35 | 9.55 | % Forest extent |
| PEAT | 10.87 | 4.65 | 5.27 | % Peat extent |
| PASTURE | 69.87 | 86.58 | 84.61 | % Pasture extent |
| ALLUV | 4.98 | 4.63 | 4.70 | % Alluvium extent |

### 6.3.2 River Reach for Case Study

The River Suir catchment in broad terms and in the context of hydrometric measuring stations where flow data is available can be considered to comprise three sub-sections. The upper reach is between Beakstown and Arglo Bridge, the middle reach is between Arglo Bridge and New Bridge and lower reach includes the river section from New Bridge downstream to Caher Park. The suitability of each catchment section for case study consideration was firstly assessed in terms of the Flood Attenuation Indicator (FAI). The FAI represents a flood polygon representing the lateral extent of flooding at a depth of 1m above surrounding bankfull river level and gives an indication of the frequency and extent of floodplain inundation. These flood polygons were developed in Work-Package 5.3 of the Flood Studies Update programme and are shown in Figure 6-1 for the three sections of the River Suir catchment under investigation.

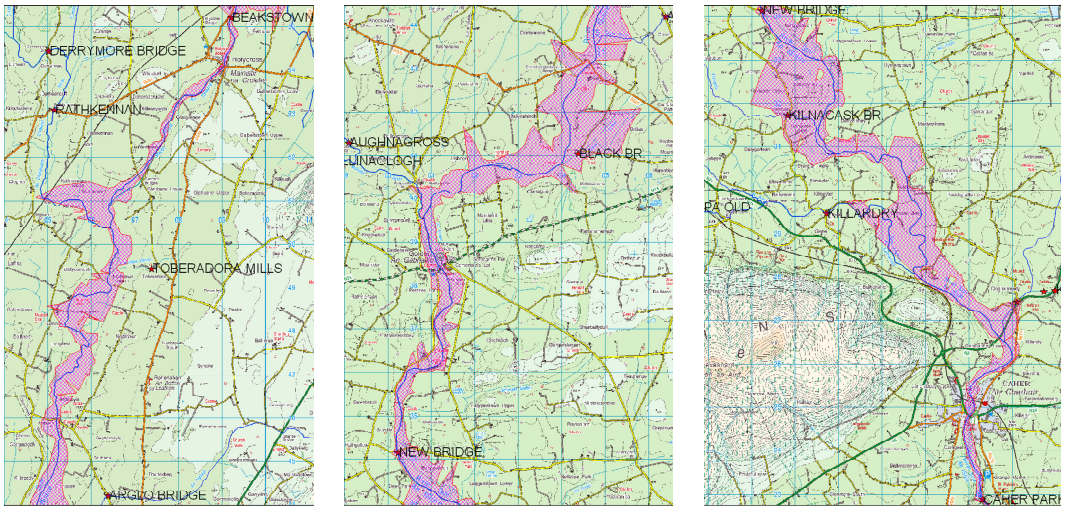


**Figure 6-1 Flood attenuation indicator polygons for River Suir reaches – Beakstown to Arglo Bridge (left), Arglo Bridge to New Bridge (middle) and New Bridge to Caher Park (right)**

Based on the extent of the flood polygon in Figure 6-1, combined with the number of, and data available for tributaries that enter between the upstream and downstream extents, the reach from New Bridge and Caher Park was selected for the case study. The River Aherlow is the most significant tributary in this reach and this river is gauged at Killardry (Station No. 16007). Three other smaller tributaries that are ungauged also join the River Suir between New Bridge and Caher Park. Site visits indicated that large areas of the floodplain within this catchment are farmland with riverside trees forming the interface between the main channel and floodplain along much of the channel. These characteristics are represented in Figure 6-2.

**Figure 6-2 Catchment images (taken 30th Oct 2008) with left floodplain at New Bridge (top right) and right floodplain at Caher Park (bottom left)**

Figure 6-2 shows that the left floodplain upstream of the Caher Park gauging station is grassland pasture. The corresponding right floodplain (viewed upstream) is more developed and includes an urbanised area that extends towards Caher town centre. At Caher Castle further downstream, a concave shaped weir controls the flows. The channel in the chosen reach can be characterised by series gravelly glides interspersed with stony runs and some deep pools. The river, at many locations is well sheltered by waterside trees and other bank-side vegetation. It was felt that these characteristics could be reasonably well represented in a hydraulic model and this supported the decision to use this lower section of the River Suir for the case study.

A range of physiographic characteristics in combination with climatic factors influence the overall shape of flood hydrographs in any catchment. In the case of the section of the Suir catchment being used in the case study, the area draining to New Bridge is 1090 $km^2$, to Caher Park is 1582 $km^2$ and that to Killardry on the River Aherlow is 273 $km^2$. The catchment's area plays an important role in various phases of the runoff process. In small catchments, the contribution of overland flow to the total flow is dominant. In larger catchments, the main proportion of the total flow is conveyed to the main channel through the tributary network rather than overland flow from nearby floodplains. Influential climatic factors for hydrograph shape include rainfall intensity, duration and the direction of storm movement. The average annual rainfall at New Bridge is 1030 mm, Caher Park is 1079 mm and that at Killardy is 1331 mm. Estimated annual rainfall losses at New Bridge and Caher Park are 483 mm and at Killardry is 455 mm.

The main stream slope (S1085) for the River Suir is approximately 1 m/km, and that for the River Aherlow is 2.84 m/km. Stream slope influences the velocity of flow in the channel and is a significant parameter in defining the shape of a flow hydrograph, particularly the recession limb of the hydrograph. High gradient channels are characterised by steeply falling recession limbs and corresponding reductions in hydrograph base widths.

Stream frequency (STMFRQ), defined in the Flood Studies Update as the number of discrete channel elements in the hydrological network upstream of a specified gauging location, also influences hydrograph shape. High values of stream frequency are conducive to quick disposal of runoff in a channel and contribute to a peak discharge that would be higher than that for a corresponding catchment with a lower stream frequency. The estimated stream frequencies at New Bridge, Caher Park and Killardry are 1195, 1810 and 468 respectively. Hydrological catchment descriptors for the River Suir and Aherlow catchments are summarised in Table 6-2

**Table 6-2 Hydrological catchment descriptors of River Aherlow (Station 16007) and River Suir catchments (Station 16008 and Station 16009)**

| | | | | **Description** |
|---|---|---|---|---|
| | **16007** | **16008** | **16009** | Station code |
| GAUGE_X | 201702 | 200193 | 205300 | Gauge location easting |
| GAUGE_Y | 129481 | 134176 | 122851 | Gauge location northing |
| MSL | 43.430 | 68.615 | 85.436 | Mainstream length (km) |
| NETLEN | 366.214 | 1074.903 | 1585.171 | Length of hydrological network (km) |
| STMFRQ | 468 | 1195 | 1810 | Number of stream segment elements in upstream river network |
| S1085 | 2.839000 | 1.038000 | 1.000000 | Slope of MSL |
| FARL | 0.999 | 0.999 | 0.998 | FARL Index value |

Patterns of land use in a catchment also impact on hydrograph shape in terms of peak and duration and represent the main factor where human activity or intervention plays a role. As noted above, the majority of the catchment in the Suir is used for agricultural purposes with a significant proportion of the remaining area being forested. Peat also features in the tributary catchment of the River Aherlow. The presence of catchment vegetation impedes overland flow and increases the infiltration into soils thereby decreasing the proportion of direct runoff.

## 6.4 Case Study Methodology

Validation of the indices developed in Chapter 5 in the case study involved hydraulic modelling of the reach between New Bridge and Caher Park on the River Suir.

### 6.4.1 Selection of Hydraulic Model

Hydraulic river models are generally chosen to provide particular information for a defined situation. As such, there are many occasions when a one-dimensional model is quite adequate and gives reasonable results and other occasions when multi-

dimensional models are required. This study included a general review (Chapter 3) and assessment (Chapter 4) of 1-D, 2-D and 3-D hydraulic modelling codes for effectively simulating data sets for the large-scale UK Flood Channel Facility. The 1-D model that was assessed was HEC-RAS and the TELEMAC code was used for 2-D and 3-D assessment. The advantage of 2-D and 3-D models is that they can simulate the 3-D characteristics of compound channel flows, particularly the turbulent momentum exchange between the main channel and floodplain. If these are significant, multi-dimensional models, can provide greater detail and accuracy than that possible in a 1-D model. Turbulent momentum exchanges between the main channel and floodplains in compound channels occur along the vertical interface between these zones and the intensity of this interaction diminishes as the lateral distance from the main channel increases. Chapter 4 contained the results of modelling of the UK Flood Channel Facility (FCF) dataset from which an assessment of 1-D (HEC-RAS), 2-D (TELEMAC 2-D) and 3-D codes (TELEMAC 3-D was made. The FCF data was used in the absence of 'real' river data which was unavailable but which would have been preferable. While it covers a limited range of situations, the FCF data set represented a reasonable compromise between data from small-scale laboratory studies of floodplain flows and data from natural rivers where Reynolds numbers would be higher. The validation in Chapter 4, while noting the constraints of a 1-D model, showed that HEC-RAS could reproduce the FCF data with physically realistic resistance properties. TELEMAC 2-D also performed well but given the difficulties regarding the availability of data and simulation time that would be required to successfully apply this code to the River Suir case study, HEC-RAS was the preferred option.

### 6.4.2 Topographical Data

The availability of good quality topographical data is essential for the development of any hydraulic model and defines the size, shape and presence of irregularities in the river, the slope of the river and the extent of river floodplains. Topographical data for this case study was made available by OPW. The most recent survey in the River Suir catchment was undertaken in the Summer of 2008 by Maltby Land Surveys for the River Suir C-FRAM project and focussed primarily on the main channel and hydraulic structures. The survey included river sections at the locations of hydrometric gauges among which, Killadry (Station 16007), New Bridge (Station 16008) and Caher Park (16009) were included.

This more recent survey data was augmented by a previous, more extensive survey of the River Suir dating to the 1960's. A review of both data sets indicated that data from 35 cross-sections was available to define the main channel and floodplain topography for the chosen case study reach between New Bridge and Caher Park. The average longitudinal distance between successive cross-sections in the reach was approximately 400m and the number of coordinates defining cross-sections varies as is shown in Table 6-3.

**Table 6-3 Number of coordinates defining numbers of cross-sections**

| Number of survey Co-ord in each x-section | Number of stations |
|---|---|
| 31-50 | 8 |
| 51-70 | 10 |
| 71-90 | 8 |
| 91-110 | 5 |
| 111-131 | 2 |
| 131-150 | 2 |

Results in Chapter 5 indicated that floodplain width is an influential parameter in both the ability of a floodplain to attenuate the flood peak and its ability to delay the propagation of a flood wave along a valley. The survey data collected in the summer of 2008 and from the 1960's indicated that the main channel width was approximately 25m but the survey extent of both the left and right floodplains was limited also to 25m. For the purpose of this study it was necessary that the full extent of the River Suir floodplains be represented and this was done by further augmenting the survey data by LIDAR data provided by OPW. The LIDAR survey provided details of floodplain topographies to widths of approximately 500m on each side of the main channel.

#### *6.4.2.1 Hydraulic Structures*

Ordnance survey maps indicated that hydraulic structures on the River Suir between New Bridge and Caher Park were limited to two bridges. The first of these was a bridge between Gaherabbey Lower and Killemly and the second was the Suir Bridge in Caher Park. The required data to include these bridges in the case study model was unavailable and they were therefore omitted from the case study model.

### 6.4.3 Hydrometric Data

Autographic gauging stations operated by OPW exist at Killardry (Station 16007), New Bridge (Station 16008) and Caher Park (Station 16009). These gauging stations were established in the period between 1953 and 1954 and the OPW is satisfied that reliable records exist for the period from installation to the current time. These three gauging stations have a common digitised 15 minutes flow records in the period of 1954 to 2007 and this data was used in the case study.

#### *6.4.3.1 Identification of Isolated Storm Events*

Although it is theoretically possible to resolve a complex hydrograph into a series of simple hydrographs, hydrologists generally prefer to use simple hydrographs that result from isolated storm events for many hydrograph studies. It was this approach that was adopted in this study and this required a detailed analysis of the 54-year flow record at Killadry, New Bridge and Caher Park. This was undertaken with the assistance of hydrograph analysis software developed in Work-Package 3.1 of the

Flood Studies Update. As might be expected, the majority of the hydrographs are complex and are characterised by kinks, multiple peaks etc. that reflect both storm and catchment peculiarities and the interactions between them. Therefore identifying isolated storm events from the 54-year, 15-minute record in the River Suir catchment would be laborious. The software assisted this hydrograph processing by allowing defined numbers of flood peaks in the flow record to be extracted and this facilitated the identification of isolated storm events that were required for the study.

Within the available record, four simple hydrographs resulting from isolated storms were identified. These events related to periods in December 1954/ January 1955, August 1986/ September 1986, July 1997/ August 1997 and October 2004/ November 2004. These hydrographs at the three gauging stations in the case study reach are shown in Figure 6-3 to Figure 6-6.

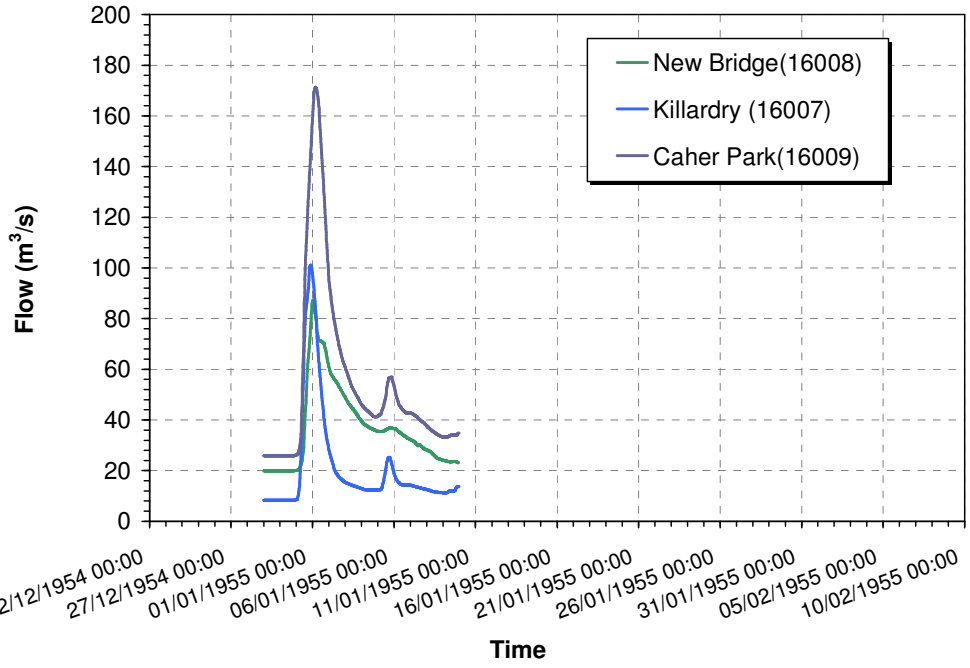


**Figure 6-3 Hydrographs at Killardry, New Bridge and Caher Park for isolated storm of December 1954/ January 1955**

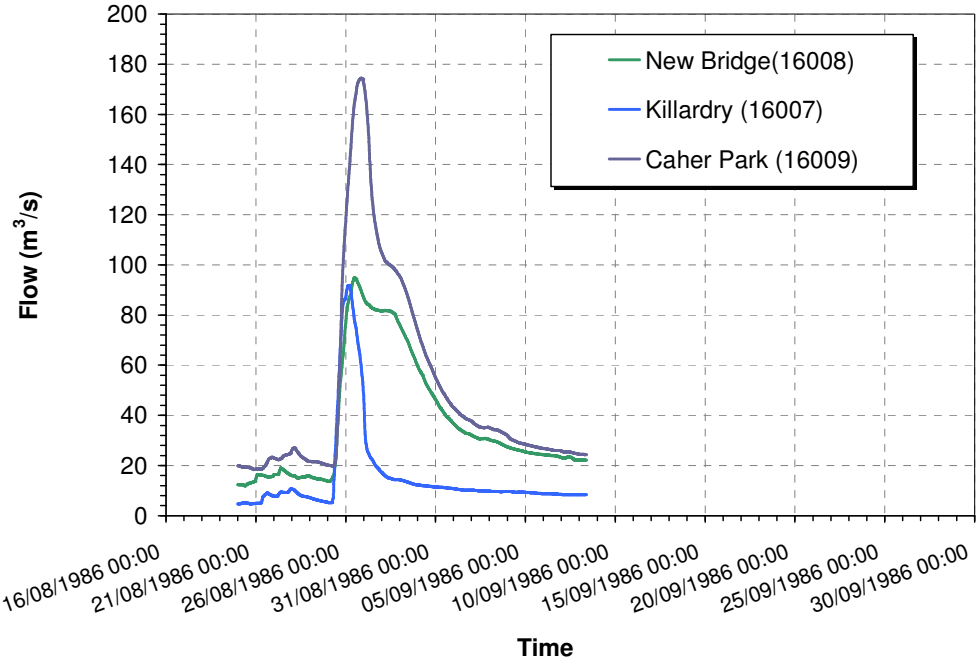


**Figure 6-4 Hydrographs at Killardry, New Bridge and Caher Park for isolated storm of August 1986/ September 1986**

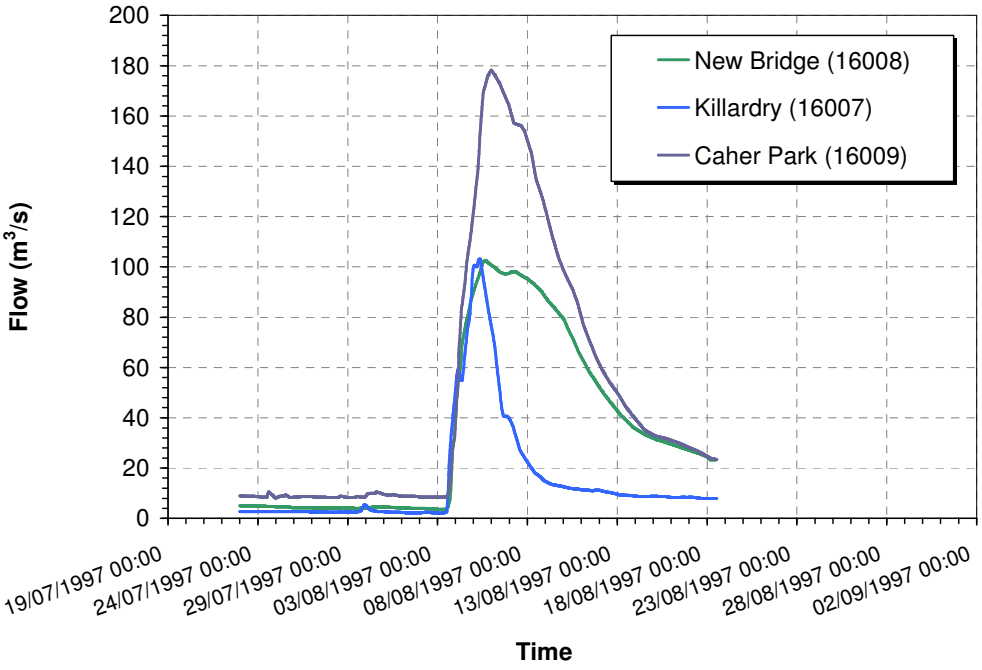


**Figure 6-5 Hydrographs at Killardry, New Bridge and Caher Park for isolated storm of July 1997/ August 1997**

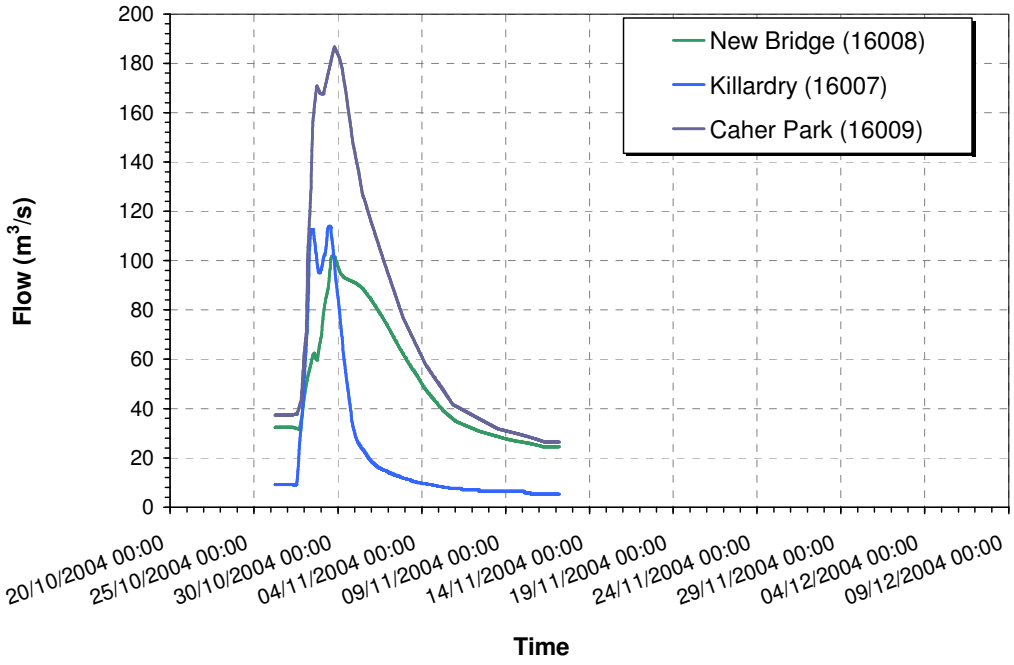


**Figure 6-6 Hydrographs at Killardry, New Bridge and Caher Park for isolated storm of October 2004/ November 2004**

Figure 6-3 to Figure 6-6 indicate that the magnitude of the flood peak at Caher Park is significantly greater that that at New Bridge and reflects the significant contribution to the flow at this station from the River Aherlow catchment. Table 6-1 and Table 6-2 show that rainfall in the Aherlow catchment (1330mm per annum) is greater that that at both New Bridge (1030mm per annum) and Caher Park (1080mm per annum) and this coupled with the steeper gradient (S1085 value of 2.84) and smaller catchment area are conducive to run-off in the Aherlow catchment being conveyed to the River Suir reasonably quickly.

### *6.4.3.2 Water Balance in Case Study*

As mentioned above, The River Suir network between New Bridge and Caher Park includes four tributaries. The most significant of these is the Aherlow River and this is gauged at Killardry (Station 16007). The remaining three tributaries are smaller channels and are ungauged. The most upstream of these is the Abhainn Fhiodachta Stream and further downstream the Mill Stream joins the River Suir. The third tributary which enters the Suir downstream of its confluence with River Aherlow is unnamed. This tributary network in the context of the River Suir is shown in schematic in Figure 6-7.

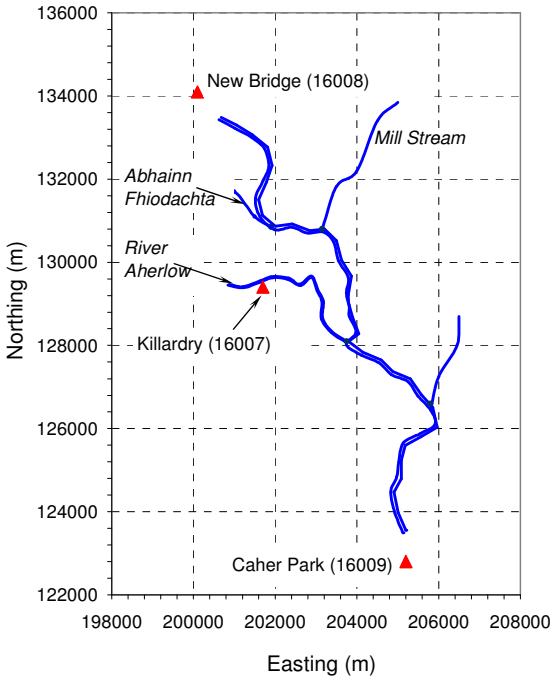


**Figure 6-7 Tributary network of River Suir between New Bridge and Caher Park**

Ideally, the case study reach between New Bridge and Caher Park should include the River Suir with all its tributaries. However, in the absence of any measured data from these tributaries, there inclusion, particularly when ascertaining how the time to peak of the hydrographs at the downstream extents of these ungauged catchments relates to the timing of the flood hydrograph from the main River Suir, is complex and uncertain. In an attempt to quantify the significance of the unmeasured tributary flows to the system, a balance of isolated hydrograph volumes for the river network was undertaken. This is based on adding the volume of the flow hydrograph at New Bridge (Station 16008) to that observed at Killardry (Station 16007) and comparing the combined volumes to the hydrograph volume observed at Caher Park (Station 16009). Results for this analysis for the four isolated storm events in the 54-year flow record are summarised in Table 6-4.

**Table 6-4 Comparison of flood volumes at Killardry, New Bridge and Caher Park for isolated storm events in 54-year flow record**

| Duration of the flood | | Inflow ($m^3$) | | Outflow ($m^3$) | % (In-Out)/ In |
|---|---|---|---|---|---|
| | | 16007 | 16008 | 16009 | |
| 30/12/1954 00:00 | 09/01/1955 22:15 | 20918209.50 | 36409981.50 | 54131346.00 | 5.58 |
| 15/08/1986 04:15 | 07/09/1986 17:15 | 27833031.00 | 68729809.50 | 91378588.50 | 5.37 |
| 29/07/1997 00:00 | 17/08/1997 17:30 | 32839308.00 | 77685034.50 | 108640669.50 | 1.70 |
| 27/10/2004 02:00 | 10/11/2004 23:00 | 32968570.50 | 68258403.00 | 100855017.00 | 0.37 |

Data in Table 6-4 indicates that the food volume at the downstream station (Caher Park) is lower than the combined volumes at Killardry and New Bridge for each of the four isolated storm events. While this loss may be contributed to by evaporation and infiltration from the river channel, a full understanding requires a broader

investigation that would include ground and surface water interactions that are beyond the scope of this project. However, for the purpose of this project, the differences which vary to maximum values of approximately 5.6% suggest that the tributary flows into the system are not particularly significant. The associated levels of uncertainty may not necessarily be improved by including these tributary flows through an ungauged catchment analysis and for this reason, the unguaged tributaries were not included in the case study model.

### 6.4.4 Model Construction

A 1-Dimensional HEC-RAS hydraulic model was constructed for the River Suir between New Bridge and Caher Park using the 35 cross-sections obtained from previous surveys of the River Suir and from LIDAR data derived from a digital elevation model (DEM). A downstream reach of the Aherlow River was also included in the model to facilitate the routing of the inflow hydrograph at Killardry. From the results of the flow balance that was undertaken (Section 6.4.3.2) which indicated that tributary flows other than that in the River Aherlow were not particularly significant, the model was limited only to the Rivers Suir and Aherlow and other tributaries were not included.

1-D HEC-RAS modelling requires that cross-sections should be perpendicular to the flow direction and for this case study, the cross-sections are as shown in Figure 6-8.

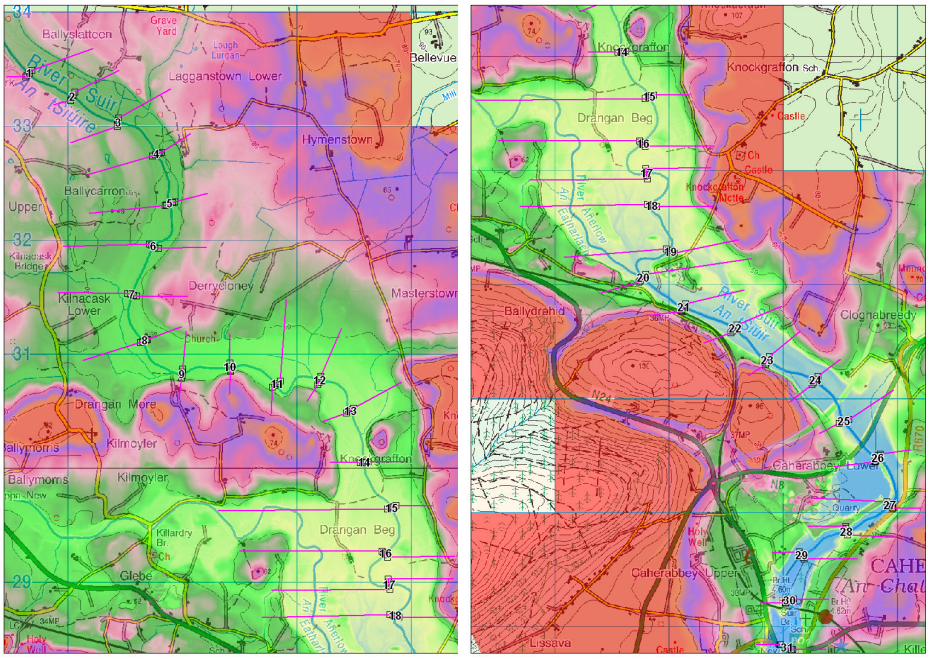


**Figure 6-8 Location of cross-sections in case study**

The channel bed profile with a typical cross-section extracted from the HEC-RAS model is shown in Figure 6-9. Main channel cross-sections were typically defined by approximately 25 coordinates with floodplains being defined by upwards of 80 coordinates. Cross-sections generally coincided with hydraulically important features

such as breaks in channel slope and within each cross-section topographic features such as bankfull levels were represented.

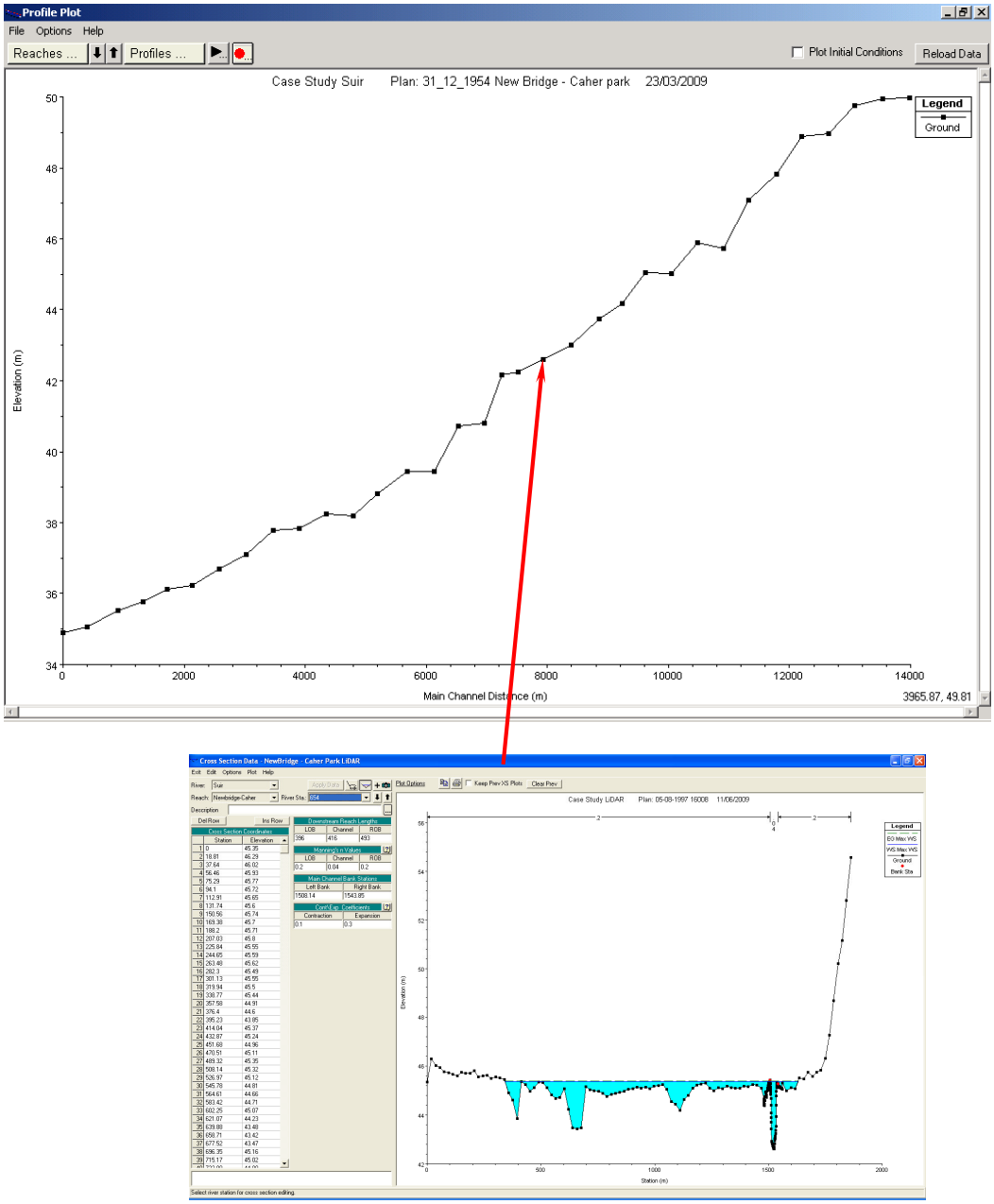


**Figure 6-9 HEC-RAS bed profile with typical cross-section**

### 6.4.5 Model Calibration

Executing the HEC-RAS model in unsteady or dynamic mode involves routing observed inflow hydrographs through the river network. The model is one dimensional, with the stream network defined by cross-sections, longitudinal distances between successive cross sections, the locations of tributary junctions, and main channel and floodplain estimates of hydraulic resistance. Hydraulic resistances

were defined in terms of Manning's *n* values. The hydrodynamic model solves the fully dynamic one-dimensional equations of conservation of mass and momentum (Saint Venant equations) applied in an implicit, finite difference framework.

Boundary conditions used for executing the model included an imposed dynamic discharge (inflow hydrograph) at the upstream end of the reach and an imposed normal depth at the downstream end. The main channel was assigned a Manning's resistance coefficient of 0.04 to represent an average value for a relatively 'clean' meandering channel with some pools and shoals.

Usually, hydrograph routing and calibration would involve simultaneous routing of the inflow hydrographs from New Bridge (Station 16008) and Killardry (Station 16007) through the case study model to produce a flow hydrograph at Caher Park that could be compared to the observed hydrograph at this location (Station 16009). Flow magnitudes and arrival times of simulated and observed hydrographs at Caher Park would then be correlated in a calibration process where resistance properties would be iteratively adjusted until acceptable agreement between simulated and observed hydrographs was obtained.

However, such an approach was not possible in this case study. Simultaneous routing of hydrographs from New Bridge and Killardry to Caher Park would have resulted in a hydrograph with an increased peak and volume compared to that at New Bridge. Determining a 'relative attenuation' in this situation would not have been possible using the index (Eqn. 5.6) in Chapter 5. Furthermore, the indices (Eqn. 5.6 and Eqn. 5.8) can be applied only to a single reach where the parameters in the index can be well estimated. The indices cannot be readily applied to a river and tributary network where sub-catchments will have different numerical values for various parameters in the indices.

In order to validate the indices that were developed, an alternative routing approach was therefore necessary. This involved executing the HEC-RAS model by routing a measured inflow hydrograph at Killardry to Caher Park while maintaining a nominal flow of insignificant magnitude (to facilitate model execution) in the reach from New Bridge to Caher Park. In a separate simulation, a hydrograph was routed from New Bridge to Caher Park while again maintaining a nominal flow in the reach from Killardry to Caher Park. This resulted in two simulated outflow hydrographs at Caher Park which were added. The resulting hydrograph was compared to the observed hydrograph at Caher Park. These simulations were repeated for each of the four isolated storm events in the 54-year flow record.

Results indicated that flows in the Aherlowe tributary between Killardry and the confluence of the tributary with the River Suir remained inbank. For this reason, calibration involved iteratively adjusting the floodplain resistance of the river reach from New Bridge to Caher Park until the combined added hydrograph from Killardry and New Bridge was in good agreement with the observed hydrograph in Caher Park. The calibrated hydrographs are shown in Figure 6-10 to Figure 6-13 where the routed hydrograph from Killardry and New Bridge to Caher Park are *16007 at 16009* and *16008 at 16009* respectively and these hydrographs when added are defined as *16009 Routed.* The observed hydrographs at Caher Park in Figure 6-10 to Figure 6-13 are defined as *16009 Observed*.

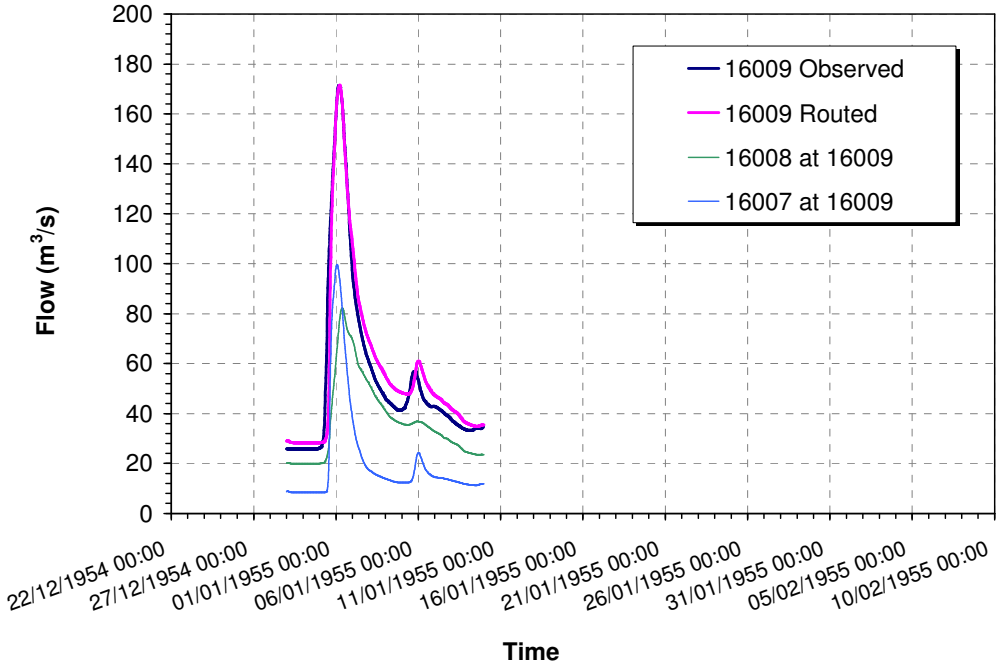


**Figure 6-10 Routed and observed hydrographs at Caher Park for isolated storm of December 1954/ January 1955**

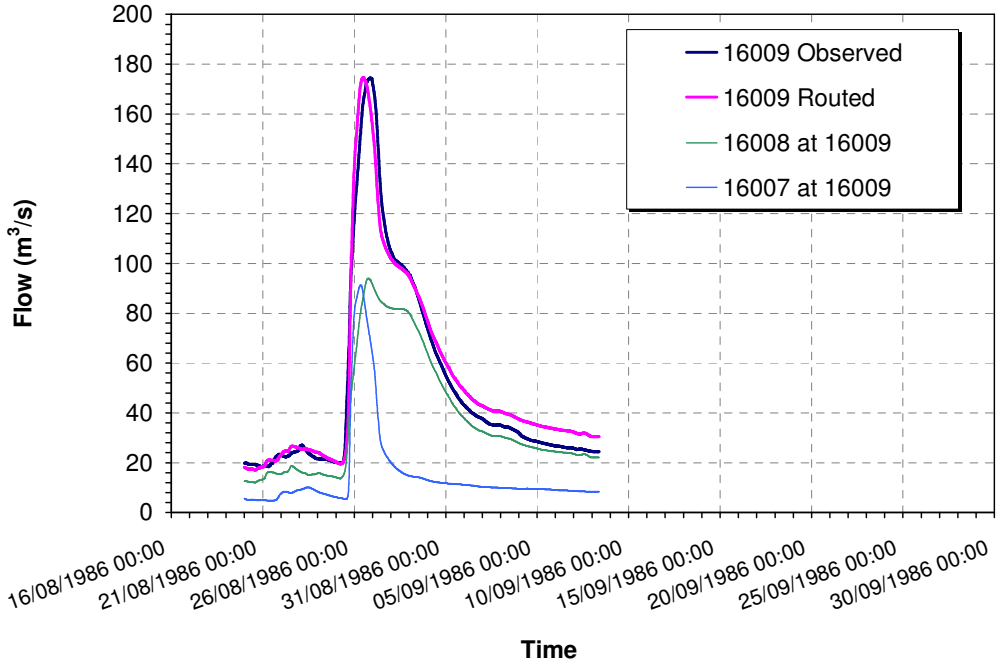


**Figure 6-11 Routed and observed hydrographs at Caher Park for isolated storm of August 1986/ September 1986**

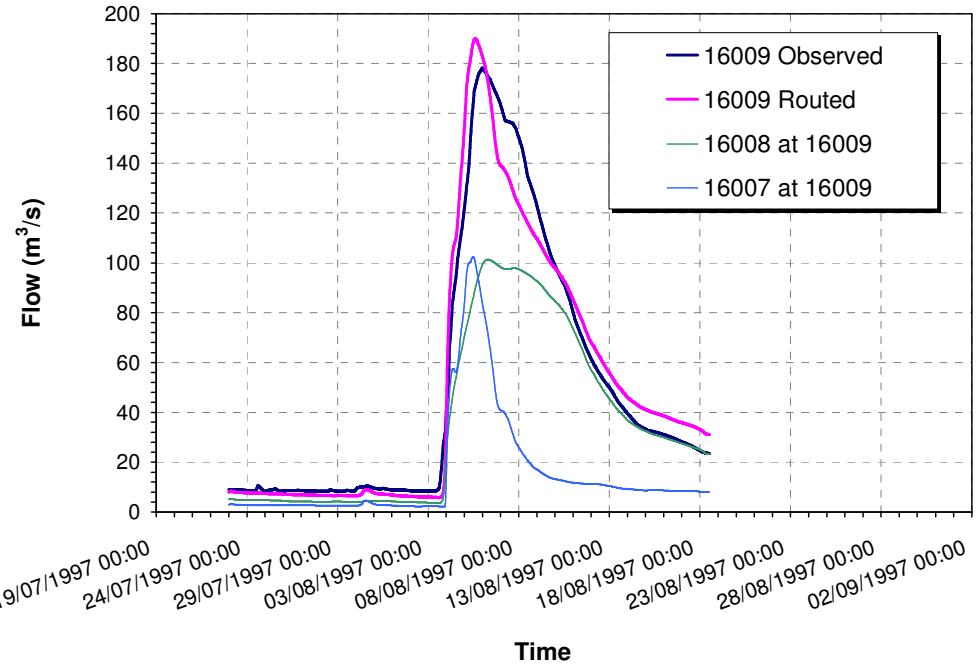


**Figure 6-12 Routed and observed hydrographs at Caher Park for isolated storm of July 1997/ August 1997**

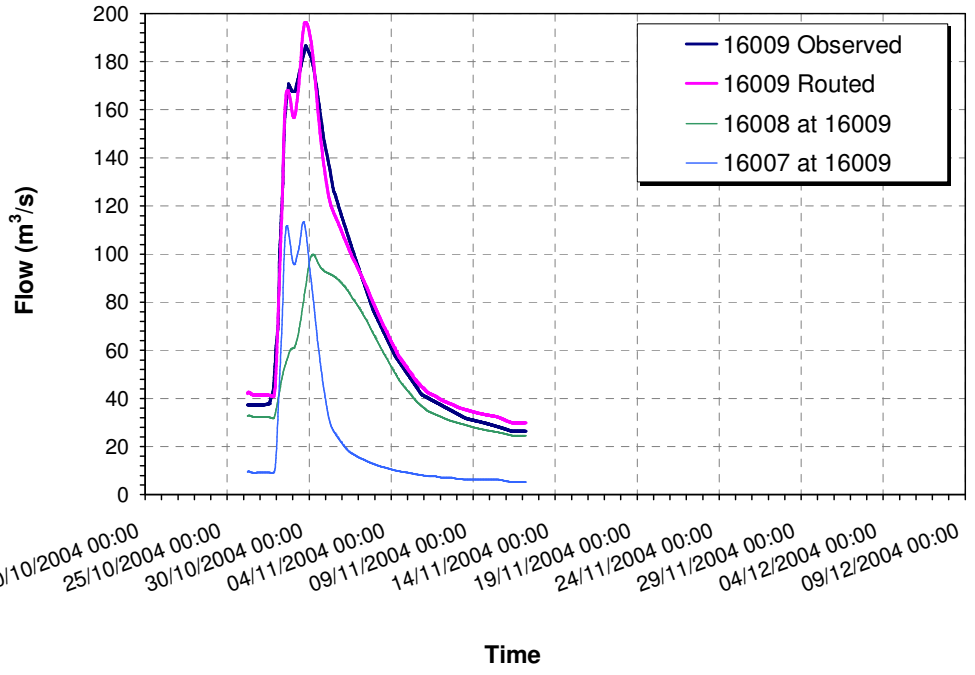


**Figure 6-13 Routed and observed hydrographs at Caher Park for isolated storm of October 2004/ November 2004**

Figure 6-10 to Figure 6-13 indicates that relatively good agreement between the observed hydrograph at Caher Park with that determined from model simulations is obtained. Floodplains of the River Suir are characterised at many locations by the

presence of roughness that would be emergent for the range of floodplain depths investigated. Roughness of this type imparts a drag resistance to the flow and is characterised by eddy shedding around individual elements. Manning's resistance strictly applies to boundary friction only. Energy losses associated with eddy shedding were represented in the calibration of the case study model by floodplain Manning's resistance values greater than those that would be predicted in published literature or from the Soil Conservation Service Method. The main channel and floodplain resistance coefficients used in this final calibration are summarised in Table 6-5.

**Table 6-5 Main channel and floodplain resistance coefficients used in calibration of the case study model**

| | 31/12/1954 | 26/08/1986 | 05/08/1997 | 29/10/2004 |
|---|---|---|---|---|
| $n_{mc}$ ($s/m^{1/3}$) | 0.04 | 0.04 | 0.04 | 0.04 |
| $n_{fp}$ ($s/m^{1/3}$) | 0.05 | 0.05 | 0.20 | 0.04 |

Coefficients of the magnitude shown are typical for floodplains covered in light brush and trees and are considered realistic for the River Suir. Calibration of the 1997 event required a floodplain resistance value of 0.2. This is not representative of the conditions in the River Suir but was required for calibration on this occasion.

The model calibration as described represents an 'artificial' representation of the interactions between the River Suir and Aherlowe tributary. In reality, these interactions would be likely to produce significant backwater effects which have not been considered in this analysis. However, given the constraints within which the indices were applied and while recognising its limitations, this calibration approach was considered acceptable.

## 6.5 Application of Hydraulic Model to Case Study

The hydraulic model of the River Suir used in the case study and calibrated as outlined in the previous section, consisted of the river reach between New Bridge and Caher Park. The case study methodology involved routing the observed inflow hydrographs for New Bridge (Station 16008 and shown in Figure 6-3 to Figure 6-6) through the case study hydraulic model to generate outflow hydrographs at Caher Park. These observed inflow and simulated outflow hydrographs are shown for the four storms being investigated in Figure 6-14. The inflow hydrographs are denoted as *16008* and represented by the solid lines in Figure 6-14 and the simulated data is denoted as *16008 at 16009* and shown in dashed format.

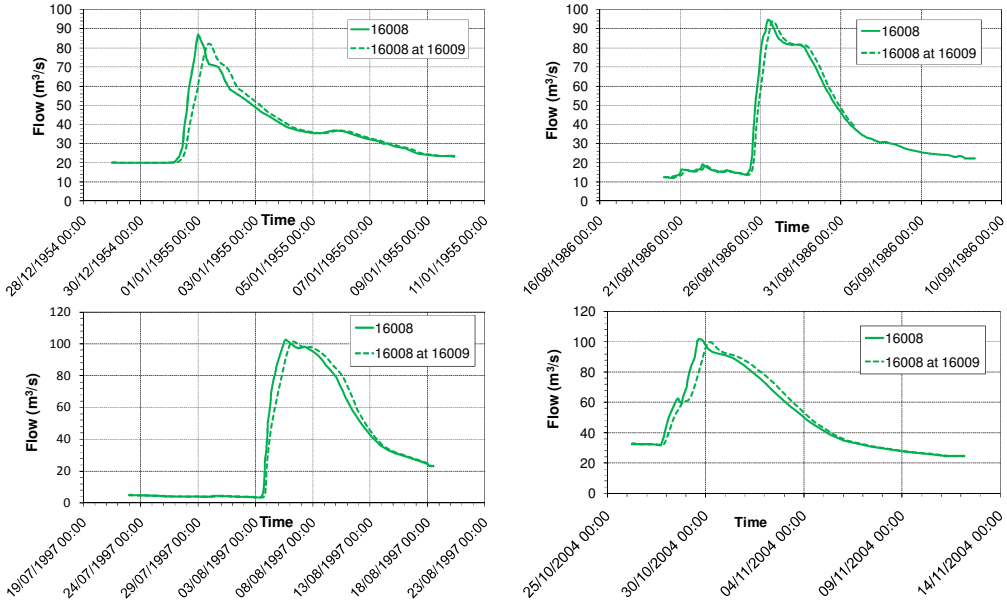


**Figure 6-14 Observed inflow hydrographs at New Bridge and simulated outflow hydrographs at Caher Park for storm events being investigated**

By comparing the inflow and outflow hydrographs in Figure 6-14, relative attenuations and relative delays were determined using the following two equations:

$$\text{Relative Attenuation } (\%) = \frac{Q_{P1} - Q_{P2}}{Q_{P1}} \qquad \textbf{Eqn. 6.1}$$

$$\text{Relative delay in time to peak } (\%) = \frac{T_{P2} - T_{P1}}{T_{P1}} \qquad \textbf{Eqn. 6.2}$$

where Q is the peak flow magnitude, T is the time to peak and subscripts P1 and P2 refer to the peaks of the inflow and outflow hydrographs (these are further defined in Figure 5-6 and Figure 5-18).

These relative attenuations and relative delays are summarised in Table 6-6.

**Table 6-6 Relative attenuations and delays determined from case study model**

| | 31/12/1954 | 26/08/1986 | 05/08/1997 | 29/10/2004 |
|---|---|---|---|---|
| $Q_p$ at New Bridge | 87.10 | 94.86 | 102.64 | 101.78 |
| $Q_p$ at Caher park | 82.22 | 94.55 | 102.38 | 99.89 |
| Time of peak at New Bridge | 01/01/1955 00:00 | 26/08/1986 11:15 | 05/08/1997 15:45 | 29/10/2004 16:30 |
| Time of peak at Caher park | 01/01/1955 09:15 | 26/08/1986 15:15 | 05/08/1997 18:30 | 30/10/2004 01:30 |
| % Obs. Rel. Attn in $Q_p$ | 5.60 | 0.33 | 0.25 | 1.86 |
| % Obs. Rel. delay in TP | 33.64 | 2.57 | 5.14 | 16.98 |

Table 6-6 indicates that large variability in the relative attenuation and delay values exists across for the four storm events investigated. The values for the 1954/ 55 storm, in particular, seem misaligned in scale with the other more recent events and require further investigation. In the absence of this investigation, data pertaining to the 1954 storm is excluded from this report for further comparison and discussion.

In addition to extracting the data in Table 6-6, case study simulations were also analysed to determine the geometrical properties of the flood inundation for application to the two regression equations developed for relative attenuation and relative delay in Sections 5.5 and 5.7. These properties were averaged for the cross-sections between New Bridge and Caher Park and are summarised in Table 6-7. Numerical values for other relevant parameters are also summarised in Table 6-7.

**Table 6-7 Geometrical and resistance properties for River Suir used in case study**

| | 31/12/1954 | 26/08/1986 | 05/08/1997 | 29/10/2004 |
|---|---|---|---|---|
| $b_{fp}$ (m) | 92.00 | 98.43 | 115.00 | 111.14 |
| $n_{fp}$ (s/m$^{1/3}$) | 0.05 | 0.05 | 0.20 | 0.04 |
| $Q_P$ (m$^3$/s) | 87.10 | 94.86 | 102.64 | 101.78 |
| $T_B$ (hrs) | 241.50 | 449.50 | 461.52 | 352.00 |
| $B_{bf}$ (m) | 25.00 | 25.00 | 25.00 | 25.00 |
| α (degree) | 5.00 | 5.00 | 5.00 | 5.00 |
| L (km) | 16.82 | 16.82 | 16.82 | 16.82 |
| $n_{mc}$ (s/m$^{1/3}$) | 0.04 | 0.04 | 0.04 | 0.04 |
| $S_{fp}$ (m/km) | 1.000 | 1.000 | 1.000 | 1.000 |

The equations for relative attenuation and delay are summarised as:

$$\%\ \text{Relative Attenuation} = 14050\frac{L\ n_{fp}\ n_{mc}\left(\frac{b_{fp}}{b_{bf}}\right)^{1.54}\left(\frac{Q_P}{B}\right)^{0.44}}{S_{fp}^{1.54}\alpha^{0.18}\left(12.97+T_B\right)^{1.96}} \qquad \textbf{Eqn. 6.3}$$

$$\%\ \text{Relative Delay} = 181\frac{L\ n_{fp}^{0.17}\ n_{mc}^{0.46}\left(\frac{b_{fp}}{b_{bf}}\right)^{0.38}}{S_{fp}^{0.55}\ \alpha^{0.07}\ T_B^{0.8}\left(\frac{Q_P}{B}\right)^{0.36}} \qquad \textbf{Eqn. 6.4}$$

where $b_{bf}$ is the bankfull width (m), $b_{fp}$ is the floodplain width (m), B is the total channel width (m), L is the floodplain length (km), $S_{fp}$ is the longitudinal floodplain slope (m/km), α is the transverse or lateral floodplain slope (degrees), $n_{mc}$ and $n_{fp}$ are the main channel and floodplain Manning's resistances respectively, $Q_P$ is the peak flow (m$^3$/s) and $T_B$ is the flood duration (hrs). Application of Eqn. 6.1 and Eqn. 6.2 require that $\alpha > 0$ and therefore horizontal floodplains are represented by a near-zero value of α. Similarly, the equations assess floodplain effects and therefore $Q_P > Q_{bf}$ where $Q_{bf}$ is the estimated bankfull discharge in the river.

Applying parameter values in Table 6-7 to equations Eqn. 6.3 and Eqn. 6.4 yields the values summarised in Table 6-8 and Table 6-9.

**Table 6-8 Comparison of observed and calculated relative attenuations (Eqn. 6.1)**

| | 26/08/1986 | 05/08/1997 | 29/10/2004 |
|---|---|---|---|
| % Obs. Rel. Attn in $Q_P$ | 0.33 | 0.25 | 1.86 |
| % Cal. Rel. Attn in $Q_P$ | 0.02 | 0.07 | 0.02 |

**Table 6-9 Comparison of observed and calculated relative delays (Eqn 6.2)**

| | 26/08/1986 | 05/08/1997 | 29/10/2004 |
|---|---|---|---|
| % Obs. Rel. delay in TP | 2.57 | 5.14 | 16.98 |
| % Cal. Rel. delay in TP | 6.27 | 8.43 | 7.80 |

Results in Table 6-8 indicate that Eqn. 6.4 massively underestimates the relative attenuations determined from the case study hydraulic model. While such large discrepancies are difficult to explain, limitations with the methodology adopted in developing the regression equations are likely to be contributing factors. Issues with roughness representation are the dominant factors in this regard. Energy losses associated with flows in real floodplains are likely to be considerably greater those represented by defining roughness through Manning's *n*. Intuitively, it would be expected that significant floodplain roughness as an example, would result in reasonably large attenuations. However, a limitation of the analysis that was undertaken is that the influence of geometrical, resistance and hydrograph properties were assessed individually. Therefore, in the case of floodplain resistance for example, high values (up to Manning's *n* of 5) were assessed in combination with constant main channel resistance values of 0.03. As the floodplain resistance increases, the proportion of flow being conveyed in the main channel increases and attenuation is very low. Results indicate that floodplain width, slope and main channel resistance are the dominant parameters on and other parameters that may be expected to have a strong influence on attenuation are much less significant.

In addition and although minimised through the calibration procedure, issues with te case study methodology are worth noting. The stability issues that necessitated the separate, rather than simultaneous, routing of the inflow hydrographs from New Bridge and Killardry to Caher Park resulted in energy losses at the confluence of the Rivers Suir and Aherlow being excluded.

Furthermore, individual routing indicated that flood hydrographs from Killardry in the absence of the flow contribution from New Bridge were primarily contained inbank. Flood flows from New Bridge in the absence of a contribution from Killardry exceed the bankfull level but result in a lower extent of flood inundation downstream of the confluence of the Aherlow and Suir Rivers than would be expected when the two hydrographs coincide. This would potentially result in floodplain flows being conveyed with overbank widths and depths and resulting hydrographs that would be different than those represented in the approach that was adopted.

The average geometrical properties from New Bridge to Caher Park based on routing the New Bridge hydrograph in Figure 6-10 to Figure 6-13 to Caher Park were extracted and are summarised in Table 6-7. Hydraulic resistance values for the River Suir floodplain required for model calibration are also shown.

The performance of Eqn. 6.4 in predicting the delay in flood wave propagation in Table 6-9 is more successful but is still likely to be influenced by the same issues as with Eqn. 6.3.

In an attempt to improve the performance of Eqn. 6.3 for the case of the River Suir, a further optimisation was undertaken. The equation from the generalised model for relative attenuation can be expressed as:

$$\% \text{ Relative Attenuation} = C \times 14050 \frac{L \; n_{fp} \; n_{mc} \left(\frac{b_{fp}}{b_{bf}}\right)^{1.54} \left(\frac{Q_P}{B}\right)^{0.44}}{S_{fp}^{1.54} \alpha^{0.18} \left(12.97+T_B\right)^{1.96}} \qquad \textbf{Eqn. 6.5}$$

Where *C* is a scaling factor that is dependent of the catchment to which the equation is being applied and remaining parameters are as previously defined.

By undertaking a further regression analysis using data from the 1986, 1997 and 2004 flood events, a value of *C* for the River Suir can be determined. With this value of C, Eqn. 6.5 becomes:

$$\% \text{ Relative Attenuation} = 5.55 \times 10^{5} \frac{L \; n_{fp} \; n_{mc} \left(\frac{b_{fp}}{b_{bf}}\right)^{1.54} \left(\frac{Q_P}{B}\right)^{0.44}}{S_{fp}^{1.54} \alpha^{0.18} \left(12.97+T_B\right)^{1.96}} \qquad \textbf{Eqn. 6.6}$$

Eqn. 6.6 is only applicable to the River Suir between Newbridge and Caher Park and an application this equation to the 1986, 1997 and 2004 flood events gives the relative attenuations shown in Table 6-10.

**Table 6-10 Comparison of observed and calculated relative attenuations (Eqn. 6.6)**

| | 26/08/1986 | 05/08/1997 | 29/10/2004 |
|---|---|---|---|
| % Obs. Rel. Attn in $Q_P$ | 0.33 | 0.25 | 1.86 |
| % Cal. Rel. Attn in $Q_P$ | 0.61 | 2.85 | 0.91 |

Table 6-10 indicates that Eqn. 6.6 represents an improvement in the relative attenuations predicted using Eqn. 6.1. However, considerable differences remain between the observed and the calculated values. It should be noted that a small number of floods in a 54-year flow record in a single catchment does not form a suitable basis for accurately determining the scale factor C for Irish catchments. It is recommended therefore, that further case study work in Irish catchments be undertaken to further refine this factor.

It should also be noted that the inclusion of an optimised scaling factor in Eqn. 6.4 for calculating the relative delay in the propagation of a flood wave did not yield improved results.

# 7 Conclusions and Recommendations for Further Work

## 7.1 Introduction

This report contains the findings of Work-Package 3.3 of the Flood Studies Update Programme. The Flood Studies Update (FSU) Programme was initiated in 2005 by the OPW in conjunction with interested state, semi-state and other relevant organisations. The title of Work-Package 3.3 of the FSU is Floodplain Attenuation Studies.

Flood flows in river channels in Ireland are commonly influenced by the effects of floodplain storage. This has significance for both single site and regional flood frequency analysis in Ireland. Failure to allow for floodplain attenuation in these analyses will potentially result in errors in estimated peak flows. Floodplain attenuation effects are inherently included in single site or regional flood frequency estimation procedures that use Annual Maximum series, resulting in calculated flows that are potentially underestimated. This presents a problem when these flows are used as inputs in river models where the flows are further attenuated. Therefore, the ability to properly account for floodplain effects in the hydrological analysis of catchments is essential to unravel this 'double accounting' of floodplain attenuation.

The project undertaken focussed on these issues. Through an extensive literature review, the role of floodplain storage on flood flows was assessed and various approaches adopted by researchers to incorporate these effects in flood risk estimation were presented. The review highlighted the full complexity of compound channel flows and suggested that influence of floodplain effects in flood risk assessment was likely to be very variable.

An objective of the report was to develop simple indices to represent floodplain effects on both flood frequency analysis. Previous research indicated that both hydraulic and hydrological routing were options for this. The approach that was adopted in this study was to use hydraulic routing of flood hydrographs in combination with a multi-variate least squares fit regression model to develop the optimal indices. Geometrical, resistance and hydrograph properties that were influential in the capacity of a river reach to attenuate a flood peak were identified and these included, length, longitudinal and lateral floodplain slopes, floodplain and bankfull widths, main channel and floodplain resistances, flood peak and flood duration. The hydraulic was undertaken in a generalised model of the River Suir, Co. Tipperary. This facilitated an assessment of the floodplain indices through case study investigation at the end of the project. Topographical and flow data for a reach of the River Suir was made available by the OPW for this purpose.

The project included an assessment of 1-D, 2-D and 3-D numerical models for simulating compound channel flows. The assessment was included to provide guidance on a suitable modelling code for completing the flood routing. HEC-RAS was the 1-D model used and this was compared with TELEMAC 2-D and TELEMAC 3-D. The Phase C experimental data from the UK Flood Channel Facility (FCF) was used in the simulations. Results from the assessment indicated that although 2-D and 3-D model can provide significantly more detailed information, a 1-D model would be sufficient for the study being undertaken. The decision to use HEC-RAS was supported by the work of Horritt and Bates (2002) where it was shown that for situations of river flood inundation, both 1-D and 2-D model types are capable of predicting flood extent and travel times to similar levels of accuracy if correctly calibrated. A further benefit of the HEC-RAS model is that it is readily available and has the required flexibility to perform flood routing for various floodplain geometric configurations.

Results of the HEC-RAS modelling formed the basis of the multi-variate regression model where the individual influences of geometrical, resistance and hydrograph properties on relative attenuation of a flood peak and relative delay of a flood wave were assessed. Indices for both relative attenuation and delay were derived from the regression model and applied to the case study of the River Suir.

## 7.2 Main Findings

The project produced single indices for floodplain attenuation and delay of flood wave propagation. These are summarised as:

$$\%\ \text{Relative Attenuation} = 14050\frac{L\ n_{fp}\ n_{mc}\left(\frac{b_{fp}}{b_{bf}}\right)^{1.54}\left(\frac{Q_P}{B}\right)^{0.44}}{S_{fp}^{1.54}\alpha^{0.18}\left(12.97+T_B\right)^{1.96}}$$

$$\%\ \text{Relative Delay} = 181\frac{L\ n_{fp}^{0.17}\ n_{mc}^{0.46}\left(\frac{b_{fp}}{b_{bf}}\right)^{0.38}}{S_{fp}^{0.55}\ \alpha^{0.07}T_B^{0.8}\left(\frac{Q_P}{B}\right)^{0.36}}$$

where $b_{bf}$ is the bankfull width (m), $b_{fp}$ is the floodplain width (m), B is the total channel width (m), L is the floodplain length (km), $S_{fp}$ is the longitudinal floodplain slope (m/km), $\alpha$ is the transverse or lateral floodplain slope (degrees), $n_{mc}$ and $n_{fp}$ are the main channel and floodplain Manning's resistances respectively, $Q_P$ is the peak flow ($m^3/s$) and $T_B$ is the flood duration (hrs). Application of Eqn. 6.1 and Eqn. 6.2 require that $\alpha > 0$ and therefore horizontal floodplains are represented by a near-zero value of $\alpha$. Similarly, the equations assess floodplain effects and therefore $Q_P > Q_{bf}$ where $Q_{bf}$ is the estimated bankfull discharge in the river.

Application of these two equations to the River Suir Case study indicated that the equations grossly underestimated the relative attenuations that were determined when routing observed hydrographs at New Bridge through the case study hydraulic model to Caher Park.

While the discrepancies are difficult to explain, limitations with the methodology adopted in developing the regression equations are likely to be contributing factors. Issues with roughness representation are the dominant factors in this regard. Energy losses associated with flows in real floodplains are likely to be considerably greater those represented by defining roughness through Manning's *n*.

An attempt was made to improve the performance of the attenuation equation by the addition of a scaling factor which is applicable to the River Suir between New Bridge and Caher Park. This was only moderately successful. The optimised equation for the River Suir that included the scaling factor was:

$$\% \text{ Relative Attenuation} = 5.55\times10^{5}\frac{L\ n_{fp}\ n_{mc}\left(\frac{b_{fp}}{b_{bf}}\right)^{1.54}\left(\frac{Q_P}{B}\right)^{0.44}}{S_{fp}^{1.54}\alpha^{0.18}\left(12.97+T_B\right)^{1.96}} \qquad \textbf{Eqn. 6.6}$$

It should be noted that a small number of floods in a 54-year flow record in a single catchment does not form a suitable basis for accurately determining a scale factor for Irish catchments. It is recommended therefore, that further case study work in Irish catchments be undertaken to further refine this factor.

The performance of the regression equation for determining the relative delay in flood wave propagation, although better, still fails to accurately represent the attenuations in the River Suir as determined in the case study.

## 7.3 Recommendations for Further Work

The study serves to illustrate the full complexities that must be understood when trying to predict 'real' hydraulics and hydrology in natural catchments and highlights in a positive way issues and limitations with using numerical models to represent these complexities. Differences between relative attenuations and delays calculated using the developed indices with those determined in the case study model emphasise again that where it is available, there is no substitute for real data in hydrological analyses.

The work undertaken in this study and presented in this report represents a genuine attempt by the researchers to produce an index that represents the effects of the significant physical factors which influence flood peak attenuation. The number of factors representing catchment and hydrograph properties that were included in the indices, reflect this complexity. The large errors that result from an application of the indices to the River Suir case study are disappointing and indicate the need for further research on the topic.

Flood attenuation indicators (FAIs) have been developed for catchments throughout

Ireland as part of the Flood Studies Update. These were used in this study to aid the selection of the river reach used in the case study. However, FAIs were not used in the developed indices. The findings of this study indicated that attenuation from floodplains is proportional to both the width and length of an inundated floodplain area. Scope may therefore exist to use FAIs to distinguish between floodplain affected (FPA) and non FPA catchments and to link FAI values to attenuations determined by comparison of upstream and downstream hydrographs within a river reach. Flood volume was also shown in this study to be an influential parameter in floodplain attenuation. Consideration therefore should be given to a hydrograph width / flood duration parameter when developing further approaches of incorporating floodplain effects in flood frequency analysis.

# 8 References

Abbott, M., 1997. Range of tidal flow modelling. *J. Hyd. Eng., 123(4), pp. 257-277.*

Ackers, P., 1992. Hydraulic design of two-stage channels. *Proceedings of the Institution of Civil Engineers, Water,Maritime & Energy, 96, No. 4, 247–257.*

Ackers, P., 1993. Flow formulae for straight two-stage channels. *Journal of Hydraulic Research, 31, No. 4, 509–531.*

Ackers, P., 1993. Stage – Discharge Functions for Two stage channels: *The Impact of New Research. Journal of the Institution of Water and Environmental Management, Vol. 7, No. 1, pp. 52-61.*

Acreman, M.C. and Sinclair, C.D., 1986. Classification of drainage basin according to their physical characteristics; an application for flood frequency analysis in Scotland. *J. Hydrol., 84, pp. 365-380.*

Ahilan, S., 2007. Flood frequency analysis based on Peaks over Threshold approach for UK and Irish catchments. *M. Appl. Sc. Thesis, National University of Ireland, Galway.*

Amein, M., 1968. An implicit method for numerical flood routing. *Water Resour. Res., 4(8): 719 - 726.*

Amein, M. and Fang, C.S., 1970. Implicit flood routing in natural channels. *J. Hydroul. Div., ASCE, 96(5): 2481-2500.*

Archer, D., 1989. Flood wave attenuation due to channel and floodplain storage and effects on flood frequency. *In Floods: Hydrological, Sedimentological and Geomorphological Implications, Beven, K. and Carling, P.A. (Eds), John Wiley and Sons: Chichester: pp 37-46.*

Bates, P., Anderson, M., Price, D., Hardy, R., Smith,C., 1996. Hydraulic Models and Floodplain flows in Floodplain Processes. *Anderson et al (ed.), Wiley, 139-181.*

Bates, B. C., Pilgrim, D. H., 1982. Investigation of storage-discharge relations for river reaches and runoff routing models in hydrology. *Water Resources Symposium, Preprints of Papers, The Institution of Engineers Australia, Canberra, pp 120-126.*

Benn, J.R., 1984. Frequency analysis of flood data from the Northumbrian and South West water authority regions. *M.Sc. dissertation, University of Newcastle upon Tyne.*

Bhowmik, N.G., 1984. Hydraulic geometry of floodplains. *In: G.E. Stout and G.H. Davis (Editors), Global Water: Science and Engineering – The Ven Te Chow Memorial Volume. J. Hydrol., 68: 369-401.*

Bousmar, D., Zech, Y., 1999. Momentum transfer for practical flow computation in compound channels. *J. Hydraul. Eng., 125(7), 696–706.*

Castro, J.M. and Jackson P.L., 2001. Bankfull discharge recurrence intervals and regional hydraulic geometry relationships patterns in the Pacific Northwest, USA. Journal of the American Water Resources Association, 37(5), pp. 1249-1262.

Chang, H.H., 1984. Variation of flow resistance through curved channels. *Journal of Hydraulic Engineering, ASCE, vol. 110, no. 12, paper no. 19348, pp. 1772-1782.*

Choudhury, P, Shrivastava, R.K. and Narulkar, S.M., 2002. Flood routing in river networks using equivalent Muskingum inflow. *J. Hydrol. Eng. 7(6): 413-419.*

Chow, V.T., 1959. *Open Channel Hydraulics*, McGraw-Hill, New York.

Corti, S., and Pennati, V., 2000. A 3-D Hydrodynamic Model of River Flow in a Delta Region. *Hydrological Processes, 14(13), pp 2301-2309.*

Cunnane, C., 1979. A note on the Poisson assumption in partial duration series models. *Water Resour. Res., 15(2), 489-493.*

Dury, G.H. 1961. Bankfull discharge: an example of its statistical relationship. *Bulletin of the International Association of Scientific Hydrology 6(3), pp. 48-55.*

EDF (1997a). TELEMAC modelling system. TELEMAC-3D. Version 2.1 - Validation Document.

EDF(1997b). TELEMAC modelling system. TELEMAC-3D. Version 2.2 - Système de modélisation TELEMAC-3D Note Théorique, HE-42/97/049/B.

EDF (2000). TELEMAC modelling system TELEMAC-2D, Version 5.0 - Validation Document.

EDF (2001). TELEMAC modelling system, TELEMAC-2D, Version 3.0 - Principle Notes. Report No. HE-43/94/052/A.

Ervine, D.A., Sellin, R.J., Willetts, B.B., 1994. Large flow structures in meandering compound channels. *2nd International conference on River Flood Hydraulics (Ed. WR White and J Watts), March, York, England, Paper 40, pp. 459-469, Published by J Wiley & Sons Ltd.*

Ghavasieh, A.R., Poulard, C. and Paquier, A., 2006. Effect of roughened strips on flood propagation: Assessment on representative virtual cases and validation. J. *Hydrol., 318: pp 121-137.*

Gillespie, D.F.T., Smith, J.A. and Bates, P.D., 2003. Attenuating reaches and the regional flood response of an urbanizing drainage basin. *Advances in Water Resources., 26: pp 673-684.*

Haider, S., 1992. Effects of floodplain inundation on flood frequency. *Trans., Am. Geophys. Union, 73(43):pp 242-243.*

Hey RD, 1976, "Geometry of River Meanders", *Nature, vol. 262, pp. 482-484.*

Hey, R.D. and Davies, J.D., 1975. Design discharge for natural channel. *In: Science Technology and Environmental Management, Saxon House: Farnbourgh: pp. 73-88.*

Harvey, A. M., 1969. Channel capacity and the adjustment of streams to hydrologic regime. *J. Hydrol., 8, pp 82-98.*

Helmiö, T., 2005. Unsteady 1D flow model of a river with partly vegetated floodplains -application to the Rhine River. *Environmental Modelling & Software, Vol. 20, pp. 361-375.*

Henderson, F.M., 1966. Open Channel Flow. *Macmillan Publishing Company, New York.*

Hervouet, J.-M., 2000. A high resolution 2-D dam-break model using parallelisation. *Hydrological Processes, 14(13), pp. 2211–2230.*

Hervouet, J.-M. (2003). Hydrodynamique des Écoulements á Surface Libre: Modélisation Numérique avec la Méthode des Éléments Finis. Presses de l'École Nationale des Ponts et Chaussées.

Hervouet, J.-M. (2004). TELEMAC Modelling system . Guide to Programming in the TELEMAC system version 5.4 Fortran 90. Report EDF HP-75/04/006/A.

Hervouet, J.-M. (2007). Hydrodynamics of Free Surface Flows: Modelling with the Finite Element Method. John Wiley and Sons, Ltd.

Hey, R.D. and Davies, J.D., 1975. Design discharge for natural channels. In Science Technology and Environmental Management. Saxon House: Farnborough: 73-88.

Holden, A.P. and James, C.S., 1989. Boundary shear distribution on flood plains. *IAHR, Journal of Hydraulic Research, January, vol. 27, no. 1, pp. 75-89.*

Hollis, G. 1975. The Effect of Urbanization on Floods of Different Recurrence Intervals. *Water Resour. Res., 11(3): pp 431–435.*

Horritt, M.S. and Bates, P.D., 2002. Evaluation of a 1D and 2D numerical models for predicting river flow inundation. Journal of Hydrol., 268: 87-99.

ICE, 1975, Discussion on Papers 7 and 8. *Proc. Flood Studies Conference*, London, 7-8 May 1975, pp. 61-66.

ICE, 2001, Learning to live with rivers. Final Report of the Institution of Civil Engineers' Presidential Commission to review the technical aspects of flood risk management in England and Wales. Institution of Civil Engineers, London.

Imamoto, H. and Kuge, T. 1974. On the basic characteristics of an open channel flow in complex cross section. *Kyoto University Diaster Prevention Research Annual Report No. 17, pp. 665-679.*

Institute of Hydrology, 1999, Flood Estimation Handbook. Vol.1 *Overview*, Vol. 2 *Rainfall Frequency Estimation*. Vol. 3 *Statistical Procedures for Flood Frequency Estimation*. Vol. 4 *Restatement and Application of the Flood Studies Report Rainfall-Runoff Method*. Vol. 5 *Catchment Descriptors, IH, Wallingford, UK*.

James, L. D., 1965. Using a digital computer to estimate the effects of urban development on flood peaks, *Water Resour. Res., 1(2), pp. 223-234.*

James, M., Brown, R.J., 1977. Geometric parameters that influence floodplain flow. *US Army Engineering Waterways Experiment Station, Vicksburg, Mississippi, June, Research report H-77-1*.

Jarvela, J., 2002. Flow resistance of flexible and stiff vegetation: a flume study with natural plants. *J. Hydrol., 269: 44-54*.

Karamisheva, R., Lyness, J., Myers, W., Cassells, J., O'Sullivan, J., 2006. Overbank flow depth prediction in alluvial compound channels. *Proceedings of the Institution of Civil Engineers, Water Management 159, Issue WM3, pp 195–205.*

Kiely, G., 1989. Experimental study of the mechanisms of flood flow in meandering channels. *Proc. Of the 23rd IAHR Congress, August, Ottawa, Canada.*

Kiely, G., 1990. Overbank flow in meandering compound channels-the important mechanisms. *International conference on River Flood Hydraulics, (Ed. White WR), Wallingford, England, September, Paper F3, pp. 207-217, Published by John Wiley & Sons Ltd.*

Kirby, W., 1969. On the random occurrence of major floods. *Water Resour. Res., 5(4): pp. 778-789*.

Knight, D.W. and Demetriou, J.D., 1983. Floodplain and main channel flow interaction. *J. Hydraul. Div., ASCE, 109(8): 1073-1092.*

Knight, D.W., Demetriou, J.D. and Hamed, M.E., 1984. Stage discharge relationships for compound channels. *Proc. 1st Int. Conf. on Hydraulic Design in Water Resource Engineering: Channel and Channel Control Structures, University of Southamption. Computational Mechanics Centre, Southampton, and Springer, Heidelberg, pp. 4.21 – 4.36.*

Knight, D.W. and Sellin, R.H.J., 1987. The SERC Flood Channel Facility. *Journal of the Institution of Water and Environmental Management, London, vol. 1, no. 2, pp. 198-204.*

Knight, D.W. and Shiono, K. 1990. Turbulence measurements in a shear layer region of a compound channel. *Journal of Hydraulic Research, IAHR. 28(2): 175-196. (Discussion in IAHR Journal, 1991, 29(2), 259-276.)*

Knight, D.W. and Shiono, K., 1996. River Channel and Floodplain Hydraulics. In: *Floodplain Processes. Anderson et al (ed.), Wiley, pp. 139-181.*

Knight, D.W., Shiono, K., and Pirt, J., 1989. Prediction of depth mean velocity and discharge in natural rivers with overbank flow. *Proc. Int. Conf on Hydraulic and Environmental modelling of Coastal, Estuarine, and River Waters, (ed. R.A. Falconer et al), University of Bradford, Gower Technical Press, Paper 38, pp. 419-428.*

Kowen, N., Fathi-Moghadam, M., 2000. Friction factors for coniferous trees along rivers. J. Hyd. Res., 126(10), pp. 732-740.

Lambert, C.P. and Walling, D.E., 1987. Floodplain sedimentation: a preliminary investigation of contemporary deposition within the lower reaches of the River Culm. Devon U.K. *Geografisko Annaler, 69(3-4): pp. 393-404.*

Lane, S., Bradbrook, K., Richards, K., Biron, P. Roy, A., 1999. The application of computational fluid dynamics to natural river channels: three-dimensional versus two-dimensional approaches. *Geomorphology 29, pp.1–20.*

Lane, S.N., Richards, K.S., Chandler, J.H., 1995. Within-reach spatial patterns of process and channel adjustment. *In: Hickin, E.J._Ed.., River Geomorphology, Wiley, Chichester, pp. 105–130.*

Laurenson, E. M., 1962. Hydrograph synthesis by runoff routing. *Rep. 66, sect. 3.3, Water Res. Lab., Univ. of New South Wales, Manly Vale, N. S. W., Australia.*

Leopold, L.B., Bagnold, R.A., Wolman, M.G. and Brush, L.M. Jr., 1960. Flow resistance in sinuous or irregular channels. *Physiographic and hydraulic studies of rivers, Professional Paper 282-D, US Coast and geodetic survey, Washington DC, pp. 111-134.*

Lewin, J. and Huges, D., 1980. Welsh Floodplain Studies II: Application of a Qualitative Inundation model. *J. Hydrol., 46: 35-49.*

Lipscomb, E.B., 1956. Hydraulic capacity of meandering channels in straight floodways. *Report T.M. no. 2-2429, Waterways Experiment Station, Vicksburg, Mississippi, USA.*

Longwell, C.R., Knopf, A., and Flint R.F., 1948. Physical Geology, *John Wiley, New York, 602 pp.*

Lyness, J.F., Myers, W.R.C., O'Sullivan J., 1999. Hydraulic characteristics of meandering mobile bed compound channels. *Proceedings of the Institution of Civil Engineers: Water, Maritime & Energy, December, vol. 130, paper 11545 pp. 179-188.*

Martens, L.A., 1968. Flood inundation and effects of urbanization in metropolitan Charlotee, N. Carolina. *U.S. Geol. Surv., Water Suppl. pap. 1591-C, 60 pp.*

Martin, L.A., Myers, W.R.C., 1991. Measurement of overbank flow in a compound river channel. *Proceedings of the Institution of Civil Engineers, London, December, vol. 91, Part 2, paper no. 9729, pp. 167-178.*

Mason, D.W., 1992. Modelling the effect of Floodplain storage on the flood frequency curve. *PhD thesis, University of Newcastle upon Tyne.*

Mason, D.W., O' Connell, P.E. and Mawdsley, J.A., 1988. The effect of floodplain storage on the flood frequency curve. *Paper presented at International Association of Hydraulics Research, Int. Symp. on Stochastic Hydraulics, Birmingham.*

McCartney, M.P. and Naden, P.S., 1995. A Semi-Empirical investigation of the influence of flood-Plain Storage on Flood Flow. *Journal of the Institution of Water and Environment Management 9(3): pp 236-246.*

Mimikou, M., 1983. A study of Drainage Basin Linearity and Non Linearity. *Journal of Hydrol., 64: 113-134.*

Mockmore, C.A., 1944. Flow around bends in stable channels. *Transactions of the ASCE, vol. 109, pp. 593-628.*

Morvan, H., Pender, G., Wright, N., Ervine, D., 2002. Three-dimensional hydrodynamics of Meandering Compound Channels. *Journal of Hydraulic Engineering, pp. 674-682.*

Murota, A., Fukuhara, T., Seta, M., 1990. Effects of channel shape and floodplain roughness on flow structure in compound cross sections. *Journal of Hydroscience and Hydraulic Engineering, December, vol. 8, no. 2.*

Myers, W.R.C., 1987. Velocity and discharge in compound channels. *Journal of the Hydraulic Engineering, ASCE, June, vol. 113, no. 6, paper no. 21549, pp. 753-766.*

Myers, W.R.C., Lyness, J.F., 1989. Flow resistance in rivers with floodplains. *Final Report on Research Grant GR5/D/45437, University of Ulster, Northern Ireland.*

Naden, P., Rameshwaran, P., Wilson, C., Malki, R., Egarr, D., Shukla, D. Shiono, K., 2006. Inter-comparison of CFD codes using data from a large-scale physical model. *7th International Conference on Hydroinformatics, Nice, France.*

Navratil, O., Albert, M.B. and Herouin, E., 2006. Determination of bankfull discharge magnitude and frequency: comparison of methods on 16 gravel bed river reaches. *Earth surf. Process. Landforms 31:pp 1345-1363.*

Neill, C. R., 1964. Alluvial processes and river channel regime, *Trans. Eng. Inst. Can, 7, pp 3-8.*

Nepf, H., 1999. Drag, turbulence and diffusion in flow through emergent vegetation. *Water Resources Research, 35(2), pp. 479-489.*

NERC (Natural Environment Research Council), 1975. Flood Studies Report. Vol. I *Hydrological Studies*. Vol II *Meteorological Studies*. Vol III *Flood Routing Studies*. Vol IV *Hydrological Data*. Vol V *Maps*, London.

Nicollet, G., Uan, M., 1979. Ecoulements permanents à surface libre en lit composés. *Houille Blanche, 35(1), pp 21–30.*

Nixon, M., 1959a. A study on the bank-full discharges of rivers in England and Wales. *Proc. Inst. Civil Eng., 12, pp. 157-174.*

Nixon, M., 1959b. A study of the bank-full discharge of rivers in England and Wales. *Proc. Inst. Civil Eng., 14, pp. 395-425.*

Nunnaly, N. R., 1967. Definition and identification of channel and over bank deposits and their respective roles in floodplain formation. *Prof. Geogr., 19: 1-4*.

Olsen, N.R.B., 2007. SSIIM User's Manual. *The Norwegian University of Science and Technology. Available from: http://www.bygg.ntnu.no/~nilsol/ssiimwin.*

Onoz, B. and Bayazit, M., 2001. Effect of the occurrence process of the peaks over threshold on the flood estimates. *J. Hydrol., 244: pp. 86-96.*

Petit, F. and Pauquet, A., 1997. Bankfull discharge recurrence interval in gravel-bed rivers. *Earth surface processes and landforms., 22, pp. 685-693.*

Petryk, S. and Bosmajian, G., 1975. Analysis of flow through vegetation, *Journal of the Hydraulics Division, ASCE*, *Vol. 101, No. HY7, pp. 871-884.*

Petts, G.E. and Foster, J. 1985. Rivers and Landscape, *Arnold, 274pp*.

Pickup, G., and Warner R. F., 1976. Effects of hydrologic regime on magnitude and frequency of dominant discharge. *J. Hydrol., 29, pp. 51-75*.

Price, R.K., 1973. Flood routing methods for British rivers. *Proc. Inst. Eng., 55, pp 913-930.*

Prinos, P., Townsend, R.D., 1983. Estimating discharge in compound open channels. *Canadian Society for Civil Engineering, Proc. 6th Canadian Hydrotechnical Conference, Ottowa, Ontario, June, vol. 1, pp. 129-146.*

Proust, S., Rivière, N., Bousmar, D., Paquier, A., Zech, Y., Morel, R., 2006. Flow in Compound Channel with Abrupt Floodplain Contraction. *Journal of Hydraulic Engineering. Vol. 132, No. 9, pp. 958-970.*

Rameshwaran, P. and Shiono, K.(2003). Computer modelling of two-stage meandering channel flows. *Proceedings of the Institution of Civil Engineers: Water and Maritime Engineering 156, pp. 325-339.*

Rameshwaran, P., Sun, X, Shiono, K., Chandler J.H., Sellin, R.H.J., 2008. The Modelling of Compound Channel Flow: Physical Model of River Blackwater. *International Conference on Fluvial hydraulics (River Flow 2008), September 3-5, Turkey.*

Richards, K. 1982. Rivers, Form and Process in Alluvial Channels. *Methuen, 358 pp.*

Roberts, C.E., 1989. Flood frequency and urban-induced channel change: some British examples. *In Floods: Hydrological, Sedimentological and Geomorphological Implications, Beven, K. and Carling, P. (Eds), Wiley, Chichester, pp. 57-82.*

Rogers, W.F., 1980. A practical Model for Linear and Nonlinear Runoff. *Journal of Hydrol., 46: 51-78.*

Samuels, P.G., 1985. Modelling open channel flow using pressman scheme. *Proc. 2nd Int. Conf. on the Hydraulics of Floods and Flood control. British Hydraulics Research Association, Wallingford, pp. 91-100.*

Sellin, R.H.J., 1964. A laboratory investigation into the interaction between the flow in the channel of a river and that over its flood plain. *La Houille Blanche, November, vol. 19, no. 7, pp. 793-801.*

Sellin, R.H.J., Ervine, D.A., Willetts, B.B., 1993. Behaviour of meandering two-stage channels. *Proceedings of the Institution of Civil Engineers: Water, Maritime & Energy, June, vol. 101, pp. 99-111.*

Shaw, E.M., 1994. Hydrology in practice. *TJ Press (Padstow) LTD, Cornwall UK. Shelton, J.S., 1966. In: Geology illustrated, 434 pp., W.H. Freeman, San Francisco, Calif.*

Shiono, K. and Knight, D. W., 1991. "Turbulent open channel flows with variable depth across the channel", *Journal of Fluid Mechanics, 222, pp.617-646.*

Shukry, A., 1949. Flow around bends in an open flume. *Transactions of the ASCE, vol. 115, pp. 751-788.*

Simm, D., Walling, D., Bates, P., Anderson, M., 1997. The potential application of finite element modelling of floodplain inundation to predict patterns of overbank deposition. *Journal of Hydrological Sciences, 42(6).*

Singh, V.P. and Aminian H., 1986. An Empirical Relation Between Volume and Peak of Direct Runoff. *Water Resources Bulletin 22: 725-730.*

Smith, C.D., 1978. Effect of channel meanders on flood stage in valley. *Journal of the Hydraulics Division, ASCE, January, vol. 104, paper HY1, pp. 49-58.*

Soil Conversation Service,1963. Guide for Selecting Roughness Coefficient "n" Values for Channels. *US Department of Agriculture, Soil Conservation Service, Washington, D.C.*

Song, Y. and Haidvogel, D.B., 1994. A Semi-Implicit ocean circulation model using a generalized topography following co-ordinate system. *J. Comp. Phys., 115(1): 228-244.*

*Speight, J. G., 1965. Flow and channel characteristics of the Angabunga River Papua. J. Hydrol., 3: pp 16-36.*

Stein, C.J., Rouve, G., 1988. 2D depth-averaged numerical predictions of the flow in a meandering channel with compound cross-section. *Hydrosoft, vol.2, no.1.*

Stephan, U. and Gutnecht, D., 2002. Hydraulic resistance of submerged flexible vegetation. *J. Hydrol., 269, pp. 27-43.*

Tate, E. C., Maidment, D. R., Olivera, F., Anderson, D. J. 2002. Creating a terrain model for floodplain mapping. *The ASCE Journal of Hydrologic Engineering, vol. 7, no. 2, March/April, pp. 100-108.*

Tewolde, M.H. and Smithers, J.C., 2006. Flood routing in ungauged catchments using Muskingum methods. *Journal of Water South Africa 32(3): pp 379-388.*

Thomas, H., Nisbet, R.S., 2007, An assessment of the impact of floodplain woodland on flood flows, *CIWEM Water and Environment Journal, 21, pp 114 – 126*.

Thornbury, W. D., 1969. Principles of Geomorphology. *2nd Ed., John Wiley, New York, 618 pp.*

Toebes, G.H., Sooky, A.A., 1967. Hydraulics of meandering rivers with flood plains. *Journal of the Waterways and Harbours Division, ASCE, vol. 93, no. 2, pp. 213-236.*

Tominaga, A. and Nezu, I., 1991. Turbulent structure in compound open channel flows. *Journalof Hydraulic Engineering, ASCE, 117(1): 21-41.*

Tominaga, A., Nezu, I., Ezaki, K., 1989. Experimental study on secondary currents in compound open channels. *Proc. Of 23rd IAHR Congress, Ottowa, Canada, August, pp A15-A22.*

UNESCO 1979. Impact of urbanisation and industrialisation on water resources planning and management. *Report of the UNESCO/IHP workshop at Zandvoort, The Netherlands, 1977, UNESCO.*

USACE (United States Army Corps of Engineers), 2008. HEC-RAS, River Analysis System Hydraulic Reference Manual. Available from: http://www.hec.usace.army.mil/software/hec-ras/documents/HEC-RAS_4.0_Reference_Manual.pdf.

Van Montfort, M.A.J. and Witter, J.V., 1985. Testing exponentiality against generalised Pareto distribution. *J. Hydrol., 78: pp. 305-315.*

Wieping Liu, James, C.S., 1997. Effects of floodplain geometry on conveyance of meandering compound channels. *Proc. Of the 3rd International Conference on River*

*Flood Hydraulics, (Ed. White WR), Stellenbosch, South Africa, Paper no. 9, pp. 81-90.*

Willetts, B.B., Hardwick, R.I., 1993. Stage dependency for overbank flow in meandering channels. *Proceedings of the Institution of Civil Engineers: Water, Maritime & Energy, vol. 101, pp. 45-55.*

Willetts, B.B., Hardwick, R.I., MacLean, A.G., 1990. Model studies of overbank flow from a meandering channel. *International conference on River Flood Hydraulics, (Ed. White WR), Wallingford, England, September, Paper F2, pp. 197-205, Published by John Wiley & Sons Ltd.*

Williams, G. P., 1978. Bank-Full discharge of rivers. *Water Resour. Res., 14(6), pp. 1141-1153.*

Wilson, C., Bates, P., Hervouet, J.-M., 2002. Comparison of turbulence models for stage-discharge rating curve reach prediction in reach-scale compound channel flows using two-dimensional finite element methods. *Journal of Hydrol., 257, pp. 42-58.*

Wilson, C., Yagci, O., Rauch, H.-P., Olsen, N., 2006. 3D numerical modelling of a willow vegetated river/floodplain system. *Journal of Hydrol., 327, pp. 13-21.*

Wiltshire, S. E., 1986. Identification of homogeneous regions for flood frequency analysis. *J. Hydrol., 84, pp. 287-302.*

Wolff, C. G. and Burges, S. J., 1994. An analysis of the influence of river channel properties on flood frequency. *J. Hydrol., 153: pp. 317-337.*

Woltemade, C.J. and Potter, K.W., 1994. A watershed modelling analysis of fluvial geomorphologic influences on flood peak attenuation. *Water Resour. Res., 30(6): pp. 1933-1942.*

Wong, T. H. F. and Laurenson, E. M., 1983. Wave speed-discharge relations in natural channels. *Water Resour. Res, 19(3), pp. 701-706.*

Woodyer, K. D., 1968. Bankfull frequency in rivers. *J. Hydrol., 6, pp. 114-142.*

Yalin M.S, 1992. "River mechanics", Pergamon Press, ISBN 0080401902

Zheleznyakov G V, 1965. "Relative deficit of mean velocity of instable river flow, kinematic effect in river beds with flood plains", *Proceedings of the 11th International congress of the Association for hydraulic research, Leningrad, USSR.*